TETRAPHOSPHINES WITH TETRAPHENYLELEMENT CORES AS LINKERS IN CATALYSIS AND SURFACE SUPPORTED SYNTHESIS

A Dissertation

by

ERIC MICHAEL STEFFENSMEIER

Submitted to the Office of Graduate and Professional Studies of
Texas A&M University
in partial fulfillment of the requirements for the degree of

DOCTOR OF PHILOSOPHY

Chair of Committee,	Janet Bluemel
Committee Members,	James Batteas
	Abraham Clearfield
	Tatyana Igumenova
Head of Department,	Simon North

December 2016

Major Subject: Chemistry

ABSTRACT

The principal directions of this thesis involve (1) the synthesis and characterization of tetraphosphine linkers with rigid tetraphenylelement cores and derivatives thereof, (2) the study of the tetraphosphines and their phosphonium salts with respect to their interactions with silica, (3) the creation, characterization and activity studies of immobilized Wilkinson-type hydrogenation catalysts, and (4) the synthesis, characterization, and performance investigation of a surface-supported Wittig reagent for alkene synthesis.

Several different tetraphenylelement scaffolds with silicon and tin centers and phosphine groups in the para positions have been synthesized. These tetraphenylelement compounds have the advantage of incorporating a rigid backbone, making them ideal immobilized linkers that prevent interactions of coordinated metal centers with the reactive silica surface, and it diminishes the probability of deactivation of the metal complexes by dimerization. A range of tetraphosphines and their derivatives have been generated by using one of two synthetic routes. The phosphines feature various substituents, for example, phenyl, cyclohexyl, *tert*-butyl, or isopropyl groups. The scaffolds were equally accessible with either silicon or tin at the core.

The tetraphosphines can be immobilized on silica via three phosphonium groups by using ethoxysilanes, which leaves one free phosphine at the top of the scaffold. The phosphines are covalently bound via the counteranions of the phosphonium groups and are not readily leached off of the surface. This was demonstrated by placing one representative immobilized scaffold in eight different solvents, where no leaching could be detected by ^{31}P NMR, even in very polar solvents like DMSO. Furthermore, impregnated phosphonium salts

were mobile on the surface of silica in the presence of solvents, but their solubilities did not correlate with the mobilities, which indicates that surface detachment is not a crucial element in the mode of mobility.

A new class of immobilized Wilkinson-type catalysts, consisting of a linker featuring four phosphine moieties with a rigid tetraphenylelement core, has been generated. These new catalysts can easily be recycled almost indefinitely, they display fast substrate conversion at very low temperatures, no active species leach into the supernatant, and they are resistant to oxidation in air. However, the catalyst was reduced during batchwise recycling, resulting in the formation of Rh nanoparticles. The presence of the latter was proven by split and poisoning tests, double bond migration studies, as well as electron microscopy. Using a chelating linker to bind to the Rh center did not prevent nanoparticle formation.

Finally, one tetraphosphine scaffold was selected to create a surface-supported Wittig reagent. This was achieved in two different ways. Using the first method, the free phosphine of the scaffold was quaternized with benzyl bromide and subsequently transformed into the ylide by deprotonation. The ylide then underwent the Wittig reaction with benzaldehyde under optimized conditions. Approximately the same yield as for the reaction with $Ph_3P{=}CHPh$ in solution (73%) was obtained, but the *E*/*Z* ratio (84%) was substantially higher. The phosphine oxide byproduct of the Wittig reaction remained tethered to the surface with no phosphine oxide leaching into solution. The second method for generating a surface-bound Wittig reagent involved synthesizing the tetraylide first, then reacting three of the ylide groups with the the silica surface. This method produced similar results with respect to the Wittig reaction to those when using the first method. However, the crucial difference was that the scaffold could easily be washed off of the silica support with THF.

DEDICATION

To my family,

for their patience and encouragement through this journey…

ACKNOWLEDGEMENTS

First, I'd like to thank my advisor, Dr. Janet Bluemel, for all of her assistance, guidance, and encouragement throughout my time in the group. This work would not have been possible without her persistence and dedication, and it led me on a path to becoming a successful chemist.

I'd also like to thank my committee members, Dr. Abraham Clearfield, Dr. James Batteas, and Dr. Tatyana Igumenova, for attending my seminars and providing insightful questions and input about my research.

I'd like to thank all of the technicians who have been helpful with the NMR instruments. Thanks goes to Steve Silber and Dr. Greg Wylie, who have been around to answer any questions and assist me with running non-routine experiments. Thanks goes especially to Dr. Vladimir Bakhmoutov, for his limitless help with the solid-state NMR, such as helping with a pulse program, or troubleshooting a problem that I couldn't diagnose.

Thank you also to my group members, both past and present. Thanks for listening to my practice talks, as well as helping me explore new directions for my research. I'd especially like to thank Johannes for teaching me about NMR, both solution and solid-state, as well as general experimental techniques. I'd also like to thank my undergraduate student, Jennifer Chavez, for all of her contributions to this research.

I'd like to dedicate this work to all of my family who have been so encouraging and patient for my entire lifetime of schooling, all the way back to pre-school. It's been a long time leading to this moment, and I'm thrilled to share it with you. I would especially like to thank my father for instilling in me a passion for chemistry as a science and an interest in chemistry as a livelihood. I'd also like to thank all of the friends I've made along the way.

You've been a source of comfort and joy throughout my time in graduate school, and I'm eternally grateful.

NOMENCLATURE

δ	chemical shift in ppm
λ	wavelength
^{29}Si	silicon nucleus (NMR)
^{13}C	carbon nucleus (NMR)
^{2}H	deuterium nucleus (NMR)
^{1}H	proton nucleus (NMR)
^{31}P	phosphorus nucleus (NMR)
$\{^{1}H\}$	proton decoupled
$\{^{31}P\}$	phosphorus decoupled
Å	Ångstrom
BET	Brunauer Emmett Teller
br	broad
Bu	butyl
COSY	COrrelation SpectroscopY (2D NMR)
CP	cross-polarization
CP/MAS	cross-polarization/magic angle spinning
CSA	chemical shift anisotropy
Cy	cyclohexyl
d	doublet (NMR), days

D	deuterium (^{2}H) atom
DBCOT	dibenzo[a,e]cyclooctatetraene
DCM	dichloromethane
DD	dipolar dephasing
DMSO	dimethylsulfoxide
D_2O	deuterium oxide
eq	equivalents, equatorial (NMR)
FID	free induction decay (NMR)
FT	Fourier Transformation
GC	gas chromatography
h	hours
HRMAS	high-resolution magic angle spinning
HSQC	heteronucular single quantum coherence spectroscopy (2D NMR)
Hz	Hertz
i	ipso
J	scalar coupling constant
IR	infrared
m	multiplet (NMR), medium (IR)
m	meta
MAS	magic angle spinning

Me	methyl
NCPh	benzonitrile
NMR	nuclear magnetic resonance
NOESY	Nuclear Overhauser Effect SpectroscopY (2D NMR)
o	ortho
p	para
Ph	phenyl
ppm	parts per million
py	pyridine
R	alkyl group
RT	RT
s	singlet (NMR), strong (IR)
sept	septet (NMR)
t	triplet (NMR)
t	tertiary
tert	tertiary
TEM	transmission electron microscopy
THF	tetrahydrofurane
TMEDA	tetramethylethylenediamine
UV	ultraviolet

$\Delta\nu_{1/2}$	signal width at half height
Vis	visible
vs	very strong (IR)
w	weak (IR)

TABLE OF CONTENTS

Page

Page

Page

LIST OF FIGURES

Page

Page

Page

LIST OF SCHEMES

Page

LIST OF TABLES

CHAPTER I

INTRODUCTION

1.1 General Introduction

1.1.1 Immobilized Ligands and Catalysts

Immobilized species are important in such diverse areas as catalysis,[1-15] combinatorial chemistry,[16] solid-phase synthesis,[17] surface modification,[18] chromatography,[19] and molecular motors.[20] Catalysis is the focus of this thesis, and a strategic selection of new linkers has been applied to cleanly immobilize homogeneous catalysts on solid supports. These immobilized catalysts were investigated thoroughly regarding their homo- or heterogeneous nature and their dynamics on the support. An attempt was made to correlate their retention on the support with their solubility. These studies ultimately led to immobilized catalysts with prolonged lifetimes, and they could be recycled many times. Studies on the mobilities of the linker systems and tethered catalysts were additionally performed to enhance the basic understanding, for example, regarding the formation of nanoparticles, and in general of surface phenomena which have an impact on catalysis at the solid/liquid interface.

Immobilized catalysts[1-15] are of immense academic and industrial interest,[11a,21] because they can combine the advantages of homogeneous with those of heterogeneous catalysts. Immobilized catalysts are highly active and selective, while they can be easily separated from the reaction mixtures and reused for example in the next batchwise catalysis cycle. The most favorable support materials are silica and neutral alumina,[18,22-24] and bifunctional monodentate phosphines[23,25-27] such as $Ph_2P(CH_2)_3Si(OEt)_3$, or chelating phosphines[23,28-31] like $Ph_2P(CH_2)_3PPh(CH_2)_3Si(OEt)_3$, are popular linkers. The syntheses of numerous other

mono-, bi-, and tridentate chelate phosphines with ethoxysilane groups have been optimized, and their coordination to metal centers mostly follows the expectation.[23] Furthermore, the immobilization reaction of ethoxysilanes with oxide supports has been studied in detail.[24] Therefore, most linkers have led to very successful immobilized Ni[12,32-34] and Rh[1,3,4,7-10,13-15,35] catalysts for the cyclotrimerization of acetylenes and olefin hydrogenation, respectively.

1.1.2 Support Materials

Oxides as supports provide many advantages as compared to polymers. For example, their pore size in different solvents is constant,[18,22] a parameter that is difficult to control with swellable polymers. This is why for the investigation in this thesis porous oxide supports have been used, so that the mobility and catalysis results are not blurred by any pore size variation depending on the solvents applied. Oxides are furthermore chemically and thermally stable in organic solvents, and their thermal conductivity prevents local overheating effects. From a practical point of view, it is favorable that oxides, especially with large particle diameters, settle quickly after the catalytic reaction, and the supernatant can easily be decanted without filtration or centrifugation. Because of these obvious advantages of oxide supports, the scope of this thesis has been limited to species immobilized on oxide supports such as silica and alumina. Furthermore, only immobilizations on pre-formed and well characterized oxide particles have been performed, since these allow better control of the distance of the metal centers or linkers from one another,[13,14] which is not possible for sol-gel derived support materials.

1.1.3 Challenges of Immobilized Catalysts

Since immobilized catalysts are immensely attractive target materials, and they get increasing attention regarding industrial applications, many groups have tried to improve the recyclabilities and lifetimes of immobilized catalysts.[11,36] However, one of the recurring and still unsolved problems is that immobilized catalysts can form nanoparticles.[37] Therefore, it is often unknown whether the catalytic reaction is propagated by the molecular, immobilized homogeneous catalyst, or by metal clusters or nanoparticles.[38,39] Although the heterogeneous species are not necessarily less catalytically active,[1,4,15] the formed nanoparticles often lead to diminished selectivity of the catalyst. Some progress has been made regarding the analysis of such scenarios,[38,39] but there are only few successful approaches for the selective formation of mono- and bimetallic nanoparticles with well-defined sizes and composition, for example encapsulated in dendrimers,[40] or intercalated in montmorillonite layers.[41] One goal of this thesis was to understand the factors that lead to nanoparticle formation during catalysis with homogeneous and immobilized molecular catalysts, and how to avoid this process.

1.1.4 Solid-State NMR Spectroscopy

For a long time progress has been hampered by the lack of readily available routine techniques for analyzing these amorphous materials.[42] For example, the first classical publications on studying complexes immobilized via linkers with solid-state NMR by Fyfe[43a] remained the only articles of this kind for many years. However, in the meantime, solid-state NMR has evolved as a routine technique[43b-f,44] and other analytical methods for solids are readily available as well.[42] Since both linkers and catalysts immobilized on oxide supports are amorphous materials, for the research performed during this thesis solid-state NMR has

turned out to be the most versatile and powerful analytical method.[1-10,15,21-35] Therefore, improving solid-state NMR techniques has been an endeavour parallel to catalysis. For example, it could be demonstrated that CP (cross polarization) measurements are not efficient for immobilized linkers and catalysts that contain only aryl groups due to the lack of alkyl protons.[9,44] The aryl protons did not readily transfer their magnetization to phosphorus or carbon under routine conditions.[9,44] Therefore, only high-power decoupling without magnetization transfer was applied for most samples, which allowed the efficient measurement of large numbers of solid samples.

The new HRMAS (high resolution magic angle spinning) technique that has been implemented recently for immobilized linkers and catalysts,[1,2,4,5,7-10,23,27,46] has been tested for rigid linkers immobilized on silica. However, the limited mobility of these systems did not allow a narrow solid-state NMR signal to be detected as linkers with flexible alkyl chains do.[1,2,4,5,7-10,23,27,45,46] Based on the results obtained during this thesis it can be concluded that HRMAS NMR can also be used to distinguish between mobile and immobile systems, such as the rigid tetraphenylelement scaffold linkers bound to silica via electrostatic interactions studied here.[47]

1.2 Introduction to Specific Phosphine Linker Systems

1.2.1 Synthesis of New Rigid Linker Systems

The rigid linkers **4-15** and **18** had been obtained previously using the synthesis displayed in Scheme 1.1 with C, Si, and Sn as the center atoms, and substituents with different electronic and steric characteristics have been incorporated in the phosphine groups.[3,6,8,9]

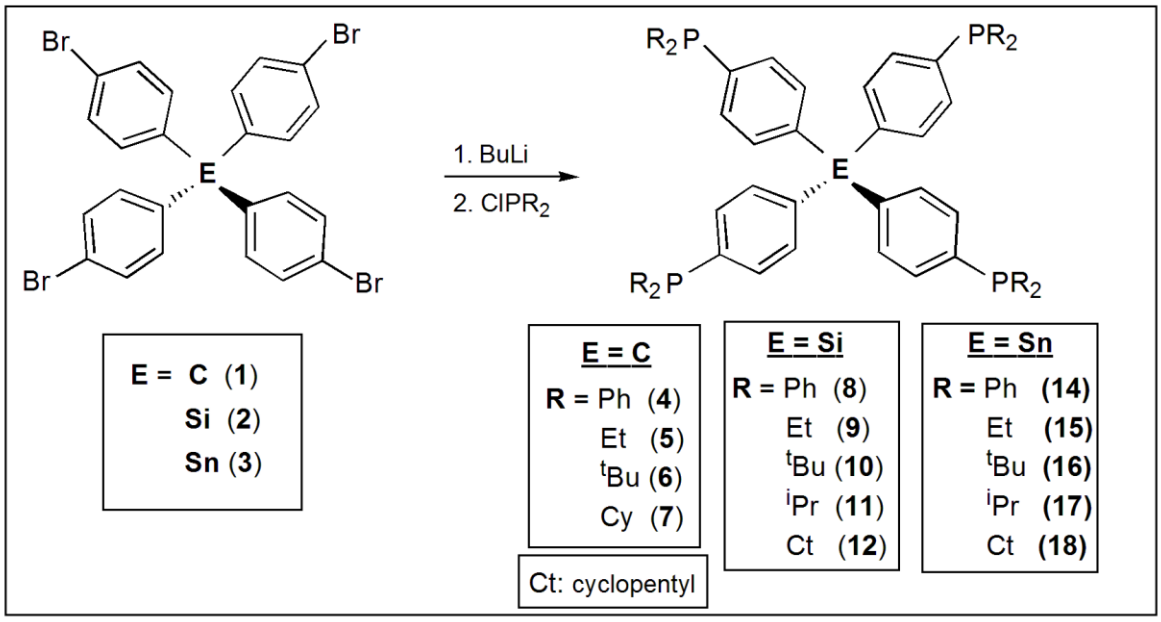

Scheme 1.1 Synthesis of tetraphosphines with tetraphenylelement cores.[3,6,8,9]

In this thesis, the new compounds **16** and **17** with E = Sn and R = ^{t}Bu and ^{i}Pr have additionally been synthesized and fully characterized (Scheme 1.1). In the case of compounds **16** and **17**, it was necessary to use ^{t}BuLi to achieve complete Br/Li exchange of compound **3**, whereas for all other compounds listed, ^{n}BuLi was sufficient. For the tetrabromo compounds **2** and **3** single crystal X-ray structures had already been obtained,[3] whose unit cells perfectly explain the different numbers of signals in the ^{29}Si and ^{119}Sn MAS NMR spectra of polycrystalline **2** and **3**.[3] Similarly interesting is the occurrence of large long-range couplings in the corresponding tetraphosphonium salts.[8] For example, the phosphonium salt Sn([*p*-$C_6H_4PPh_2CD_3$]$^{+}$I^{-})$_4$, derived from treating **14** with CD_3I, shows a quintet with $^{5}J(^{119}\text{Sn-}^{31}\text{P})$ = 19.7 Hz in its ^{119}Sn NMR spectrum, while for the phosphines no coupling is found.[6,9] The general nature of this phenomenon could be confirmed with more independent examples in this work.

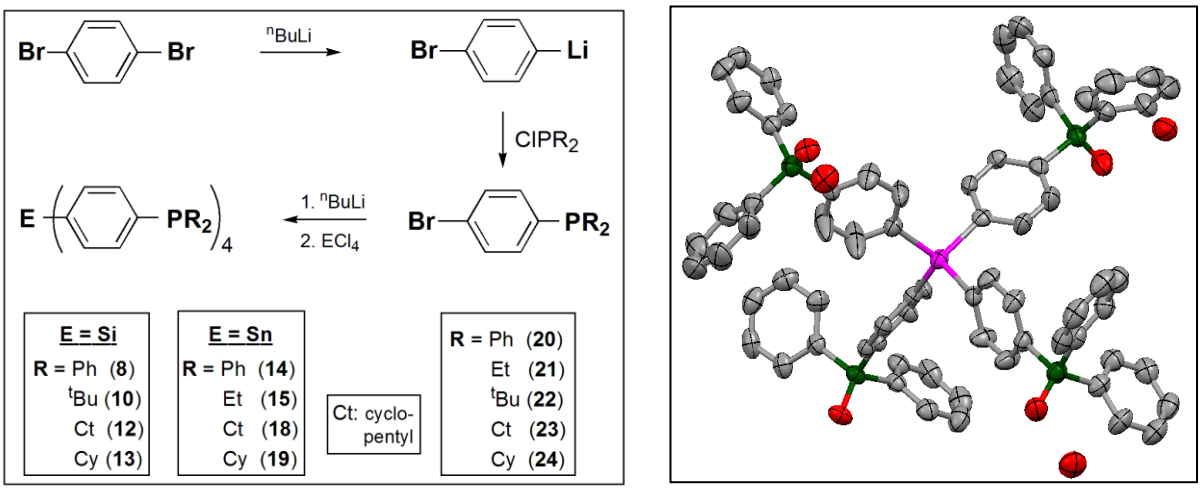

Scheme 1.2 Alternative synthesis route for tetraphosphine ligands (left) and single crystal X-ray structure of the tetroxide Sn(*p*-$C_6H_4P(O)Ph_2)_4$ (right, three included H_2O molecules shown).[7]

Six of the tetraphosphines have been obtained by an alternative synthesis (Scheme 1.2) via the *p*-bromophenyl phosphines **20**-**24**.[6,9] Both synthesis routes led to the clean products in yields of 70 to 80%. For the compounds **13** and **19**, where E = Si or Sn and R = Cy, the syntheses had to be adjusted individually. In contrast to PPh_3 all tetraphosphines, even the triarylphosphines, oxidize in air. An X-ray structure of the tetroxide of **13** had been obtained (Scheme 1.2), which provided an exact intramolecular P···P distance, and also confirmed that phosphine oxides can be hygroscopic.[48]

Since oxidation processes are important when working with air-sensitive phosphines, and for this thesis it is necessary to avoid oxidation products, or at least know how to quickly identify and separate them from the phosphines, a thorough study regarding phosphine oxide synthesis and characterization had been undertaken.[48] Selected important results are, for example, that phosphine oxides and their H_2O_2 and H_2O adducts are distinctly different species.[48a] Besides their unexpectedly large chemical shift differences, the polycrystalline

solids give very different ^{31}P MAS spectra.[48a] While there is only one isotropic line for the phosphine oxides, for example $Ph_3P{=}O$, there are two for its H_2O_2 adduct (Figure 1.1, left), due to the number of magnetically independent P nuclei in the unit cell. For the H_2O_2 adduct of $Cy_3P{=}O$ a single crystal X-ray structure had been obtained (Figure 1.1, right).[48a] It reveals a dimeric structure with two hydrogen-bonded bridging H_2O_2 molecules, and with all oxygen atoms assuming a chair conformation. This thorough study helped to identify and control the phosphines and their oxides during the work on this thesis.

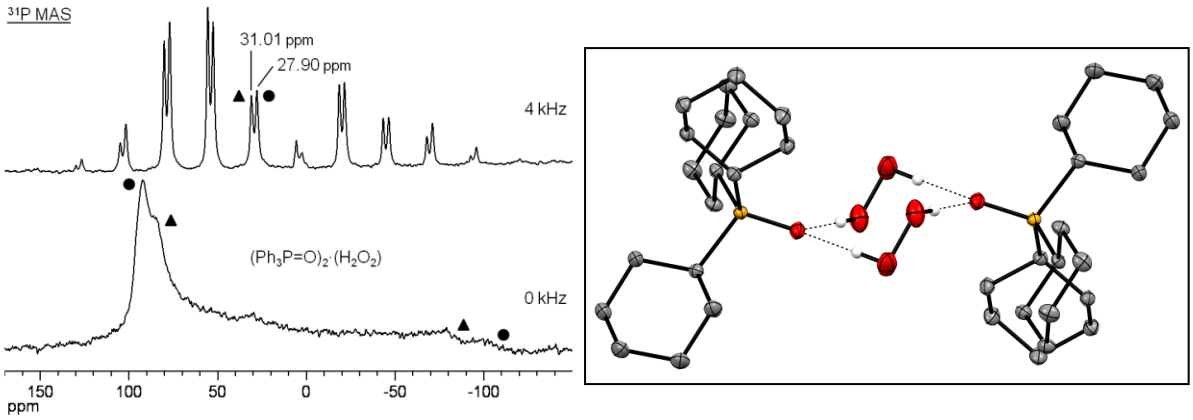

Figure 1.1 ^{31}P MAS (top) and wideline (bottom) spectra of $(Ph_3P{=}O)_2{\cdot}(H_2O_2)$ and single crystal X-ray structure of $[Cy_3P{=}O{\cdot}(H_2O_2)]_2$.[48a]

1.2.2 Immobilization of the New Rigid Linker Systems

It has been confirmed in this thesis that all rigid scaffold linkers can be bound to the support via electrostatic interactions selectively by one, two, or three phosphonium groups.[3,6-8] The mechanism of the phosphonium group formation has been proven,[7-9] and the main result is that the quaternization takes place by the phosphine groups scavenging an ethyl group from one of the residual Si(OEt) groups of the ethoxysilane linker. During the work on

this thesis it has been confirmed that for immobilizing the new tetraphosphine scaffolds **8**, **13**, and **19** on a silica surface via three phosphonium groups, an excess of triethoxysilane is still needed.[3,6-9] The scaffold can in all cases be selectively bound via one phosphonium group by modifying the silica surface with ethoxysilanes in a sub-monolayer surface coverage prior to the reaction with the tetraphosphines.[3]

The strength of binding of the phosphonium groups to the support[8] has been investigated by leaching experiments using different solvents. The tetraphosphine bound to the support via three phosphonium groups can not be detached from the surface, even by treating the silica with hot protic solvents, such as MeOH.[8] When the surface is impregnated with model phosphonium salts like $[Ph_3PMe]^+I^-$, they stay on the support with unpolar (pentane, hexanes, toluene) and with aprotic solvents (ether, DCM, THF), but they can be removed in 50 to 100% amounts when the silica is washed with very polar and protic solvents like acetone, MeOH, MeCN, or DMSO.[8] Obviously, the number of phosphonium binding sites per linker molecule is crucial. The influence of the counteranion (I^-, Br^-, Cl^-, BF_4^-) on the leaching of the model phosphonium salts is negligible.[8] Similarly, using the deuterated versions of the model phosphonium salts, $[(p\text{-}DC_6H_4)_3PMe]^+I^-$ and $[Ph_3PCD_3]^+I^-$, for ^2H MAS and HRMAS studies, fast translational mobility across the surface has been found.[8] In contrast to this, the tetraphosphine bound to the surface via three phosphonium groups is immobile, and the same result has been obtained with tetraphosphonium salts of the tetraphenylelement linkers applied to the silica surface by impregnation.[8] This corroborates the result that the tetraphosphine scaffolds bound to silica via electrostatic interactions are not mobile, based on the NMR behavior towards CP/MAS and high-power decoupling.

The diphosphines **25** to **33** shown in Scheme 1.3 had been synthesized previously and

fully characterized.[9,47] It had been demonstrated earlier that, depending on the reaction conditions, all diphosphines can be attached to a silica surface via one or two phosphonium groups.[9,47] The leaching experiments, as described for the model phosphonium salts above have also been performed for **30** (Scheme 1.3), immobilized via one phosphonium group, and similar results have been obtained.[8] Leaching takes place in polar and protic solvents when the binding occurs only via one phosphonium group. There is no leaching for surface-bound diphosphonium salts, which again speaks for the firm attachment of the tetraphosphine scaffold linkers to silica via three phosphonium groups per linker molecule.[8]

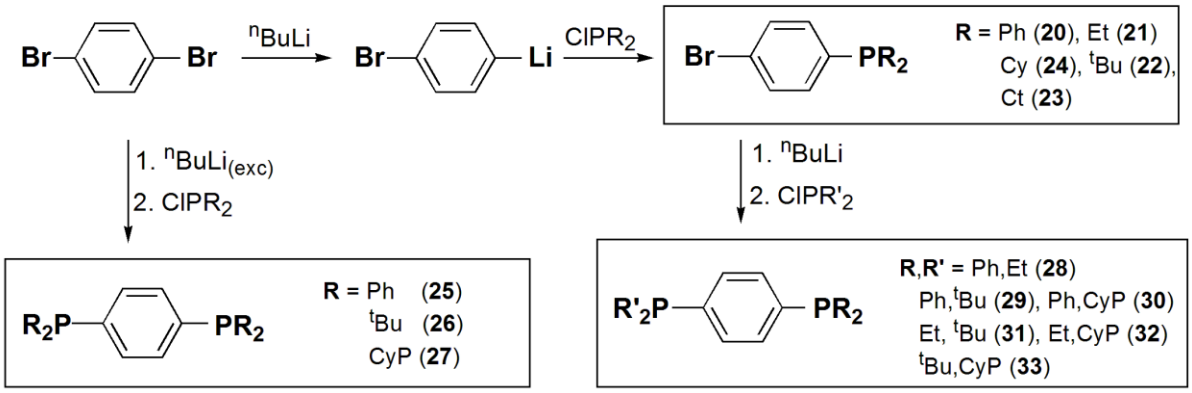

Scheme 1.3 Synthesis of symmetric and unsymmetric diphosphines with phenyl spacers.[9,47]

1.2.3 Immobilized Rhodium Hydrogenation Catalysts

Rh hydrogenation catalysts bound to a rigid diphosphine linker that is attached to the support via one phosphonium group could only be recycled 3 to 4 times.[3] Therefore, diphosphine linkers with phenyl or biphenyl spacers have not been pursued as ligands for immobilized catalysts any further. The poor recyclability might also be due to the translational surface mobility of monophosphonium salts,[8] which allows deactivation of the bound catalysts by dimerization. The possible formation of diphosphonium salts also

indicates, together with ^{2}H MAS results of deuterated versions,[8] that the linkers can "bend down" to the surface and allow decomposition of bound metal complexes at the reactive silica surface. However, the unsymmetric diphosphines **28** to **33** have been successfully used for establishing a basicity scale of phosphine groups using quasi an intramolecular standard. It has been demonstrated by ^{31}P MAS that under mild reaction conditions it is always the more basic of the two phosphine groups that is quaternized on the silica surface in the presence of ethoxysilanes, while the steric hindrance of bulky substituents such as ^{t}Bu or Cy plays a subordinate role.[9]

The most successful immobilized catalyst obtained so far is a Wilkinson-type Rh catalyst immobilized by the linker scaffold shown in Figure 1.2.[3] This olefin hydrogenation catalyst can be recycled for a record 30 times in a batchwise manner. In this thesis it could be demonstrated that the Sn in the core of the linker did not influence the catalytic activity. When Si was used in the center of the scaffold linker, the analogous Rh catalyst could also be recycled 30 times. Therefore, this success must be due to the large footprint of the linker scaffolds that does not allow any contact of the metal centers and subsequent deactivation by dimerization (Figure 1.2). Furthermore, the scaffold sterically prevents any interaction with the reactive silica surface. Most noteworthy with respect to future work is that Rh nanoparticles have been found on the spent catalyst. For comparison, catalytic runs using flexible chelate phosphines have been limited to 13 cycles.[13,14] Only very long alkyl chains matched the characteristics of a Rh catalyst immobilized by the rigid scaffolds with 30 successful repeats of catalytic runs.[1] This indicates that, in the case of linkers with alkyl chains of moderate lengths, the catalyst can get deactivated by contact with the surface. However, as compared to fully flexible chelate linkers, this scaffold is still superior, taking

into account that here the metal center is only bound by a monodentate phosphine.

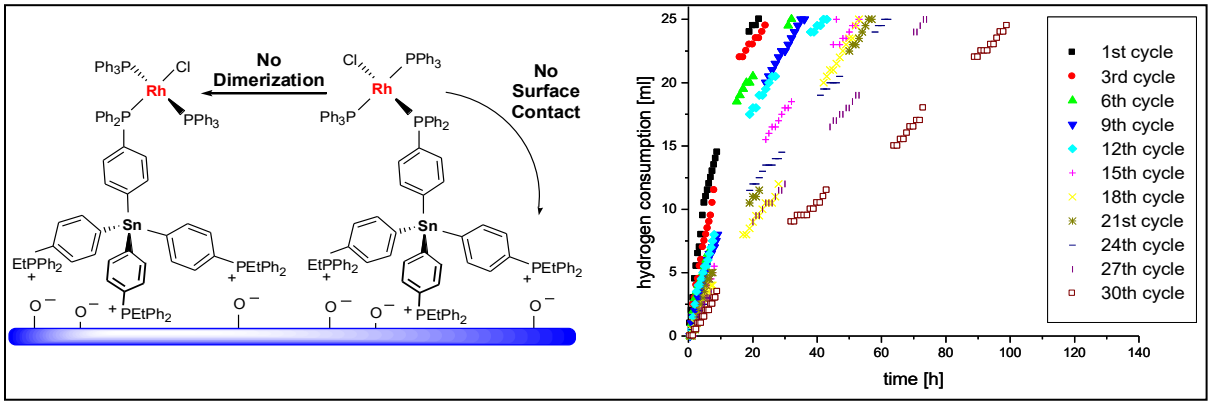

Figure 1.2 Structure and recycling characteristics of an immobilized Rh catalyst for the hydrogenation of dodecene.[3]

Most important for the work presented here was that the formation of nanoparticles during catalysis with immobilized metal complexes depends on the linker. Rh nanoparticles always formed when linkers with flexible alkyl chains were used for the hydrogenation of dodecene.[1,4] Hereby, the lengths of the alkyl chains (C_1 to C_{11}) did not play a crucial role.[1,4] The heterogeneous nature of the catalyst has been determined by poisoning-, split-, and three-phase tests.[1,4] Heterogeneous Rh catalysts also shift double bonds within olefins, in contrast to molecular Rh catalysts, such as $ClRh(PPh_3)_3$.[1] The time frame for the nanoparticle formation had been determined to be about 5 h from the start of the reaction by checking the double bond migration in dodecene. The nanoparticle size, as determined by TEM, was dictated by the pore diameter of the support.[1] Interestingly, the Rh nanoparticles were highly active catalysts, they could be recycled 30 times in a batchwise manner,[1] and they were not air-sensitive.[4] Leaching was not detected by AAS, because the nanoparticles were stuck within the pores of the silica. One goal of this thesis was to investigate whether nanoparticles

would also be formed when Wilkinson-type Rh catalysts were immobilized via the rigid scaffold linkers.

CHAPTER II

SYNTHESIS AND CHARACTERIZATION OF NEW TETRAPHOSPHINE SCAFFOLDS INCORPORATING TETRAPHENYLELEMENT CORES

2.1 Introduction

As described in the general introduction of the previous chapter, linker molecules are important for tethering homogeneous metal complexes to oxide surfaces. The traditional linkers consist of an ethoxysilane group that connects with the surface and a phosphine moiety for coordinating a metal complex. Ethoxysilane groups form covalent bonds, for example, with silica surfaces, via siloxane group formation. Phosphines are favorable because of their coordinating power and inertness against reactive oxide surfaces.[25,26] Flexible alkyl chains bridging the ethoxysilane with the phosphine groups, however, are not favorable in every case, as outlined in the previous chapter. Therefore, new rigid tetraphosphine scaffolds incorporating tetraphenylelement cores are targeted. The binding to the surface is performed via electrostatic interactions after phosphonium formation of three of the originally four phosphine groups. In this way, one phosphine group remains on top of the rigid scaffold for coordinating to a metal center. The rigid nature of the scaffold linkers prevents dimerization of the metal complexes on the surface and interactions with the reactive surface. Therefore, catalysts with longer lifetimes and improved recyclability are expected when using the scaffold linkers. In this chapter the synthesis and characterization of two new scaffolds incorporating a Si center and derivatives thereof will be described.

2.2 Results and Discussion

2.2.1 Synthesis

As demonstrated previously, tetraphenylelement scaffolds are readily synthesized in good yields,[3,9,47] and they can be obtained via different synthetic routes. This is important because certain synthetic pathways may not be possible or may be very problematic, and it is beneficial to have alternative routes available if indicated.

One advantage of the route 1 synthesis (Scheme 2.1) is that different elements can be placed at the core. The two main elements used for the cores are silicon and tin, and the differences between them will be an area of study throughout this chapter and thesis.

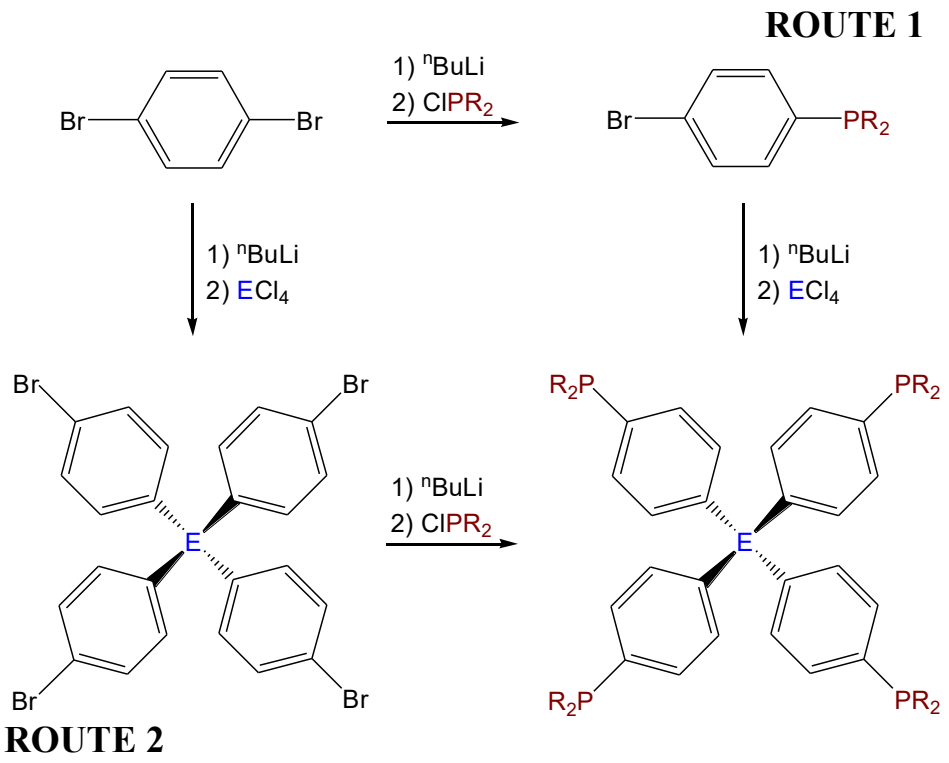

Scheme 2.1 General synthesis outline for generating tetraphosphine scaffolds via two different routes. E = Si, Sn; R = alkyl, aryl.

These scaffolds also allow one to selectively modify the substituents at phosphorus in the *para* position. The advantage of this is that each scaffold can be fine-tuned to the application it is needed for. One area of study in this chapter is how the scaffold can be modified to meet the needs of the corresponding application.

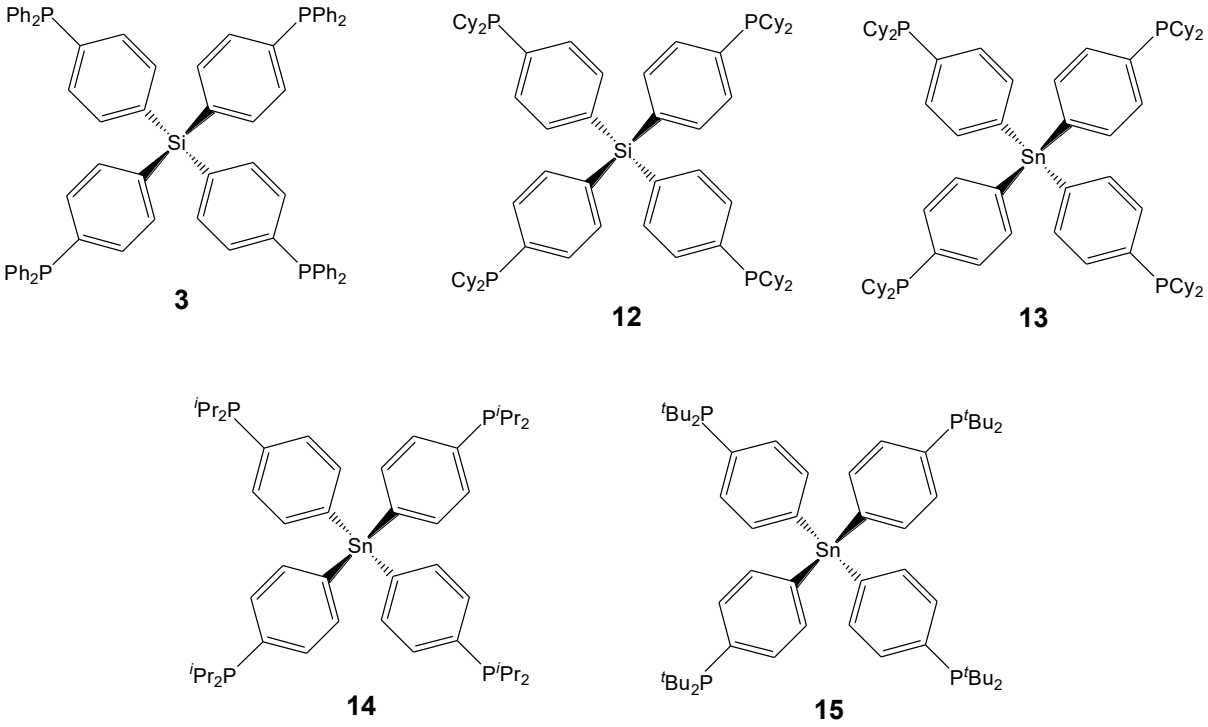

Scheme 2.2 The tetraphosphine scaffolds synthesized in this project.

The scaffolds synthesized for this project are compounds **3**, **12**, **13**, **14**, and **15** (Scheme 2.2). For all of these compounds, the synthesis of the tetraphosphine could be achieved using either one of the two routes outlined in Scheme 2.1.

Route 1 involves attaching the phosphine first, then forming a tetraaryl system in the second step. The main advantage to this route is that certain compounds can only be made using this route, as Sn-C bonds are cleaved easily when using an excess of ^{n}BuLi. Therefore,

route 1 is sometimes necessary to synthesize a desired tetraphosphine. Another advantage is that this method usually requires no excess of ^{n}BuLi, which means there is no phosphine side product to be removed, which can prove troublesome in some cases. Also, the reactions performed using this route usually have slightly higher yields, although not all syntheses have been studied using both routes.

Route 2 creates a tetraarylbromide in the first step, followed by tetraphosphine formation in the second step. The largest benefit to this route is that the intermediate tetrabromide is not oxygen sensitive, and can thus be handled in the open atmosphere, and therefore this method facilitates large scale reactions.

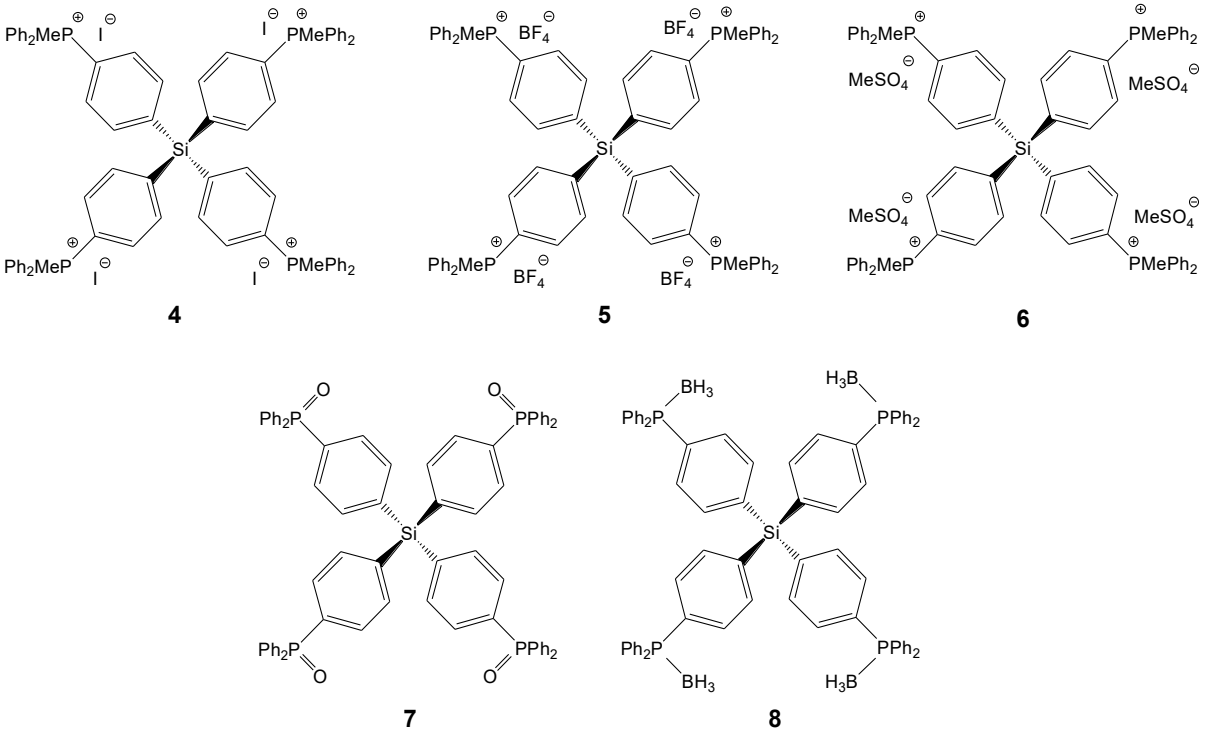

Scheme 2.3 Synthesized derivatives of compound **3** presented in this chapter.

2.2.2 Derivatives of Compound 3

Starting from compound **3**, it was possible to synthesize the new derivatives **4**, **5**, **6**, **7**, and **8** (Scheme 2.3). This was partly done in an attempt to obtain a single crystal suitable to determine crystallographic data of any of these molecules, but this undertaking proved elusive despite numerous attempts. However, the derivatives could be fully characterized, and several interesting features were detected.

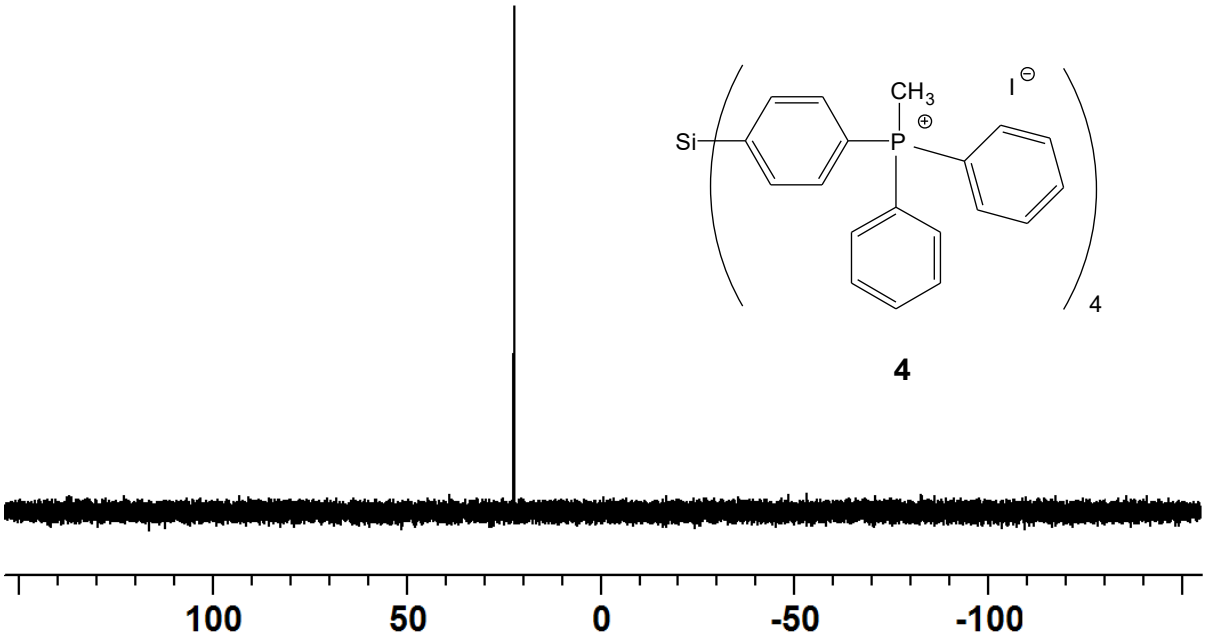

Figure 2.1 ^{31}P NMR spectrum of compound **4** in DMSO-d_6.

Two phosphonium salts have been synthesized for studies of their surface mobility and leaching as detailed in the following chapter. An excess of methyl iodide is added to quaternize tetraphosphine **3** to form the tetraphosphonium salt **4** (Scheme 2.3). For the second, anion exchange is performed on **4** using $AgBF_4$ to form **5**. The yields for each

reaction product are very high at about 99%. Obviously, the NMR data of these two compounds are similar, given that they only differ in the counteranion. The ^{1}H and ^{13}C NMR spectra are consistent with expected values for analogous monophosphonium salts.[26] The ^{31}P NMR signal shows a significant downfield shift relative to **3** to δ = 22.46 for **4** and δ = 22.52 for **5**, consistent with the chemical shift of the monophosphine analog $[Ph_3PMe]^+Cl^-$, which is δ = 18.9.[26]

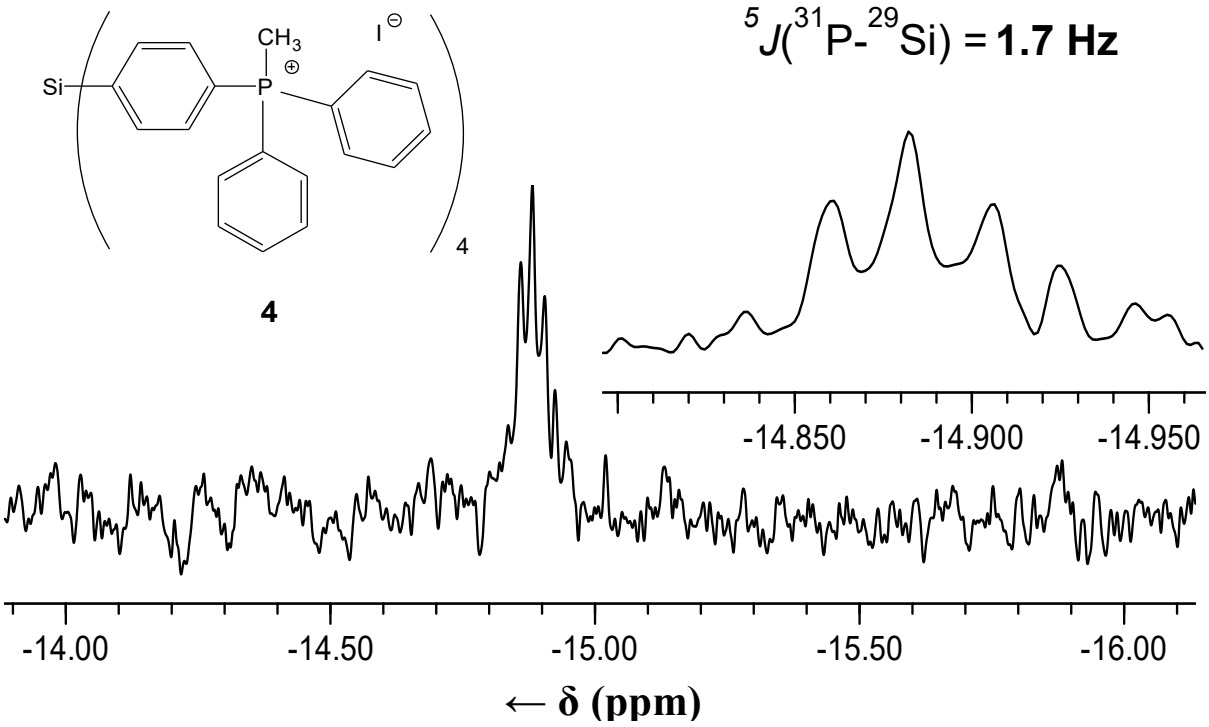

Figure 2.2 ^{29}Si NMR spectrum of compound **4** in DMSO-d_6.

One of the more remarkable properties of compound **4** is found in the ^{29}Si NMR spectrum. A long range phosphorus-silicon spin-spin coupling $^{5}J(^{31}P\text{-}^{29}Si)$ = 1.7 Hz is observed. This coupling spans five bonds, and it is the largest $^{31}P\text{-}^{29}Si$ indirect coupling value reported so far. This long range coupling may be assisted by the molecule offering two

coupling pathways through the electron rich phenyl rings, and the rigid nature of the backbone.

The last tetraphosphonium salt created is synthesized by the reaction of tetraphosphine **3** with dimethylsulfate, forming phosphonium salt **6**. According to expectation, the NMR data very closely match those of compounds **4** and **5**.

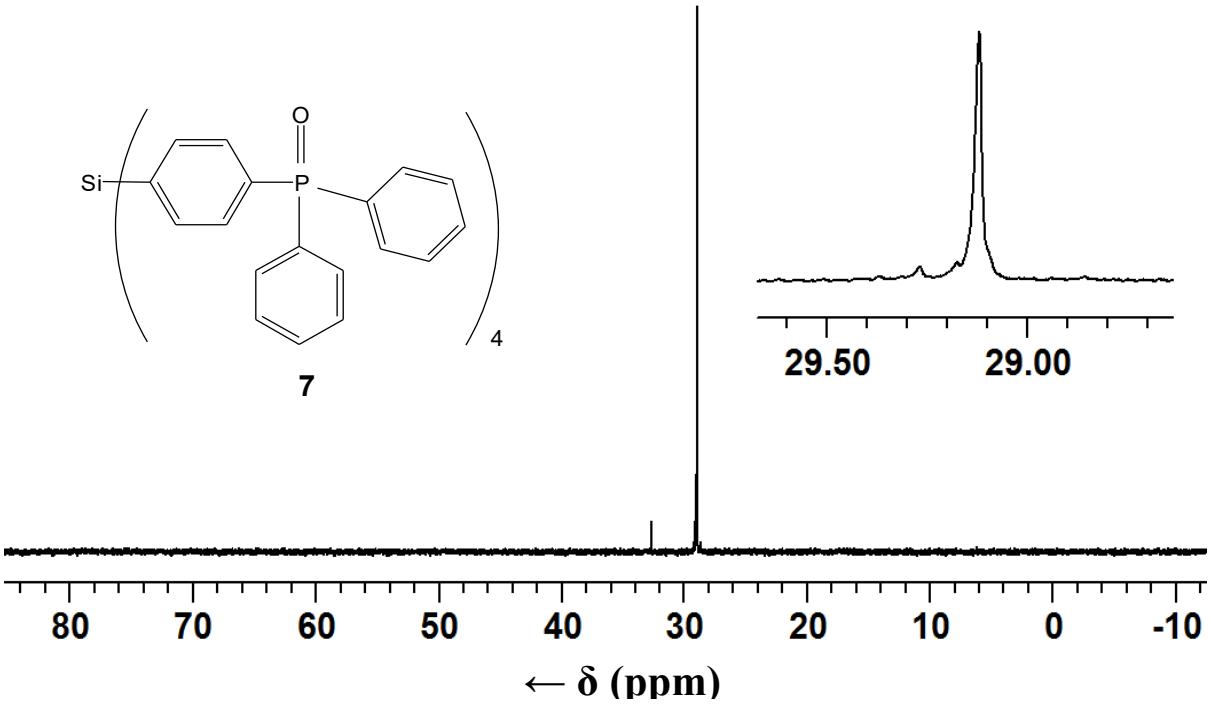

Figure 2.3 ^{31}P NMR spectrum of compound **7** in $CDCl_3$.

Furthermore, the tetraphosphine tetroxide **7** was synthesized (Scheme 2.3) for later use in phosphine oxide adsorption studies.[48c] Compound **7** is obtained from **3** using a biphasic solution of methylene chloride and aqueous hydrogen peroxide. Upon removal of the aqueous layer, molecular sieves are added to the organic layer. This procedure for destroying the hydrogen peroxide adduct that forms when hydrogen peroxide is used and

removing the residual hydrogen-bonded water follows a procedure pioneered by Hilliard.[48a] The product **7** is obtained as a white powder with a yield of 94.5%. IR analysis (Figure 2.4) shows that the P=O stretching band has a wavenumber of 1192 cm^{-1}, which is close to the literature value of triphenylphosphine oxide in the absence of the hydrogen peroxide adduct.[48a] The absence of an OH stretching band proves that the product is water free. The ^{1}H, ^{13}C, and ^{31}P NMR spectra all have similar signal assignments compared to the values for triphenylphosphine oxide found in the literature.[48a]

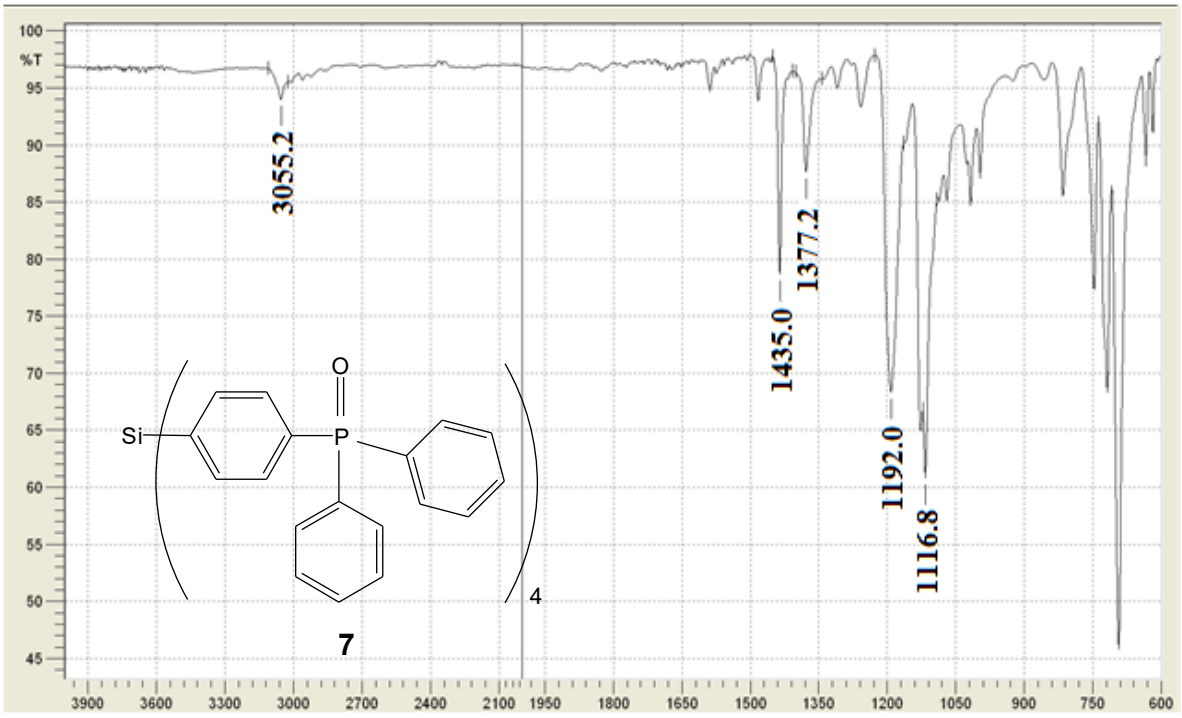

Figure 2.4 IR spectrum of compound **7**.

The borane adduct **8** was formed as an air-stable species that facilitates chromatographic purification of **3** by addition of a stoichiometric amount of $H_3B{\cdot}THF$ to **3** in

toluene. The yield was very high at 96% and the compound only decomposes above 320 °C. Additionally, **8** proved to be curiously insoluble, as only $CHCl_3$ was able to dissolve the compound, and only as much as 2.1 mg/mL. Fortunately, this was sufficient for NMR spectroscopic characterization. The ^{1}H and ^{13}C NMR spectra show the expected signals. Regarding the ^{31}P NMR spectrum (Figure 2.5), it is apparent that the borane is greatly increasing the halfwidth of the signal to $\nu_{1/2}$ = 44 Hz. This is expected, as boron is a quadrupolar nucleus (I = 3/2), which causes the ^{31}P nucleus to undergo relaxation much more rapidly. The shift of δ = 20.92 is similar to that of the analogous monophosphine borane adduct $Ph_3P{\cdot}BH_3$ found in the literature.[51]

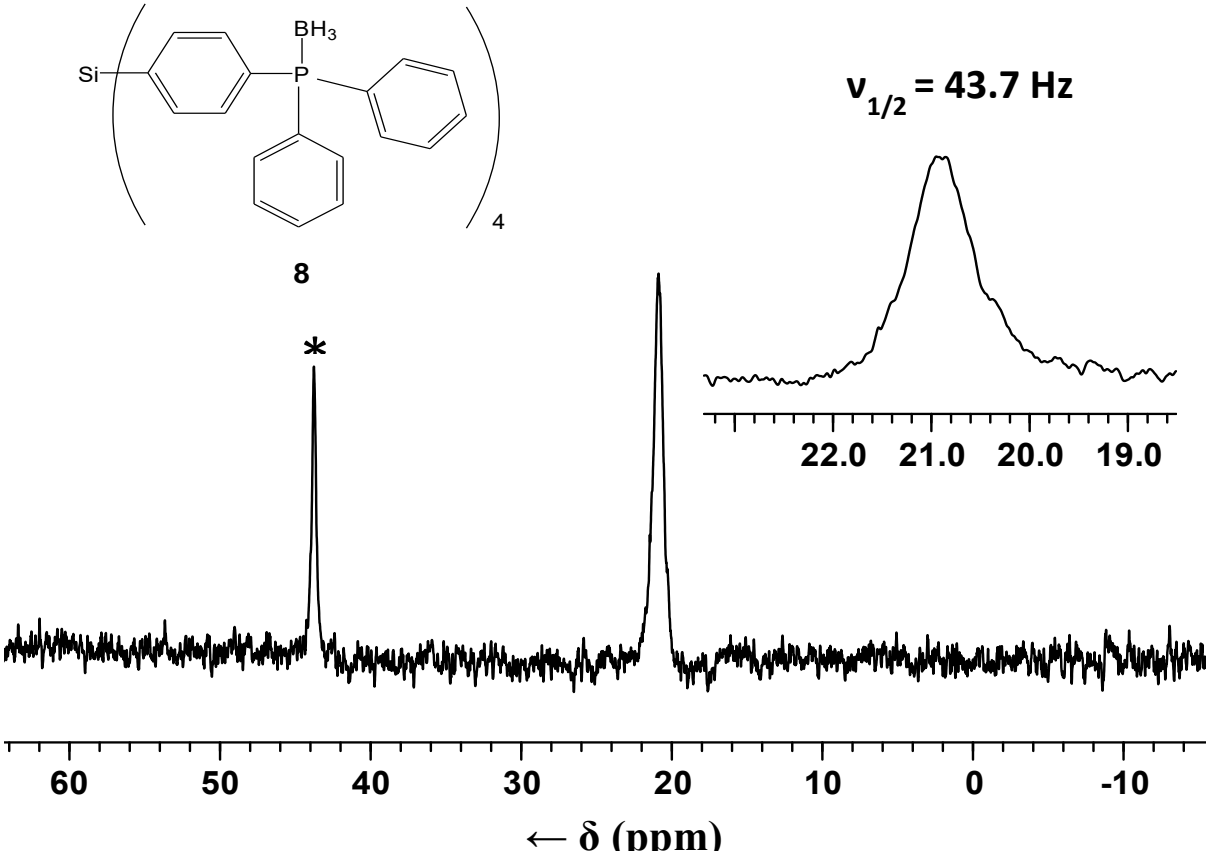

Figure 2.5 ^{31}P NMR spectrum of compound **8** in $CDCl_3$. The asterisk denotes an impurity ($Ph_2P(O)Cl$) in the capillary standard (Ph_2PCl).

2.2.3 Tetraphenylelement Compounds with Alternate Substituents

Compound **3** was the first tetraphosphine that has been described in the group.[47] However, it is possible to modify the phosphines while keeping the tetraphenylsilane core to create tetraphosphines with different substituents at phosphorus. Previously, several such phosphines have been synthesized,[3,6,7-9,47] but the derivative featuring a dicyclohexylphosphine on each phenyl ring, **12**, had been elusive. Attempts to synthesize this compound using route 2 (Scheme 2.1) presented the problem of separating the product from the byproduct $BuCy_2P$. Therefore, it is preferable to use route 1 to synthesize compound **12**.

Compound **11**, as the intermediate in this process, is synthesized in the first step. This is accomplished by adding ^{n}BuLi to *p*-dibromobenzene prior to quenching with Cy_2PCl. The product represents a clear colorless oil with a yield of 94%.[9] Subsequently, the intermediate **11** is subjected to a Br/Li exchange again, before the addition of $SiCl_4$ forms compound **12**. This compound is a sticky, white solid with a relatively low yield of 13.9% for the second step after purification.

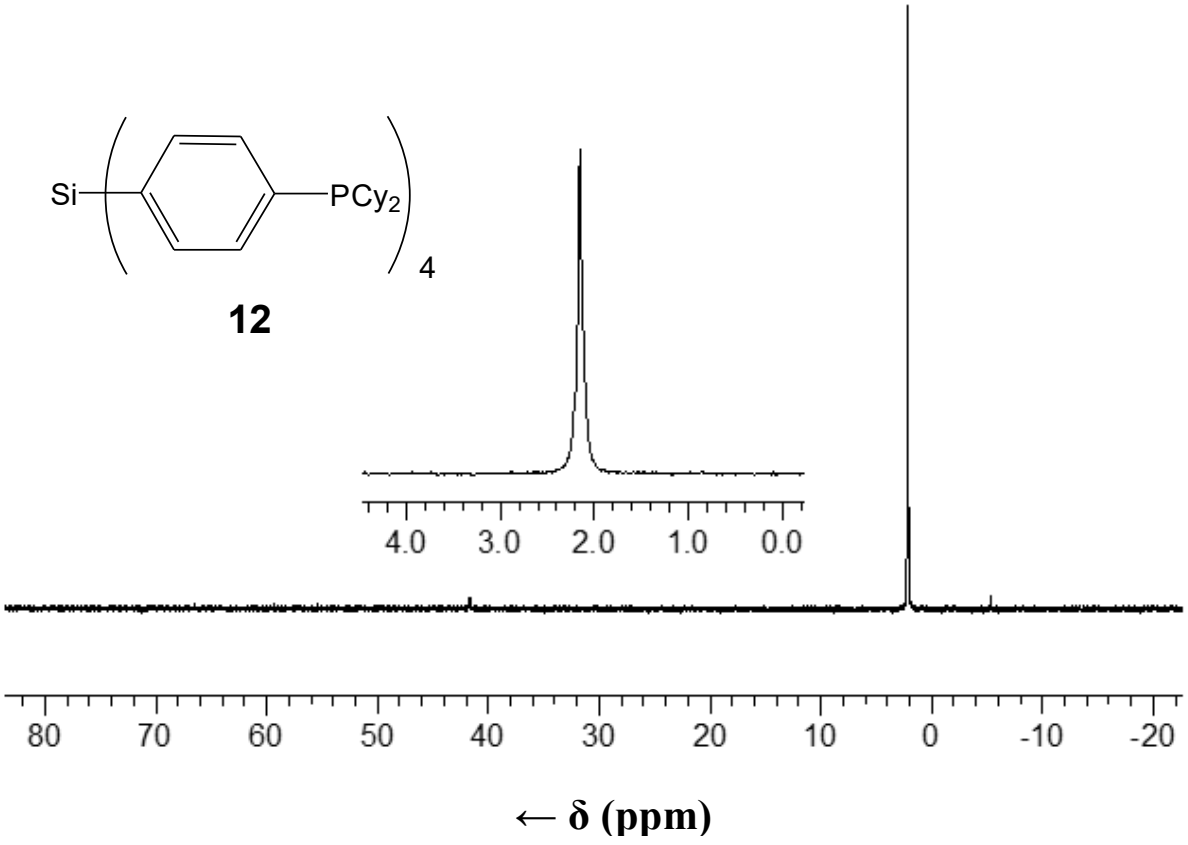

Figure 2.6 ^{31}P NMR spectrum of compound **12** in C_6D_6.

For this compound, the ^{31}P NMR chemical shift matches the literature value of the analogous phosphine $PhPCy_2$ (Figure 2.6),[52] but an interesting phenomenon occurs in the ^{13}C NMR spectrum. The aryl region displays four carbon signals as expected, however, in the aliphatic region, six signals are observed (Figure 2.7). The reason is that the carbon pairs 6/10 and 7/9 are diastereotopic because carbon 5 is a prochiral center (Figure 2.7). This can be demonstrated in a Gedanken experiment by replacing one of the carbon atoms within a pair by ^{13}C. This renders both, carbon atom 5 and phosphorus, a stereocenter. Therefore, carbons 6 and 10, as well as carbons 7 and 9, each result in different ^{13}C NMR signals. Additional proof for this feature comes from the literature.[52] Schraml and coworkers applied

an INADEQUATE pulse sequence to observe the $^{1}J(^{13}C\text{-}^{13}C)$ couplings, and could demonstrate that all six different carbon nuclei reside within the same ring.[52] Therefore, the appearance of the six carbon signals in the aliphatic region of the ^{13}C NMR spectrum is not due to the presence of two cyclohexyl rings.

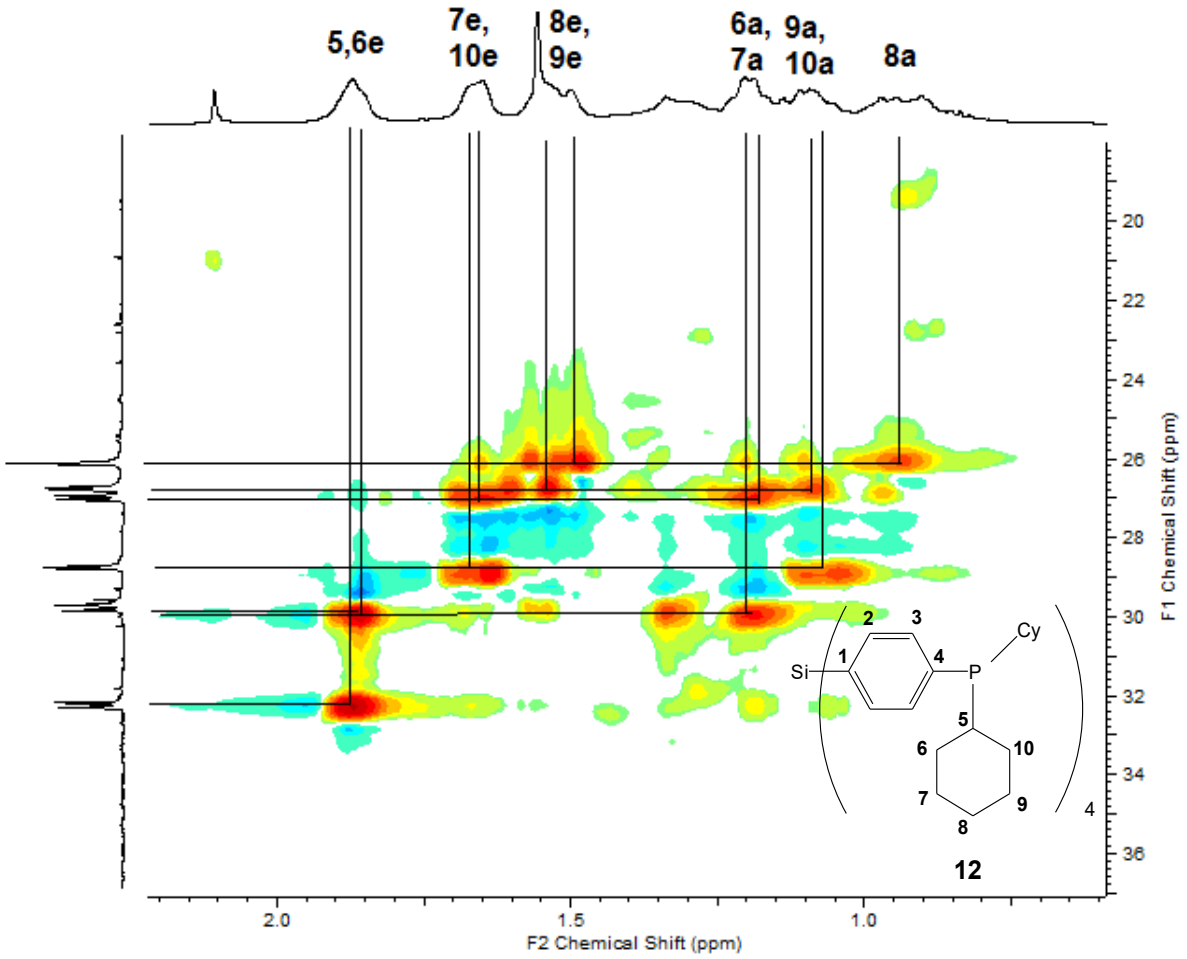

Figure 2.7 Expansion of the aliphatic region of the $^{13}C\text{-}^{1}H$ HSQC spectrum of compound **12** in C_6D_6.

Knowing this feature, one can follow through with the ^{1}H and ^{13}C NMR signal assignments using the two-dimensional $^{1}H\text{-}^{1}H$ and $^{13}C\text{-}^{1}H$ COSY NMR spectra (Figures 2.7

and 2.8). The $^{1/2/3}J(^{31}P\text{-}^{13}C)$ values in the ^{13}C NMR spectra provide additional information for the signal assignments. As usual for cyclic aliphatic rings, axial (a) and equatorial (e) protons of the methylene groups have different chemical shifts.

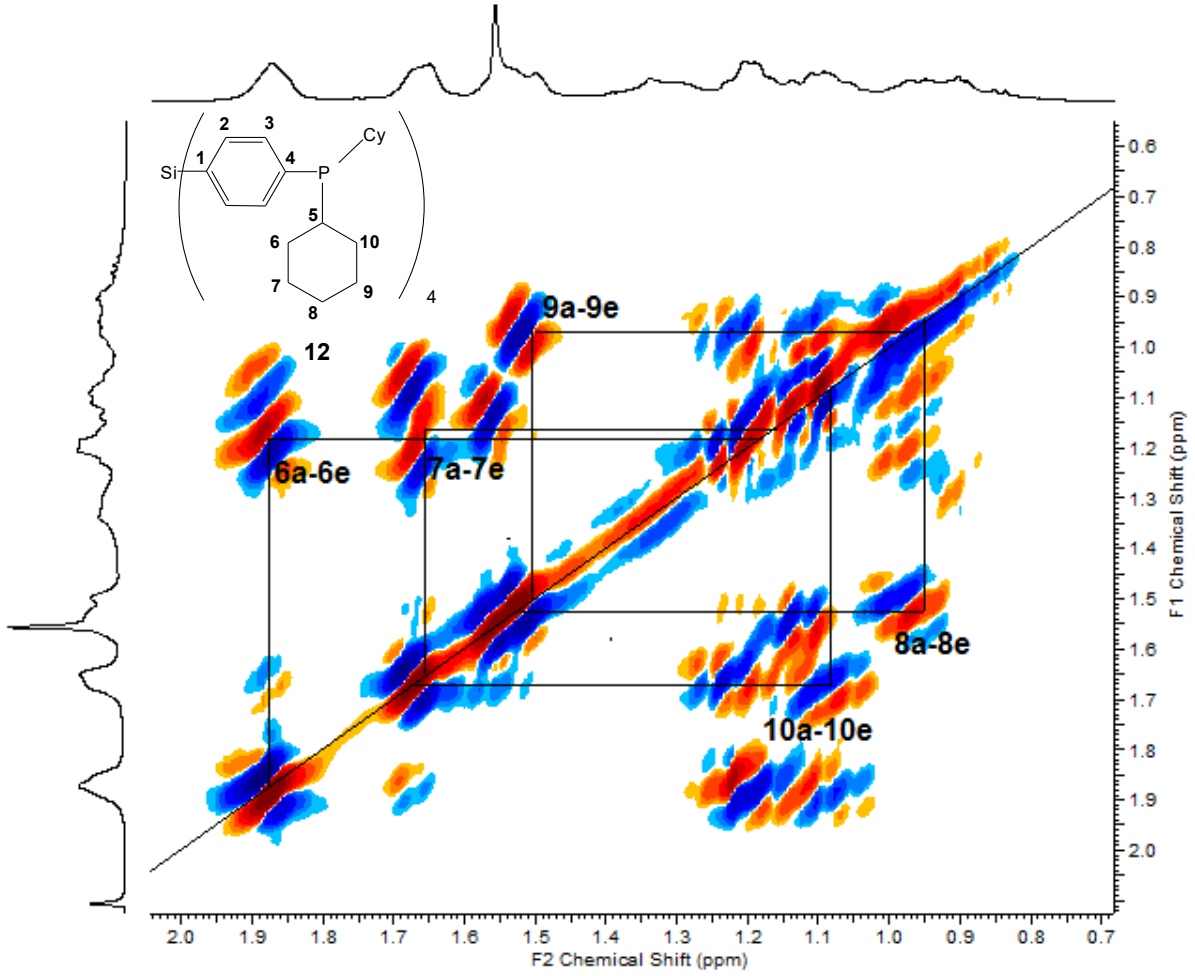

Figure 2.8 Expansion of the aliphatic region of the $^{1}H\text{-}^{1}H$ COSY spectrum of compound **12** in C_6D_6.

Compound **12** is synthesized to incorporate a Si atom in the center. By altering the synthesis accordingly, a scaffold molecule with a Sn core, compound **13**, can be obtained

(Figure 2.9). Other than using $SnCl_4$ instead of $SiCl_4$ the synthesis works exactly the same way (Scheme 2.1, route 1), and the ^{1}H, ^{13}C, and ^{31}P NMR data are almost identical.

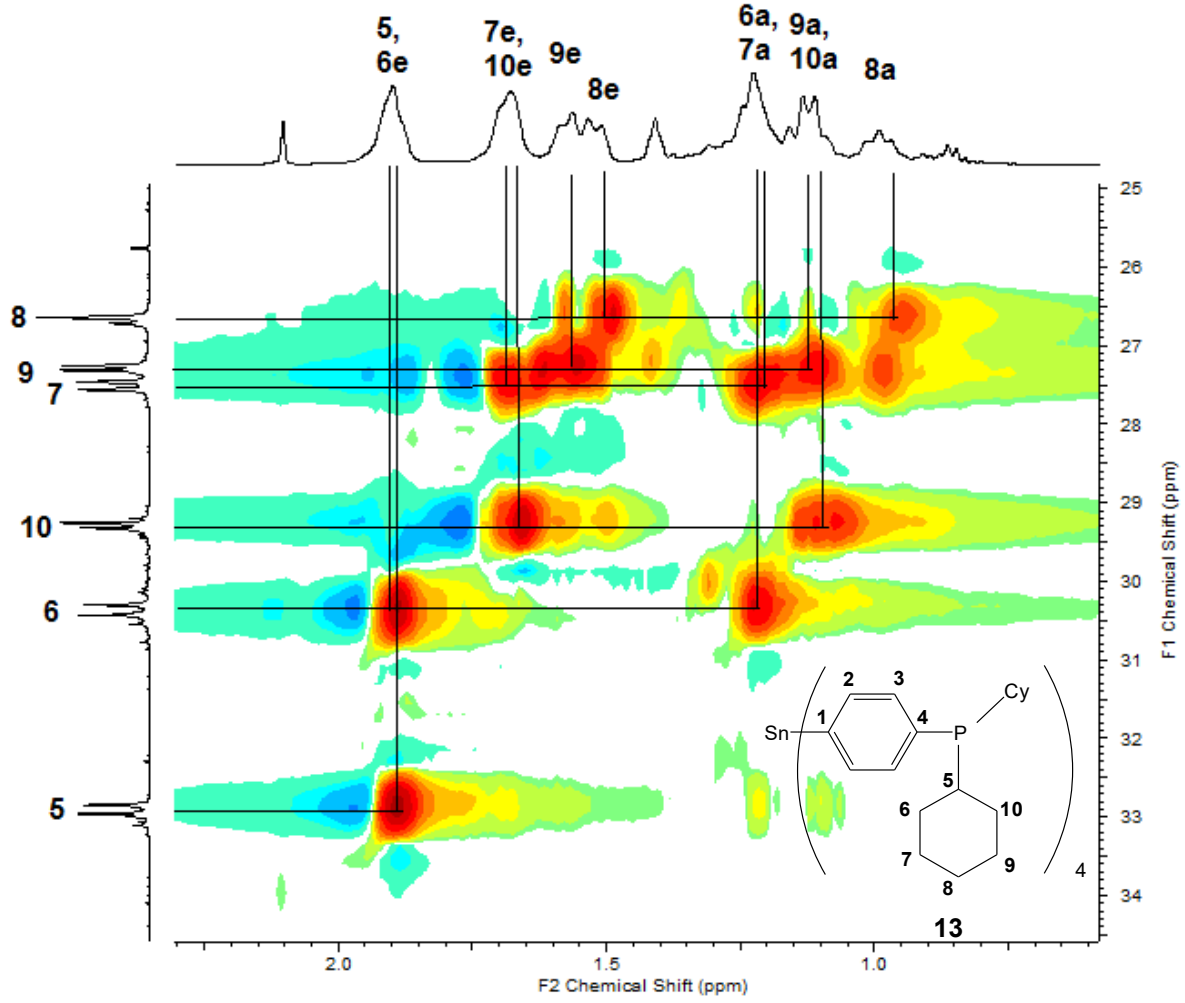

Figure 2.9 Expansion of the aliphatic region of the ^{13}C-^{1}H HSQC spectrum of compound **13** in C_6D_6.

Other important tetraphosphines with a Sn core had been elusive previously, namely compounds **14** and **15**. When attempting their synthesis via route 1, a complication develops because $ClP^{i}Pr_2$ and $ClP^{t}Bu_2$ do not readily form the monobromo intermediates from the monolithiated precursor. Even using MeLi or a mixture of ^{n}BuLi and TMEDA could not make this reaction proceed. This is problematic, because research in the group has shown that

^{n}BuLi cannot be used with the tetrabromo compound **2** directly, as it cleaves the Sn-C bonds. Thus, a new synthetic route is needed for compounds **14** and **15**, and eventually the tetradeutero compound Sn(*p*-$C_6H_4D)_4$ (**16**).

The suspicion is that ^{n}BuLi is sterically unencumbered enough that the nucleophilic butyl group can attack the core of the tetraarylstannane. To avoid this problem, the sterically bulky ^{t}BuLi is used to tetralithiate compound **2** without cleaving the Sn-C bonds. Then the chlorophosphines or D_2O can be added to form the desired products.

This change proved effective for synthesizing compounds **14** and **15**. Compound **14** has been purified by hexane extraction. The product is obtained in a yield of 64% as a white powder. ^{1}H and ^{31}P NMR spectra in C_6D_6 can be recorded, and the data obtained are similar to the literature values of the analogous compound PhP^{i}Pr$_2$.[53] The ^{13}C NMR data are also consistent with this compound.[53] Figure 2.10 displays the ^{31}P NMR spectrum of **14** as a representative example for the compounds in this category.

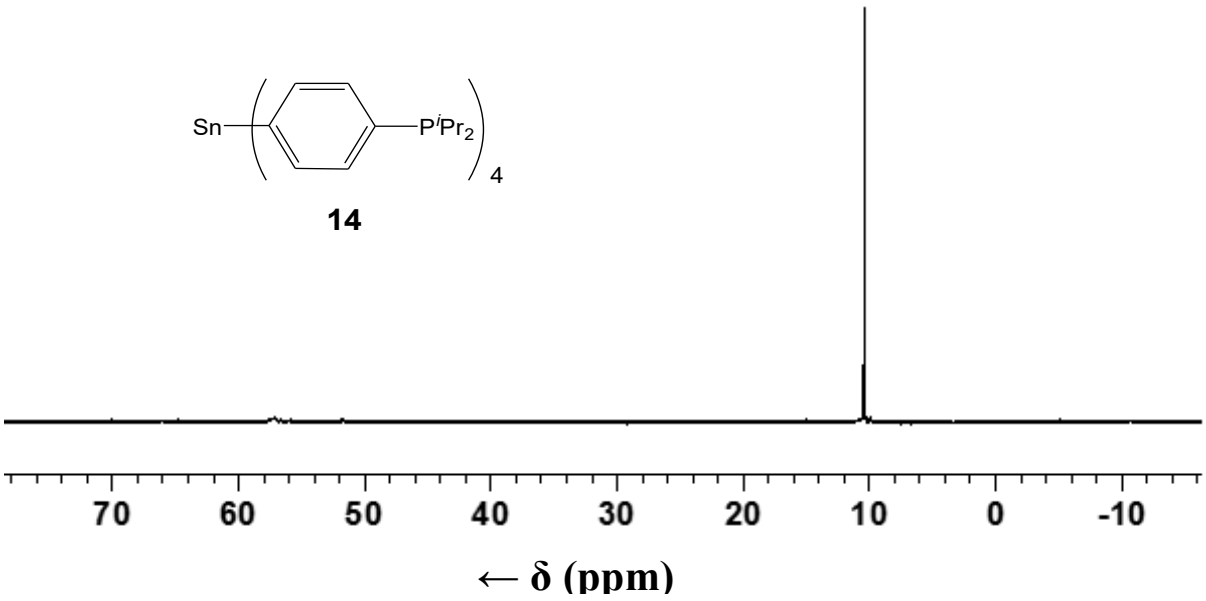

Figure 2.10 ^{31}P NMR spectrum of compound **14** in C_6D_6.

Compound **15** is made using ClP^tBu_2, but otherwise the synthesis works in the same way, and the NMR data are consistent with the expected values based on the comparative monophosphine PhP^tBu_2.[54]

The last tetraarylelement scaffold synthesized, **16**, is not a phosphine, but the tetradeuterated version of $SnPh_4$. This compound was desired for later use in surface adsorption studies, allowing ^2H NMR to investigate surface mobilities of adsorbed molecules.[48c] Using the knowledge that compound **2** can be lithiated with ^{t}BuLi, it is now possible to add any Lewis acid to form a new compound. This includes D_2O, and the deuterium should bond to the aryl ring, and leave lithium hydroxide as

Figure 2.11 ^{31}P NMR of compound **15** in C_6D_6.

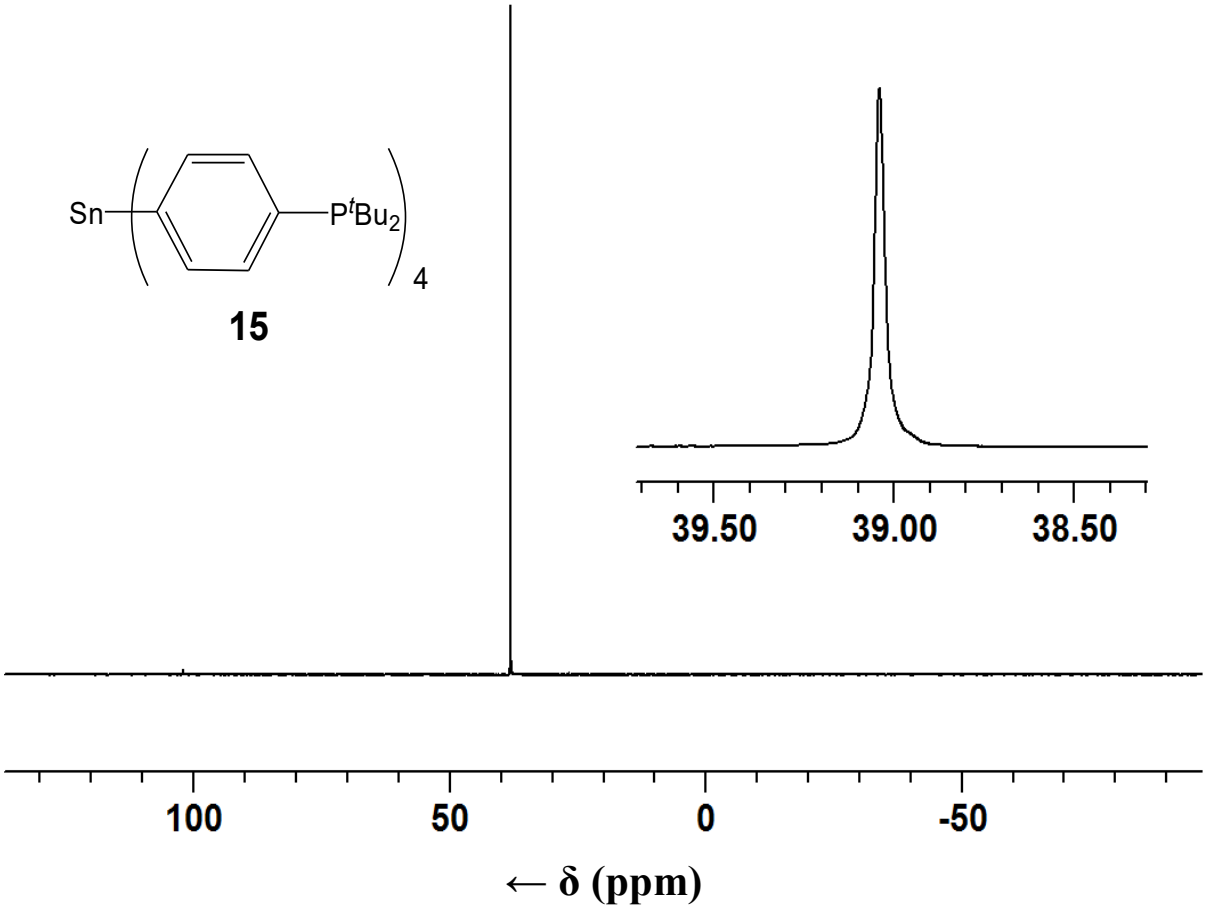

Figure 2.11. 31P NMR spectrum of compound 15 in C_6D_6.

a byproduct. This actually occurs, and the resulting product is compound **16** (Figure 2.12). Although Sn satellites for the two non-quaternary carbons are seen, the signal for the carbon bound directly to the deuteron is not detected.

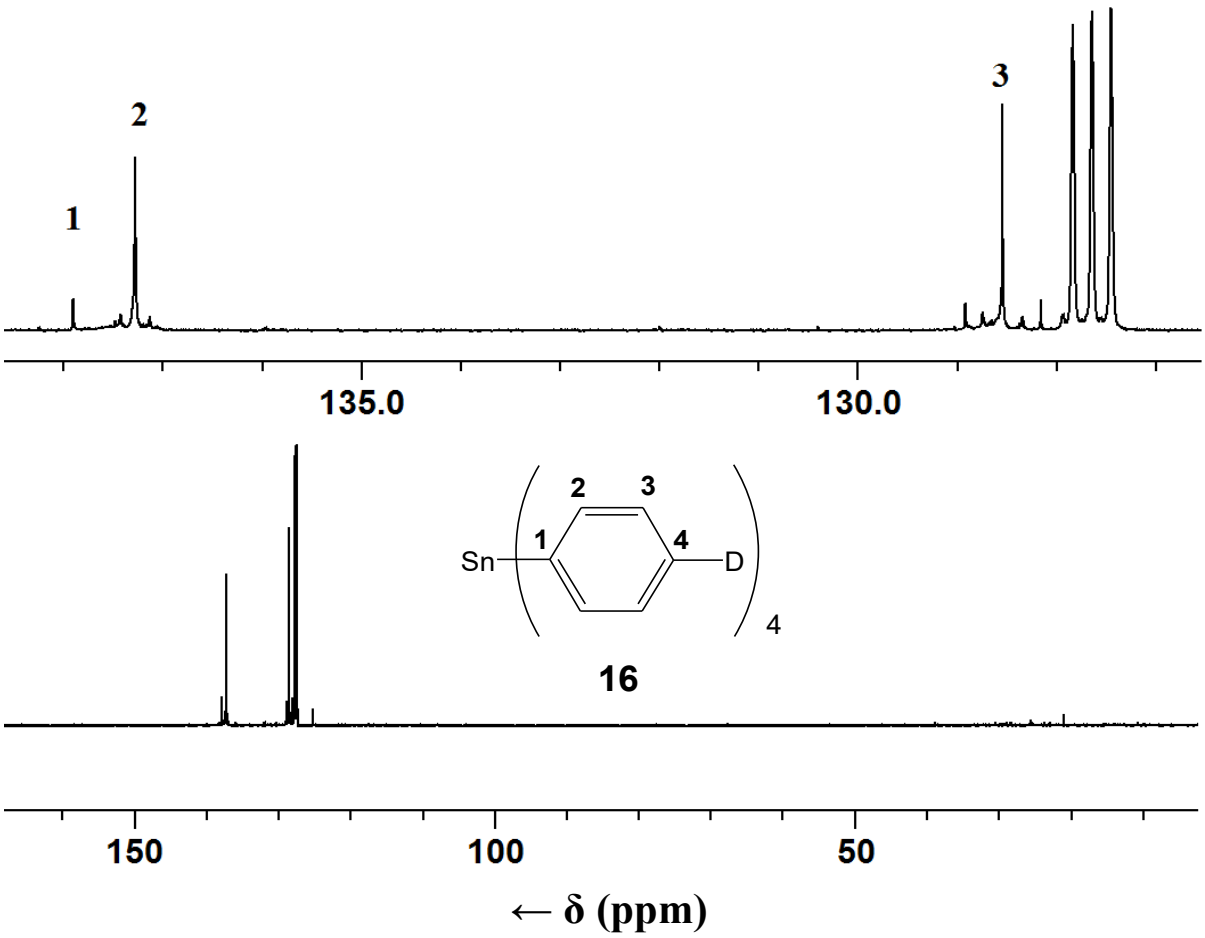

Figure 2.12 ^{13}C NMR spectrum of compound **16** in C_6D_6.

2.3 Conclusion

Various tetraphenylelement scaffolds have been synthesized. These tetraarylelement compounds have the advantage of incorporating a rigid backbone. This feature makes them ideal linkers that prevent interactions of the metal complexes with the reactive silica surface

after being immobilized, and it diminishes the probability of deactivation of the metal complexes by dimerization. Modifications and derivatives of these molecules can be made in a straightforward manner to meet the needs of the application desired.

There are two principal routes to synthesizing these scaffolds, depending on whether the tetraaryl core is generated in the first or second step. Both routes are used to synthesize compound **3**, as well as derivatives thereof. All of these compounds have been synthesized and characterized. The long range coupling between ^{31}P and ^{29}Si is particularly noteworthy.

It is also possible to modify the scaffold by incorporating different substituents in the phosphine groups and to choose alternative elements from the carbon group at the core. For example, compounds with four dicyclohexylphosphine groups can be formed, and a Sn, or alternatively a Si core can be chosen. This is demonstrated for compounds **12**, **13**, and **14**. For ease of purification, the phosphine is added prior to incorporating the core element. All of the scaffolds with cyclohexylphosphines display an interesting ^{13}C NMR phenomenon where six aliphatic signals are found per cyclohexyl ring where four would be expected at first glance. This is due to stereocenters in the molecule.

For synthesizing compounds **14**, **15**, and **16**, it is necessary to use ^{t}BuLi to lithiate compound **2**, which proves to be the only successful method of synthesis. The synthesis then proceeds in a straightforward manner, and the resulting products can be characterized.

2.4 Experimental Section

2.4.1 General Information and Procedures

All reactions are carried out using standard Schlenk techniques and a purified N_2 atmosphere, if not stated otherwise. Reagents purchased from Sigma Aldrich or VWR are used without further purification. Solvents are dried by boiling them over Na, distilled, and stored under N_2. CH_2Cl_2 and hexanes are obtained from a solvent purification system. The silica gel used for purifications is Silicycle SiliaFlash G15 (60-200 μm particle size and variable pore size) and used as received without further purification.

2.4.2 Instruments and Measurements

The ^{1}H, ^{13}C, and ^{31}P NMR spectra of liquids were recorded at 500.13, 125.66, and 202.28 MHz on a 500 MHz Varian spectrometer and referenced as follows: ^{1}H: residual internal $CHCl_3$ (δ, 7.26 ppm) or benzene-d_6 (δ, 7.16 ppm); ^{13}C: internal $CDCl_3$ (δ, 77.23 ppm) or benzene- d_6 (δ, 128.06 ppm). ^{31}P NMR spectra are referenced to neat Ph_2PCl (δ, 81.92 ppm) which is placed in a capillary centered in the NMR sample tube. The ^{13}C and ^{31}P spectra are recorded with ^{1}H decoupling if not stated otherwise. The ^{2}H, ^{29}Si, and ^{119}Sn NMR spectra of liquids were recorded at 61.41, 79.46, and 149.09 MHz on a 400 MHz Varian spectrometer and referenced as follows: ^{2}H: residual internal $CHDCl_2$ (δ, 4.79 ppm); ^{29}Si: external hexamethyldisiloxane (δ, 6.53 ppm); ^{119}Sn: external tetraphenyltin (δ, -130.65).[49] The solid-state NMR spectra are measured with a Bruker Avance 400 widebore NMR spectrometer with a multinuclear 4 mm MAS probehead. For the ^{31}P and ^{29}Si CP/MAS and MAS measurements ^{1}H high-power decoupling was applied. The recycle delays are 3 s for CP/MAS and 10 s for MAS spectra.

IR measurements are performed using a Shimadzu IRAffinity-1 FTIR spectrophotometer. Melting point determinations were done using a SRS Optimelt MPA100 Automated Melting Point System.

2.4.3 Synthesis of 3

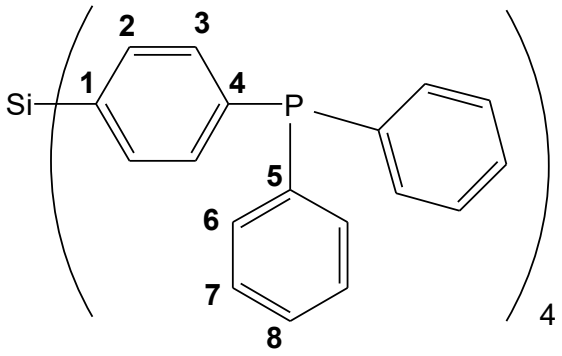

$C_{72}H_{56}P_4Si$

Mol. Wt.: 1073.196 g/mol

Tetrabromide compound **1** (1.370 g, 2.10 mmol) is dissolved in Et_2O (100 mL) and cooled to -78 °C for 10 minutes. 2.5 M ^{n}Buli (6.72 mL, 16.8 mmol, 8.0 eq) is slowly added. The solution is allowed to warm to RT over 2h, then cooled to -78 °C. Chlorodiphenylphosphine (3.05 mL, 3.75 g, 17.0 mmol, 8.1 eq.) is added slowly, and the solution is gradually warmed to RT and allowed to react overnight. The Et_2O is then removed *in vacuo*, and **3** is washed with hexane (3 times, 30 mL), and extracted with toluene (2x, 50 mL). The toluene is removed in vacuo, leaving a white powder of **3** (1.309 g, 1.220 mmol, 58.1%).

^{1}H NMR (C_6D_6, 300 MHz)

δ = 7.50 (dd, 8H, H-2, $^3J(^1H\text{-}^1H)$ = 7.9 Hz, $^4J(^{31}P\text{-}^1H)$ = 0.9 Hz), 7.40-7.34 (m, 16H, H-6), 7.30 (dd, 8H, H-3, $^3J(^1H\text{-}^1H)$ = 7.9 Hz, $^3J(^{31}P\text{-}^1H)$ = 7.4 Hz), 7.04-7.00 (m, 24H, H-7, H-8).

^{13}C NMR (C_6D_6, 75.43 MHz)

δ = 141.78 (d, C-4, $^{1}J(^{31}P\text{-}^{13}C)$ = 14.3 Hz), 137.21 (d, C-5, $^{1}J(^{31}P\text{-}^{13}C)$ = 11.6 Hz), 135.49 (d, C-2, $^{3}J(^{31}P\text{-}^{13}C)$ = 6.1 Hz), 134.37 (d, C-6, $^{2}J(^{31}P\text{-}^{13}C)$ = 20.1 Hz), 133.41 (d, C-3, $^{2}J(^{31}P\text{-}^{13}C)$ = 18.6 Hz), 133.04 (s, C-1), 129.10 (s, C-8), 128.90 (d, C-7, $^{3}J(^{31}P\text{-}^{13}C)$ = 7.1 Hz).

^{29}Si NMR (C_6D_6, 79.46 MHz)

δ = -14.42 (s)

^{31}P NMR (C_6D_6, 202.28 MHz)

δ = -5.19 (s)

2.4.4 Synthesis of 4

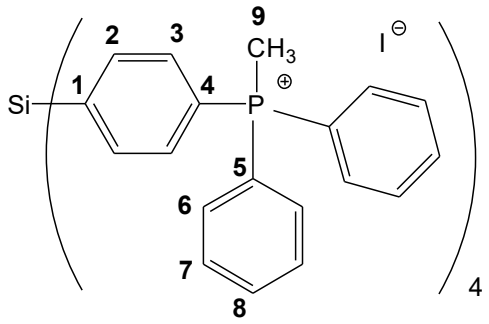

4

$C_{76}H_{68}P_4I_4Si$

Mol. Wt.: 1640.952 g/mol

Tetraphosphine **3** (0.113 g, 0.105 mmol) was combined with iodomethane (0.5 mL, 0.8 mmol, 7.6 eq.) in dimethylsulfoxide (10 mL) and stirred overnight. The product was left under vacuum at 50 ºC for 10 hours, leaving the white powder **4** (0.125 g, 0.0762 mmol, 98%).

^{1}H NMR (DMSO-*d*$_6$, 300 MHz)

δ = 7.72-7.86 (m, 56H), 3.18 (d, H-9, $^{2}J(^{31}P\text{-}^{1}H)$ = 14.4 Hz).

^{13}C NMR (DMSO-d_6, 75.43 MHz)

δ = 137.97 (d, C-1, $^{4}J(^{31}P\text{-}^{13}C)$ = 2.5 Hz), 137.08 (d, C-2, $^{3}J(^{31}P\text{-}^{13}C)$ = 11.9 Hz), 134.90 (d, C-8, $^{4}J(^{31}P\text{-}^{13}C)$ = 2.8 Hz), 133.25 (d, C-7, $^{3}J(^{31}P\text{-}^{13}C)$ = 10.9 Hz), 132.75 (d, C-3, $^{2}J(^{31}P\text{-}^{13}C)$ = 10.6 Hz), 130.10 (d, C-6, $^{2}J(^{31}P\text{-}^{13}C)$ = 12.8 Hz), 122.69 (d, C-4, $^{1}J(^{31}P\text{-}^{13}C)$ = 86.4 Hz), 119.25 (d, C-5, $^{1}J(^{31}P\text{-}^{13}C)$ = 88.2 Hz), 7.40 (d, C-9, $^{1}J(^{31}P\text{-}^{13}C)$ = 55.6 Hz).

^{29}Si NMR (DMSO-d_6, 79.46 MHz)

δ = -14.88 (quint., $^{5}J(^{31}P\text{-}^{29}Si)$ = 1.7 Hz).

^{31}P NMR (DMSO-d_6, 202.28 MHz)

δ = 22.46

2.4.5 Synthesis of 5

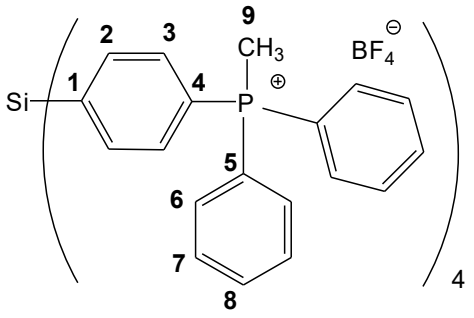

5

$C_{76}H_{68}B_4F_{16}P_4Si$

Mol. Wt.: 1480.552 g/mol

Tetraphosphonium salt **4** (0.095 g, 0.059 mmol) was combined with $AgBF_4$ (0.049 g, 0.25 mmol) in methanol (20 mL) and stirred for 30 min, during which time a white precipitate formed. The reaction mixture was then filtered, and the solvent of the supernatant was removed under vacuum, leaving the white powder product **5** (0.071 g, 0.048 mmol, 81.4%).

^{1}H NMR (DMSO-d_6, 500.13 MHz)

δ = 7.63-7.92 (m, 56H), 3.02 (d, H-9, $^{2}J(^{31}P\text{-}^{1}H)$ = 13.3 Hz).

^{13}C NMR (DMSO-d_6, 125.66 MHz)

δ = 137.83 (d, C-1, $^{4}J(^{31}P\text{-}^{13}C)$ = 2.7 Hz), 134.76 (d, C-8, $^{4}J(^{31}P\text{-}^{13}C)$ = 2.5 Hz), 133.15 (d, C-6, $^{2}J(^{31}P\text{-}^{13}C)$ = 10.9 Hz), 132.67 (d, C-3, $^{2}J(^{31}P\text{-}^{13}C)$ = 10.6 Hz), 131.67 (d, C-2, $^{3}J(^{31}P\text{-}^{13}C)$ = 9.8 Hz), 129.97 (d, C-7, $^{3}J(^{31}P\text{-}^{13}C)$ = 12.8 Hz), 122.55 (d, C-4, $^{1}J(^{31}P\text{-}^{13}C)$ = 86.5 Hz), 119.08 (d, C-5, $^{1}J(^{31}P\text{-}^{13}C)$ = 88.2 Hz), 7.41 (d, C-9, $^{1}J(^{31}P\text{-}^{13}C)$ = 55.2 Hz).

^{29}Si NMR (DMSO-d_6, 79.46 MHz)

δ = -14.87 (s)

^{31}P NMR (DMSO-d_6, 202.28 MHz)

δ = 22.52 (s)

2.4.6 Synthesis of 6

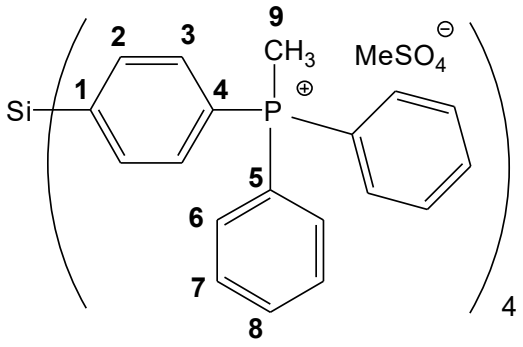

6

$C_{80}H_{80}O_{16}P_4S_4Si$

Mol. Wt.: 1577.722 g/mol

Tetraphosphine **3** (0.500 g, 0.466 mmol) was reacted with dimethylsulfate (0.235 g, 1.86 mmol) in DMF (50 mL) and stirred overnight. The solvent is removed in vacuo, leaving behind the product **6** as a white powder (0.694 g, 0.440 mmol, 94.4%).

^{1}H NMR ($CDCl_3$, 300 MHz)

δ = 7.10-7.90 (m, 56H), 3.12 (d, H-9, $^{2}J(^{31}P\text{-}^{1}H)$ = 14.5 Hz).

^{13}C NMR ($CDCl_3$, 75.43 MHz)

δ = 138.36 (d, C-1, $^{4}J(^{31}P\text{-}^{13}C)$ = 3.0 Hz), 137.86 (d, C-2, $^{3}J(^{31}P\text{-}^{13}C)$ = 12.4 Hz), 135.12 (d, C-8, $^{4}J(^{31}P\text{-}^{13}C)$ = 2.9 Hz), 133.13 (d, C-7, $^{3}J(^{31}P\text{-}^{13}C)$ = 10.8 Hz), 133.02 (d, C-3, $^{2}J(^{31}P\text{-}^{13}C)$ = 10.8 Hz), 130.46 (d, C-6, $^{2}J(^{31}P\text{-}^{13}C)$ = 13.0 Hz), 121.34 (d, C-4, $^{1}J(^{31}P\text{-}^{13}C)$ = 87.0 Hz), 117.92 (d, C-5, $^{1}J(^{31}P\text{-}^{13}C)$ = 88.6 Hz), 11.15 (d, C-9, $^{1}J(^{31}P\text{-}^{13}C)$ = 57.1Hz).

^{29}Si NMR ($CDCl_3$, 79.46 MHz)

δ = -14.79 (s)

^{31}P NMR ($CDCl_3$, 202.28 MHz)

δ = 22.15 (s)

2.4.7 Synthesis of 7

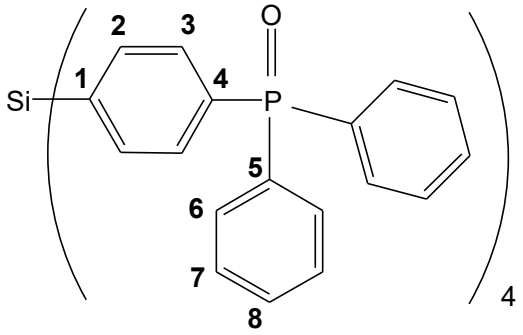

7

$C_{76}H_{64}O_4P_4Si$

Mol. Wt.: 1193.300 g/mol

Tetraphosphine **3** (0.118 g, 0.110 mmol) is stirred in dichloromethane (10 mL), followed by addition of H_2O_2 (2 mL, 35 wt%). The solution was stirred for 2 h, then the aqueous layer was removed with a pipette.[48a] Activated molecular sieves were added, and the solution was stirred slowly overnight. The solution was then extracted, followed by removal of the solvent under vacuum. The product **7** is a white powder with a yield of 0.118 g (0.104 mmol, 94.5%).

^{1}H NMR ($CDCl_3$, 500.13 MHz)

δ = 7.66 (dd, H-3, H-6, $^{3}J(^{31}H\text{-}^{1}H)$ = 11.5 Hz, $^{3}J(^{1}H\text{-}^{1}H)$ = 7.9 Hz), 7.58 (dd, H-2, $^{3}J(^{1}H\text{-}^{1}H)$ = 8.2 Hz, $^{4}J(^{31}P\text{-}^{1}H)$ = 3.0 Hz), 7.54 (dq, H-8, $^{3}J(^{1}H\text{-}^{1}H)$ = 7.5 Hz, $^{4}J(^{1}H\text{-}^{1}H)$ = 2.8 Hz) 7.45 (td, H-7, $^{3}J(^{1}H\text{-}^{1}H)$ = 8.0 Hz, $^{4}J(^{31}P\text{-}^{1}H)$ = 2.7 Hz).

^{13}C NMR ($CDCl_3$, 125.66 MHz)

δ = 136.62 (d, C-1, $^{4}J(^{31}P\text{-}^{13}C)$ = 2.5 Hz), 136.08 (d, C-2, $^{3}J(^{31}P\text{-}^{13}C)$ = 11.6 Hz), 134.94 (d, C-4, $^{1}J(^{31}P\text{-}^{13}C)$ = 101.7 Hz), 132.09 (d, C-8, $^{4}J(^{31}P\text{-}^{13}C)$ = 2.7 Hz), 131.98 (d, C-6, $^{2}J(^{31}P\text{-}^{13}C)$ = 9.9 Hz), 131.84 (d, C-5, $^{1}J(^{31}P\text{-}^{13}C)$ = 104.4 Hz), 131.44 (d, C-3, $^{2}J(^{31}P\text{-}^{13}C)$ = 9.5 Hz), 128.55 (d, C-7, $^{3}J(^{31}P\text{-}^{13}C)$ = 12.2 Hz).

^{29}Si NMR ($CDCl_3$, 79.46 MHz)

δ = -14.78

^{31}P NMR ($CDCl_3$, 202.28 MHz)

δ = 29.12

2.4.8 Synthesis of 8

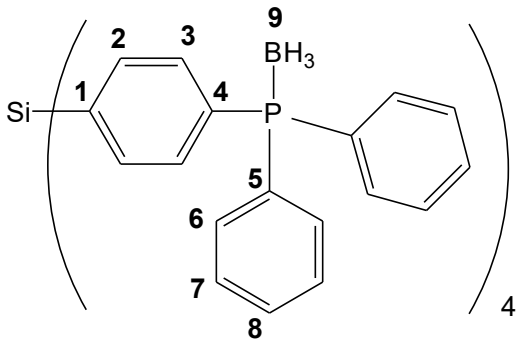

8

$C_{76}H_{80}B_4P_4Si$

Mol. Wt.: 1188.673 g/mol

Tetraphosphine **3** (0.116 g, 0.108 mmol) is dissolved in toluene (20 mL). Then BH_3·THF (1 mmol) was added and the reaction mixture stirred overnight. The solvent and excess borane were removed under vacuum. The product **8** remains behind as a white solid (0.113 g, 96%).

^{1}H NMR ($CDCl_3$, 500.13 MHz)

δ = 7.62-7.55 (m, H-2, H-3, H-6, 32H), 7.49 (td, H-8, 8H, $^{3}J(^{1}H\text{-}^{1}H)$ = 7.3 Hz), $^{4}J(^{1}H\text{-}^{1}H)$ = 1.3 Hz), 7.42 (td, H-7, 16H, $^{3}J(^{1}H\text{-}^{1}H)$ = 7.7 Hz), $^{3}J(^{31}P\text{-}^{1}H)$ = 1.9 Hz), 1.30 (s (br), H-9).

^{13}C NMR ($CDCl_3$, 125.66 MHz)

δ = 136.32 (d, C-3, $^{3}J(^{31}P\text{-}^{13}C)$ = 9.7 Hz), 135.80 (d, C-1, $^{4}J(^{31}P\text{-}^{13}C)$ = 2.1 Hz), 133.25 (d, C-6, $^{2}J(^{31}P\text{-}^{13}C)$ = 9.7 Hz), 132.52 (d, C-2, $^{3}J(^{31}P\text{-}^{13}C)$ = 9.3 Hz), 132.07 (d, C-4, $^{1}J(^{31}P\text{-}^{13}C)$ = 56.0 Hz), 131.44 (d, C-8, $^{4}J(^{31}P\text{-}^{13}C)$ = 2.3 Hz), 128.87 (d, C-7, $^{3}J(^{31}P\text{-}^{13}C)$ = 10.2 Hz), 128.54 (d, C-5, $^{1}J(^{31}P\text{-}^{13}C)$ = 58.0 Hz).

^{29}Si NMR ($CDCl_3$, 79.46 MHz)

δ = -14.76

^{31}P NMR ($CDCl_3$, 202.28 MHz)

$\delta = 20.92$ (br), $\Delta\nu_{1/2} = 43.7$ Hz

Melting Point

320 °C (decomp.)

Solubility

2.13 g/L ($CHCl_3$)

2.4.9 Synthesis of 12

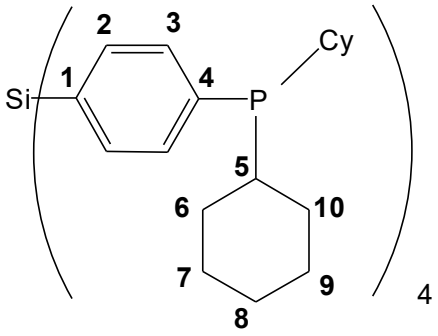

12

$C_{72}H_{104}P_4Si$

Mol. Wt.: 1121.577 g/mol

Compound **11** (0.335 g, 0.514 mmol) was dissolved in Et_2O (100 mL) and cooled to -78 °C for 10 minutes. 2.5 M ^{n}BuLi (1.65 mL, 4.13 mmol, 8.0 eq.) was added and the reaction mixture was warmed to RT for 2 h. The reaction mixture was cooled to -78 °C for 10 minutes, and chlorodicyclohexylphosphine (0.96 g, 4.12 mmol, 8.0 eq.) was added. The solution was stirred overnight, then the Et_2O and butyldicyclohexylphosphine were removed *in vacuo*. Dry silica was added to remove phosphine oxide after dissolution in toluene, and

the product was extracted three times with 30 mL of toluene. The product **12** was recovered as a sticky, white solid (0.080 g, 0.071 mmol, 13.9%).

^{1}H NMR (C_6D_6, 500 MHz)

δ = 7.67 (d, H-2, $^{3}J(^{1}H\text{-}^{1}H)$ = 7.6 Hz), 7.47 (t, H-3, $^{3}J(^{1}H\text{-}^{1}H)$ = 7.6 Hz, $^{2}J(^{31}P\text{-}^{1}H)$ = 6.8 Hz), 1.87 (m, H-5, H-6_{eq}), 1.65 (m, H-7_{eq}, H-10_{eq}), 1.56 (m, H-8_{eq}), 1.54 (m, H-9_{eq}), 1.20 (m, H-6_{ax}, H-7_{ax}), 1.10 (m, H-9_{ax}, H-10_{ax}), 0.90 (m, H-8_{ax}). Signals were assigned using the chemical shift values for dicyclohexylphenylphosphine and triphenylphosphine.[48a]

^{13}C NMR (C_6D_6, 125.7 MHz)

δ = 137.73 (s, C-1), 136.26 (d, C-2, $^{3}J(^{31}P\text{-}^{13}C)$ = 6.6 Hz) 136.18 (d, C-4, , $^{1}J(^{31}P\text{-}^{13}C)$ = 93.7 Hz), 134.65 (d, C-3, $^{2}J(^{31}P\text{-}^{13}C)$ = 18.2 Hz), 32.76 (d, C-5, $^{1}J(^{31}P\text{-}^{13}C)$ = 13.7 Hz), 30.30 (d, C-6, $^{2}J(^{31}P\text{-}^{13}C)$ = 16.5 Hz), 29.29 (d, C-10, $^{2}J(^{31}P\text{-}^{13}C)$ = 7.7 Hz), 27.52 (d, C-7, $^{3}J(^{31}P\text{-}^{13}C)$ = 12.1 Hz), 27.28 (d, C-9, $^{3}J(^{31}P\text{-}^{13}C)$ = 7.2 Hz), 26.65 (s, C-8).

^{29}Si NMR (C_6D_6, 79.46 MHz)

δ = -15.11 (s)

^{31}P NMR (C_6D_6, 202.4 MHz)

δ = 2.15 (s)

^{31}P CP/MAS NMR (ν_{rot} = 10.0 kHz)

δ = 2.62 (s)

^{29}Si CP/MAS NMR (ν_{rot} = 10.0 kHz)

δ = -14.28 (s)

2.4.10 Synthesis of 13

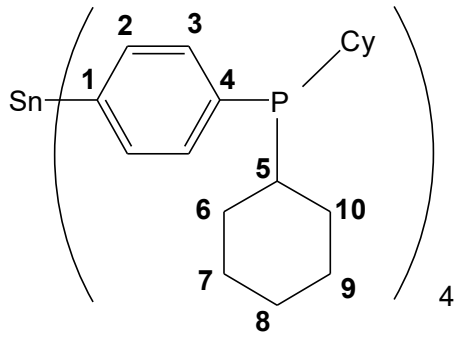

13

$C_{72}H_{104}P_4Sn$

Mol. Wt.: 1212.201 g/mol

Compound **11** (1.3673 g, 3.87 mmol) is dissolved in Et_2O (100 mL) and cooled to -78 ^oC for 10 minutes. 2.5 M ^{n}Buli (1.54 mL, 3.85 mmol, 1 eq) is slowly added. The solution is warmed to RT over 2h, then cooled to -78 °C. Tetrachlorostannane (0.252 g, 0.967 mmol, 0.25 eq.) is dissolved in pentane (10 mL) and added slowly, and the solution is gradually warmed to RT and allowed to react overnight. The Et_2O is then removed *in vacuo*, and **13** is extracted 2 times with pentane (30 mL). The pentane is then removed *in vacuo*, leaving **13** behind as a white powder (0.760 g, 64%).

^{1}H NMR (C_6D_6, 500.13 MHz)

δ = 7.63 (8H, H-2, $^3J(^1H\text{-}^1H)$ = 7.1 Hz), 7.50 (8H, H-3, $^3J(^1H\text{-}^1H)$ = 7.1 Hz, $^3J(^{31}P\text{-}^1H)$ = 6.8 Hz), 1.89 (8H, H-5, s), (8H, H-6_{eq}, s), 1.68 (8H, H-7_{eq}, s), 1.66 (8H, H-10_{eq}, s), 1.56 (8H, H-9_{eq}, s), 1.49 (8H, H-8_{eq}, s), 1.22 (8H, H-6_{ax}, s), (8H, H-7_{ax}, s), 1.12 (8H, H-9_{ax}, s), 1.11 (8H, H-10_{ax}, s), 0.95 (8H, H-8_{ax}, s).

^{13}C NMR (C_6D_6, 125.76 MHz)

δ = 138.57 (C-1, s), 137.14 (C-2, $^3J(^{31}P\text{-}^{13}C)$ = 6.6 Hz, $^2J(^{119}Sn\text{-}^{13}C)$ = 22.1 Hz, $^2J(^{117}Sn\text{-}^{13}C)$ = 15.3 Hz), 135.36 (C-3, $^2J(^{31}P\text{-}^{13}C)$ = 19.1 Hz, $^3J(^{119}Sn\text{-}^{13}C)$ = 34.6 Hz, $^3J(^{117}Sn\text{-}^{13}C)$ = 32.2

Hz), 128.89 (C-4, $^{3}J(^{31}P\text{-}^{13}C)$ = 96.3 Hz), 32.90 (C-5, $^{1}J(^{31}P\text{-}^{13}C)$ = 13.8 Hz), 30.36 (C-6, $^{2}J(^{31}P\text{-}^{13}C)$ = 16.6 Hz), 29.29 (C-10, $^{2}J(^{31}P\text{-}^{13}C)$ = 8.0 Hz), 27.51 (C-7, $^{3}J(^{31}P\text{-}^{13}C)$ = 12.1 Hz), 27.28 (C-9, $^{3}J(^{31}P\text{-}^{13}C)$ = 7.2 Hz), 26.34 (C-8, s).

^{119}Sn NMR (C_6D_6, 148.97 MHz)

δ = -125.92 (quint., $^{5}J(^{119}Sn\text{-}^{31}P)$ = 11.6 Hz).

^{31}P NMR (C_6D_6, 202.28 MHz)

δ = 2.35 (s)

2.4.11 Synthesis of 14

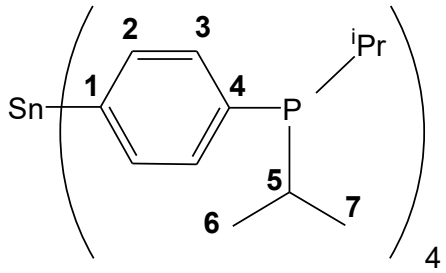

14

$C_{48}H_{72}P_4Sn$

Mol. Wt.: 891.690 g/mol

1.5 M ^{t}BuLi (0.70 mL, 1.1 mmol, 10 eq.) is added to a solution of **2** (0.0808 g, 0.1088 mmol) in diethyl ether (80 mL) at -78 °C. Then the reaction mixture was allowed to warm up and stirred at room temperature for 1 h. After cooling to -78 °C, chlorodiisopropylphosphine (0.304 g, 1.99 mmol, 18.3 eq.) was added, and the solution was stirred overnight. Then the solvent was removed *in vacuo*. The product was purified by extraction with toluene, and by heating the product *in vacuo* at 120 ºC for 2 hours. The product **14** was recovered in as a sticky, white solid (0.0760 g, 0.0852 mmol, 78.3%).

^{1}H NMR (C_6D_6 , 499.69 MHz)

δ = 7.64 (dd, 8H, H-2, $^{3}J(^{1}H\text{-}^{1}H)$ = 8.0 Hz, $^{4}J(^{31}P\text{-}^{1}H)$ = 1.0 Hz), 7.47 (dd, 8H, H-3 , $^{3}J(^{1}H\text{-}^{1}H)$ = 8.0 Hz, $^{3}J(^{31}P\text{-}^{1}H)$ = 6.5 Hz), 1.94 (ds, 8H, $^{3}J(^{1}H\text{-}^{1}H)$ = 7.0 Hz, $^{2}J(^{31}P\text{-}^{1}H)$ = 1.3 Hz), 1.04 (dd, 8H, $^{3}J(^{1}H\text{-}^{1}H)$ = 7.0 Hz, $^{3}J(^{31}P\text{-}^{1}H)$ = 14.8 Hz), 0.89 (dd, 8H, $^{3}J(^{1}H\text{-}^{1}H)$ = 6.9 Hz, $^{3}J(^{31}P\text{-}^{1}H)$ = 11.1 Hz).

^{13}C NMR (C_6D_6, 125.66 MHz)

δ = 138.25 (s, C-1, $^{1}J(^{119}Sn\text{-}^{13}C)$ = 124.1 Hz, $^{1}J(^{117}Sn\text{-}^{13}C)$ = 119.7 Hz), 136.69 (d, C-2), $^{3}J(^{31}P\text{-}^{13}C)$ = 6.5 Hz, $^{2}J(^{119}Sn\text{-}^{13}C)$ = 24.7 Hz, $^{2}J(^{117}Sn\text{-}^{13}C)$ = 22.4 Hz), 134.81 (d, C-3, $^{2}J(^{31}P\text{-}^{13}C)$ = 6.5 Hz, $^{3}J(^{119}Sn\text{-}^{13}C)$ = 34.9 Hz, $^{3}J(^{117}Sn\text{-}^{13}C)$ = 33.9 Hz), 128.88 (d, C-4), $^{1}J(^{31}P\text{-}^{13}C)$ = 96.1 Hz), 22.64 (d, $^{1}J(^{31}P\text{-}^{13}C)$ = 13.4 Hz), 19.63 (d, $^{2}J(^{31}P\text{-}^{13}C)$ = 18.6 Hz), 18.65 (d, $^{2}J(^{31}P\text{-}^{13}C)$ = 9.0 Hz).

^{31}P NMR (C_6D_6, 202.28 MHz)

δ = 9.94 (s).

^{119}Sn NMR (C_6D_6, 148.97 MHz)

δ = -128.94 (s).

2.4.12 Synthesis of 15

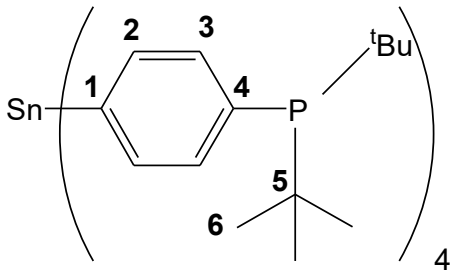

15

$C_{56}H_{88}P_4Sn$

Mol. Wt.: 1004.086 g/mol

1.5 M ^{t}BuLi (0.70 mL, 1.1 mmol, 10 eq.) is added to a solution of **2** (0.0808 g, 0.1088 mmol) in diethyl ether (80 mL) and cooled to -78 °C. The reaction mixture was stirred at room temperature for 1 h, then cooled to -78 °C. Chlorodi-*tert*-butylphosphine (0.304 g, 1.99 mmol, 18.3 eq.) was added, and the solution was stirred overnight. The solvent was removed *in vacuo*. The product was purified by extraction with toluene, and by heating the product *in vacuo* at 120 ºC for 2 hours. The product **15** was recovered in as a sticky, white solid (0.0760 g, 0.0852 mmol, 78.3%).

^{1}H NMR (C_6D_6 , 499.69 MHz)

δ = 7.52 (t, 8H, H-3, $^3J(^1H\text{-}^1H)$ = 7.2 Hz, $^3J(^{31}P\text{-}^1H)$ = 7.2 Hz), 7.22 (d, 8H, H-2 , $^3J(^1H\text{-}^1H)$ = 7.2 Hz), 0.98 (d, 36H, H-6 , $^3J(^{31}P\text{-}^1H)$ = 11.7 Hz).

^{13}C NMR (C_6D_6, 125.66 MHz)

δ = 138.25 (s, C-1), 138.40 (d, C-4), $^1J(^{31}P\text{-}^{13}C)$ = 25.1 Hz), 136.27 (d, C-3, $^2J(^{31}P\text{-}^{13}C)$ = 22.9 Hz), 132.73 (d, C-2), $^3J(^{31}P\text{-}^{13}C)$ = 8.0 Hz), 32.15 (d, C-5), $^1J(^{31}P\text{-}^{13}C)$ = 23.4 Hz), 30.87 (d, C-6), $^2J(^{31}P\text{-}^{13}C)$ = 14.9 Hz).

^{31}P NMR (C_6D_6, 202.28 MHz)

δ = 39.04 (s).

^{119}Sn NMR (C_6D_6, 148.97 MHz)

δ = -123.21

2.4.13 Synthesis of 16

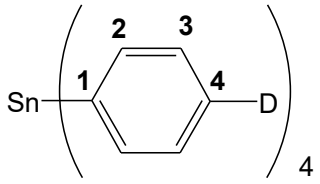

16

$C_{24}H_{16}D_4Sn$

Mol. Wt.: 431.150 g/mol

1.5 M ^{t}BuLi (0.75 mL, 1.1 mmol, 10 eq.) is added to a solution of **2** (0.083 g, 0.111 mmol) in 80 mL diethyl ether, cooled to -78 °C. The reaction mixture was stirred at room temperature for 1 h, then cooled to -78 °C. D_2O (0.50 mL, 25.0 mmol, 225 eq.) is added and the reaction mixture is stirred overnight. Then the solvent was removed *in vacuo* and the product was cleaned by washing with toluene. The product **16** was recovered as a white powder (0.041 g, 0.095 mmol, 85.7%).

^{1}H NMR (C_6D_6, 499.69 MHz)

δ = 7.61 (d, 8H, H-2), $^3J(^1H\text{-}^1H)$ = 8.0 Hz), 7.16 (d, 8H, H-3, $^3J(^1H\text{-}^1H)$ = 7.9 Hz).

^{2}H NMR (C_6D_6, 61.32 MHz)

δ = 7.34.

^{13}C NMR (C_6D_6, 125.66 MHz)

δ = 138.25 (s, C-1), 137.63 (s, C-2, $^2J(^{119}Sn\text{-}^{13}C)$ = 18.9 Hz, $^2J(^{117}Sn\text{-}^{13}C)$ = 18.1 Hz), 128.90 (s, C-3, $^3J(^{119}Sn\text{-}^{13}C)$ = 26.0 Hz, $^3J(^{117}Sn\text{-}^{13}C)$ = 24.8 Hz).

^{119}Sn NMR (C_6D_6, 148.97 MHz)

δ = -128.44(s).

^{2}H MAS NMR (C_6D_6, 61.32 MHz)

δ_{iso} = 7.24 (Q_{cc} = 181.5 kHz)

CHAPTER III

PHOSPHONIUM SALTS:

IMMOBILIZATION ON SILICA, LEACHING, AND SOLUBILITY

3.1 Introduction

Surface chemistry has always been an important area of scientific study and it has grown rapidly in previous decades, with applications in catalysis, materials chemistry, the separation sciences, nanotechnology, surfactants, polymers, and medicine.[11,16-19] Most of the surface species and their behaviors are amenable to solid-state NMR which is a powerful analytical method to investigate amorphous materials.[43] Different optimized pulse sequences and techniques allow the selective measurements of oxide or polymer supports, adsorbed or covalently bound species, or salts bound to surfaces via electrostatic interactions. Furthermore, dynamic effects, coordination chemistry and reactivity can be investigated with the corresponding techniques (see Introduction, Chapter I).[23]

As described in the previous chapter, tetraphosphines with rigid tetraphenyl element cores can be applied as linkers for tethering homogeneous catalysts to solid oxide supports such as silica. In a first step, the tetraphosphines have to be immobilized on the support. This is done *in situ* using an ethoxysilane reagent to form a phosphonium salt on the surface, as described previously.[3,47] During the reaction of the ethoxysilanes with the silica surface phosphines are quaternized to phosphonium groups by taking up ethyl groups from the activated ethoxysilane moieties.[26] The counteranions of the generated ethylphosphonium groups are siloxide anions which are covalently bound to the silica surface. Due to the tetrahedral sterics of the tetraphosphines only maximally three of the phosphines per

molecule can form phosphonium salts and be bound to the surface. In this way, the linker scaffold stands upright on the surface, bound via three "legs", while one phosphine group remains to coordinate to a metal complex.[3]

The principle of this immobilization reaction has been demonstrated for tetraarylphosphines with a Sn core previously, and a highly active and recyclable Wilkinson-type Rh catalyst has been obtained.[3] However, it could not be excluded at that time that the Sn core did not enhance the activity of the catalyst, for example, by activating the hydrogen prior to its binding to the metal center. Therefore, in this thesis, several analogous linker scaffolds with inert Si cores that do not interact with hydrogen, were synthesized and investigated. Furthermore, the substituents at phosphorus were varied in order to explore, for example, the electronic influence of dialkylarylphosphine groups on the catalytic activity.

One advantage of using a linker molecule containing four phosphine groups is that it can be immobilized via one, two, or three phosphonium groups. The first phosphonium group can form on any surface site where an ethoxysilane group has been bound. The second phosphine has the first phosphonium group as a fixed pivot point, but rotation about that point is feasible and the second phosphonium formation can take place at any point on a circle with the given radius, as illustrated in Figure 3.1. Since two points are set, the third phosphonium group can only form at two locations on the surface (Figure 3.1, right). Therefore, an excess of ethoxysilane reagent has to be applied for threefold bonding to ensure the presence of an active ethoxysilane group at least at one of the two surface sites accessible by the third phosphine group of the linker.

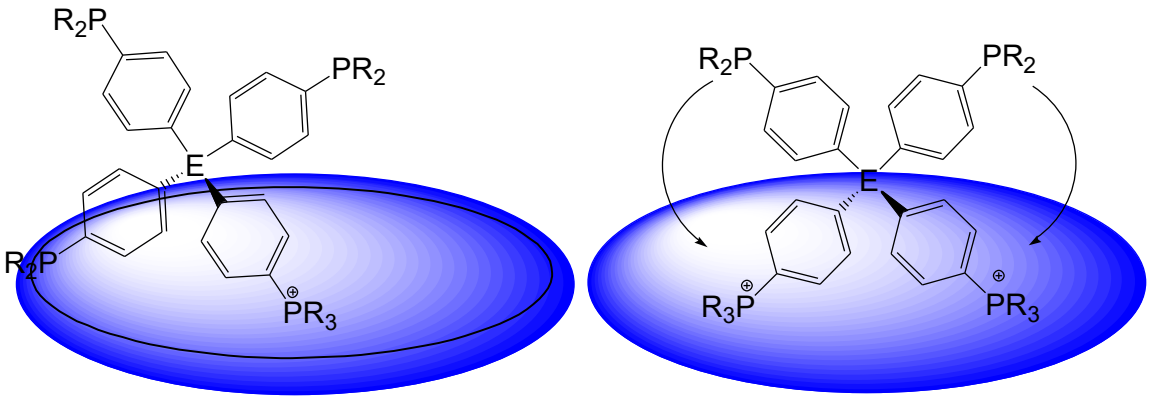

Figure 3.1 Representation of the immobilization of the second phosphonium group (left) and the third phosphonium group (right).

For the purposes of this project, the binding to the support via three phosphonium groups is preferred, as the resulting large footprint ensures sufficient spacing between the remaining phosphine groups, so that the coordinated metal complexes cannot become deactivated by dimer formation.[13] Additionally, due to the rigid nature of the scaffold, the metal centers are kept away from the reactive surface and in this way decomposition of the catalysts is diminished (Figure 3.2). Binding the tetrahedral scaffold with only one or two phosphonium groups to the surface would still allow contact with the surface, as the electrostatic interactions with the surface are not directional. Therefore, catalyst deactivation occurs faster.[3]

Although immobilized homogeneous catalysts have shown their merits over the past decades and have led to a catalyst with unprecedented lifetime and optimal recyclability,[3] some challenges remain. One of them involves the leaching of the catalyst into solution, leading to the loss of metal catalyst and diminished catalytic activity of the remaining material. This leaching can occur due to detachment of the metal center from the phosphine ligand, as recently investigated with Pd complexes tethered to silica via chelate phosphine

linkers.[27b] This scenario is less likely for Rh complexes of the Wilkinson type that are studied in this thesis.[1,3] However, leaching can also be the result of linker detachment from the support, which ultimately leads to a loss of metal complexes. Since the tetraphosphine linkers and bonding by electrostatic interactions are still a relatively new concept, this type of leaching has been investigated in the thesis in more detail.

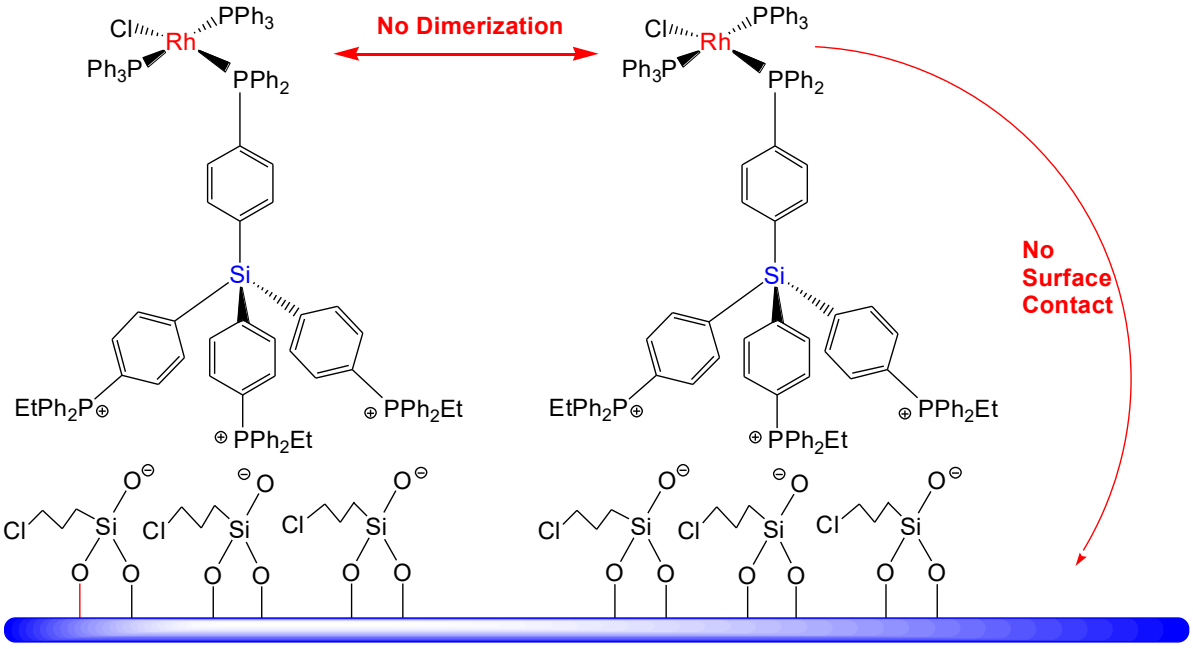

Figure 3.2 Schematic representation showing how the new rigid linker scaffolds prevent the deactivation pathways of rhodium complex dimerization and contact with the silica surface.

Another area of study relating to surface chemistry involves the dynamic properties of phosphonium salts on supports. In order to illuminate issues of metal complex dimerization on the surface it is important to understand the underlying principle. One possibility is that the linker molecules are mobile on the surface. Ethoxysilane linkers that are covalently bound via siloxane bonds are stationary at their surface site.[13] However, previous work suggested that electrostatic interactions of phosphonium salts, in case their counteranions are

not covalently bound, with silica surfaces allow their translational mobility across the surface.[8]

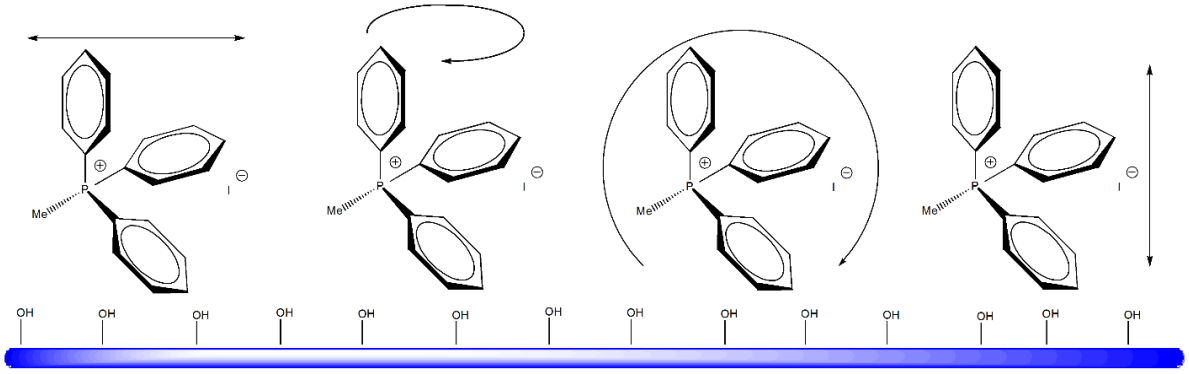

Figure 3.3 Depiction of the four types of motion possible for a model phosphonium salt on a silica surface, namely (left to right) translational motion, spinning, rolling, and "hopping" on the surface.

However, the nature of the motion remains unclear, as there are various manners in which an object might move on a surface (Figure 3.3). It could, for example, slide translationally in two dimensions across the surface with the molecular reorientation not being limited to one surface site. Alternatively, a phosphonium salt could spin in place like a top, roll across the surface like a tumbleweed, or, in the presence of a solvent, leach into solution before getting reattached to the surface.

By using solid-state NMR and solubility studies, in conjunction with previous data, it should be possible to better understand the nature of this molecular motion. If solubility data correlate with the molecular motion, it would strongly suggest that the motion observed involves detachment from the surface in the presence of a solvent. If there is no correlation, the mobility should only occur while the phosphonium salt resides on the surface. This

phenomenon has been described for adsorbed metallocenes[55] and phosphine oxides[48a,c] earlier.

The last area of analysis presented in this chapter involves leaching of surface-bound materials into solution in the presence of different solvents. As mentioned above, in the field of immobilized catalysts, this is of vital importance as a means of ensuring that the catalyst is not being removed from the surface into solution during the catalytic cycle. Although it has previously been demonstrated that phosphonium salts without covalent attachment to the support are leached off of silica in polar solvents,[8] the newer type of immobilized tetraphosphines has never been probed. Therefore, the novel phosphonium salts formed on silica *in situ* by the reaction of tetraphosphines with rigid tetraphenylsilane cores with an excess of ethoxysilanes will be suspended in a variety of representative solvents, and the leaching will be quantified.

3.2 Results and Discussion

3.2.1 Immobilization of Scaffolds

Previously, it has been shown that phosphines can be immobilized onto oxide supports in the presence of $(EtO)_3Si$ groups at elevated temperatures.[23,25,26]

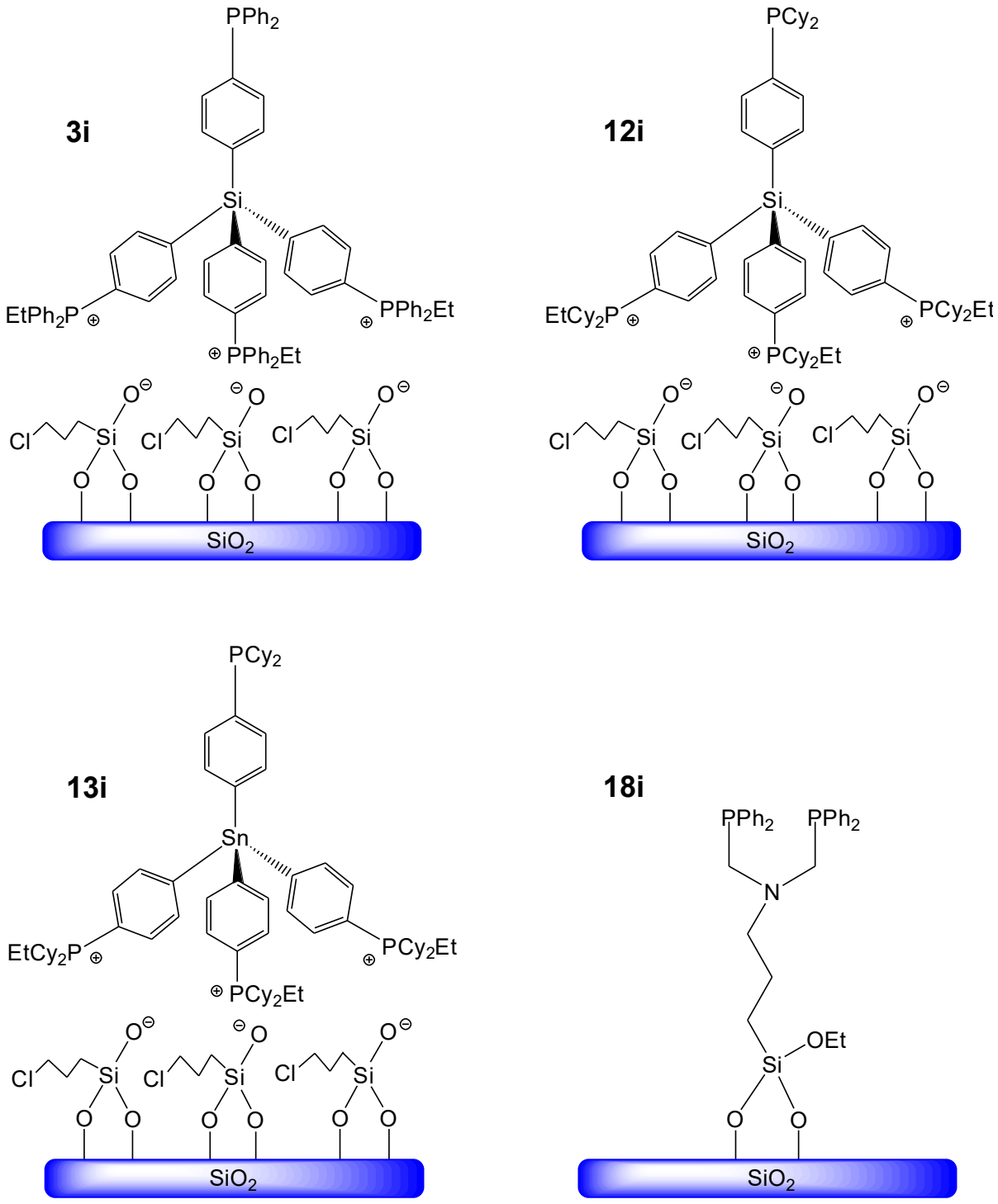

Scheme 3.1 Diagram of immobilized linkers **3i**, **12i**, **13i**, and **18i**.

Table 3.1 Surface coverages of the linker-modified silica **3i**, **12i**, **13i**, and **18i**.

Immobilized Linker	molecules per 100 nm^2 of surface	mg of linker/complex per g of SiO_2	mmol of linker/complex per g of SiO_2
3i	3.0	48	0.045
12i	3.8	47	0.042
13i	3.2	42	0.034
18i	2.6	19	0.031

The tetraphosphine ligands **12** and **13** have been synthesized by procedures described in Chapter II. Compounds **3**, **12**, and **13** were immobilized on silica using 3-chloropropyltriethoxysilane to generate the phosphonium groups binding **3i**, **12i**, and **13i** to the support via electrostatic interactions (Scheme 3.1). Another material generated was **18i**, which has been described previously.[46] The synthesis was performed for this thesis using the same procedure. One pending question was if a chelating phosphine ligand would result in a stronger attachment to the metal center, which could result in slower deactivation of the catalyst. In addition to the work presented by Merckle,[13,14] one can compare chelating linkers with the monodentate linker scaffolds. Therefore, it was desired that the immobilization would proceed until the scaffold was immobilized via three phosphonium groups, as described above.

Table 3.1 provides the surface coverages for all immobilized linkers. The surface coverages for **3i**, **12i**, and **13i** are lower than those usually determined for immobilized

linkers with alkyl chains.[23] Because the base of the scaffold with three tethered phosphonium centers spans about 13 Å in diameter, the surface cannot be loaded as fully with the scaffolds as with smaller linkers.[1-5,8-10,13,14,46] Generally, all linkers are immobilized completely, leaving no excess linker in the supernatant after the immobilization. **18i** has been applied in a lower surface coverage on purpose to ensure that dimerization of the metal centers did not occur during catalysis.

In the field of immobilized catalysts, solid-state NMR is the primary tool for characterizing amorphous supports and surface-bound species. The ^{31}P solid-state NMR spectra displayed in Figures 3.4, 3.5, and 3.6 show that the immobilizations proceeded cleanly, and only traces of oxidic byproducts are formed. This can occur during the measurements which take typically several hours in a rotor with Kel-F caps that are not completely air tight.

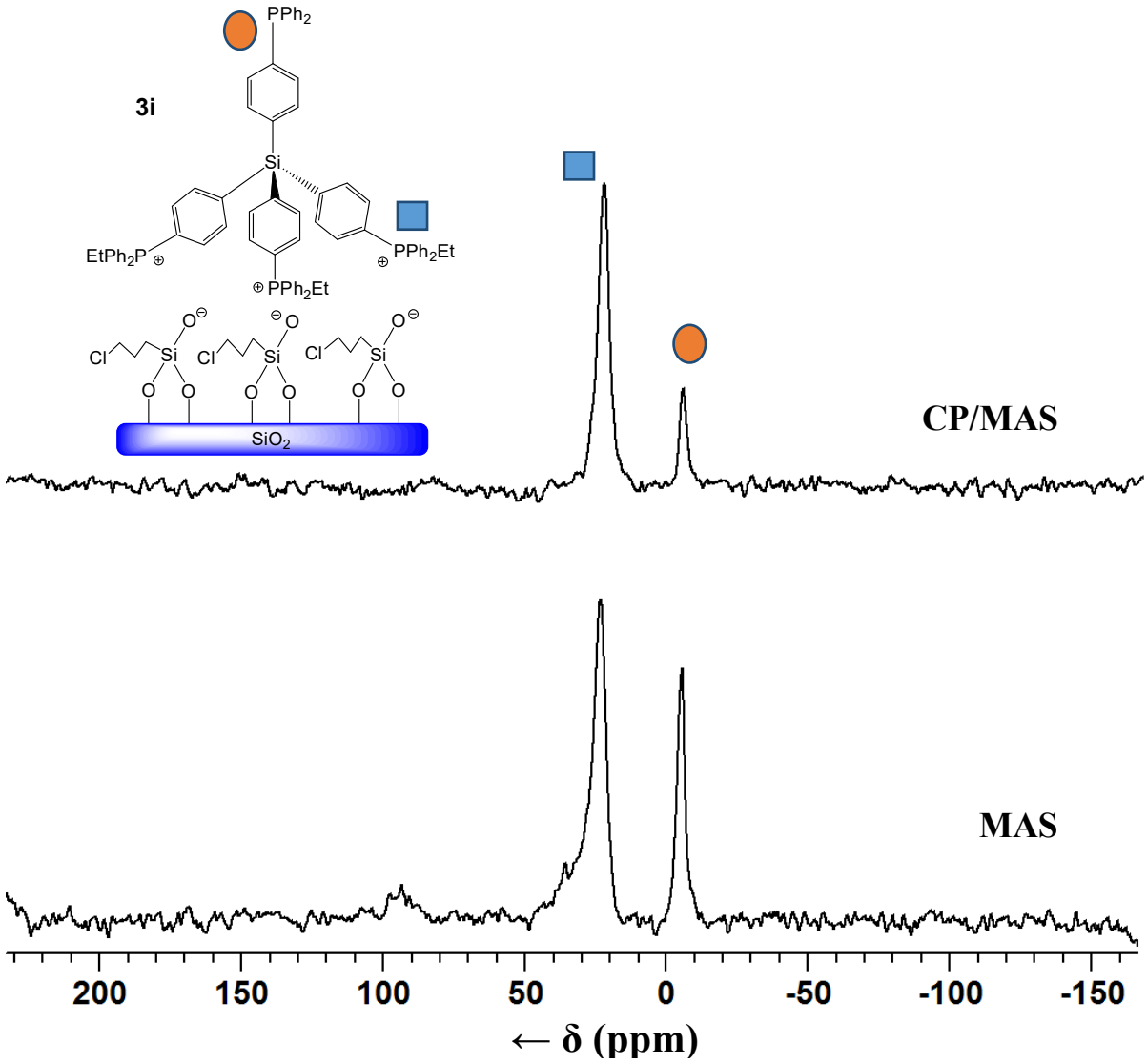

Figure 3.4 ^{31}P CP/MAS (top) and MAS (bottom) NMR spectra of **3i**. ν_{rot} = 10 kHz.

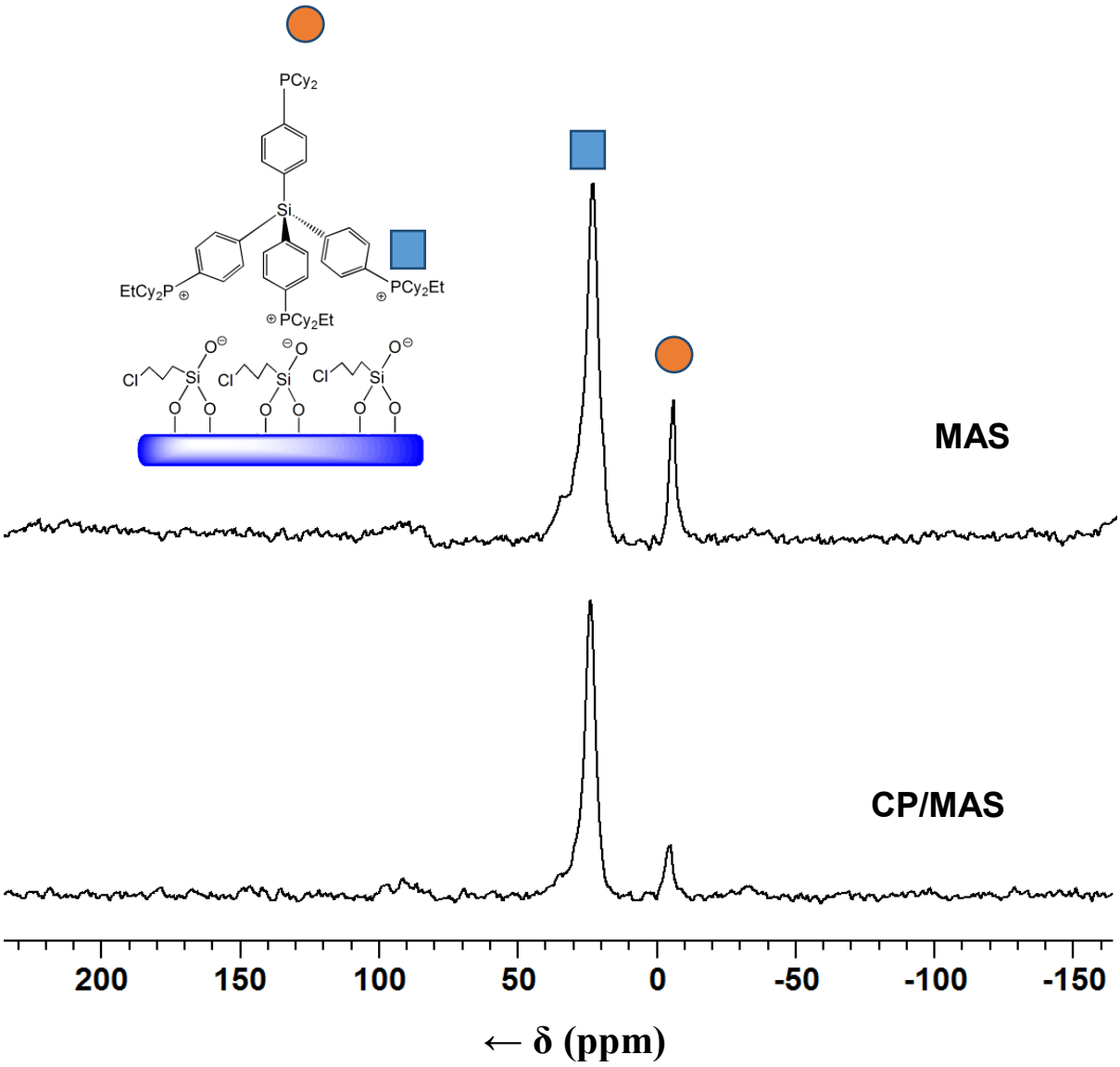

Figure 3.5 ^{31}P CP/MAS (bottom) and MAS (top) NMR spectra of **12i**. ν_{rot} = 10 kHz.

The two pulse programs mainly used in this thesis are simple high-power proton decoupling in combination with Magic Angle Spinning (MAS) and cross polarization/magic angle spinning (CP/MAS). Cross polarization involves the transfer of magnetization from the proton reservoir to phosphorus nuclei, resulting in shorter measurement times due to shorter recycle delays and higher intensities of the signals. The main drawback is that the relative

signal intensities are no longer reliable, as the ^{31}P nuclei closer to alkyl protons get a boost in intensity, while those with only aryl groups in the vicinity do not. MAS NMR spectra are recorded with no magnetization transfer and only high-power ^{1}H decoupling. Together with long relaxation delays MAS gives more reliable intensity data. This effect is experimentally known, and is demonstrated here in all Figures 3.4, 3.5, and 3.6, when comparing the intensities of signals stemming from ethylphosphonium and phosphine groups. Using CP/MAS, the signals of the ethylphosphonium groups around 25 to 30 ppm experience a boost in intensity, because the ethyl protons easily transfer their magnetization to the ^{31}P nucleus. The signals of the phosphine groups, where the ^{31}P nucleus is only surrounded by aryl protons, remain comparatively small. Only when MAS, in combination with a long recycle delay, is applied can a more accurate ratio of the signals, about 3 : 1, can be obtained spectroscopically.

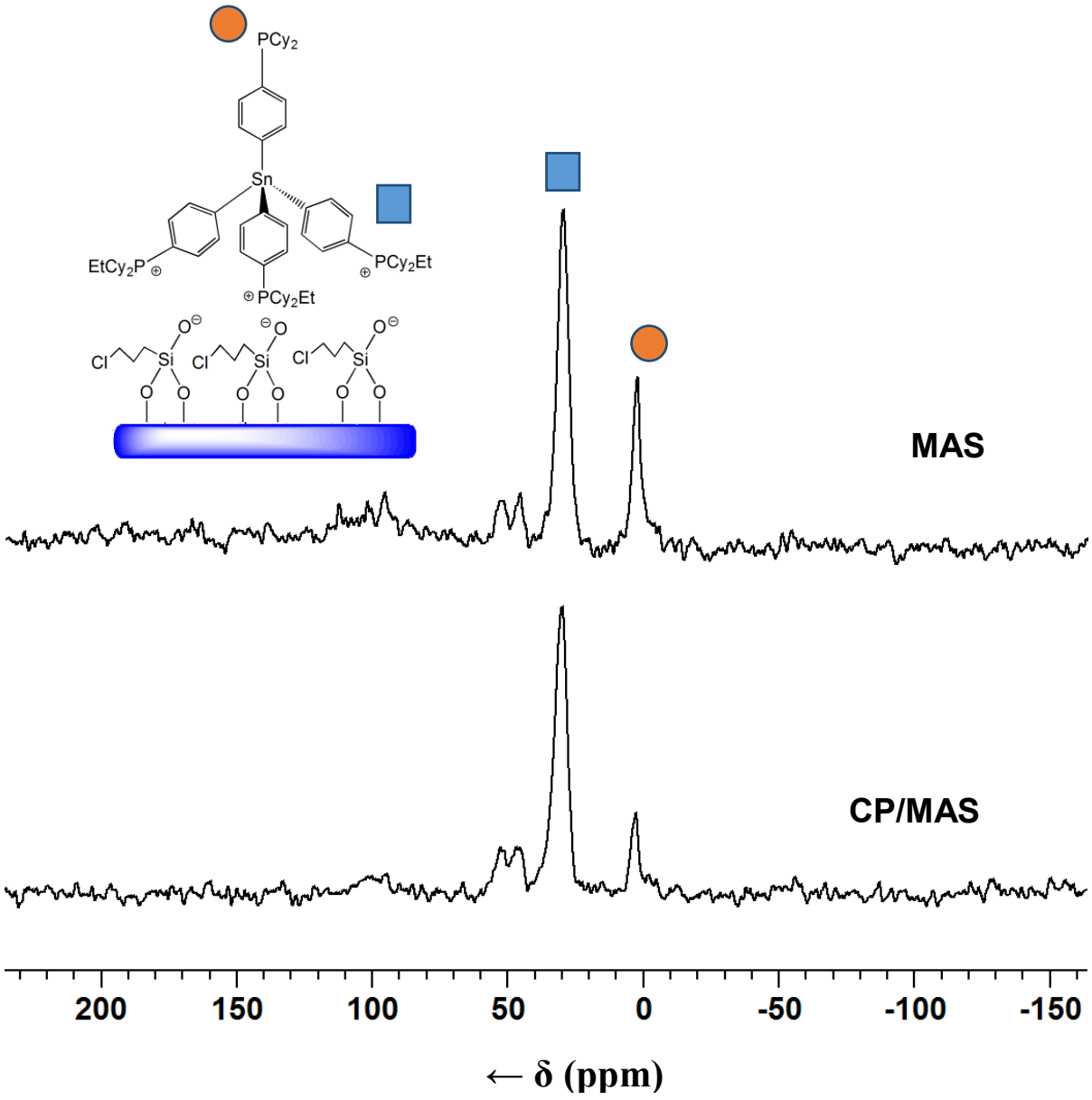

Figure 3.6 ^{31}P CP/MAS (bottom) and MAS (top) NMR spectra of **13i**. ν_{rot} = 10 kHz.

Concerning compound **18i**, it can be seen from the ^{31}P solid-state NMR spectrum in Figure 3.7 that the expected ^{31}P chemical shift of δ = -26.85 is attained,[46] resulting from the two equivalent free phosphine groups. There are no phosphonium peaks, as this compound is immobilized by reacting the silanol groups of the surface with the ethoxysilane compound **18**

to form a covalent bond, so phosphorus is not involved in the immobilization. Figure 3.7 shows that **18i** has been generated successfully.

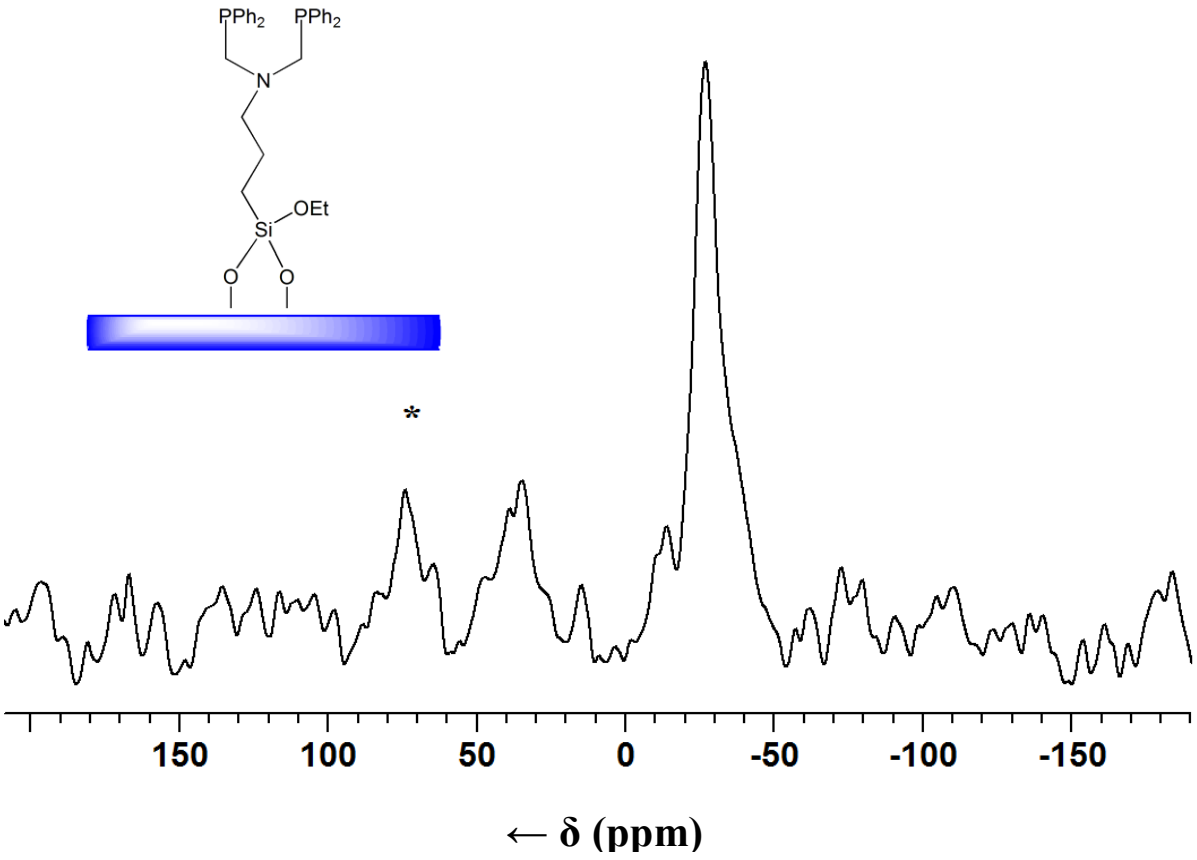

Figure 3.7 ^{31}P MAS NMR spectrum of **18i**. ν_{rot} = 6 kHz. The asterisk denotes a rotational sideband. The peak at δ = 37 ppm is a phosphine oxide impurity.

3.2.2 Solubility

A selection of four different methyltriarylphosphonium salts, as depicted in Scheme 3.2, was studied. These specific salts were chosen to test 1) how the anion affects solubility and 2) whether there would be any cooperative effects on the solubility which may result from having four phosphonium moieties within one molecule. From the results outlined in

Table 3.2 and depicted in Figure 3.8, one can see that nonpolar solvents are basically unable to dissolve these inorganic salts. As the polarity of the solvent increases, the salt generally becomes more soluble. However, DMSO and acetonitrile are less solubilizing than the protic solvent methanol.

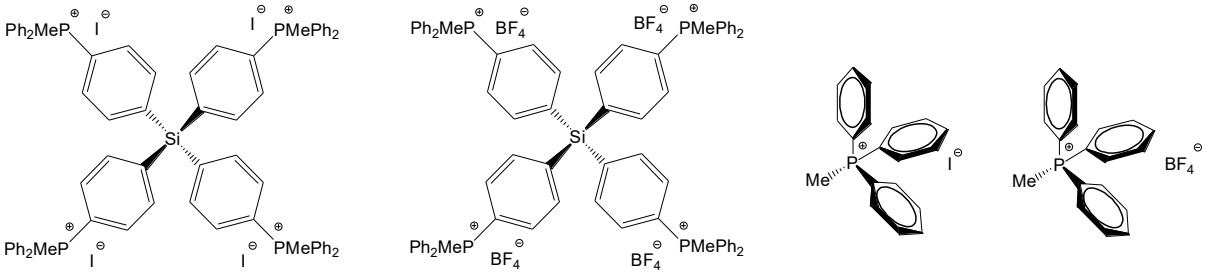

Scheme 3.2 Four representative phosphonium salts for solubility tests in various solvents.

In general, one expected result is that the tetraphosphonium salts are less soluble than their corresponding monophosphonium analogs. This is understandable, given that there are four ionic moieties in one molecule. It is also evident, given the similarity of solubilities of mono- and tetraphosphonium salts relative to a solvent, that there is no intramolecular cooperative effect between the phosphonium groups that would diminish the polarities of the molecules.

Table 3.2 Solubility data of phosphonium salts in various solvents.

	Solubility (mg/mL)			
	$[MePPh_3]^+ I^-$	**$[MePPh_3]^+[BF_4]^-$**	**Compound 4**	**Compound 5**
Toluene	0.0004	0.0003	0.0002	0.0002
Ether	0.0013	0.0005	0.00024	0.00029
DCM	360	320	185	180
THF	0.52	0.73	0.387	0.281
Acetone	29	471	11.9	74
MeOH	527	391	140	136
MeCN	288	297	126	122
DMSO	177	172	83	83

Changing the anion from BF_4^- to I^- had very little effect for the same cation in a given solvent. An oddity in the results occurs with the discrepancy between the solubility of the phosphonium salts in acetone being much more soluble with a tetrafluoroborate counteranion as compared to an iodide anion (Table 3.2, Figure 3.8). It was suspected that the acetone contained traces of water, which resulted in hydrogen bonding between the water and the fluorine atoms. However, the solubilities remained unchanged even when using acetone that has been dried thoroughly. Therefore, the increased solubility is more likely the result of intermolecular interactions between the tetrafluoroborate anion and the acetone, although the nature of the interactions is unknown. It might be speculated that the nucleophilic fluorine atoms of the BF_4^- anions interact with the carbons of the CO groups in acetone.

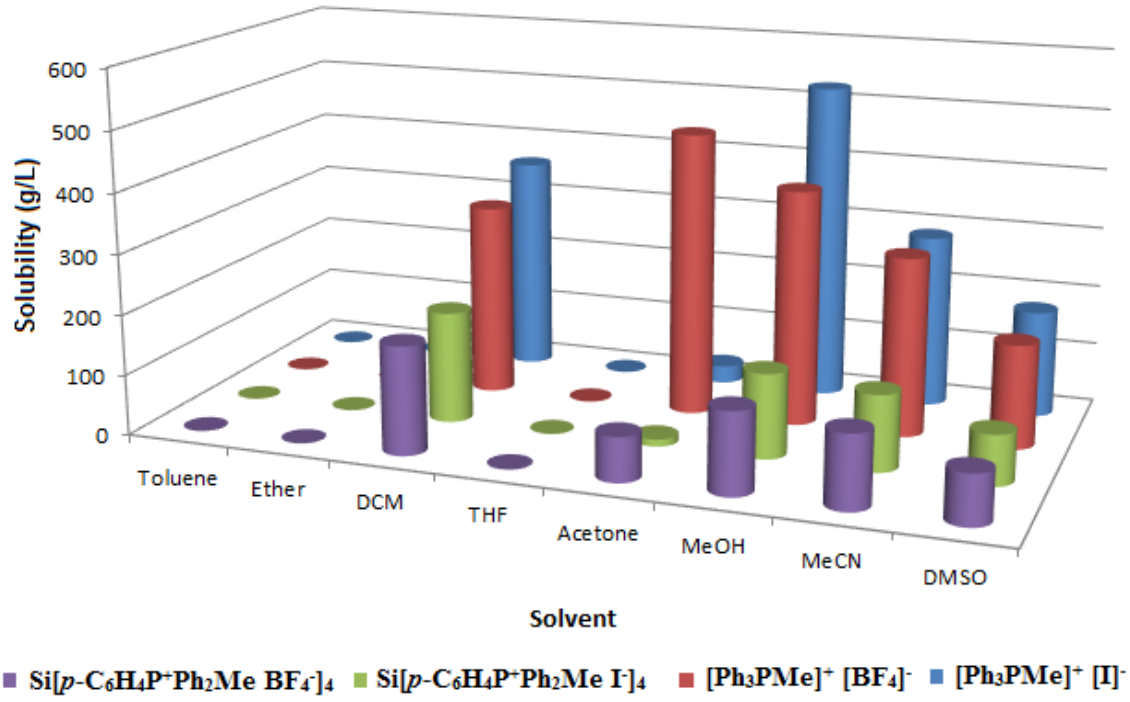

Figure 3.8 Solubilities of different phosphonium salts in selected solvents.

The data can also be compared with the dynamic properties of phosphonium salts on surfaces investigated by the Bluemel group previously.[8] The ^{31}P HRMAS spectra of the phosphonium salts in the presence of solvents were recorded. The halfwidths of the ^{31}P signals were determined, because in general a smaller halfwidth indicates a higher mobility. All mono- and tetraphosphonium salts were more mobile on the silica surface in the presence of polar solvents.[8] However, the nature of this motion remained unknown. If the salts were moving by being leached off of the surface into solution, then dropping back down, that should correlate with the solubility of the phosphonium salts.

As shown in Figure 3.8 the solubilities of phosphonium salts generally correlate with solvent polarity, as would be expected. However, any correlation with the surface mobilities determined by ^{31}P HRMAS is not obvious.[8] DMSO results in the highest surface mobility,[8]

but the phosphonium salts are only about half as soluble in this solvent as in methanol. Additionally, dichloromethane, THF, and acetone lead to similar mobilities, but they display very different solubilizing qualities. Based on this comparison, it can be concluded that the hopping motion (Figure 3.3) is not the primary form of surface mobility, and that the mobility of the phosphonium salts is likely some combination of translational motion, spinning, and rolling on the surface.

3.2.3 Leaching

Information about the interactions of the phosphonium groups with the surface is vital with respect to later potential leaching issues of the catalysts. Previously, the Bluemel research group has measured the HRMAS spectrum of the Sn analog of the immobilized species **3i**.[8] No signal has been observed, meaning that phosphines immobilized using SiO_2 and ethoxysilanes exhibit no mobility on the surface, even in the presence of a solvent.

The next question is whether any solvent is capable of leaching the scaffold from the support. Previous results indicate that phosphonium salts impregnated on the surface of the SiO_2 remain adsorbed in the presence of nonpolar and aprotic solvents. However, the phosphonium salts are washed off by more polar solvents.[8] This would only apply to impregnated phosphonium salts, where the anion is not covalently bound to the surface. It remains to be seen if this applies even to phosphonium salts immobilized on the surface using ethoxysilanes.

^{31}P NMR was used to measure the amount of leached phosphorus species in the supernatant solutions. A constant amount of **3i** was placed in an NMR tube, along with a given volume of a solvent. For all solvents, this was done in the same NMR tube. 16 hours

were allowed to give the solvent an opportunity to leach the linker off of the support. Then a capillary containing chlorodiphenylphosphine was placed in the center of the NMR tube as a chemical shift and intensity standard. By measuring the intensity of the signal of the phosphonium peaks that result in the supernatant and comparing them to a calibration curve, it should be possible to analyze the amount of phosphonium salt leached off from the support.

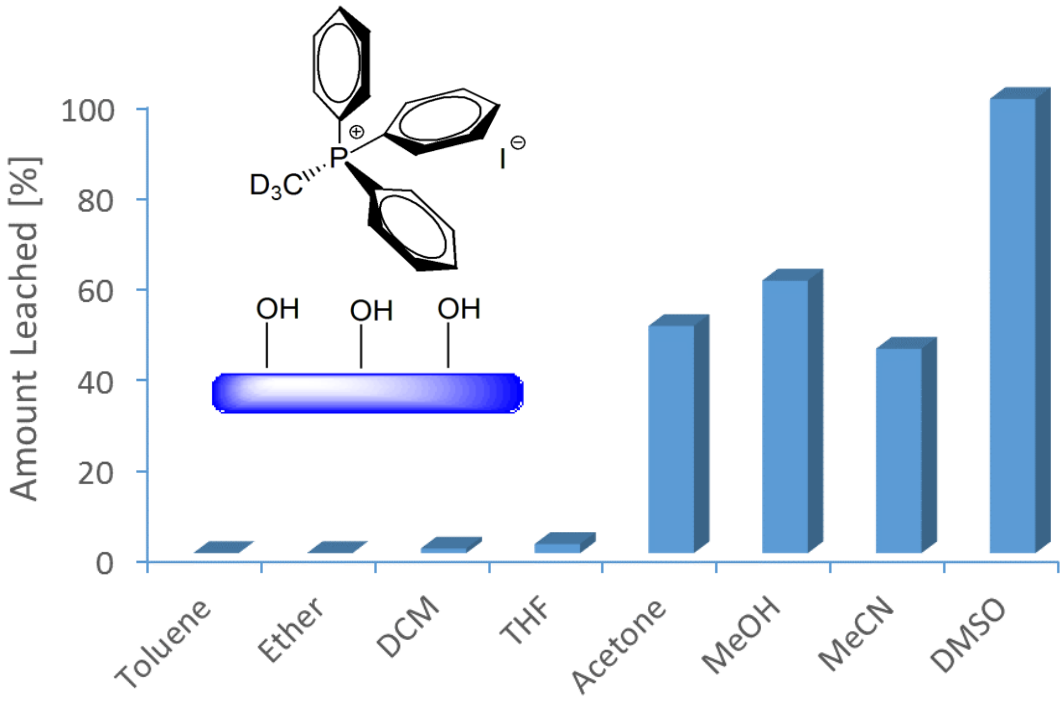

Figure 3.9 Leaching studies of impregnated phosphonium salts on the surface of silica.[8]

Eight solvents have been tested on **3i** with a range of polarities: toluene, diethyl ether, dichloromethane, THF, acetone, methanol, acetonitrile, and DMSO. ^{31}P NMR shows no signal for any of the supernatants (Figure 3.10). This is true even though the limit of detection for this method would be around 3% of the linker being leached off. This shows

that the linker scaffold is not leaching into the solvent and should also stay on the support during the catalytic runs.

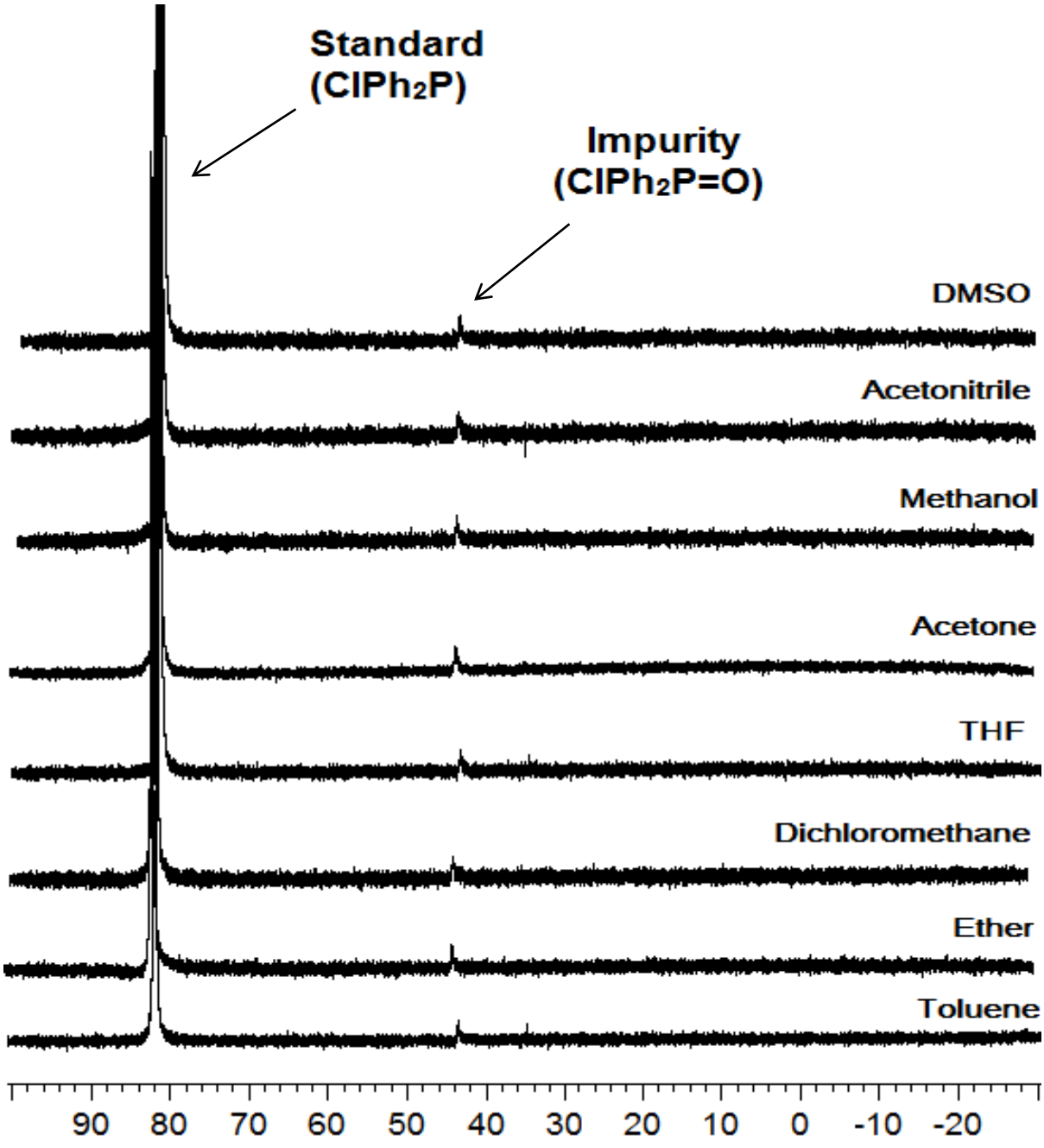

Figure 3.10 ^{31}P NMR spectra of the eight leaching experiments. No phosphonium peaks in the range of 20 to 30 ppm were detectable.

3.2.4 Dynamic Properties

From previous work in the group it is known that various compounds, including alkanes, fullerenes, and metallocenes can be mobile on favorable surfaces.[55] In contrast, compounds which cannot align with the surface of the support due to steric reasons, such as tetraphenylmethane, dicarbonyl bis(triphenylphosphine)nickel, and triptycene, are immobile on the surface of silica. [55]

Based on this, it is not expected that compound **16**, a tetradeuterated derivative of tetraphenyltin, which is very similar sterically to tetraphenylmethane, would be mobile on the surface. However, after adsorbing an excess of compound **16** onto silica by removing solvent from a dissolved suspension of **16** with silica, ^{2}H solid-state NMR reveals the formation of an intensive center signal without rotational sidebands (Figure 3.11), indicative of translational movement of the substance on the surface which leads to the elimination of quadrupolar interactions.[55b] In the figure, there is an excess of **16** relative to the amount of silica needed to form a monolayer, which means there is still some polycrystalline **16** left in the sample. This is why there are sidebands in addition to the isotropic peak at $\delta = 7.84$, the presence of which is very apparent in Figure 3.11. It remains unknown why this molecule moves on the surface, given that similar molecules and the analogous deuterated tetraphenylmethane do not, or what type of motion is occurring. One explanation could be that tetraphenyltin reacts with the silica surface, forming deuterated benzene, for example, by hydrolysis. Planar aromatic systems and benzene in particular are very mobile on silica surfaces and this could result in the narrow signal observed (Figure 3.11). However, after washing the silica, compound **16** was recovered, as confirmed by solution NMR measurements.

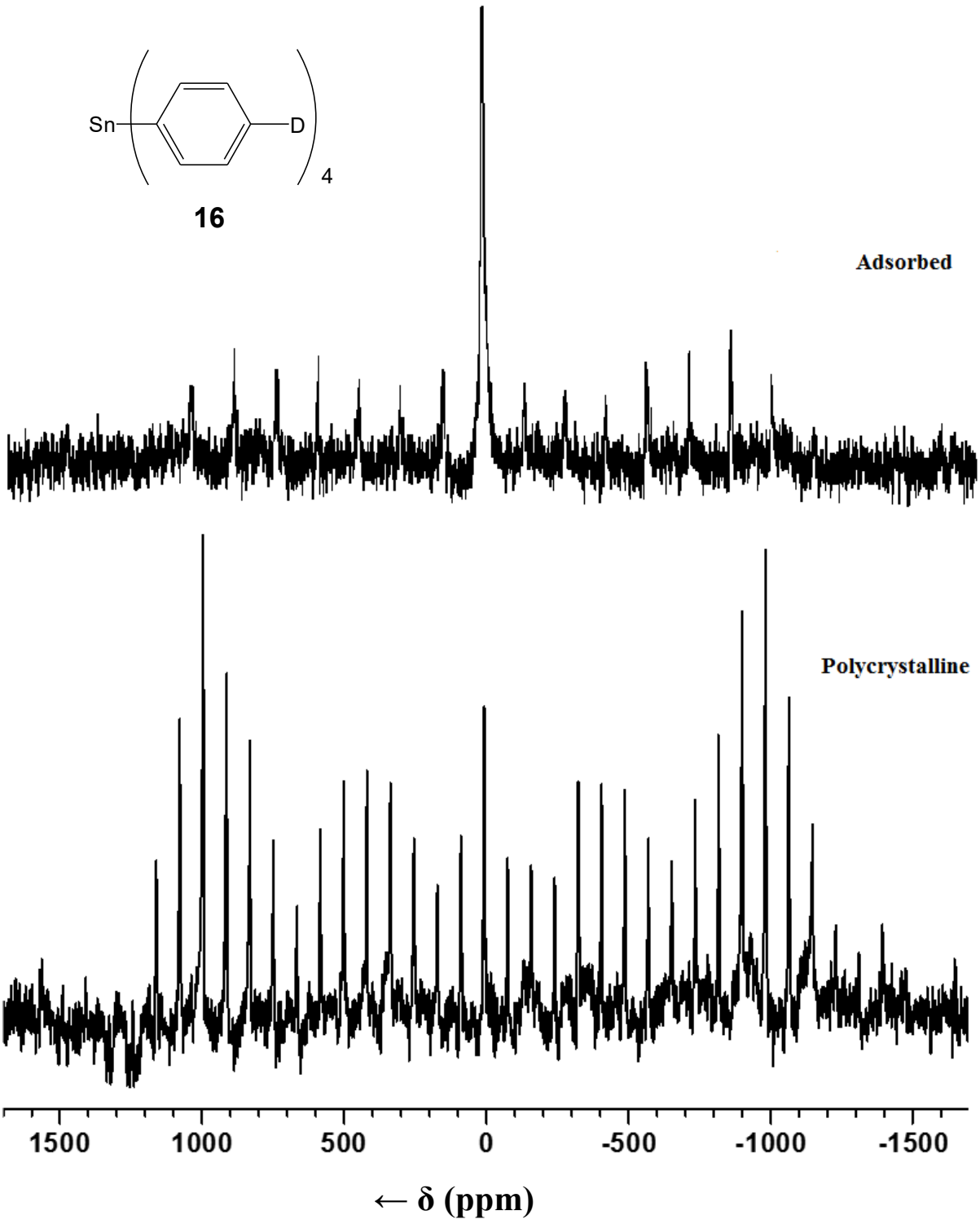

Figure 3.11 ^{2}H MAS spectrum (Hahn Echo) of polycrystalline compound **16** (bottom) and compound **16** adsorbed on silica (top). The excess of the compound remains polycrystalline material, which accounts for the sidebands.

3.3 Conclusion

The tetraphosphine scaffolds synthesized in chapter II can be immobilized onto silica using ethoxysilanes. ^{31}P solid-state NMR confirms the immobilization is occurring via three immobilized phosphonium groups, leaving one free phosphine that will eventually be coordinated to a catalyst or transformed into a reagent. The chelating compound **18** has been synthesized and immobilized for comparison with the monophosphines of the surface-bound scaffold linkers.

Monophosphonium salts are mobile on surfaces in the presence of solvents. To determine the modes of mobility, four salts were checked regarding their solubility, and whether this correlates with the ^{31}P HRMAS linewidths. There was no strong correlation, and therefore the hopping mechanism could be ruled out with respect to the surface mobility of phosphonium salts.

Furthermore, while simply impregnated phosphonium salts can be leached off the surface, they are not detached after being immobilized with ethoxysilanes, as in these cases the counteranions are covalently tethered to the support. This was demonstrated by placing batches of **3i** in eight different solvents, where less than 3% leaching occurred, even in very polar solvents like DMSO, as determined by ^{31}P NMR.

Finally, the tetradeuterated derivative of tetraphenyltin, **16**, was found to be mobile on the silica surface. ^{2}H solid-state NMR revealed the formation of an intensive center signal without rotational sidebands, indicative of translational mobility of the substance on the surface which leads to the elimination of quadrupolar interactions.

3.4 Experimental Section

3.4.1 General Information and Procedures

The ^{1}H, ^{13}C, and ^{31}P NMR spectra of liquids were recorded at 499.70, 125.66, and 470.17 MHz on a 500 MHz Varian spectrometer and referenced as follows. ^{1}H: residual internal $CHCl_3$ (δ, 7.26 ppm) or benzene-d_6 (δ, 7.16 ppm); ^{13}C: internal $CDCl_3$ (δ, 77.23 ppm) or benzene-d_6 (δ, 128.06 ppm). ^{31}P NMR spectra are referenced to neat Ph_2PCl (δ, 81.92 ppm) which is placed in a capillary centered in the NMR sample tube. The ^{13}C and ^{31}P NMR spectra are recorded with ^{1}H decoupling if not stated otherwise.

All reactions are carried out using standard Schlenk techniques and a purified N_2 atmosphere, if not stated otherwise. Reagents purchased from Sigma Aldrich or VWR are used without further purification. Toluene, diethyl ether, and THF are dried by boiling them over Na, distilled, and stored under N_2. CH_2Cl_2 is obtained from a solvent purification system. Acetonitrile, acetone, and methanol are recondensed and dried over molecular sieves (3 Å pore size). DMSO is degassed and dried over molecular sieves (3 Å pore size). The silica (Merck, 40 Å average pore diameter, 0.063 to 0.2 mm average particle size, specific surface area 750 m^2/g) is rigorously dried in vacuo at 250 °C for 4 days to remove adsorbed water and condense surface silanol groups.

3.4.2 Instruments and Measurements

The solid-state NMR spectra are measured with a Bruker Avance 400 widebore NMR spectrometer with a multinuclear 4 mm MAS probehead. For the ^{31}P CP/MAS and MAS measurements ^{1}H high-power decoupling was applied. For ^{29}Si, the Hartmann-Hahn matching condition was optimized using tetrakistrimethylsilylsilane at 5 kHz, and for ^{31}P, the

Hartmann-Hahn matching condition was optimized using sodium monohydrogen phosphate. The recycle delays are 5 s for CP/MAS and 10 s for MAS spectra. For the ^{2}H Hahn-Echo measurements, liquid D2O was used as a standard, and the recycle delay was 2 s.

3.4.3 General Procedure for Solubility Measurement

A weighed amount of a phosphonium salt is placed in a vessel. Using a micropipette, one of the eight solvents is added until all of the solid is dissolved, and the total volume needed is recorded.

3.4.4 Immobilization of Tetraphosphine Scaffold 3

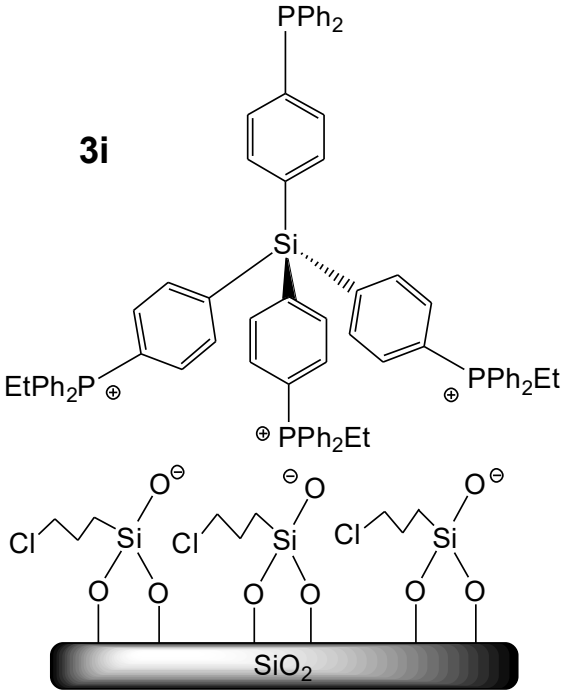

Tetraphosphine linker **3** (0.059 g, 0.055 mmol) is dissolved in toluene (50 mL). This solution is added to a suspension of SiO_2 (1.483 g) in toluene (10 mL). An excess of 3-chloropropyltriethoxysilane (1.31 mL, 5.51 mmol, 100 eq.) is added, and the flask is sealed

and vented. The reaction mixture is heated for 6 d at 100 °C. Then the flask is cooled to RT and the solid is allowed to settle. The solution is decanted, and the product **3i** is washed with toluene (2x, 40 mL), leaving the pure product **3i** (1.506 g, 3.0 particles/100 nm^2, 48 mg/g, 0.045 mmol/g). No phosphorus signal is observed in the supernatant by ^{31}P NMR.

3.4.5 Immobilization of Tetraphosphine Scaffold 12

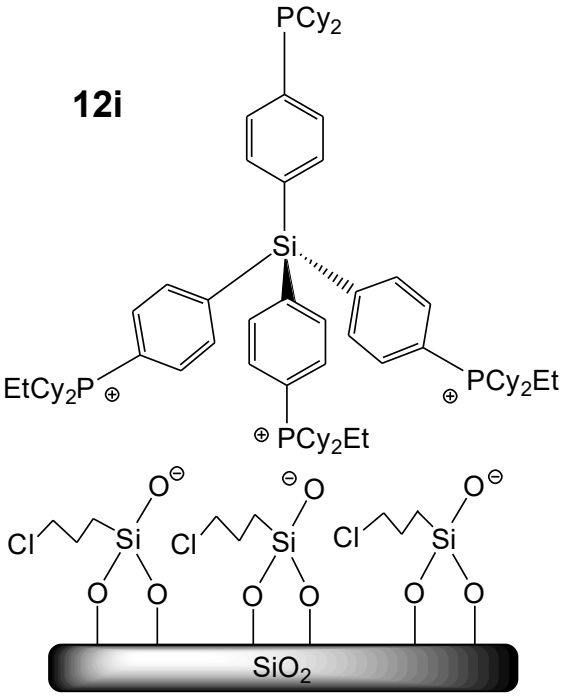

Tetraphosphine linker **12** (0.071 g, 0.063 mmol) is dissolved in toluene (50 mL). This solution is added to a suspension of SiO_2 (1.343 g) in toluene (10 mL). An excess of 3-chloropropyltriethoxysilane (3.00 mL, 12.5 mmol, 198 eq.) is added, and the flask is sealed and vented. The flask is then heated for 6 d at 100 °C. Subsequently, the flask is cooled to RT and the modified silica is allowed to settle. The solution is decanted, and the product **12i** is washed with toluene (2x, 40 mL), resulting in the product **12i** (1.137 g, 3.8 particles/100 nm^2, 47 mg/g, 0.042 mmol/g). No phosphorus signal is observed in the supernatant by ^{31}P NMR.

3.4.6 Immobilization of Tetraphosphine Scaffold 13

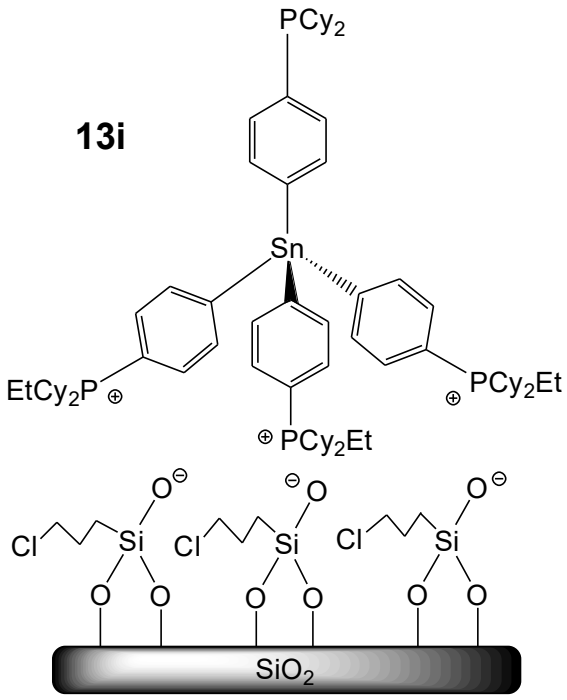

Tetraphosphine linker **13** (0.082 g, 0.068 mmol) is dissolved in toluene (50 mL). This solution is added to a suspension of SiO_2 (1.673 g) in toluene (10 mL). An excess of 3-chloropropyltriethoxysilane (3.00 mL, 12.5 mmol, 184 eq.) is added, and the flask is sealed and vented. The reaction mixture is then heated for 6 d at 100 °C. After this time, the flask is cooled to RT and the insoluble material is allowed to settle. The supernatant is decanted, and the product **13i** is washed with toluene (2x, 40 mL), yielding the product **13i** (1.972 g, 3.2 particles/100 nm^2, 42 mg/g, 0.034 mmol/g). No phosphorus signal is observed in the supernatant by ^{31}P NMR.

3.4.7 Immobilization of Chelate Phosphine 18

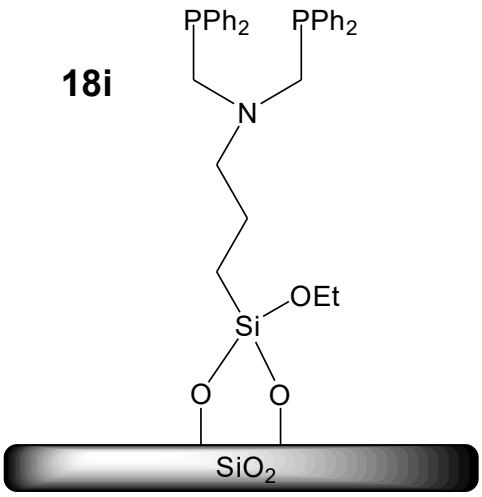

Phosphine **18** (0.056 g, 0.091 mmol) is dissolved in toluene (50 mL). This solution is added to a suspension of SiO_2 (2.782 g) in toluene (10 mL). The flask is sealed and vented. The reaction mixture is then heated for 3 d at 60 °C. After this time, the flask is cooled to RT and the solid is allowed to settle. The supernatant is decanted, and the product **18i** is washed with toluene (2x, 50 mL), resulting in **18i** (2.925 g, 2.6 particles/100 nm^2, 19 mg/g, 0.031 mmol/g). No phosphorus signal is observed in the supernatant by ^{31}P NMR.

3.4.8 Representative Procedure for Leaching Measurements

0.100 g of the immobilized species **3i** are placed into an NMR tube and suspended in 0.500 mL of a chosen solvent. After waiting for 1h, the supernatant is removed and transferred to a new NMR tube. The capillary standard $ClPPh_2$ is added, and the NMR spectrum is obtained without locking or shimming. For all eight solvents, the same NMR tube and the same capillary standard were used. The integral of the phosphonium signal serves for quantifying the concentration of potentially leached material.

3.4.9 Adsorption of Compound 16 onto Silica

Compound **16** (0.102 g, 0.237 mmol) is dissolved in THF (20 mL). Wet SiO_2 (0.244 g) is added to this solution. The THF is then removed in vacuo, leaving compound **16** adsorbed onto SiO_2 (0.367 g, 77.7 particles/100 nm^2, 277 mg **16**/g, 0.64 mmol **16**/g)

CHAPTER IV

CATALYSTS IMMOBILIZED ON SILICA VIA RIGID TETRAPHENYLELEMENT SCAFFOLDS

4.1 Introduction

Catalysis is one of the most widely used and studied fields both in industry and academia. One of the most important catalytic chemical processes in the modern world is hydrogenation, as it plays a very important role in the petrochemical, medical, and food industries.[56]

The most common molecular hydrogenation catalysts is Wilkinson's catalyst, a Rh-based catalyst developed by Dr. Geoffrey Wilkinson. Wilkinson's catalyst, $ClRh(PPh_3)_3$, can also be used for the hydroboration or hydrosilylation of alkenes or the reduction of unsaturated carbonyl compounds, but its principal use is in the hydrogenation of alkenes. Wilkinson's catalyst, and similar Rh catalysts, remain among the most studied homogeneous catalysts for hydrogenation.[56]

In order to differentiate catalysts, it is necessary to draw a distinction between homogeneous and heterogeneous catalysts. Homogeneous catalysts are usually highly active and selective, in general well understood and characterized, and capable of fine tuning to a specific reaction. However, these same catalysts often decompose under the reaction conditions or during work-up and can only rarely be recovered and recycled for subsequent reactions. Alternatively, heterogeneous catalysts are often cheaper to produce and are very conveniently separated and reused. However, they are usually less active and selective due to the presence of many different species which display different activities and selectivities.

An immobilized catalyst combines the advantages of both homogeneous and heterogeneous catalysts. The idea is to tether a homogeneous catalyst to support materials such as zeolites, activated carbon, oxides like silica or alumina, or insoluble polymers. For most applications, silica turns out to be the most favorable support.[22] The immobilized catalyst, once tethered, can retain the selectivity and much of the reactivity of the homogeneous catalyst and overcome the problem of separation and recycling.

Immobilized species have had a major impact in such diverse areas as combinatorial chemistry, solid-phase synthesis, and catalysis. Therefore, they are of immense academic and industrial interest. Being recyclable, immobilized catalysts reduce energy and resource consumption, and help to make chemistry "greener". Many analytical methods are available that enable the researcher to characterize surface-bound catalysts, elucidate their mechanistic features, and thus direct the researcher to improved catalysts. The most useful methods are solid-state NMR, *in situ* IR spectroscopy, X-ray powder diffraction, electron microscopy, and methods for probing surface and particle characteristics.[15,42]

In industry, hydrogenation is catalyzed by heterogeneous late transition metals, like Ni or Pd. Although this is effective at fully hydrogenating alkenes, it also leads to double bond migration, as well as isomerization about the double bond if the alkenes are only partially hydrogenated, as depicted in Scheme 4.1. Wilkinson's catalyst, a homogeneous catalyst with its well defined reaction mechanism (Scheme 4.1, left), does not allow this, but it cannot be recycled after each batchwise run, and must be separated in tedious processes from the reaction product after catalysis. It is hoped that, by immobilizing Wilkinson's catalyst on silica, it will retain its selectivity and activity, while being easily separable from reaction mixtures and recyclable.

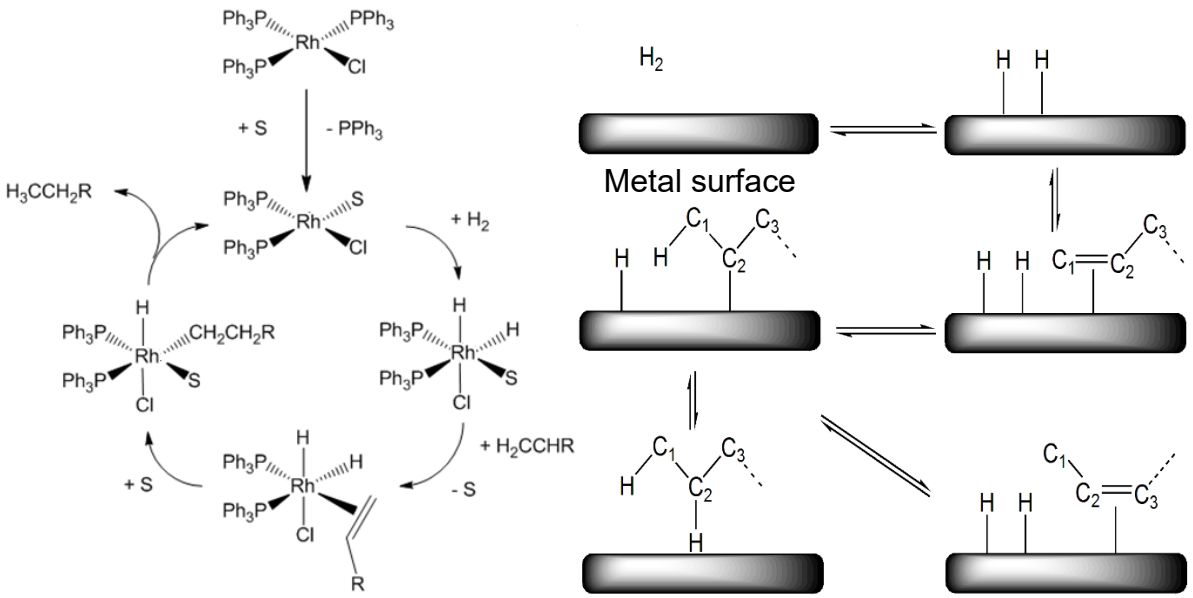

Scheme 4.1 Mechanism of hydrogenation of alkenes to alkanes with both the dihydride formation for homogeneous Wilkinson's catalyst (left) and the Langmuir-Hinshelwood mechanism using a metal surface as an example for a heterogeneous catalyst (right).

One potential complication that can occur during catalysis with immobilized Rh catalysts involves the formation of Rh nanoparticles. Previously, it has been observed that other derivatives of immobilized Wilkinson's catalyst bound with flexible linkers decompose to form Rh nanoparticles in the pores of the support material during catalysis.[1,4] It is believed that the principal pathway of decomposition for this is interaction of the catalyst with the surface of the silica support in combination with dimerization of the metal complexes.[13] Therefore, the rigid linker scaffolds presented here should be optimal to prevent this interaction. It is hoped that their unique tetrahedral sterics will prevent nanoparticle formation.

The major goals of this project are (1) to synthesize an immobilized version of Wilkinson's catalyst using a rigid tetraphenylelement linker on SiO_2, (2) to use the catalyst to perform hydrogenation of a representative alkene, and (3) to test the catalyst for recyclability

in a batchwise manner, optimally indefinitely without decomposition or byproduct formation of the catalyst.

4.2 Results and Discussion

4.2.1 General Aspects of Catalytic Hydrogenation

For hydrogenation, the alkene to be hydrogenated is 1-dodecene (Scheme 4.2), which is used for several reasons. First, it is an alkene that can be readily hydrogenated to form dodecane. Second, NMR can be used to monitor the reaction. Furthermore, due to the fact that the boiling point of 220 °C for both the alkene and alkane are too high to be removed *in vacuo*, determining exact yields without loss of starting material or product will be straightforward, for example, by GC. Due to the high boiling points NMR samples can simply be prepared by removing the solvent *in vacuo*, then adding a deuterated solvent. Third, by choosing a terminal alkene, double bond migration can be readily observed with NMR, as the chemical shifts of terminal alkenes are different from those of internal alkenes.

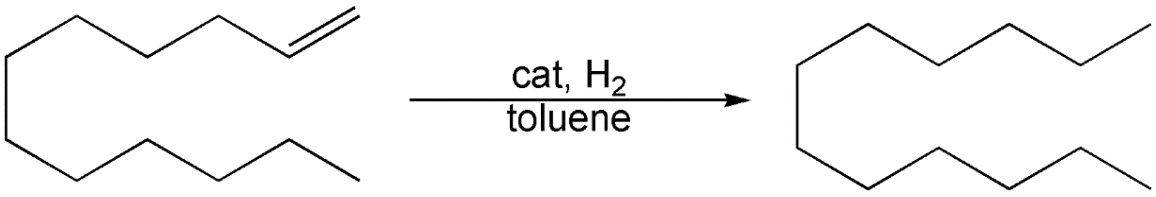

Scheme 4.2 Reaction scheme showing 1-dodecene being hydrogenated to dodecane in the presence of a catalyst.

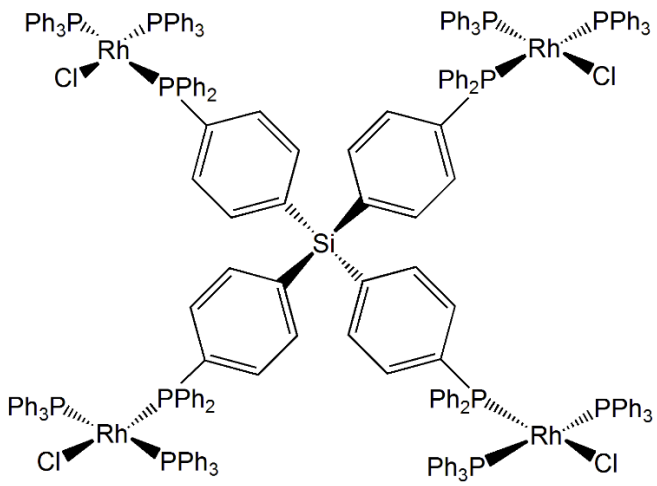

10

Scheme 4.3 Compound **10**, which is used to measure cooperative effects in hydrogenation using Wilkinson's catalyst.

4.2.2 Cooperative Effects

Wilkinson's catalyst is very active for hydrogenation, and its activity is dependent on its concentration in solution. However, it remains unclear if this is due to any cooperative effects of the catalyst which might occur at higher concentrations. In the case of four Rh centers bound to one rigid tetraphenylelement linker the question arises whether the presence of one Rh center on the scaffold affects the other Rh centers and whether there is a consequent difference in the catalytic activity. To test this, compound **3** was added to a batch of Wilkinson's catalyst, creating compound **10** (Scheme 4.3) and the hydrogenation was allowed to proceed under the standard conditions (see Experimental Section).[1,10,15] The data was then compared to those obtained from a catalytic run with an equal amount of Wilkinson's catalyst, along with one equivalent of added phosphine. The catalysis, summarized in Figure 4.1, shows no cooperative effects, as the catalytic characteristics are practically identical in both cases.

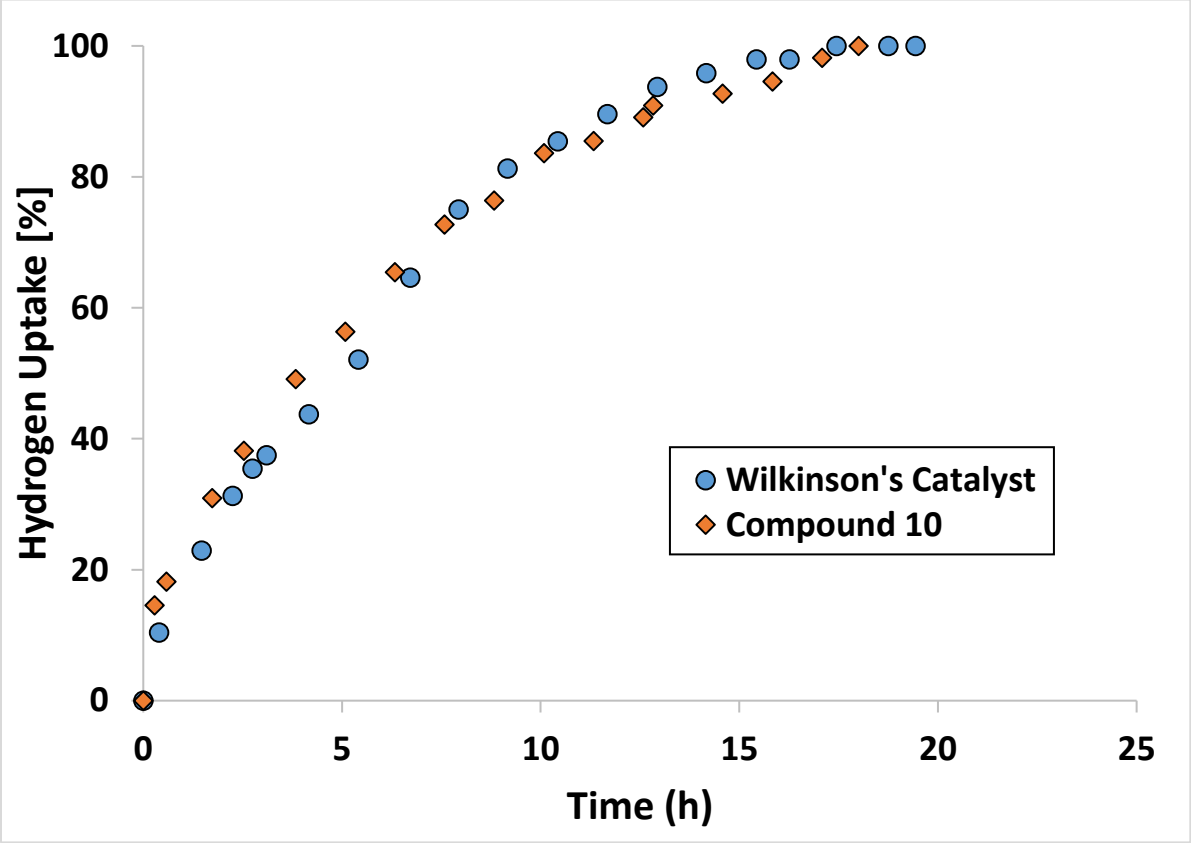

Figure 4.1 Hydrogenation of 1-dodecene using Wilkinson's catalyst with added compound **3**, compared with hydrogenation of 1-dodecene using Wilkinson's catalyst with an equal amount of added triphenylphosphine.

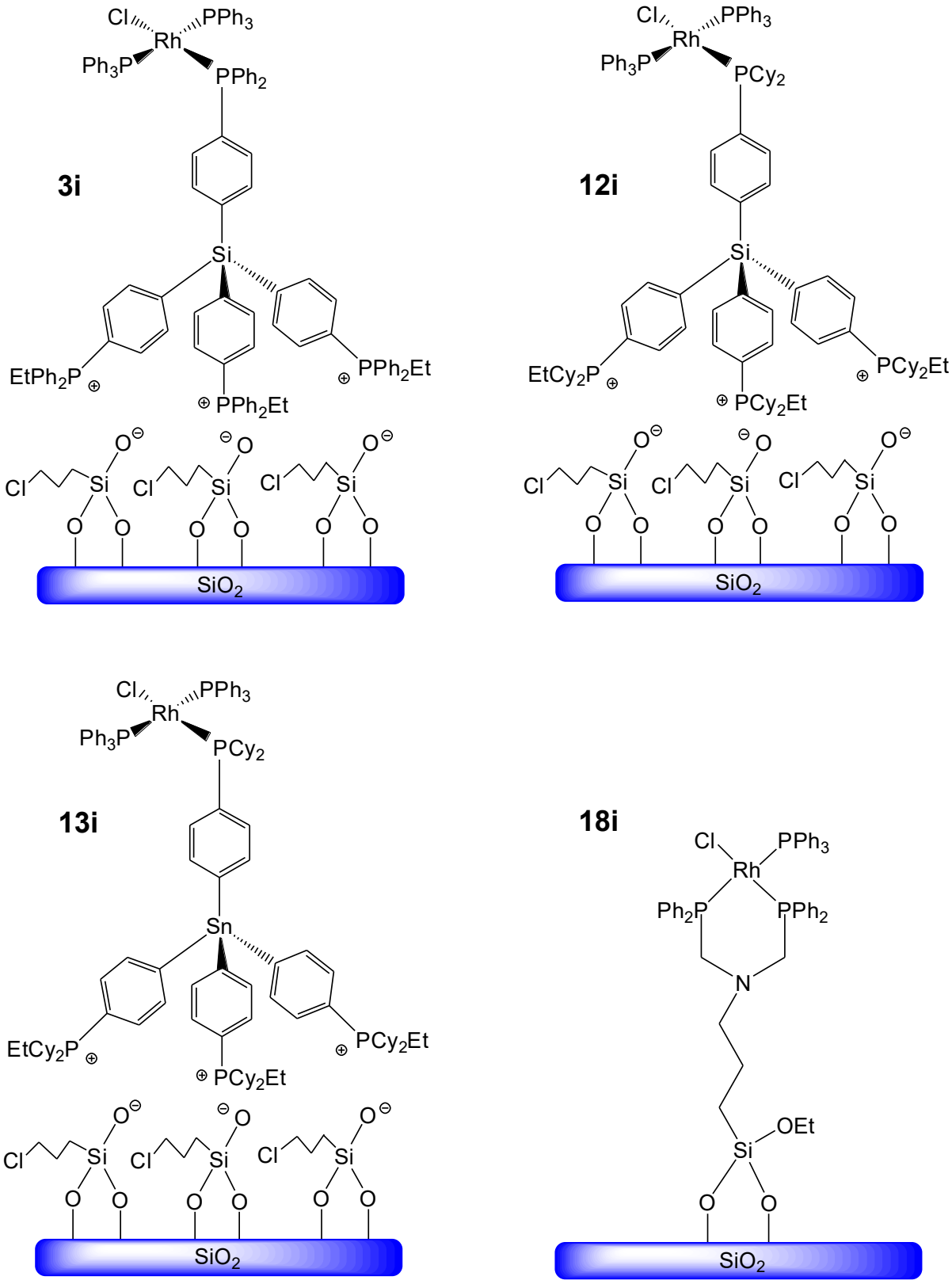

Scheme 4.4 Immobilized Wilkinson-type catalysts **3iRh**, **12iRh**, **13iRh**, and **18iRh**.

4.2.3 Synthesis of Immobilized Catalysts

The immobilized catalysts **3iRh**, **12iRh**, **13iRh**, and **18iRh** (Scheme 4.4) can be generated by ligand exchange with Wilkinson's catalyst starting from the immobilized linker scaffolds. Hereby, the catalyst attaches to the linker via phosphine ligand exchange, as the phosphine of the linker replaces a triphenylphosphine ligand of Wilkinson's catalyst. The released PPh_3 can be removed from the solid product by washing with toluene.

4.2.4 Characterizing the Immobilized Catalysts

All immobilized Wilkinson-type catalysts could be characterized by solid-state NMR spectroscopy, as described above for the immobilized linkers. The signals of immobilized metal complexes are in general broader due to the presence of trace amounts of paramagnetic impurities. Furthermore, in the case of Wilkinson's catalyst several magnetically slightly different ^{31}P environments come into existence, which leads to overlapping signals. However, the characteristic patterns of immobilized Wilkinson-type complexes are known from earlier work,[35] and the presence of phosphine oxides or other byproducts can still be excluded.

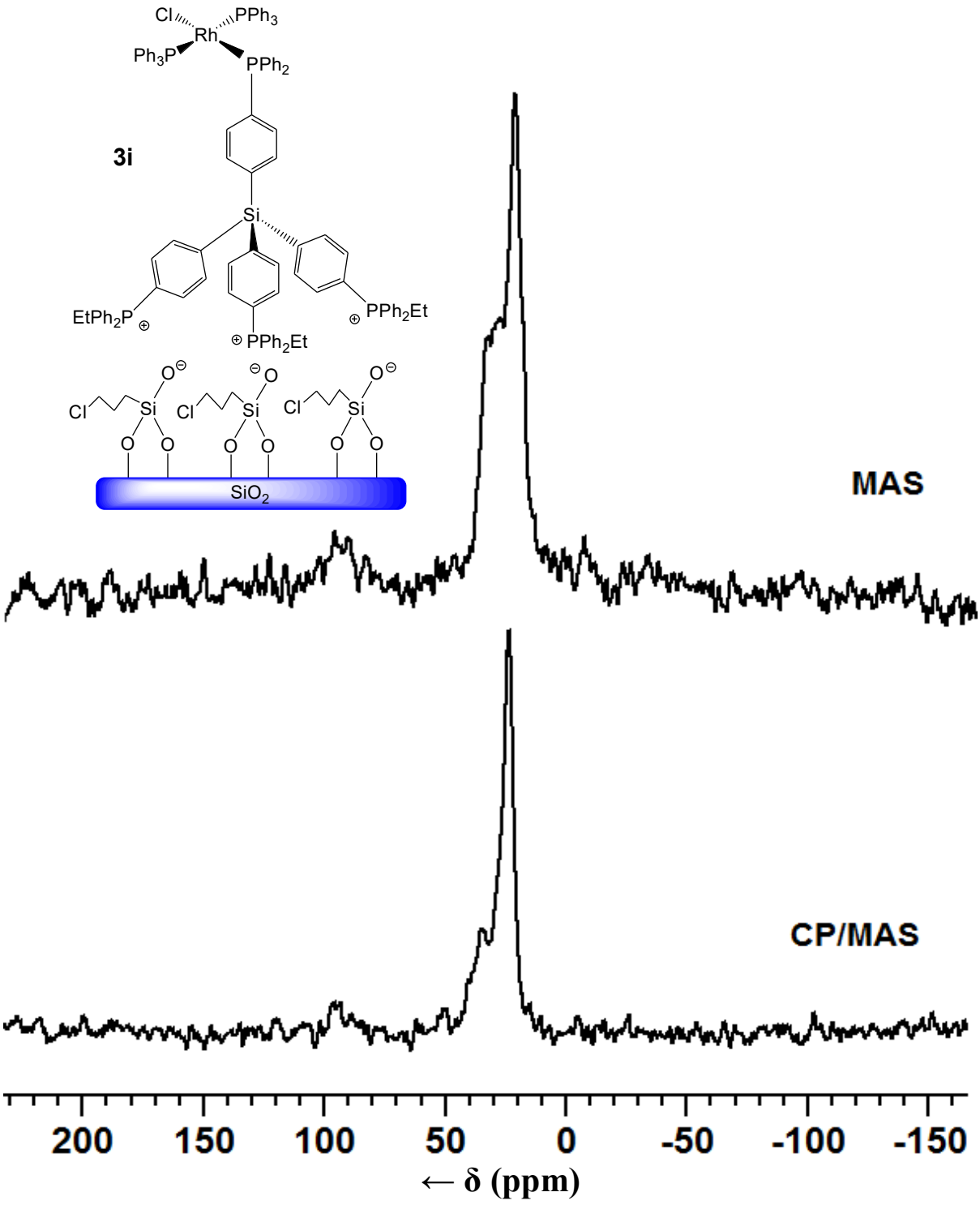

Figure 4.2 ^{31}P CP/MAS (bottom) and MAS (top) NMR spectra of **3iRh**. Rotational speed 10 kHz.

As can be seen from the ^{31}P solid-state NMR spectra shown in the previous chapter, material **3i** contains three phosphonium groups (δ = 23 ppm), along with one free phosphine (δ = -5 ppm). There is a small shoulder downfield from the phosphonium peak, representing a phosphine oxide impurity accrued during the immobilization of the linker or the measurement. After adding Wilkinson's catalyst, it is observed that the free phosphine peak disappears, leaving three overlapping peaks (Figure 4.2). Besides the signal from traces of phosphine oxide, the phosphonium resonance, and the signals of phosphines coordinated to Rh are compiled at around δ = 25 ppm. This result is in agreement with earlier descriptions[35] and it confirms that the ligand exchange and generation of the immobilized catalyst **3iRh** have taken place. As another indicator for the successful immobilization, the color of the silica support changed from white to bright orange, indicative of the presence of an originally wine red Rh(I) complex on the surface.

For **12iRh**, the ^{31}P NMR peaks shift, as the phenyl groups attached to the phosphine group are replaced by cyclohexyl groups (Figure 4.3). The immobilized version of the linker **12i** contains three phosphonium groups (δ = 29 ppm), along with one free phosphine (δ = 2 ppm), as described in the previous chapter. After adding Wilkinson's catalyst, it is observed that the signal of the uncoordinated phosphine disappears, leaving three overlapping resonances around δ = 28 ppm. These stem from traces of phosphine oxide, the surface-bound phosphonium groups, and the phosphine coordinated to Rh. The absence of the phosphine and the characteristic shift of the resonance of the metal bound phosphine group confirm that the ligand exchange was quantitative and the immobilized metal complex **12iRh** had formed. For this material, compared to **3iRh**, there is a slightly larger phosphine oxide peak, as cyclohexyl phosphines are more oxygen-sensitive than phenyl phosphines due to

increased electron donation from the cyclohexyl groups to phosphorus. This results in a more basic compound, which reacts with ambient oxygen more readily. This same increase in basicity also means the ligand exchange proceeded easier than for **3iRh**, as the linker binds to the Rh center more strongly. The color change of the support from white to orange once again corroborates the assumption that **12iRh** has been generated successfully.

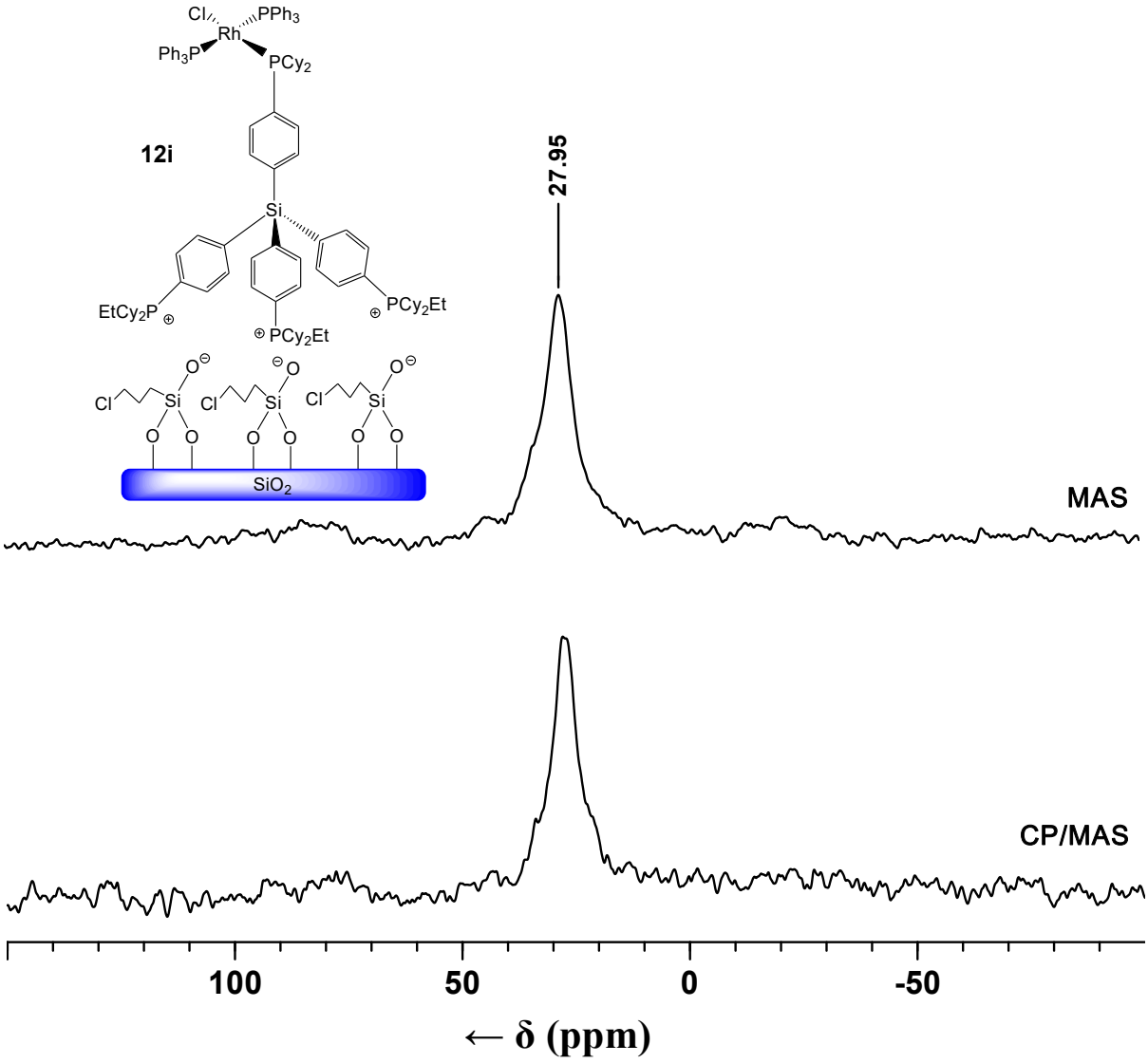

Figure 4.3 ^{31}P CP/MAS (bottom) and MAS (top) spectra of **12iRh**. Rotational speed 10 kHz.

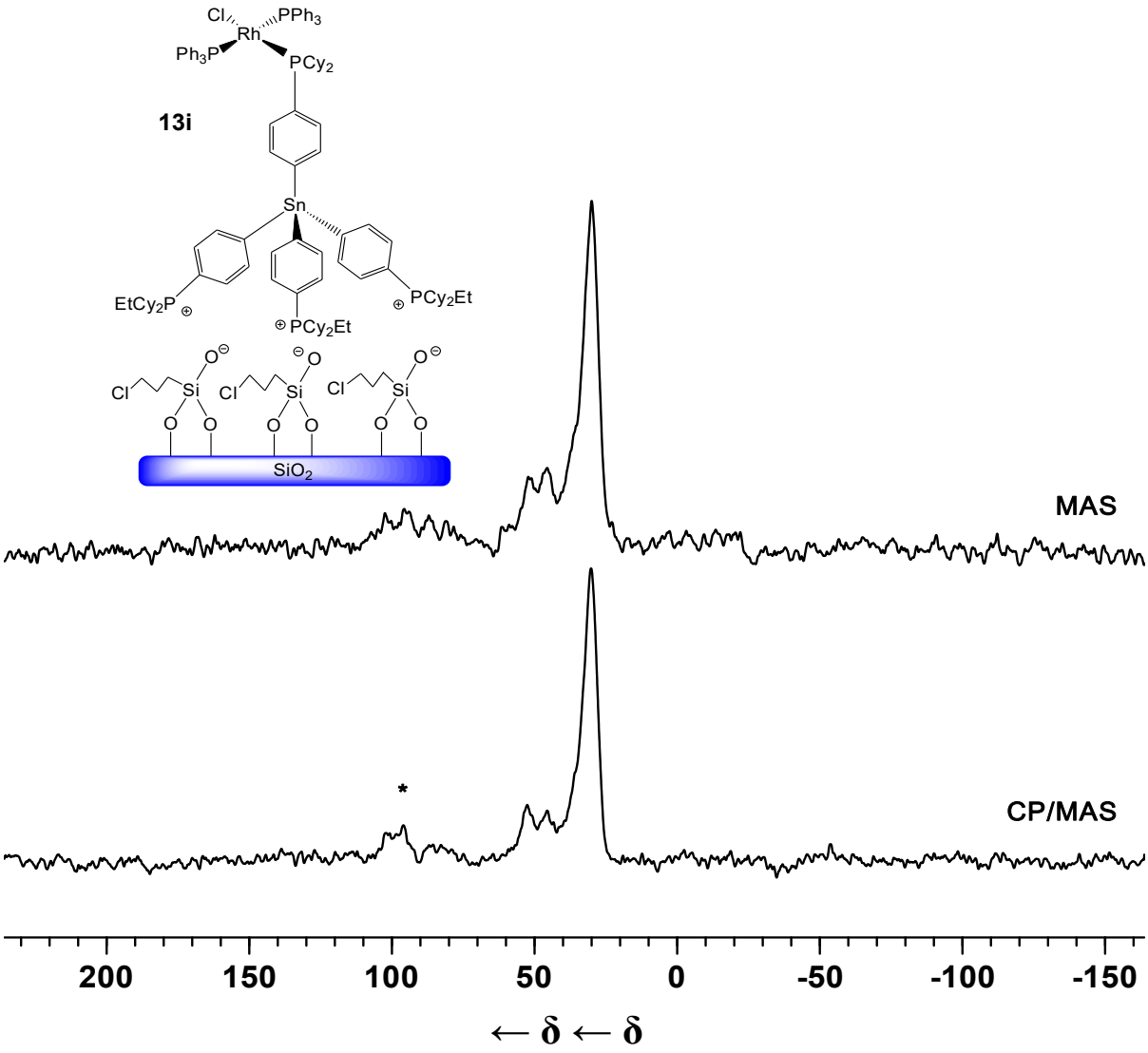

Figure 4.4 ^{31}P CP/MAS (bottom) and MAS (top) spectra of **13iRh**. Rotational speed 10 kHz.

13iRh was synthesized from **13i** using the same procedure as applied for the other two rigid scaffolds **3iRh** and **12iRh**. The ^{31}P solid-state NMR chemical shifts are almost identical to those of **12iRh**, as the compounds have similar substituents at phosphorus (Figure 4.4). The disappearance of the free phosphine peak, as well as the characteristic color change of the material after the ligand exchange, were again observed.

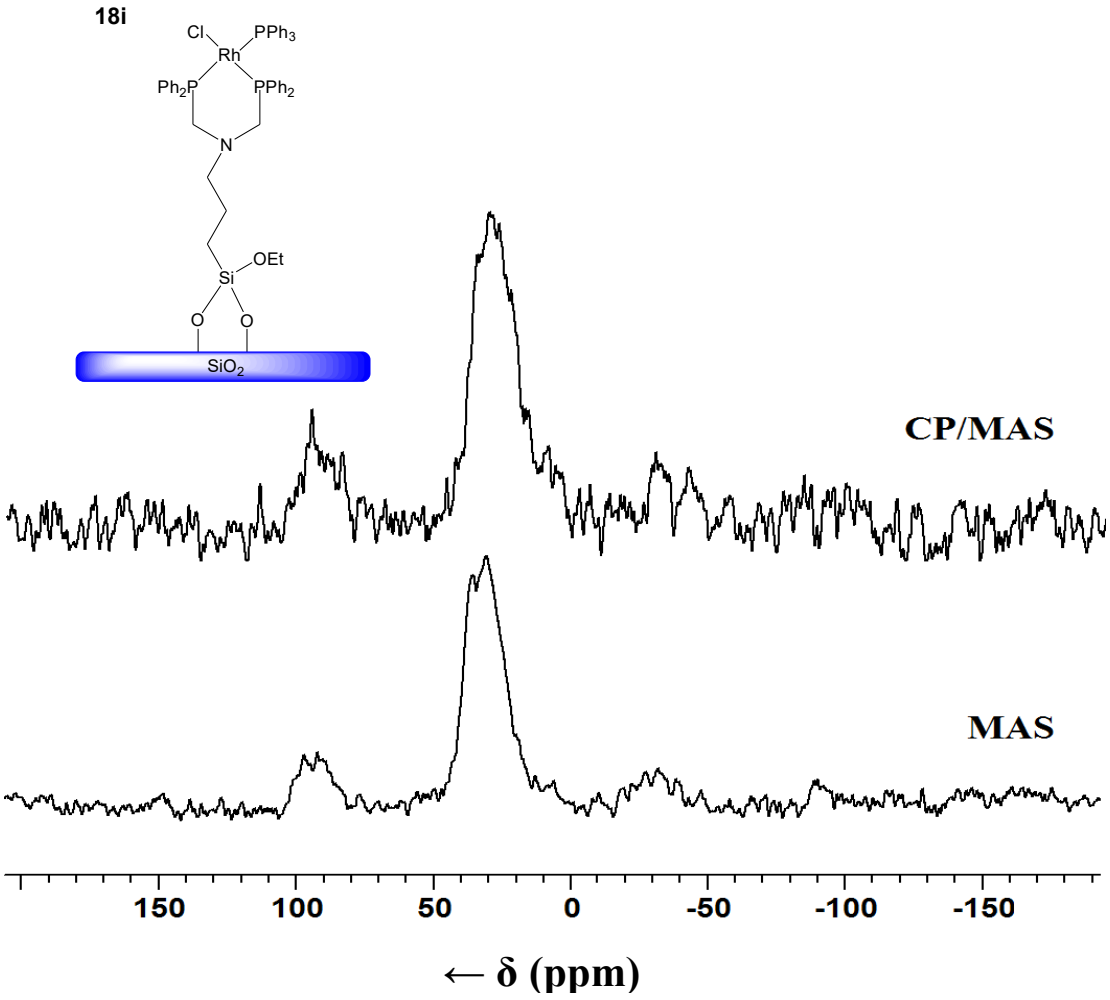

Figure 4.5 ^{31}P CP/MAS (top) and MAS (bottom) spectra of **18iRh**. Rotational speed 10 kHz.

18iRh was generated from **18i**, which has been previously synthesized and characterized by the Bluemel group.[46] In ^{31}P solid-state NMR **18i** displays only one phosphine signal at δ = -29 ppm, which is close to the value in solution. The immobilization of the catalyst proceeds in the same way discussed previously, but the solid-state NMR spectrum looks very different. As the immobilization occurs without phosphonium groups, there are only two phosphorus peaks at about 30 ppm, which are overlapping (Figure 4.5).

4.2.5 Catalysis with Immobilized Wilkinson-type Complexes

The immobilized catalyst **3iRh** hydrogenated 1-dodecene at room temperature. It is noteworthy that there was no induction period during the first cycle. The catalyst could be recycled for an additional 29 cycles, until the catalysis was stopped (Figure 4.6). ^{1}H NMR was used to confirm the absence of any olefins in the supernatant for each cycle, ensuring complete hydrogenation. Also, gas chromatography is sometimes used to ensure complete hydrogenation. The catalysis would likely have continued indefinitely, but for the fact that some **3iRh** is lost with each washing, causing the rate of catalysis to slow down. It is also noteworthy that the catalyst changed color during the catalysis from a light orange to a dark brown color, which has been observed before[1,15] and likely indicates Rh nanoparticle formation.

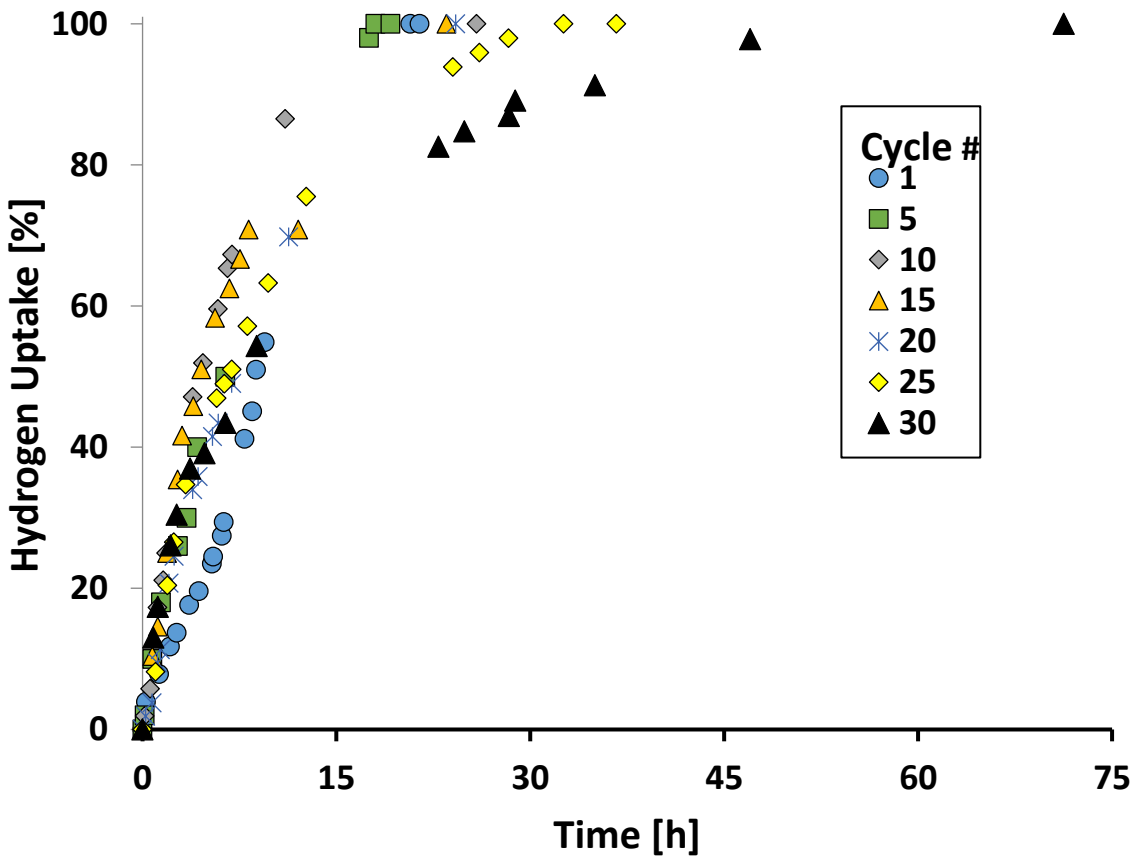

Figure 4.6 Batchwise hydrogenation runs of 1-dodecene using catalyst **3iRh** in toluene at room temperature.

To gauge the nature of the catalytically active species, a series of tests on the used catalyst were performed. The first of these is known as a split test, wherein catalysis is allowed to proceed in a standard manner until about 50% conversion, then it is stopped. The immobilized catalyst settles to the bottom of the flask, leaving a supernatant above it. Subsequently, half of the supernatant is extracted and filtered into a new tube, while half remains with the solid. Catalysis is allowed to continue on each sample, which should demonstrate if the catalyst is being leached off of the support into solution during catalysis, or remains immobilized.

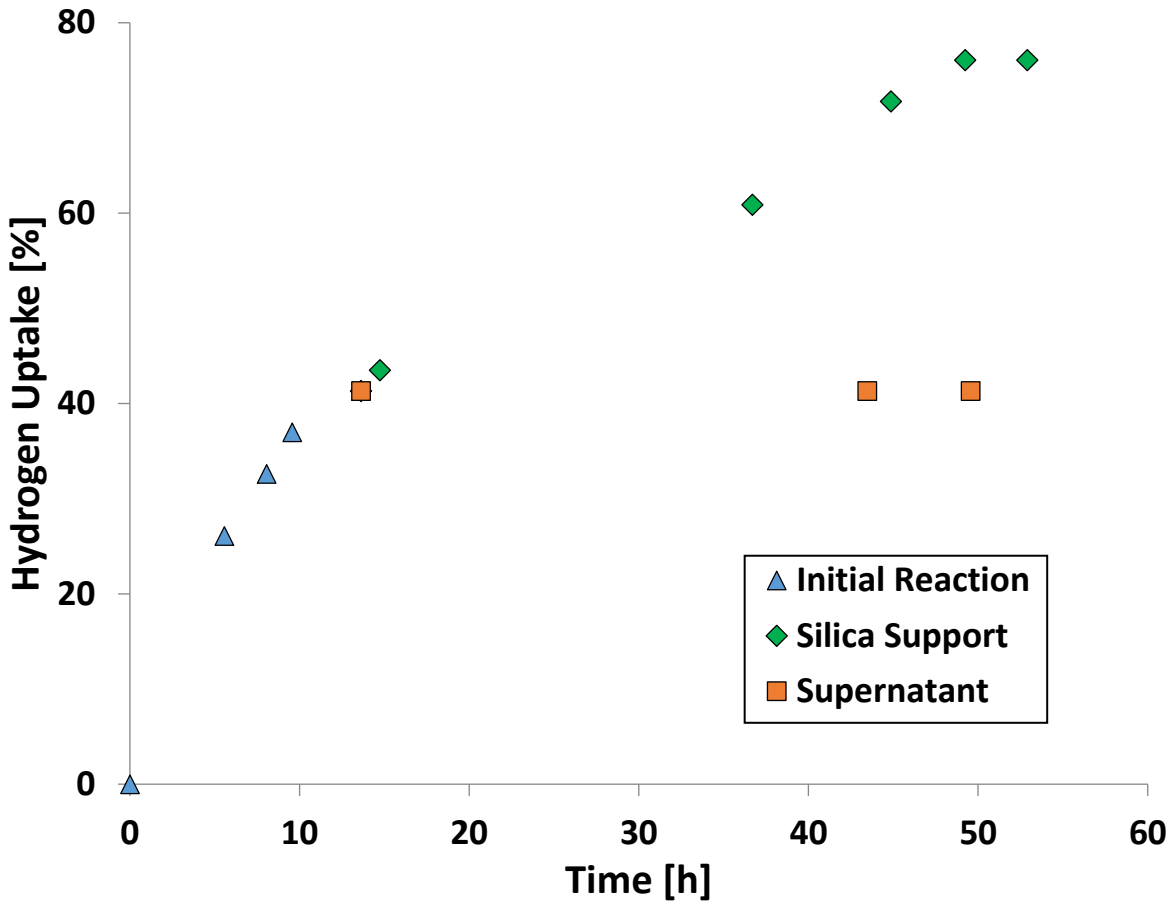

Figure 4.7 Split test for the hydrogenation of 1-dodecene with used catalyst **3iRh** in toluene.

The results of the split test (Figure 4.7) show that the catalysis proceeds in the usual way until it was stopped after about 15 hours. From here, the supernatant with the immobilized catalyst proceeded to the finish of ~75%, which is expected, as some of the 1-dodecene was removed during the split. The most important finding is that the filtered supernatant did not catalyze any hydrogenation, meaning that the catalyst is not leaching off, and that all catalytically active species remain on the support.

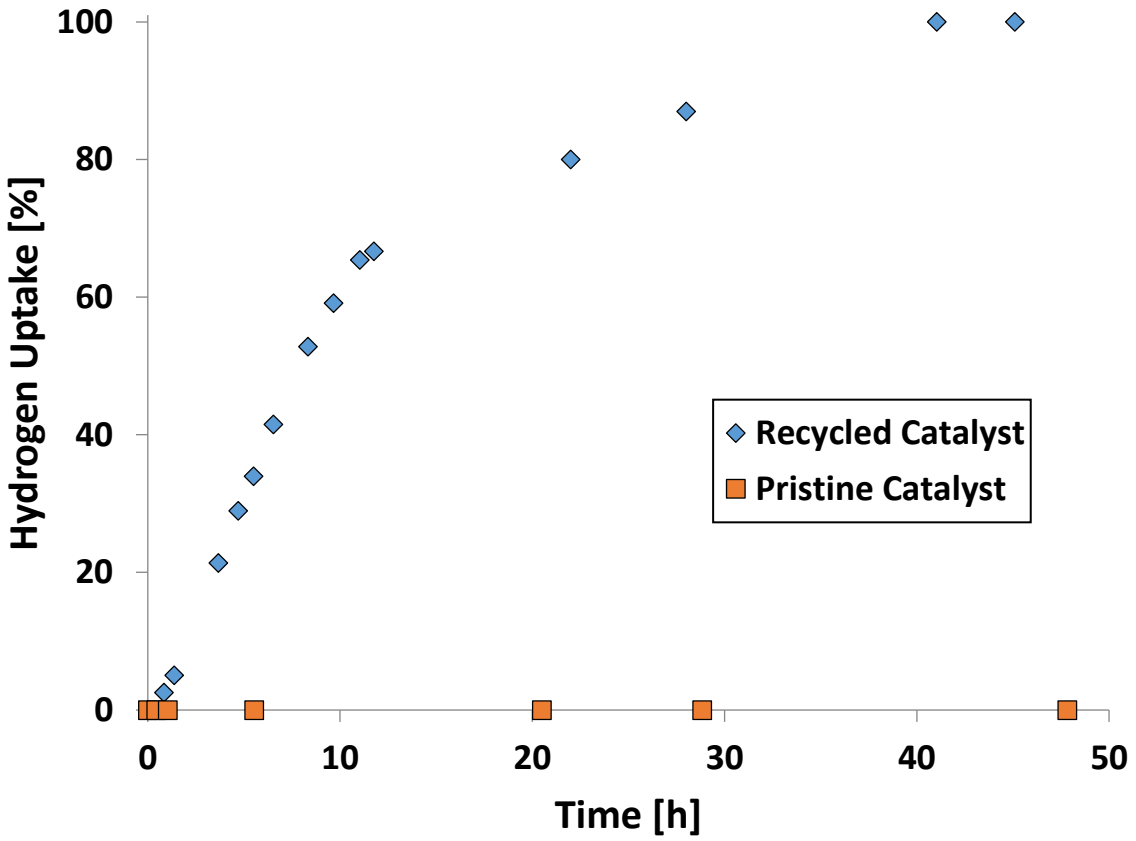

Figure 4.8 Catalytic activities of the recycled and the pristine catalyst **3iRh** after exposure to ambient oxygen.

The active catalyst remaining on the support could be still homogeneous in nature, being tethered to the silica by the linker. Alternatively, nanoparticles could have come into existence, which would be deposited on the support and act like a heterogeneous catalyst. Therefore, it is desirable to know if exposure to oxygen impacts the performance of the catalyst. The homogeneous Wilkinson's catalyst is oxygen sensitive and decomposes quickly to inactive species upon exposure to oxygen. Metal catalysts, in particular Rh nanoparticles, on the other hand, are robust towards oxygen.[1,4] To test whether the catalyst had changed in nature during catalysis, the spent catalyst and a batch of pristine catalyst **3iRh** are stirred

separately in toluene in open flasks for two hours. After this time, 1-dodecene is added, and the flasks are connected to the hydrogenation apparatus.

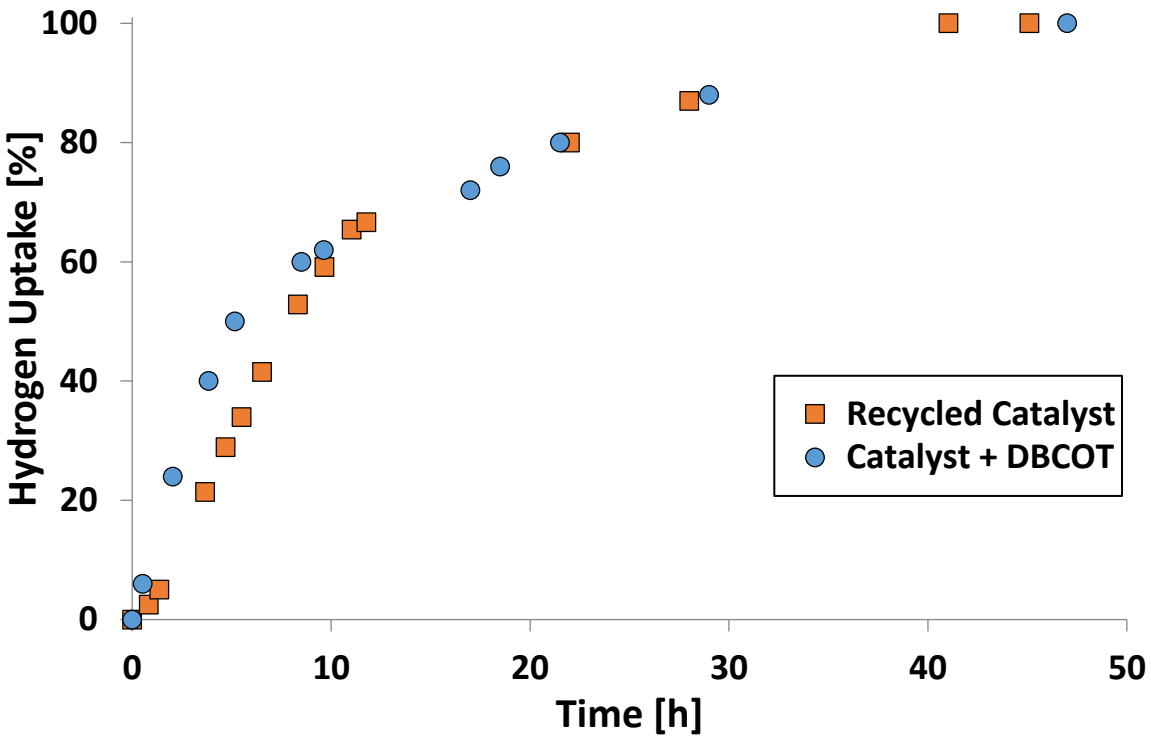

Figure 4.9 Hydrogenation of 1-dodecene using catalyst **3iRh** with and without addition of DBCOT inhibitor.

It is clear from the catalysis curves displayed in Figure 4.8 that the used catalyst is not affected by exposure to oxygen, while the pristine catalyst is rendered catalytically inactive. This indicates that at the beginning the catalyst is homogeneous, but in later runs the active species most likely consists of Rh nanoparticles resulting from the reduction of Wilkinson's catalyst with hydrogen.[1,4]

Next, a poisoning test was performed to confirm the presence of nanoparticles by adding dibenzo[a,e]cyclooctatetraene (DBCOT) to the immobilized catalyst **3iRh** after being

used for several runs. DBCOT functions as a ligand for a homogeneous, molecular Rh catalysts, but will not bind to a metal surface. Therefore, a nanoparticle catalyst should not be affected by the poisoning agent. When a catalytic cycle is performed without DBCOT addition, and subsequently carried out with DBCOT, it is possible to distinguish whether the catalyst is homogeneous or heterogeneous in nature. The catalysis curves in Figure 4.9 are practically identical and show no deceleration in the catalytic activity between the two samples. This corroborates the assumption that nanoparticles form in the course of catalysis.

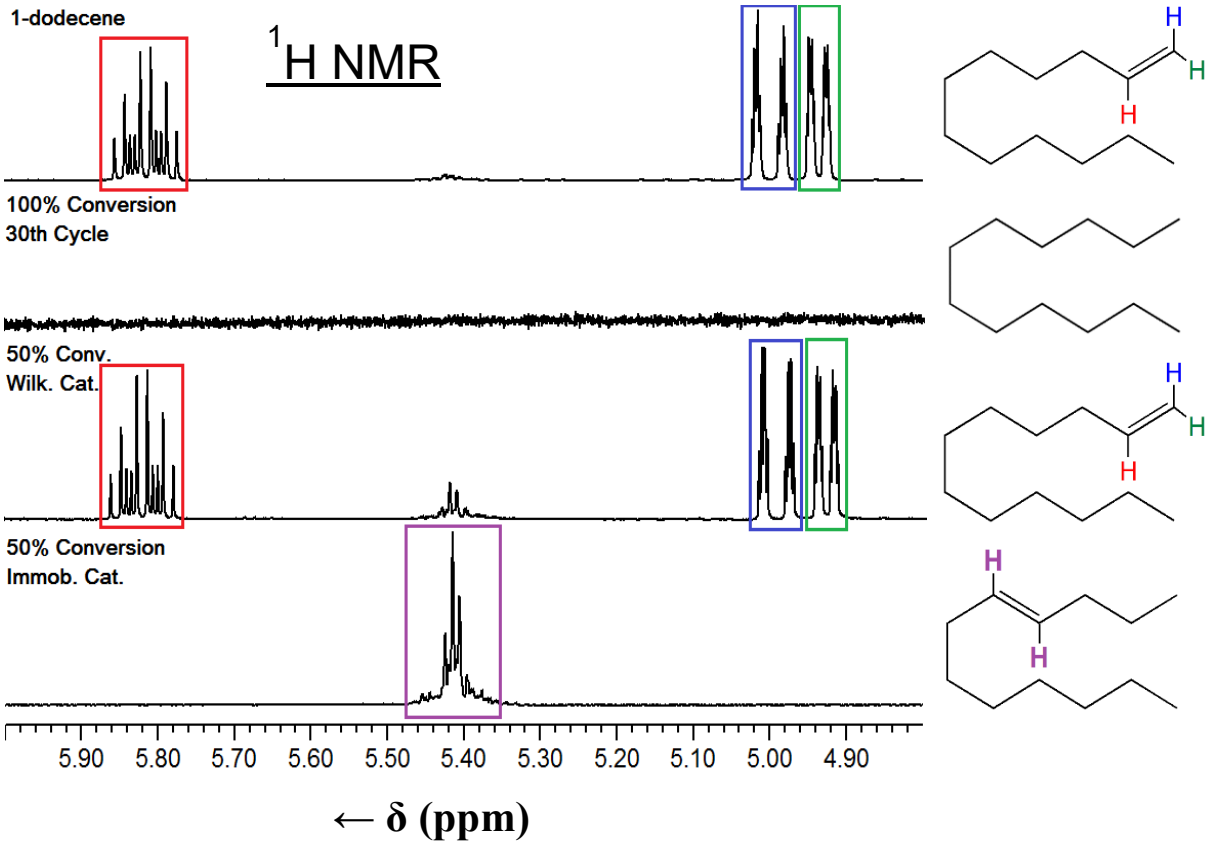

Figure 4.10 ^{1}H NMR spectra showing (from top to bottom) an expansion of the alkene region of the starting alkene, the supernatant after 100% conversion of the 30th cycle, the alkene after 50% conversion using homogeneous Wilkinson's catalyst, and the alkene after 50% conversion using the spent catalyst **3iRh**.

Another reason to suspect nanoparticle formation is the migration of the double bond within the alkene. 1-Dodecene, a terminal alkene, was used so that any migration of the double bond, resulting from the process outlined in Scheme 4.1, can be easily observed by ^{1}H NMR. In Figure 4.10 the alkene regions of the ^{1}H NMR spectra of the products are shown. 1-Dodecene has three distinct olefin ^{1}H NMR signals: one bound to the internal carbon of the alkene (red), one for the terminal hydrogen *cis* to the first hydrogen (green), and one that is *trans* to the first hydrogen (blue). Almost completely absent in the top spectrum are the peaks in the middle, which represent hydrogens on internal double bonds (purple). There are multiple internal positions available in dodecene, which is why there are many overlapping peaks. The top spectrum represents the olefin before any exposure to the catalyst. The second spectrum from the top in Figure 4.10 shows that after the 30th cycle, there are no more olefin protons, meaning that the catalyst is still completely hydrogenating 1-dodecene even after 30 cycles. The bottom two spectra show the different outcomes from Wilkinson's catalyst in its homogeneous form and the aged immobilized catalyst **3iRh**. Homogeneous Wilkinson's catalyst shows only little double bond migration after 50% conversion, represented by the relatively small intensity of the signals at δ = 5.41 ppm. However, in the bottom spectrum, after applying the aged catalyst **3iRh** for 50% conversion, almost all of the double bonds have migrated to an internal position. This double bond migration also indicates that aged **3iRh** is a heterogeneous catalyst.

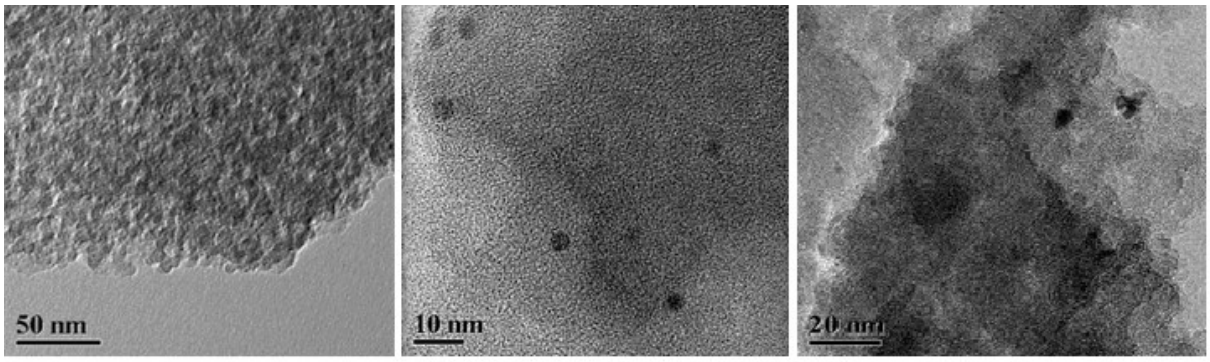

Figure 4.11 TEM images of the pristine catalyst **3iRh** (left), aged catalyst **3iRh** before oxygen exposure (middle), and aged **3iRh** after catalysis with exposure to oxygen (right).

The presence of nanoparticles was also confirmed using TEM imaging. The TEM of the pristine catalyst shows no nanoparticles, while the spent catalyst displays nanoparticles that are clearly visible in Figure 4.11. This serves to confirm what was suspected from visual observation of the catalyst after catalysis was begun, where the catalyst changed color from orange to dark brown. Interestingly, the nanoparticles generated in the oxygen-free conditions tended to be a uniform size of about 3-4 nm, as seen in the histogram in Figure 4.12. This is significant because the silica support used has an average pore size of 4 nm, which strongly suggests that the nanoparticles are forming in the pores of the silica. This also explains the extraordinary longevity of the catalyst. The size of the particles was larger for the catalyst after exposure to oxygen, as shown in Figure 4.12. However, the size of the nanoparticles does not seem to be crucial for the catalytic activity in this diameter range, as the catalyst performed equally well in the presence of oxygen as under inert gas atmosphere.

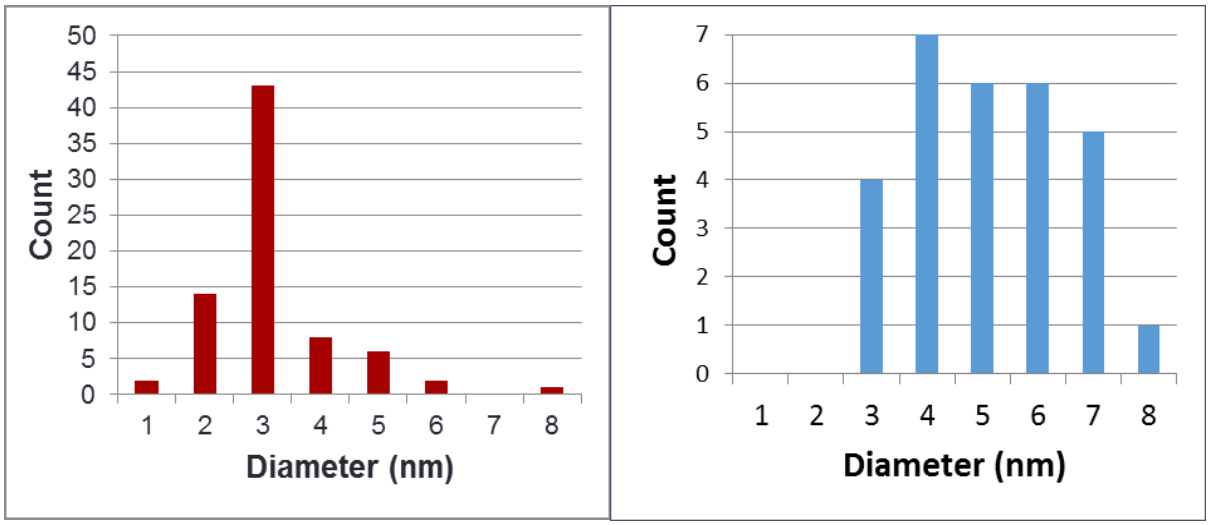

Figure 4.12 Histograms of the size distribution of nanoparticles found for aged catalyst **3iRh** with no oxygen exposure (left) and after catalysis with oxygen exposure (right).

With catalyst **12iRh** the hydrogenation of 1-dodecene proceeded over 15 cycles before it was terminated (Figure 4.13). However, it was necessary to heat the sample to 50 °C for catalysis to start. This could possibly be explained by the increased basicity of the dicyclohexylphosphine ligand that is bound to the metal. Obviously this diminishes the catalytic activity of the complex. Regardless, after a slow first cycle, it was apparent that the color of the catalyst was changing from orange to dark brown. After this, subsequent cycles proceeded at an accelerated rate relative to the first cycle. Therefore, it can be concluded that the nanoparticles are catalytically more active than the initial homogeneous immobilized Rh complex **12iRh**.

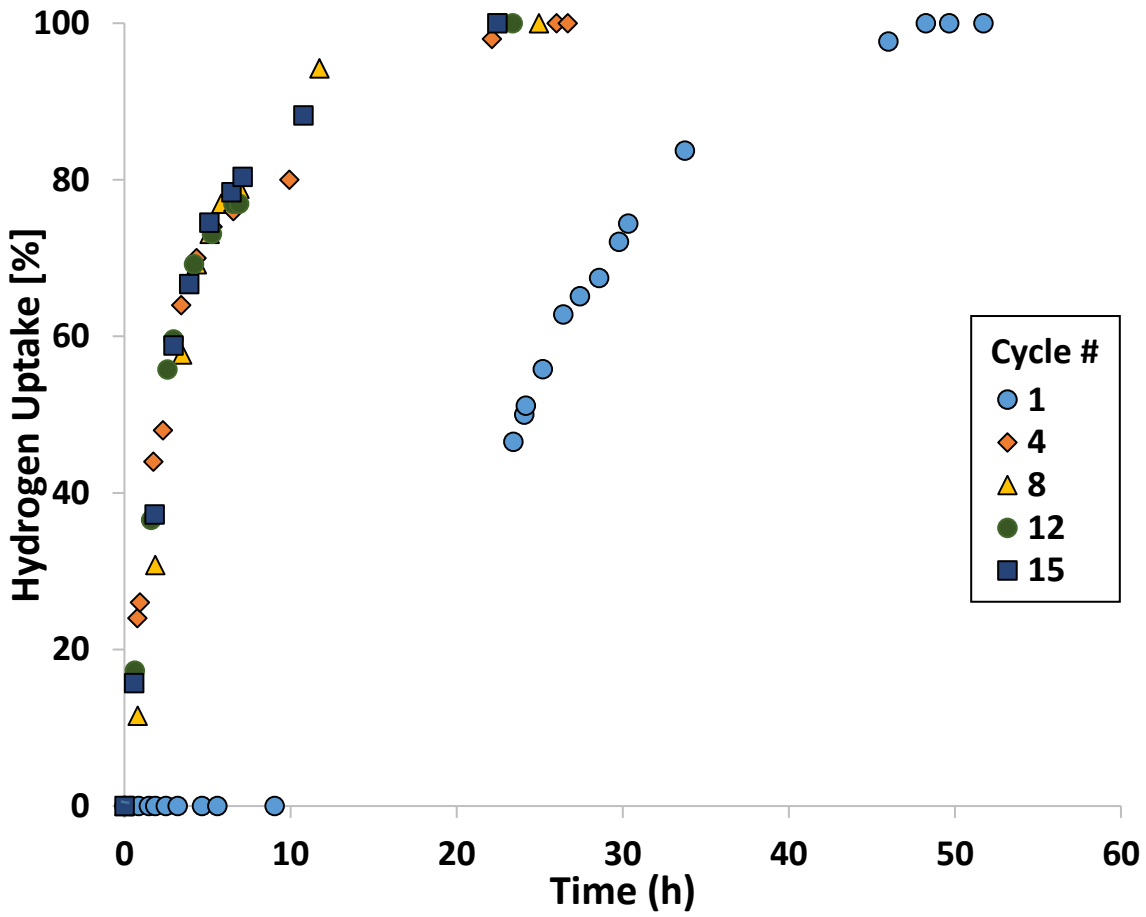

Figure 4.13 Hydrogenation cycles of 1-dodecene using catalyst **12iRh** in toluene.

To confirm the heterogeneous nature of the catalyst in the aged material **12iRh**, a split test was performed, as described above for **3iRh**. For this split test, unlike with **3iRh**, it was necessary to filter the supernatant at 50 °C to more closely mimic the catalytic conditions. It can easily be observed that catalysis proceeds with the immobilized catalyst present in the sample (Figure 4.14). For the filtered supernatant, however, irrespective of some fluctuation due to measurement errors, there was no residual catalytic activity. As with **3iRh**, this means that there is no catalytically active species in the supernatant, and all Rh centers remain bound to the support.

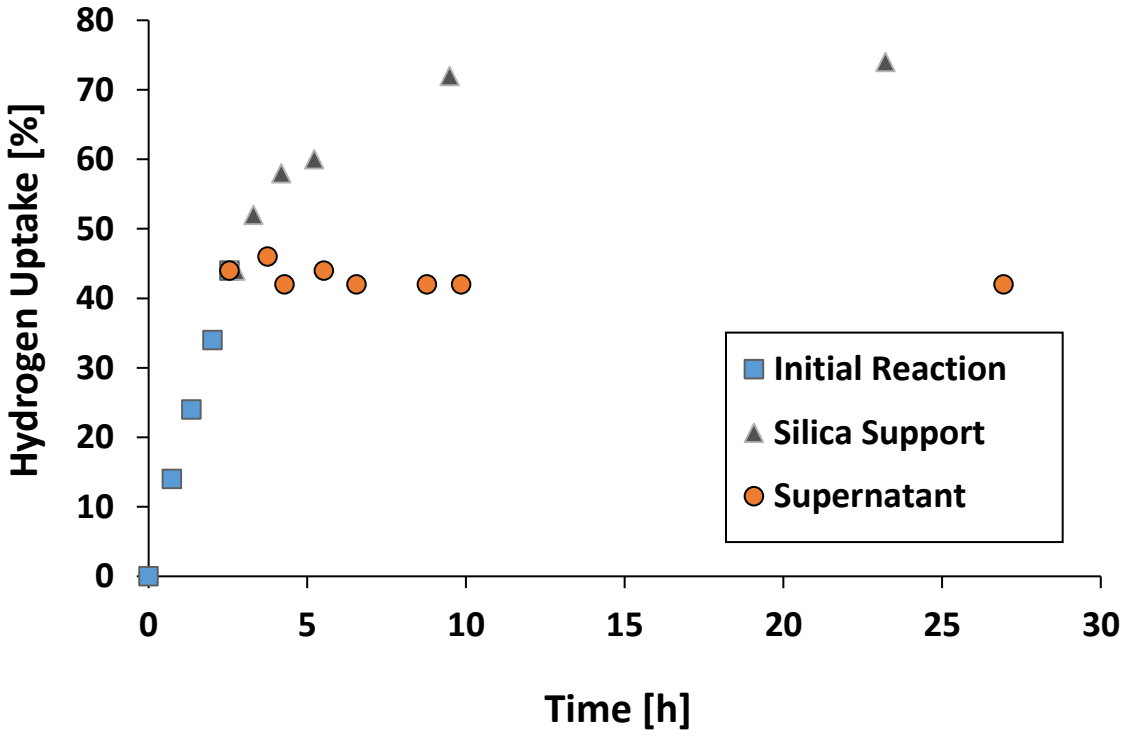

Figure 4.14 Split test characteristics for the hydrogenation of 1-dodecene with the aged catalyst **12iRh** in toluene.

Next, the used catalyst was exposed to oxygen, and its catalytic activity was compared with that of the pristine catalyst after oxygen exposure. In Figure 4.15 it can be seen that the pristine catalyst displays no catalytic activity after being exposed to oxygen, while the used catalyst remains catalytically active after exposure to oxygen. Therefore, one can conclude that the aged catalyst consists of Rh nanoparticles, while the pristine catalyst is immobilized, but homogeneous in nature.

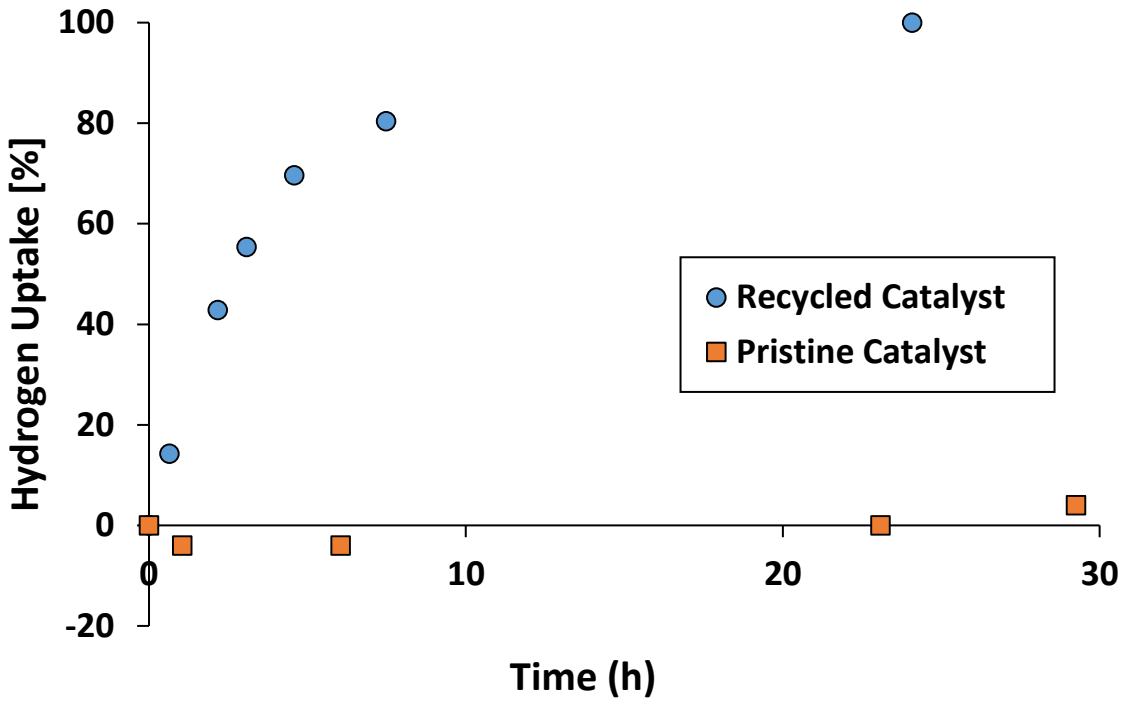

Figure 4.15 Catalytic activities of the aged catalyst and the pristine catalyst **12iRh** after exposure to ambient oxygen.

For catalyst **13iRh** the catalysis characteristics were very similar to those of **12iRh**, as the catalyst was recyclable, but required 50 °C to initiate the catalytic reaction (Figure 4.16). This catalyst could be recycled ten times, but was stopped due to time reasons. It is also similar in that the color changed from orange to dark brown during the first cycle, which again indicates the formation of nanoparticles.

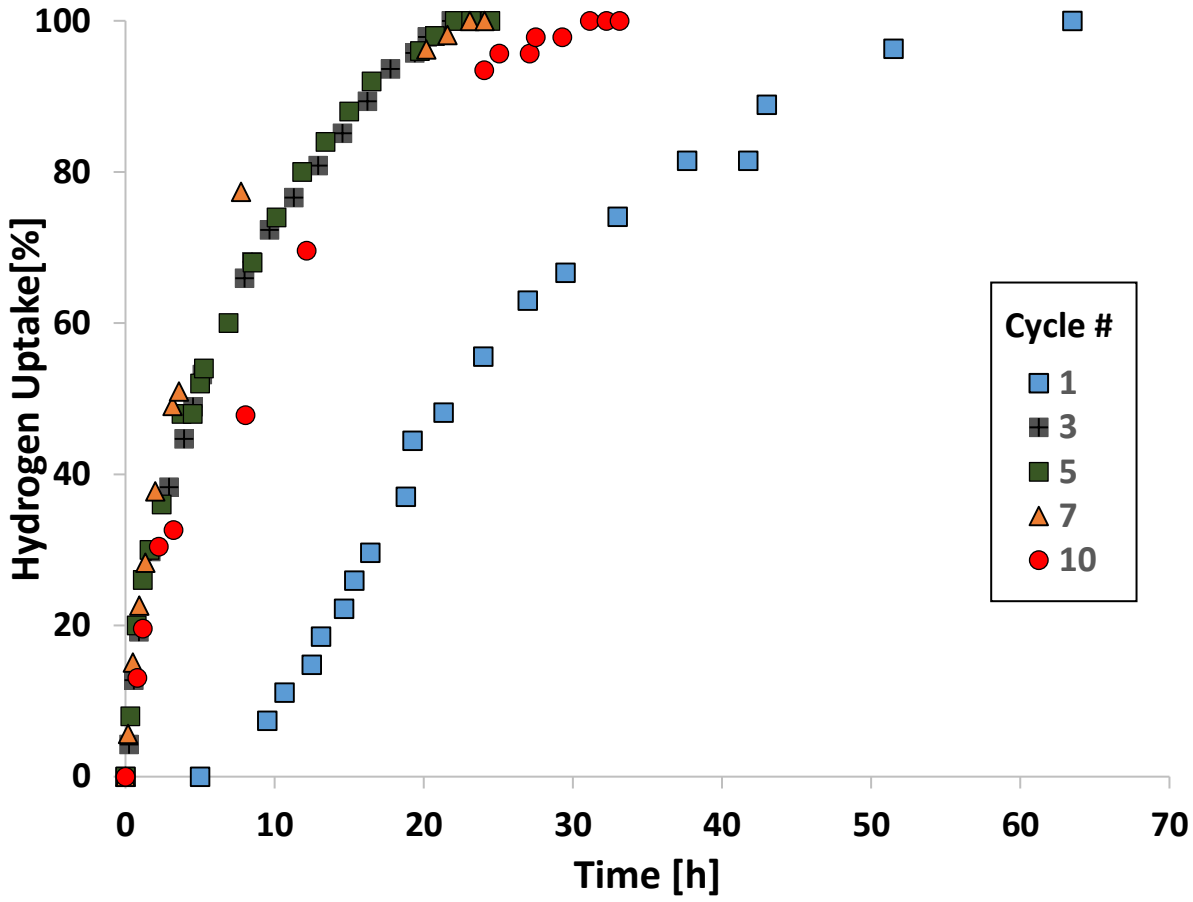

Figure 4.16 Hydrogenation cycles of 1-dodecene with catalyst **13iRh** in toluene. All runs were performed at 50 °C.

Again, a split test was performed on catalyst **13iRh** to check whether any active species is present in the supernatant during catalysis. As in the previous cases, the reaction was stopped after 50% conversion, and the catalyst was allowed to settle. Half of the supernatant was filtered at 50 °C, while the other half remained with the catalyst. While the supernatant did not display any residual catalytic activity, the solid material went on to achieve about 70% conversion (Figure 4.17).

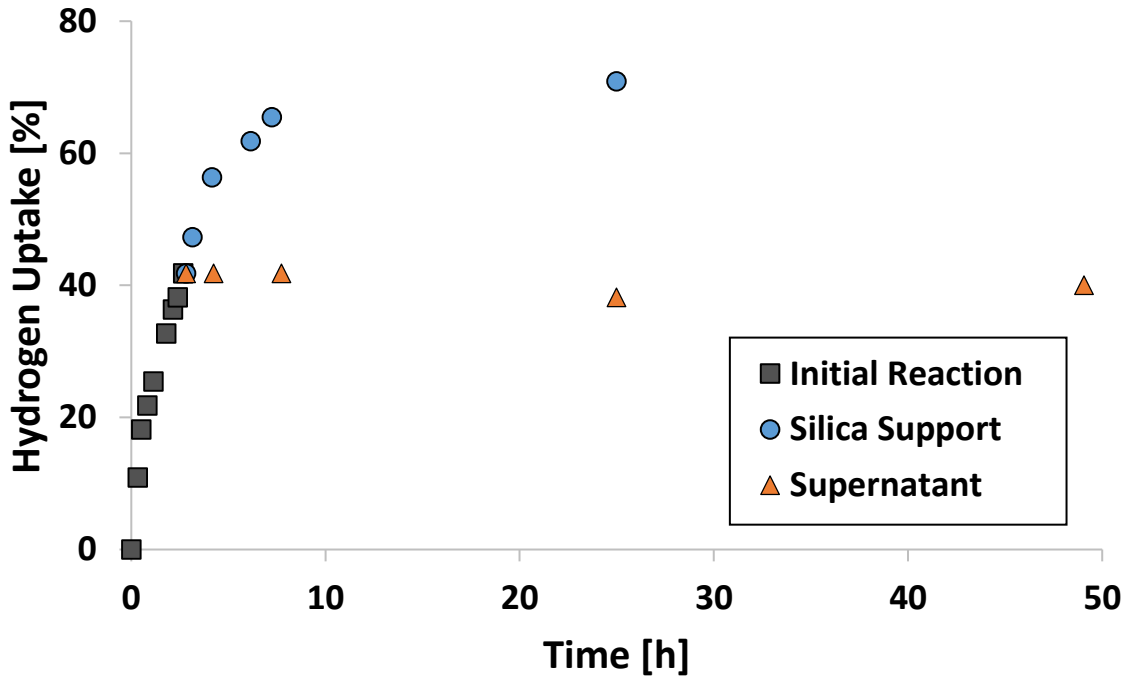

Figure 4.17 Split test curves of catalyst **13iRh** for the hydrogenation of 1-dodecene.

Next, the aged catalyst was exposed to oxygen, and its catalytic activity was compared to that of the pristine catalyst after oxygen exposure. In Figure 4.18 it can be seen that the pristine catalyst displays no catalytic activity after being exposed to oxygen, while the aged catalyst remains catalytically active after exposure to oxygen. From this, it seems again likely that the recycled catalyst is comprised of Rh nanoparticles.

The final catalyst studied is **18iRh**, which is the only catalyst that features a chelating functionality and a flexible, alkyl chain in the linker. The base of the linker is also much smaller, which could result in Rh dimerization if the linkers are loaded onto the surface too densely. For this reason, a low surface coverage of 2.5 particles/100 nm^2 is applied.

When tested for hydrogenation activity, the reaction did proceed at room temperature. It can be seen from Figure 4.19 that there was an induction period in cycle 1, as there was

little hydrogenation occurring during the first four hours. However, as the color started to change, the hydrogenation accelerated. By the second and third cycle, the catalyst had about the same activity as the previous catalysts bound via rigid linkers. The catalyst could be recycled an additional 7 times, however, there was still substantial activity during the tenth cycle. As with **3iRh**, it is suspected that the decrease in activity over time is the result of loss of **18iRh** particles when washing between cycles. Again, the catalyst changed color from orange to dark brown, indicating the formation of Rh nanoparticles.[1,15] It seems clear that chelation of the Rh center did not prevent nanoparticle formation.

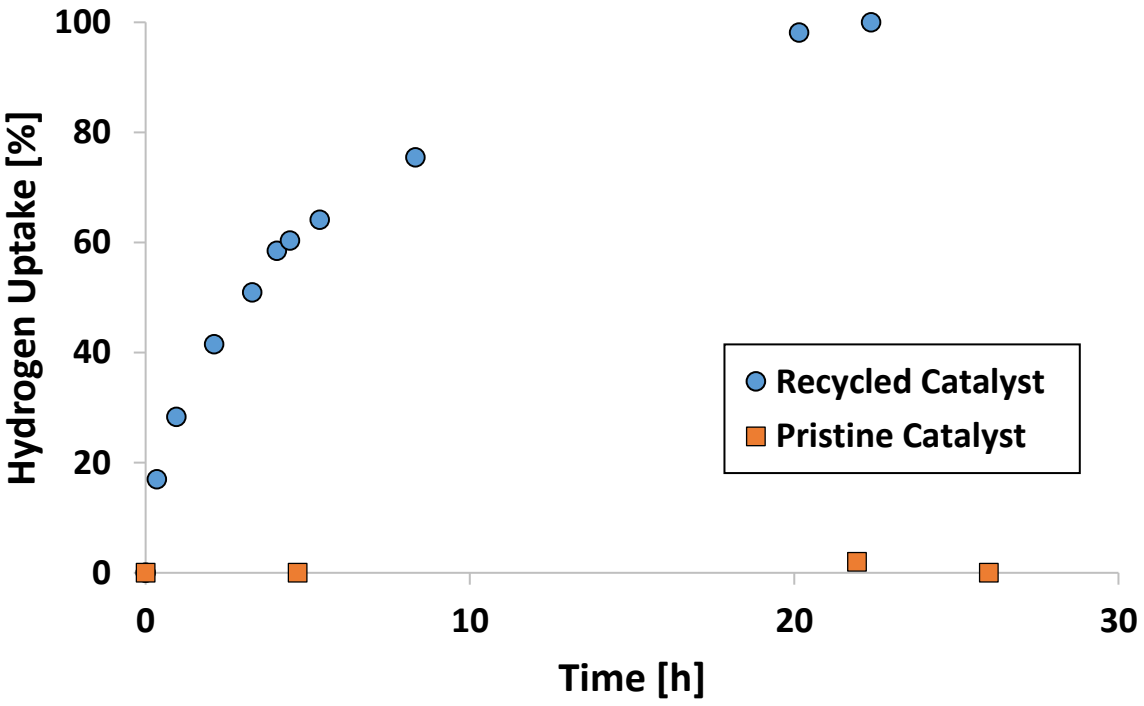

Figure 4.18 Test showing the aged and the pristine catalyst **13iRh** after exposure to ambient atmosphere.

Again, a split test was performed on catalyst **18iRh** to check whether any active species are present in the supernatant during catalysis. As in the previous cases, the reaction

was stopped after partial conversion, and the catalyst was allowed to settle. Half of the supernatant was filtered at 50 °C, while the other half remained with the catalyst. While the supernatant did not display any residual catalytic activity, even after 96 hours, the solid material went on to achieve about 70% conversion (Figure 4.20).

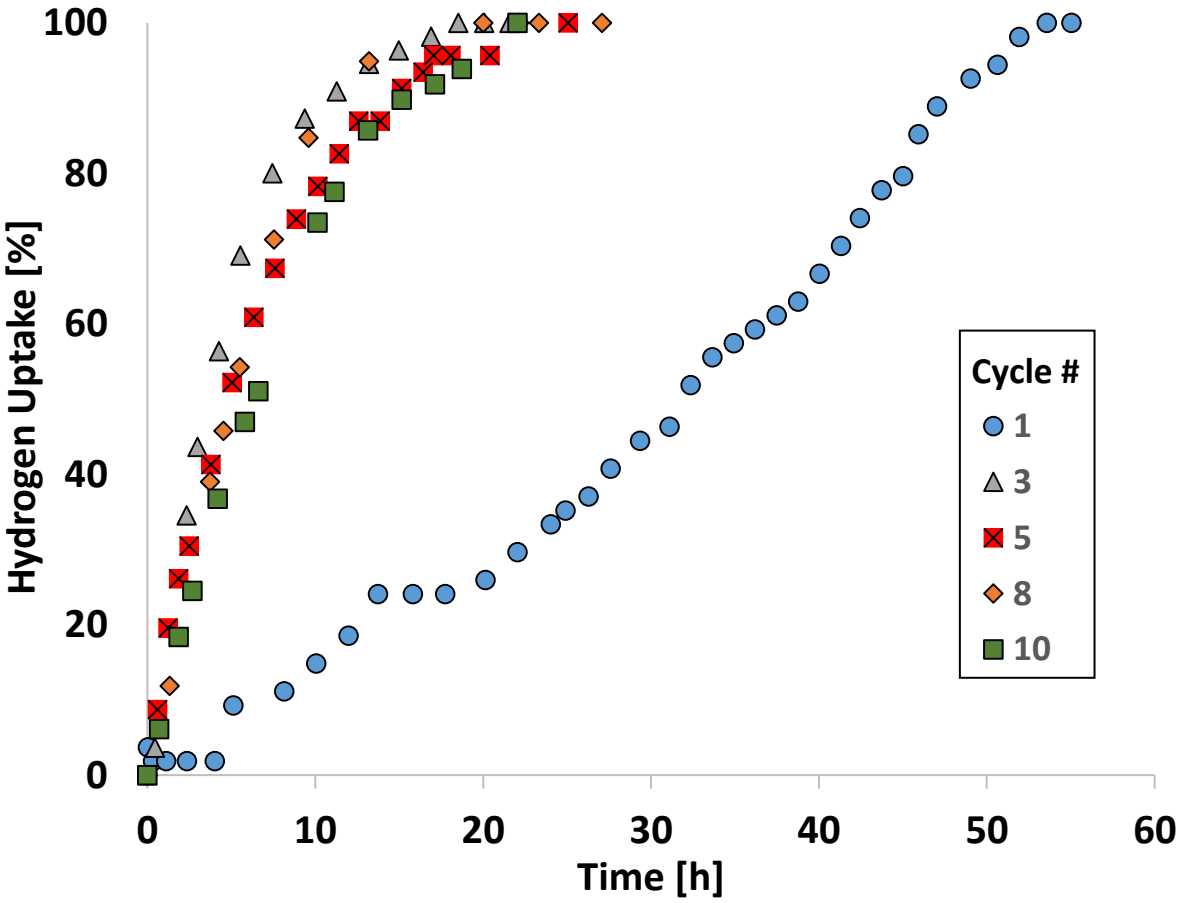

Figure 4.19 Hydrogenation cycles of 1-dodecene using catalyst **18iRh** in toluene.

The next test consists of exposing the aged catalyst **18iRh** to oxygen, and comparing its catalytic activity to the pristine catalyst after oxygen exposure. It can be seen in Figure 4.21 that the pristine catalyst displays no catalytic activity after being exposed to oxygen,

while the used catalyst remains catalytically active after exposure to oxygen. Therefore, it is assumed that the recycled catalyst is comprised of Rh nanoparticles.

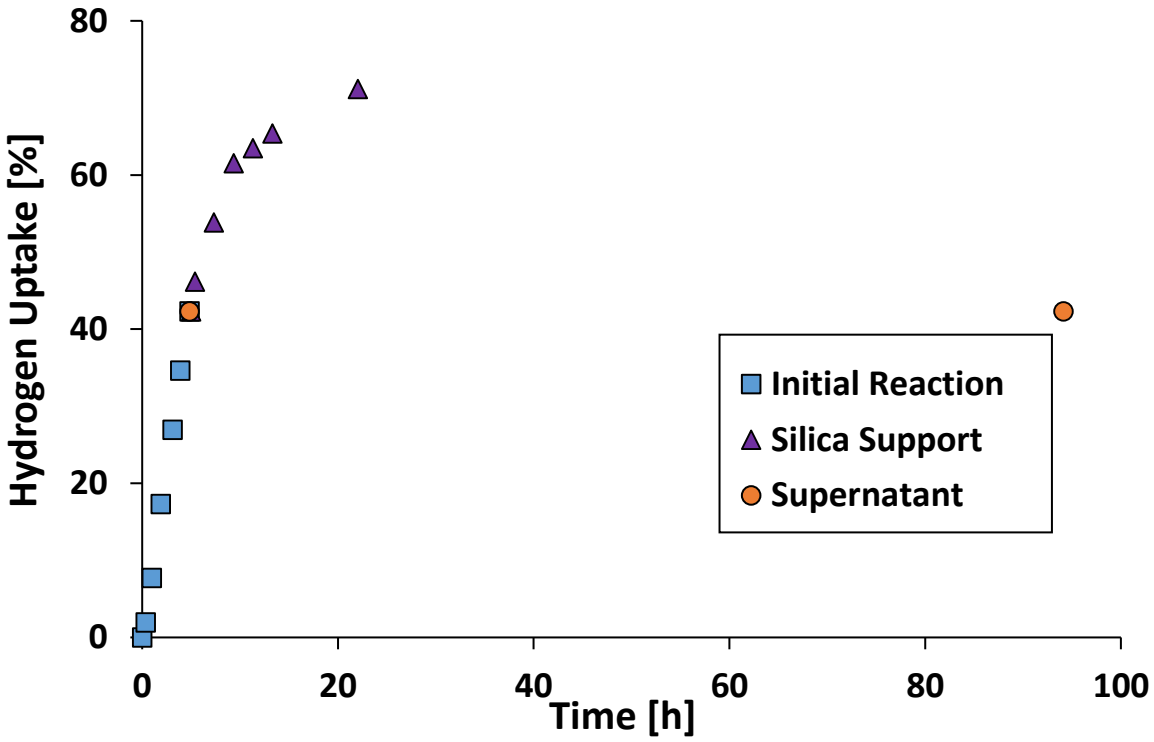

Figure 4.20 Split test for the hydrogenation of 1-dodecene with the aged catalyst **18iRh** in toluene.

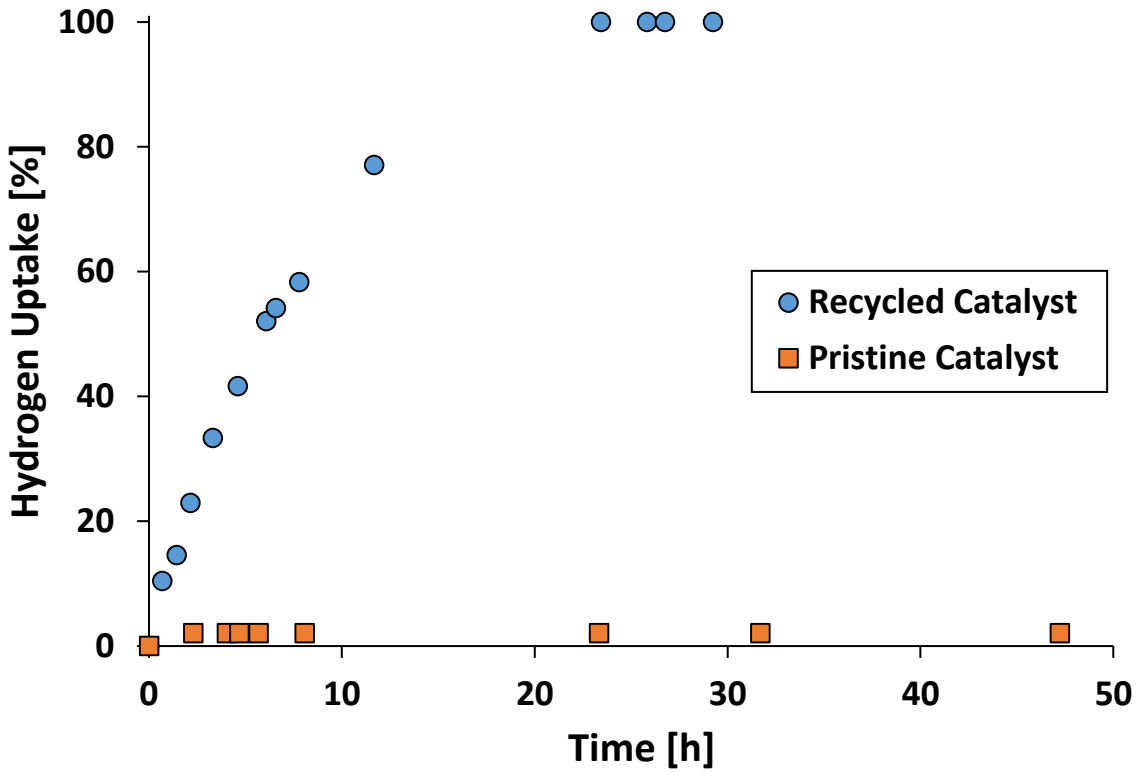

Figure 4.21 Activities of the aged and the pristine catalysts **18iRh** after exposure to ambient oxygen.

4.3 Conclusion

A new class of immobilized catalysts, **3iRh**, **12iRh**, and **13iRh**, consisting of a linker featuring four phosphine moieties with a rigid tetraphenylelement core, has been synthesized. The catalyst can be added to the immobilized scaffold via a simple ligand exchange, leaving a catalyst that is incapable of dimerization or surface contact. ^{31}P solid-state NMR confirms that the product is formed, as the free phosphine peak vanishes.

These new catalysts can easily be recycled almost indefinitely, they work at very low temperatures, have no active species being leached into the supernatant, and are resistant to oxidation. The only functional difference between the catalysts is that **12iRh** and **13iRh** required 50 °C temperatures to initiate catalytic activity, while **3iRh** was already active at

room temperature. Unfortunately, the catalyst is reduced during this process, resulting in the formation of Rh nanoparticles. Importantly, it could be demonstrated that the core element of the scaffold linker, Si or Sn, plays no part in catalysis.

The last catalyst synthesized was **18iRh**, which is distinct from the other catalysts because it does not feature a rigid linker, and the Rh center was coordinated in a chelating manner. The catalyst is added to the linker via a ligand exchange, and the product is characterized using solid-state NMR. The catalyst is effective at room temperature, but also forms nanoparticles before any catalytic activity can commence. Therefore, it can be concluded that using a chelating linker to bind to the Rh center did not prevent nanoparticle formation.

4.4 Experimental Section

4.4.1 General Information and Procedures

All reactions are carried out using standard Schlenk techniques and a purified N_2 atmosphere, if not stated otherwise. Reagents purchased from Sigma Aldrich or VWR are used without further purification. Toluene is dried by boiling over Na, distilled, and stored under N_2. The silica (Merck, 40 Å average pore diameter, 0.063 to 0.2 mm average particle size, specific surface area 750 m^2/g) is rigorously dried in vacuo at 250 °C for 4 days to remove adsorbed water and condense surface silanol groups.

4.4.2 Instruments and Measurements

The ^1H and ^{31}P NMR spectra of liquids were recorded at 499.70 and 202.28 MHz on a 500 MHz Varian spectrometer and referenced as follows. ^1H: residual internal $CHCl_3$ (δ, 7.26 ppm). ^{31}P NMR spectra are referenced to neat Ph_2PCl (δ, 81.92 ppm) which is placed in

a capillary centered in the NMR sample tube. The ^{31}P NMR spectra are recorded with ^{1}H decoupling if not stated otherwise.

The solid-state NMR spectra are measured with a Bruker Avance 400 widebore NMR spectrometer with a multinuclear 4 mm MAS probehead. For the ^{31}P CP/MAS and MAS measurements ^{1}H high-power decoupling was applied. For ^{29}Si, the Hartmann-Hahn matching condition was optimized using tetrakistrimethylsilylsilane at 5 kHz, and for ^{31}P, the Hartmann-Hahn matching condition was optimized using sodium monohydrogen phosphate. The recycle delays are 5 s for CP/MAS and 10 s for MAS spectra.

4.4.3 Synthesis of 10

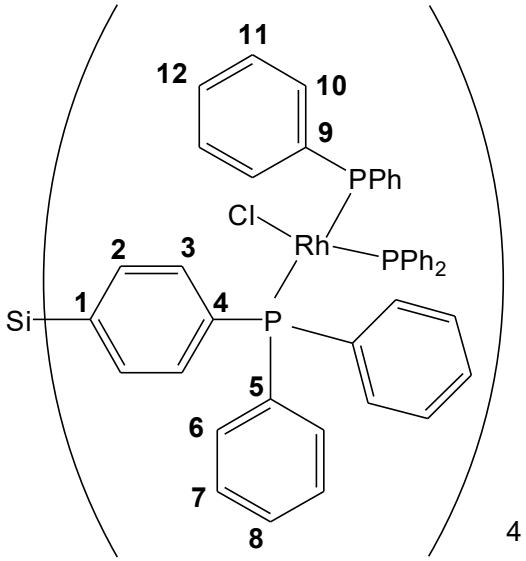

10

$C_{239}H_{248}Cl_4P_{12}Rh_4Si$

Mol. Wt.: 4073.731 g/mol

Tetraphosphine **3** (0.054 g, 0.050 mmol) was dissolved in toluene (20 mL). Wilkinson's Catalyst (0.186 g, 0.201 mmol) in toluene (30 mL) added and stirred overnight.

The crude product is filtered through Celite, then the solvent is removed *in vacuo*, leaving an orange powder **10** (0.187 g, 0.046 mmol, 92.0%).

4.4.4 General Procedure for Catalyst Immobilization

$ClRh(PPh_3)_3$ (56 mg, 0.060 mmol), dissolved in 30 mL of toluene, was added to a slurry of the functionalized silica **3i** (1.3247 g, 0.060 mmol ligand) in 10 mL of toluene. The mixture was stirred overnight at RT, then the silica was allowed to settle and the supernatant was removed. The catalyst-containing silica **3iRh** was washed with toluene (3×10 mL) and dried *in vacuo* for 2 h. The supernatant and the washing portions were combined and the solvent was removed *in vacuo*, and ^{31}P NMR verified that only liberated PPh_3 was present in solution.

4.4.5 General procedure for the catalytic hydrogenation

The immobilized catalyst **3i** (225 mg, 0.010 mmol Rh) was added to 5 ml of toluene in a Schlenk flask. Then the Schlenk flask was attached to the standardized hydrogenation apparatus[35] and warmed up to 60 °C. The apparatus was allowed to stand under H_2 prior to catalysis in order to make sure that H_2 is not lost due to leakage. Additionally, any loss of H_2 after 100% conversion of the substrate was monitored and excluded. To start the catalysis, 1 mmol of 1-dodecene, dissolved in 1 ml of toluene, was added to the suspension through the stopcock via syringe. Then the suspension was stirred vigorously with a magnetic stir bar and the hydrogen uptake was monitored. After complete consumption of the hydrogen the silica was allowed to settle, the supernatant was removed and the silica was washed with toluene

(2×10 mL). The supernatant was analyzed by ^{1}H NMR to confirm quantitative conversion of the olefin to dodecane.

4.4.6 Procedure for the split test

Immobilized catalyst **3iRh** (225 mg, 0.010 mmol Rh) was added to 5 mL of toluene in a Schlenk flask. Then the Schlenk flask was attached to the standardized hydrogenation apparatus.[35] To start the catalysis 1-dodecene (1 mmol, dissolved in 1 mL of toluene) was added. The hydrogen consumption was monitored and after ca. 40% conversion the hydrogen reservoir was disconnected and the silica support was allowed to settle. Then 3 mL of the supernatant were removed with a syringe and filtered through a filter paper. Both the remaining reaction mixture with the silica support and the filtered supernatant were reconnected to separate hydrogenation apparatuses, and the hydrogen consumption was monitored for both samples. After the hydrogen uptake had stopped, for both cases the reaction mixtures were analyzed by ^{1}H NMR.

4.4.7 General Procedure for Catalysis after Oxygen Exposure

The immobilized catalyst **3iRh** (225 mg, 0.010 mmol Rh), either pristine or recycled, was stirred in 5 mL of toluene in an open Schlenk flask for 2 h at RT. The Schlenk flask was attached to the standardized hydrogenation apparatus.[35] Then 1 mmol of 1-dodecene, dissolved in 1 ml of toluene, was added to the slurry through the stopcock via syringe. While the mixture was stirred, the hydrogen uptake was monitored. After complete conversion the silica was allowed to settle down. Then the supernatant was removed and the silica was

washed with toluene (2×10 mL). The supernatant was analyzed by ^{1}H NMR to confirm 100% conversion.

4.4.8 Catalyst Poisoning Experiment with DBCOT

The immobilized catalyst **3iRh** (225 mg, 0.010 mmol Rh) was stirred in 5 mL of toluene in a Schlenk flask. Then dibenzo[*a,e*]cyclooctatetraene DBCOT (4 mg, 0.020 mmol) was added and the mixture was stirred for 2 h at RT. The Schlenk flask was attached to the standardized hydrogenation apparatus.[35] Then 1 mmol of 1-dodecene, dissolved in 1 ml of toluene, was added to the slurry through the stopcock via syringe. While the mixture was stirred, the hydrogen uptake was monitored. After complete conversion the silica was allowed to settle. Then the supernatant was removed and the silica was washed with toluene (2×10 mL). The supernatant was analyzed by ^{1}H NMR to confirm 100% conversion.

CHAPTER V

SYNTHESIS, CHARACTERIZATION, AND PERFORMANCE OF AN IMMOBILIZED WITTIG REAGENT

5.1 Introduction

A rapidly growing area of modern chemistry is the field of surface-supported reagents,[17,57] which involves tethering a reagent onto an insoluble support via a linker. This has been performed for a range of organic and inorganic reactions, including reductions,[57a] oxidations,[57b] and brominations.[57c]

There are many advantages of binding a reagent to a solid surface. First, these reagents can be easily removed from reaction mixtures by filtration, in contrast to a reagent in solution, which would have to be removed by column chromatography, precipitation, distillation, recrystallization, or some form of extraction. Another advantage of surface-bound reagents is that, in some cases, excess reagent can be used to drive reactions to completion that otherwise would not go to 100% conversion, while there is no complication brought about by the removal of the excess reagent. Additionally, the reagent on a solid support may react differently, perhaps more selectively, after being placed on a surface. A final advantage is that the reagents could potentially be reused, which makes the reagent more efficient and environmentally friendly.[11c,17]

The Wittig reaction[58] is a well-known and important transformation in organic chemistry, discovered by Georg Wittig in 1954. It is the reaction of an aldehyde or ketone and a triarylphosphonium ylide, also known as a Wittig reagent, resulting in a new alkene and a phosphine oxide as the products (Schemes 5.1, bottom, and 5.2).[58] This reaction can be

used to create double bonds at one specific position in the molecule. Therefore, the Wittig reaction is much more favorable than, for example, elimination reactions which produce a mixture of isomers with various locations for the double bond.

The goals of this project are 1) to determine optimal reaction conditions and reagents for a Wittig reaction that can be applied to a surface-supported system later, 2) to synthesize a surface-supported Wittig reagent using the rigid, immobilized scaffold, and 3) to analyze the outcome of the Wittig reaction for the benefits of better understanding surface-supported reactions in general.

Although this reaction is effective in solution, it has the obvious disadvantage of having the desired product along with the phosphine oxide byproduct in solution. The phosphine oxide has to be removed from the reaction mixture, for example, by tedious and expensive column chromatography. If the ylide were bound to an insoluble support (Scheme 5.1), this step could be avoided, as the solution containing the alkene could be easily decanted along with the pure product.

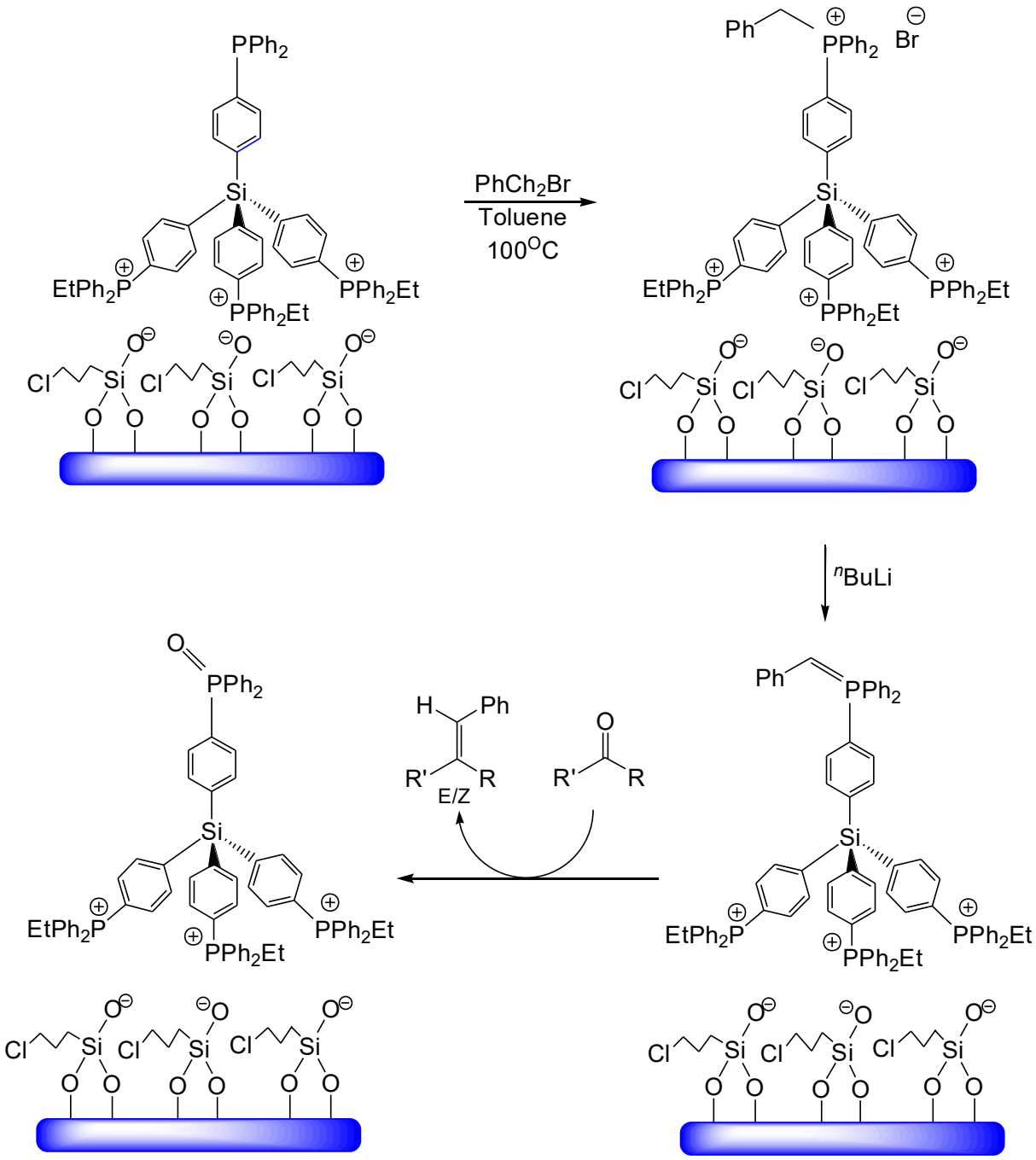

Scheme 5.1 Proposed synthesis steps for the reaction of an immobilized Wittig reagent with a carbonyl compound.

In this project, the reaction conditions for a surface-supported Wittig reaction will be optimized using a model reaction. Following this, the surface-supported Wittig reagent will

be synthesized in two different ways, both of which will be used to facilitate this reaction. All reagents and byproducts will be analyzed. Scheme 5.1 outlines the steps to be undertaken.

5.2 Results and Discussion

5.2.1 Model Compound

The first goal of the project was to optimize the reaction conditions for the Wittig reaction. The immobilized Wittig reagent is chosen as depicted in Scheme 5.1, but the type of aldehyde or ketone, temperature, and solvent can be optimized regarding yield and stereochemistry. To do this, a representative ylide (Scheme 5.2) was synthesized using known procedures,[59] and various reaction conditions were screened.

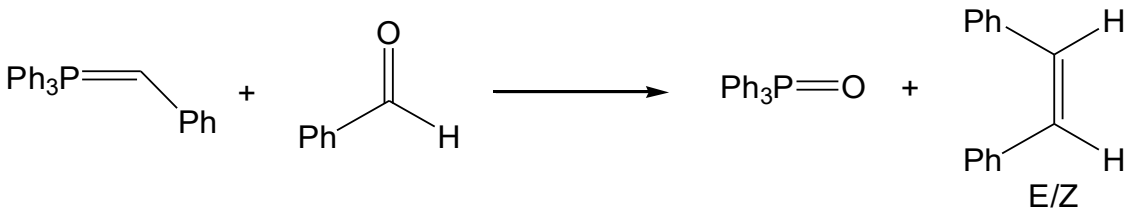

Scheme 5.2 General Wittig reaction scheme using a representative ylide.

Using a symmetrical ketone in a first step, an analysis of a product mixture can be avoided, as the product does not consist of E/Z isomers. However, it can be seen from Table 5.1 that the symmetrical ketones acetone, benzophenone, and cyclohexanone were mostly unreactive with this model ylide. After switching to benzaldehyde, the reaction proceeds rapidly. The orange color of the ylide disappears within seconds after the addition of benzaldehyde. Furthermore, THF as the solvent leads to better yields than diethyl ether. The temperature of the reaction in THF is inconsequential with respect to the obtained isomer

ratio, but room temperature results in the highest overall yield of 82%. Therefore, for the following reactions with the immobilized ylide, benzaldehyde will be used as the carbonyl reagent, while THF will be the solvent, and the reaction will be carried out at 22 °C.

Table 5.1 Summary of results using the molecular ylide Ph_3P=CHPh to screen conditions for the reaction depicted in Scheme 5.2.

Carbonyl Compound	Solvent	Temperature (°C)	Overall Yield (%)	*E* Isomer (%)
Acetone	THF	60	0	N/A
Benzophenone	THF	60	0	N/A
Cyclohexanone	THF	60	~8	N/A
Benzaldehyde	THF	0	75	55
Benzaldehyde	THF	22	82	54
Benzaldehyde	THF	60	65	52
Benzaldehyde	Et_2O	22	59	70

Additionally, an experiment was performed using the tetraylide compound **21** to test if a molecule with four ylide groups would react in the same way as the monofunctional ylide Ph_3P=CHPh. This is also important for a later test, when this tetraylide will be immobilized on SiO_2 and reacted. The tetraylide was synthesized by reaction of benzyl bromide with the tetraphosphine **3**, followed by deprotonation with ^{n}BuLi. When used for the Wittig reaction under the optimized conditions described above, the olefin yield was 48%, and the product mixture contained 63% of the *E* isomer. Although the yield was lower than in optimal cases

(Table 5.1), there was no detrimental inhibition of the Wittig reaction when using a tetraylide.

5.2.2 Synthesis and Immobilization

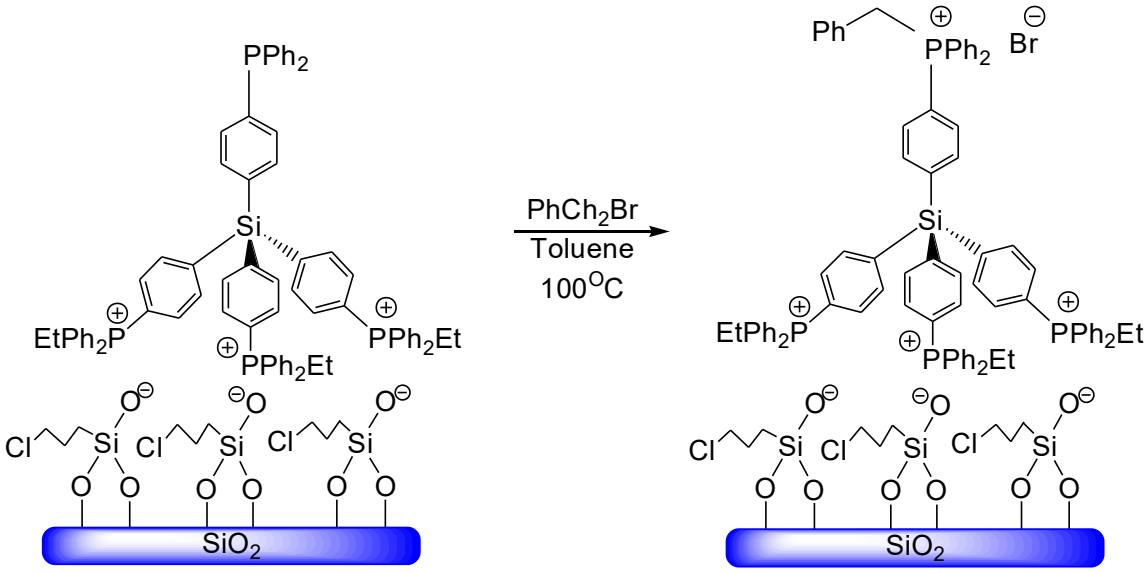

3i **22i**

Scheme 5.3 Quaternization of the phosphine group of **3i** using benzyl bromide to generate **22i**.

In Chapter III it has been demonstrated that **3i** can be synthesized in the presence of ethoxysilanes, resulting in a scaffold immobilized via three phosphonium centers. The remaining phosphine group can be reacted with an excess of benzyl bromide, which generates the immobilized phosphonium salt **22i** (Scheme 5.3). In the ^{31}P solid-state NMR spectrum of **22i** (Figure 5.1) the signal of the phosphine group is gone, which suggests the phosphine has been quaternized quantitatively. The new phosphonium signal is overlapping with the ethyl phosphonium signals bound to the silica surface via electrostatic interactions.

There is also some phosphine oxide present, as indicated by the rotational sideband downfield of the signal, which is characteristic for phosphine oxides.

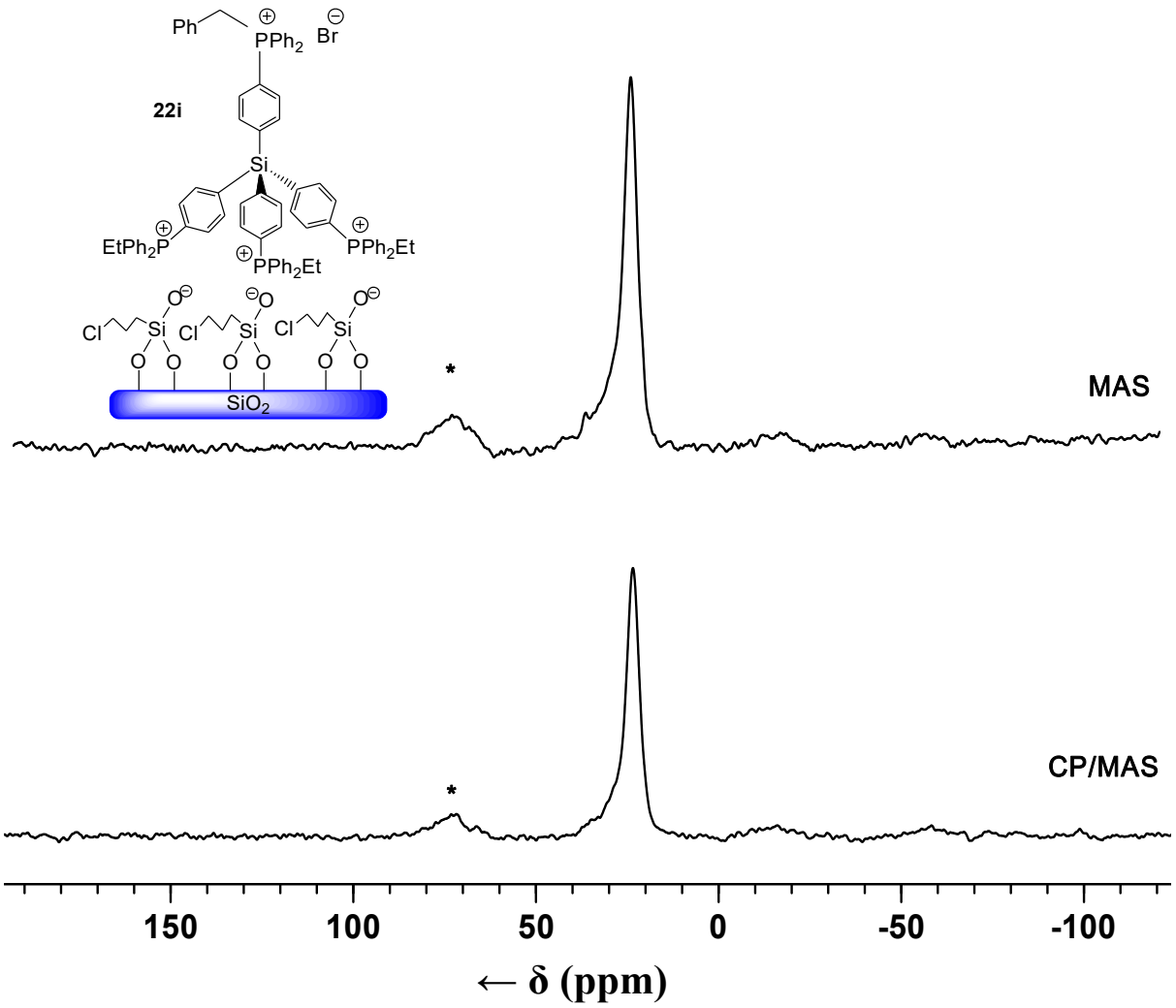

Figure 5.1 ^{31}P CP/MAS and MAS spectra of **22i**. Asterisks denote rotational sidebands of the oxide signals. Rotational speed 8 kHz.

The next step involves the abstraction of a proton from the methylene group of the benzyl phosphonium functionality (Scheme 5.4). This is accomplished using the strong base *n*-butyllithium. When the immobilized ylide **23i** is formed, the solid assumes a light orange

color, which is characteristic of benzyltriphenyl ylides and which was also observed for the molecular ylide $Ph_3P{=}CHPh$ (Scheme 5.2).

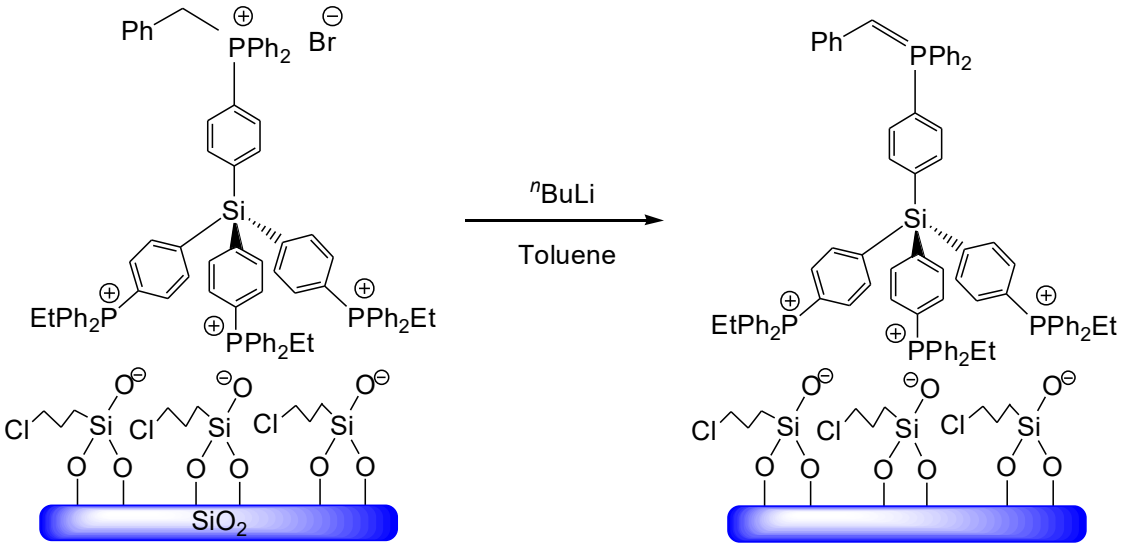

Scheme 5.4 Formation of immobilized ylide **23i** from **22i**.

In the ^{31}P CP/MAS NMR spectrum (Figure 5.2, top), the new signal at 8 ppm proves that the surface-bound ylide has formed. However, this signal is comparatively small in CP/MAS and not present in the MAS NMR spectrum (Figure 5.2, bottom). The likely cause of this is that in the MAS measurement the ylide phosphorus signal does not profit from the magnetization transfer from the vicinal proton and thus the signal intensity is diminished. On the other hand, the phosphonium ^{31}P nuclei close to the surface outnumber the ylide phosphine by a factor of three and additionally profit from the transfer of magnetization from the ethyl groups in CP/MAS. Finally, the sample was exposed to oxygen during the measurements, leading to oxidation of the ylide and some phosphine oxide formation.

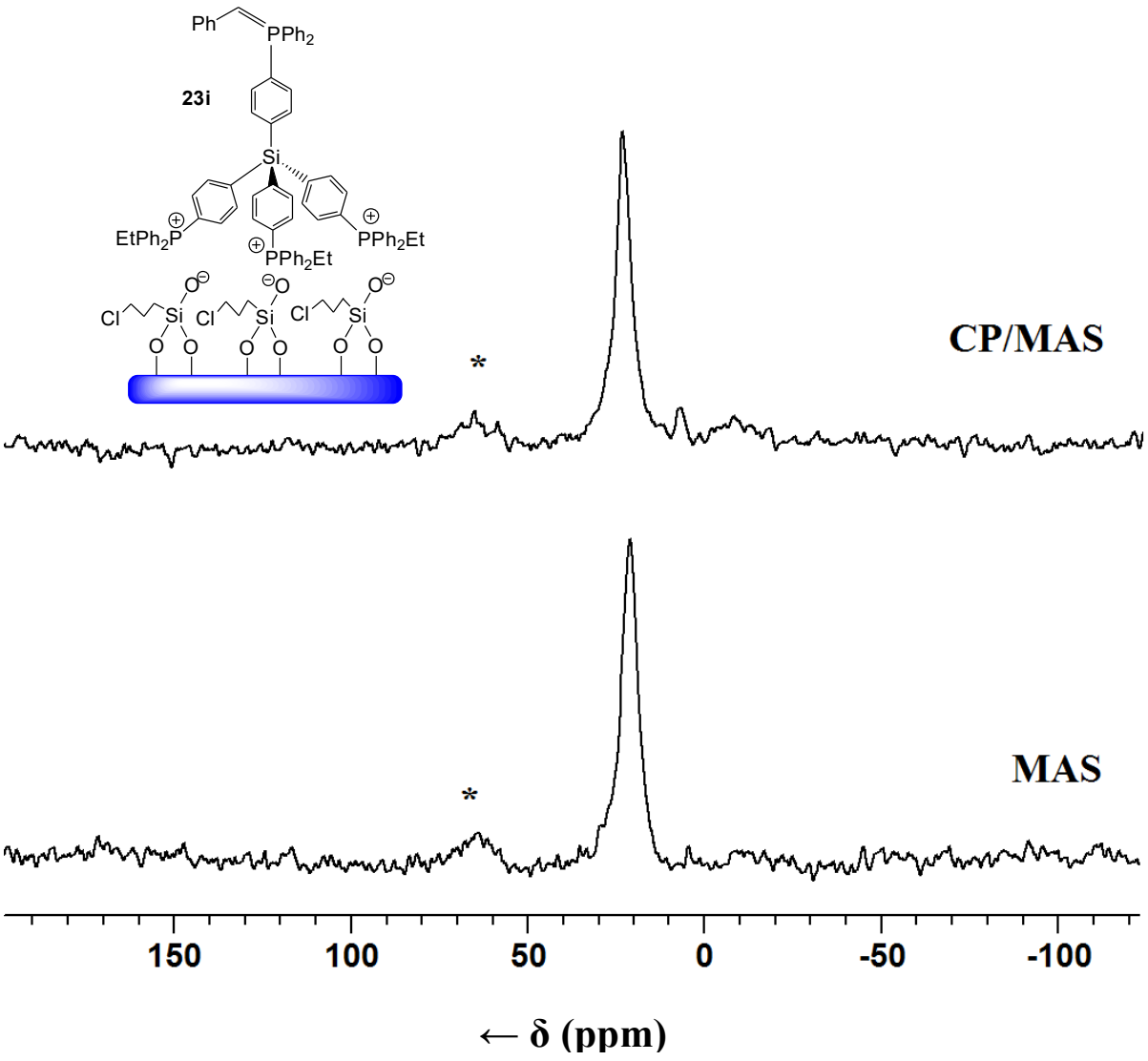

Figure 5.2 ^{31}P CP/MAS (top) and MAS (bottom) spectra of **23i**. Asterisks denote rotational sidebands. Rotational speed 7 kHz.

Next, an alternative method for generating an immobilized ylide reagent is developed. It is known from previous work by Yang[60] that ylides are reacting irreversibly with SiO_2 surfaces. It has been assumed that surface silanol groups reprotonate three of the four ylide groups, in this way regenerating the benzylphosphonium groups, which are then bound to the support by electrostatic interactions (Scheme 5.5). This presents a possible new venue for

forming an immobilized ylide by starting from the tetraylide **21** and allowing it to react with SiO_2. When the tetraylide **21** is dissolved in THF and added to SiO_2, the color of the solid changes to orange indicating that indeed the modified version of **21i** with benzyl instead of ethylphosphonium groups at the base of the scaffold has formed (Scheme 5.5).

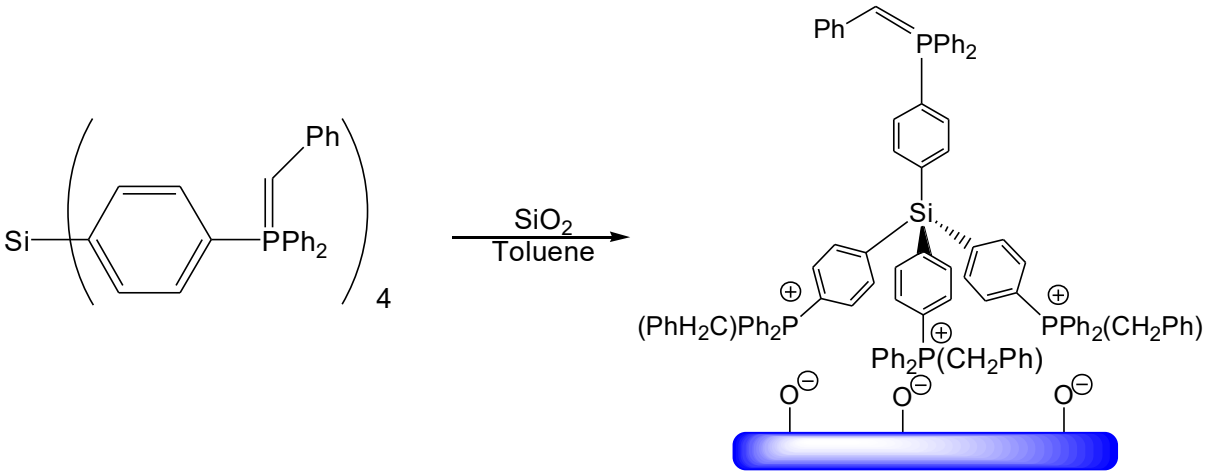

21 **21i**

Scheme 5.5 Immobilization of scaffold **21** on SiO_2 to form **21i**.

5.2.3 Surface-Supported Wittig Reaction

Once the Wittig reagent has been generated in its immobilized version on the surface the actual Wittig reaction can be tested. Previously, it has been observed that benzaldehyde was the most favorable carbonyl compound and using THF as the solvent results in the highest yields at room temperature, while the latter had very little effect on the *E*/*Z* isomer ratio (Table 5.1). Adding a stoichiometric amount of benzaldehyde to the immobilized Wittig reagent **23i** results in the formation of both isomers of stilbene and the immobilized phosphine oxide **24i** (Scheme 5.6).

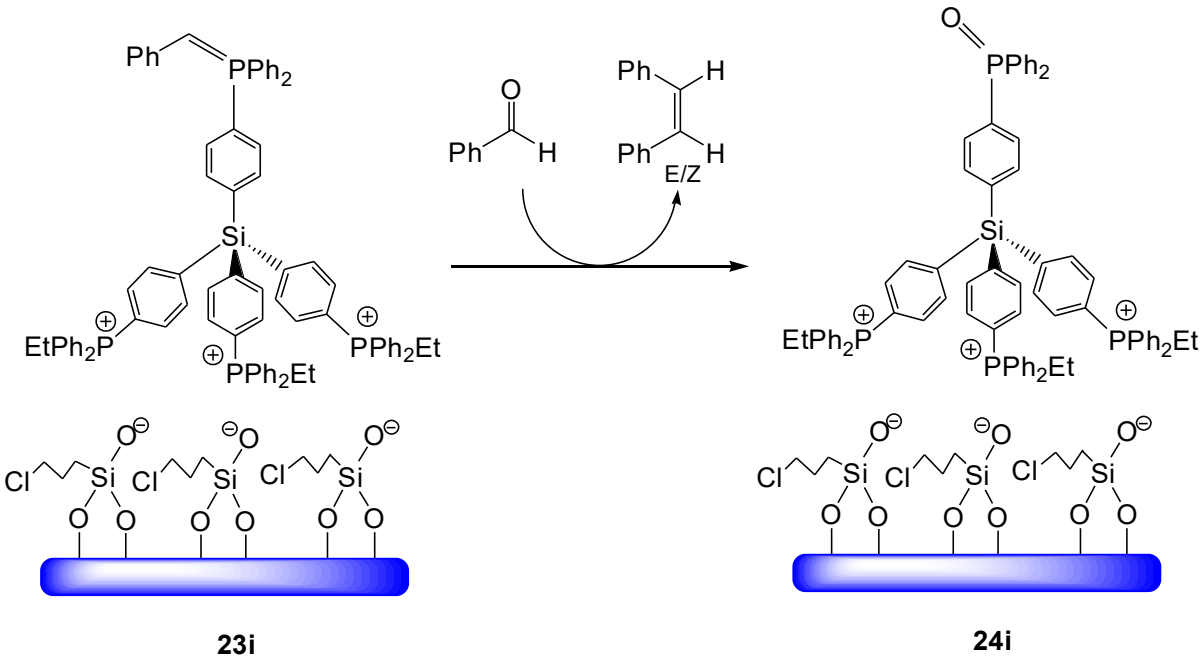

23i **24i**

Scheme 5.6 Wittig reaction using immobilized ylide **23i** to yield stilbene and **24i**.

After the reaction, the supernatant containing *E* and *Z* stilbene can be decanted from the insoluble **24i**, resulting in a clean product without further purification. The yield of the stilbene (73%) can be determined easily by weighing the residue after the solvent and excess benzaldehyde has been removed from the supernatant *in vacuo*.

To determine the *E*/*Z* ratio, ^{1}H NMR spectroscopy of the product mixture is used. In the ^{1}H NMR spectrum (Figure 5.3), it can be seen that there are two peaks at $\delta = 7.05$ and $\delta = 6.53$ ppm. These correspond to the *E* and *Z* isomers, respectively,[61] and integration of these signals gives the *E*/*Z* ratio.

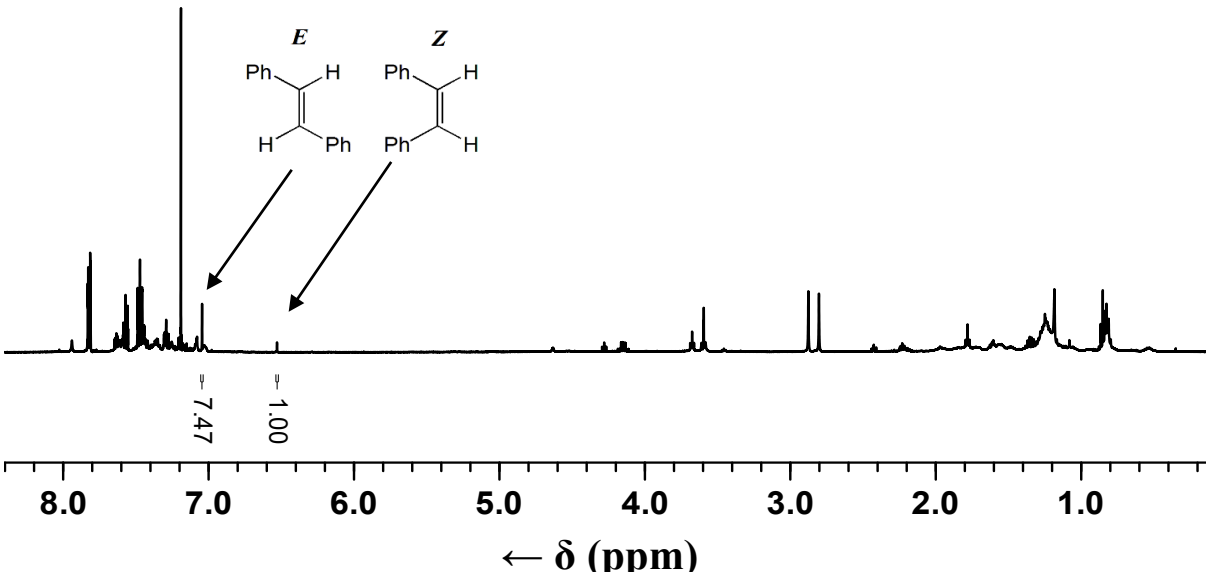

Figure 5.3 Representative ^{1}H NMR spectrum (C_6D_6) of a typical product mixture.

After the Wittig reaction, the decanted supernatant contains mainly the alkenes, while the phosphine oxide byproduct remains immobilized on the SiO_2 support. This is shown by the fact that there is no signal in the ^{31}P NMR spectrum of the decanted solution. Furthermore, the ^{31}P MAS NMR spectrum of the support after the Wittig reaction is consistent with the presence of immobilized phosphine oxide (Figure 5.4).

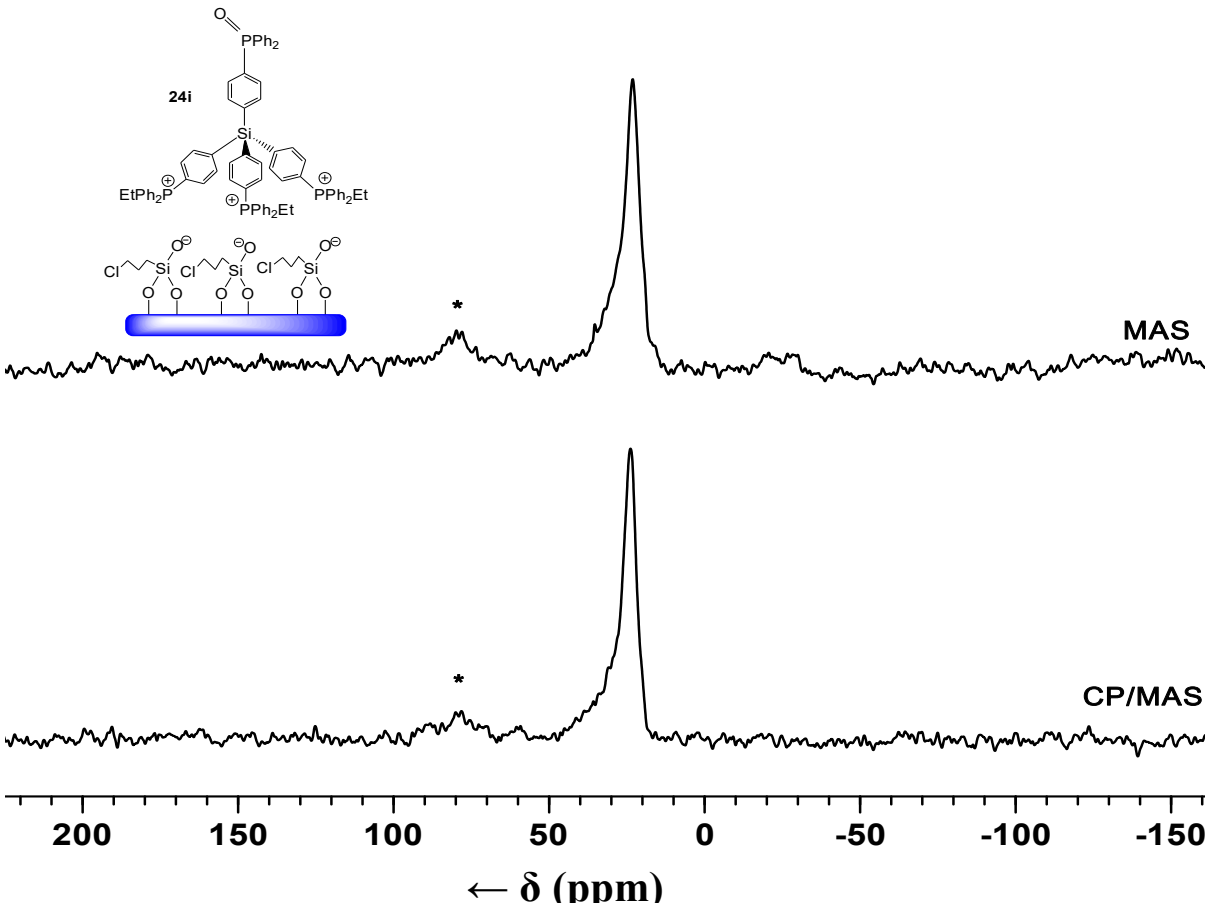

Figure 5.4 ^{31}P solid-state NMR spectra of **24i** after the Wittig reaction. Rotational speed 8 kHz. The asterisks denote rotational sidebands of the oxide signal.

It can be seen in the spectra displayed in Figure 5.4 that there is a large shoulder downfield of the phosphonium signal at 23 ppm. This broad signal, with only one rotational sideband downfield of the peak, is very characteristic of a phosphine oxide resonance. This confirms that it is possible to generate an immobilized Wittig reagent, to use it for a Wittig reaction, and to separate the surface-tethered phosphine oxide byproduct by decanting the supernatant that contains the pure product.

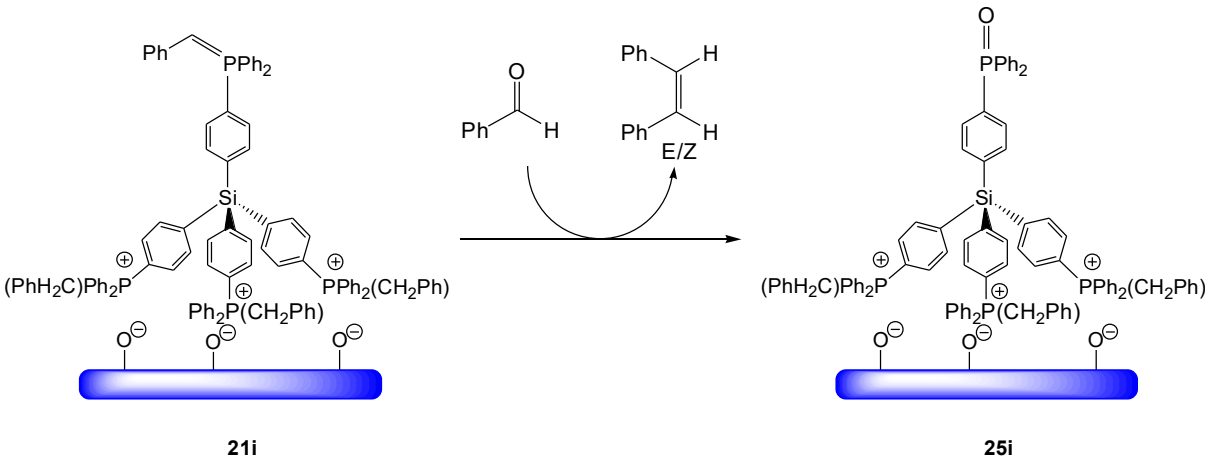

Scheme 5.7 Wittig reaction using immobilized ylide **21i** to yield stilbene and **25i**.

The Wittig reaction works in the case of immobilizing the scaffold, then forming the ylide on an already immobilized phosphine. It remains to be seen if the slightly altered version **21i**, which is generated by placing a tetraylide onto SiO_2 directly will achieve the same results (Scheme 5.7). After generating this immobilized Wittig reagent, the procedure follows the one previously described for **25i**.

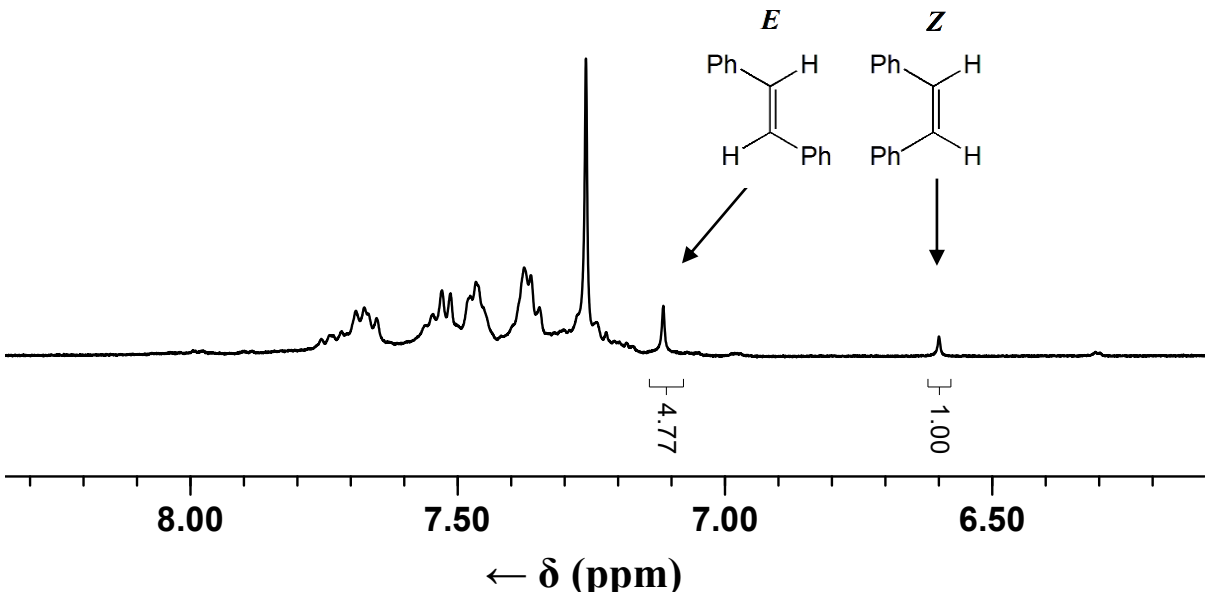

Figure 5.5 ^{1}H NMR (C_6D_6) of the supernatant after removal of the solvent.

It can be seen from the expansion of the ^{1}H NMR spectrum in Figure 5.5 that this reaction was successful as well. The signature chemical shifts of the resonances corresponding to the *E* and *Z* isomers are present. The data for the Wittig reaction are listed in Table 5.2.

Table 5.2 Results of the Wittig reaction using the tetraphosphine scaffold **21i** and **23i**.

Ylide	Carbonyl Compound	Solvent	Temperature (°C)	Overall Yield (%)	*E* Isomer (%)
23i	Benzaldehyde	THF	22	73	84
21i	Benzaldehyde	THF	22	75	87

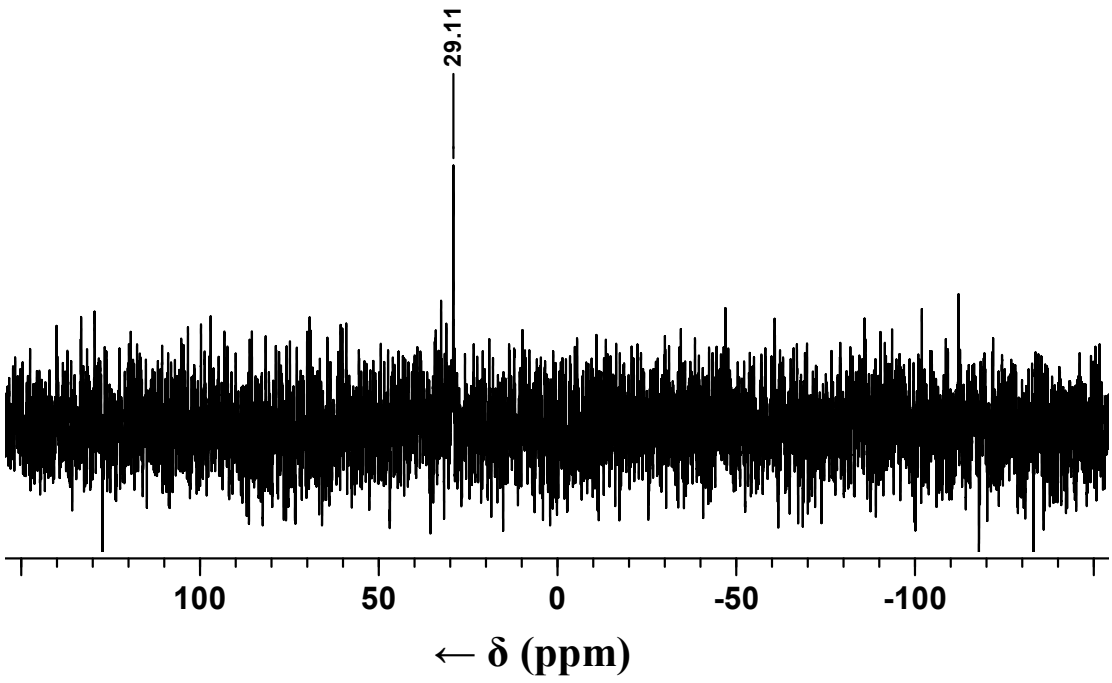

Figure 5.6 ^{31}P NMR of the supernatant above **25i** in C_6D_6 after undergoing a Wittig reaction.

Next it was investigated whether the modified surface-bound Wittig reagent **21i** remains as strongly bound to SiO_2 as **23i**. The ^{31}P NMR spectrum of the supernatant after the Wittig reaction (Figure 5.6) shows a signal with low intensity, but its chemical shift is very suggestive of phosphine oxide. This indicates that the scaffold **21i** is not remaining adsorbed on the SiO_2 and is leaching into solution.

This is confirmed by measuring ^{31}P solid-state NMR spectra of the remaining support. The spectra displayed in Figure 5.7 show no ^{31}P signal, meaning that all of the scaffold has been washed off. This means that the tetraylide was not bound as firmly to SiO_2 as phosphonium salts immobilized with ethoxysilanes. Impregnating a silica surface with tetraylides is, therefore, not a sustainable way to immobilize phosphonium salts irreversibly on SiO_2.

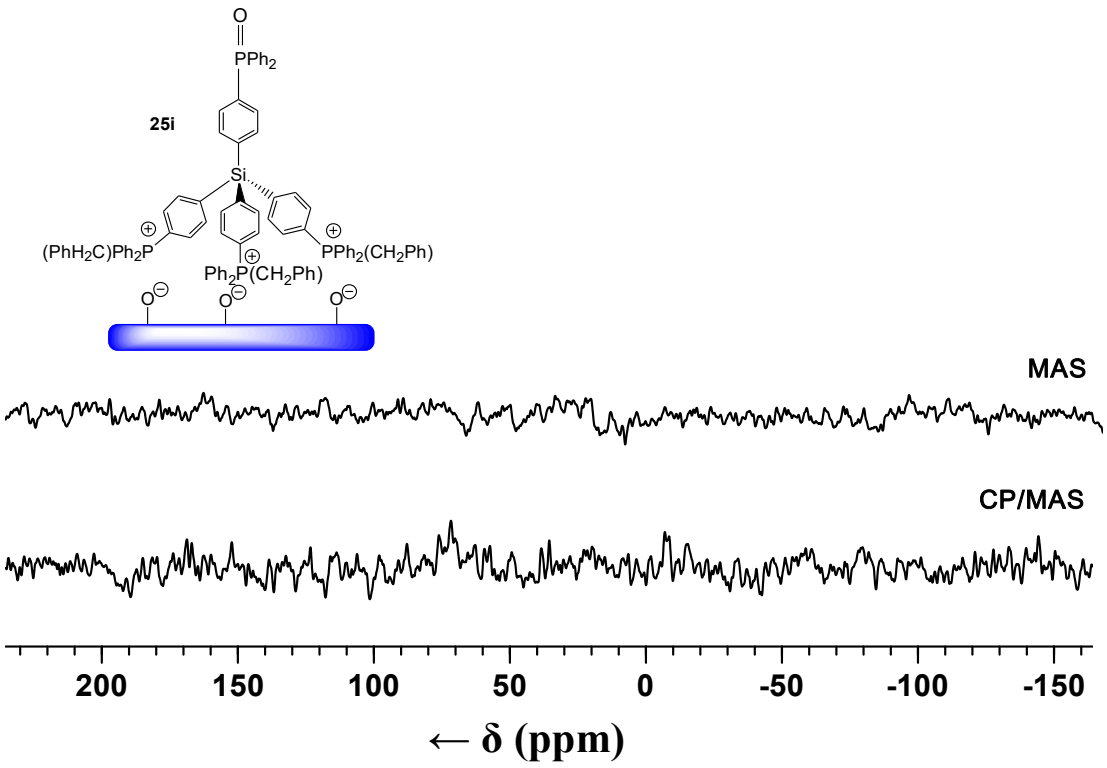

Figure 5.7 ^{31}P Solid-state NMR spectra of **25i** after undergoing a Wittig reaction. Rotational speed 8 kHz.

One of the most interesting and unexpected results is that binding the Wittig reagent to a surface has an effect on the ratio of the resulting structural isomers. The ratio of *E* and *Z* isomers of stilbene is about the same for the molecular ylide Ph_3P=CHPh in THF regardless of temperature (52-55%, Table 5.1). However, for the immobilized ylides, **23i** formed 84% *E*-stilbene and **21i** formed 87% *E*-stilbene (Table 5.2). Although it is known that surface-bound reagents can produce different isomer ratios than reagents in solution,[11c,17] it was unexpected in this case, given how the ylide group at the top of the linker scaffold is relatively unchanged by the support.

5.3 Conclusion

First, conditions were optimized using a molecular Wittig reagent, Ph_3P=CHPh. It was found that THF was the best solvent, while temperature changed the overall yield, but did not alter the product ratio in a decisive way, and symmetrical ketones were unreactive with the molecular ylide. When benzaldehyde was used as the carbonyl compound, it reacted quickly and gave good yields. The Wittig reaction produces two isomers of stilbene, *E* and *Z*, and Ph_3P=CHPh in solution produces them in nearly equal amounts. To test for any cooperative effects, and also to ensure that the Si center did not alter the reaction outcome, compound **21** was used for a Wittig reaction. The outcome was a slightly lower yield, but otherwise the result of the reaction was comparable to that in the case of using Ph_3P=CHPh.

In the next step the immobilized ylide was synthesized. This was done in two different ways. With the first method, the free phosphine of the scaffold, which had already been immobilized via three phosphonium centers (Chapter III), was quaternized with benzyl bromide, then transformed into the ylide **23i** using ^{n}BuLi. Solid-state NMR confirmed that the synthesis was successful. This ylide **23i** then underwent the Wittig reaction under the optimized conditions. The result was approximately the same yield as for the reaction with Ph_3P=CHPh in solution (73%), but with a substantially higher *E*/*Z* ratio (84%). The leftover phosphine oxide remained on the surface with no scaffold being leached into solution, as evidenced by solid-state NMR of the support and solution NMR of the supernatant.

The second method involved synthesizing the tetraylide **21** using the tetraphosphine **3**, then adding benzyl bromide to form **20**, before adding ^{n}BuLi to deprotonate the tetraphosphonium salt. The tetraylide was adsorbed by adding dissolved **21** to SiO_2 to create **21i**. This method produced results that were similar to those when using the first method

(75% yield, 87% *E* isomer), but the crucial difference to this method was that the scaffold was easily washed off with THF. This was readily seen in NMR of the supernatant and solid-state NMR of the remaining support.

5.4 Experimental Section

5.4.1 General Information and Procedures

All reactions are carried out using standard Schlenk techniques and a purified N_2 atmosphere, if not stated otherwise. Reagents purchased from Sigma Aldrich or VWR are used without further purification. Solvents are dried by boiling them over Na, distilled, and stored under N_2. CH_2Cl_2 and hexanes are obtained from a solvent purification system. The silica (Merck, 40 Å average pore diameter, 0.063 to 0.2 mm average particle size, specific surface area 750 m^2/g) is rigorously dried in vacuo at 250 °C for 4 days to remove adsorbed water and condense surface silanol groups.

5.4.2 Instruments and Measurements

The ^{1}H, ^{13}C, and ^{31}P NMR spectra of liquids were recorded at 499.70, 125.66, and 470.17 MHz on a 500 MHz Varian spectrometer and referenced as follows: ^{1}H: residual internal $CHCl_3$ (δ, 7.26 ppm) or benzene-d_6 (δ, 7.16 ppm); ^{13}C: internal $CDCl_3$ (δ, 77.23 ppm) or benzene-d_6 (δ, 128.06 ppm). ^{31}P NMR spectra are referenced to neat Ph_2PCl (δ, 81.92 ppm) which is placed in a capillary centered in the NMR sample tube. The ^{13}C and ^{31}P spectra are recorded with ^{1}H decoupling if not stated otherwise. The ^{29}Si NMR spectra of liquids were recorded at 79.46 on a 400 MHz Varian spectrometer and referenced as follows: ^{29}Si: external hexamethyldisiloxane (δ, 6.53 ppm). The solid-state NMR spectra are

measured with a Bruker Avance 400 widebore NMR spectrometer with a multinuclear 4 mm MAS probehead. For the ^{31}P CP/MAS and MAS measurements ^{1}H high-power decoupling was applied. The recycle delays are 3 s for CP/MAS and 10 s for MAS spectra.

5.4.3 Synthesis of 20

Tetraphosphine **3** (0.213 g, 0.198 mmol) is suspended in 50 mL DMF. Then 0.1573 g benzyl bromide (0.9197 mmol, 4.64 eq.) is added and the solution is heated to 60 °C and stirred for 16 h. The DMF is removed *in vacuo* and the residual solid is washed twice with 20 mL toluene. The product **20** is a white solid (0.407 g, 119%).

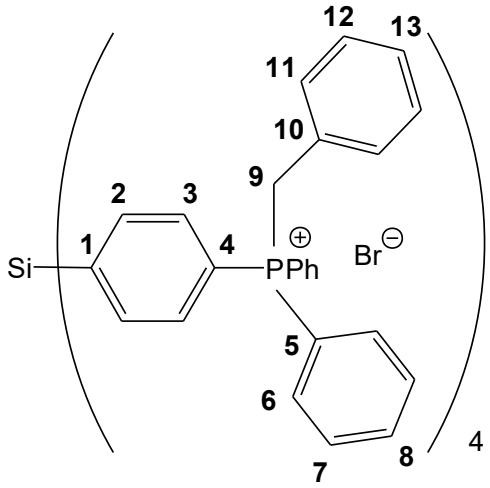

20

$C_{100}H_{84}Br_4P_4Si$

Mol. Wt.: 1757.334 g/mol

^{1}H NMR ($CDCl_3$, 499.69 MHz)

δ = 8.00 (8H, H-3, dd, $^{3}J(^{1}H\text{-}^{1}H)$ = 8.1 Hz, $^{3}J(^{31}P\text{-}^{1}H)$ = 4.5 Hz), 7.87 (8H, H-2, dd, $^{3}J(^{1}H\text{-}^{1}H)$ = 7.8 Hz, $^{4}J(^{31}P\text{-}^{1}H)$ = 3.2 Hz), 7.75 (8H, H-8, t, $^{3}J(^{1}H\text{-}^{1}H)$ = 7.7 Hz), 7.65 (32H, H-6/H-7, m) 7.19 (4H, H-13, d, $^{3}J(^{1}H\text{-}^{1}H)$ = 8.5 Hz), 7.09 (16H, H-11/H-12, m), 5.23 (8H, H-9, d, $^{2}J(^{31}P\text{-}^{1}H)$ = 14.4 Hz).

^{13}C NMR ($CDCl_3$, 125.66 MHz)

δ = 138.71 (s, C-1), 137.72 (d, C-2, $^{3}J(^{31}P\text{-}^{13}C)$ = 12.1 Hz), 135.21 (d, C-8, $^{4}J(^{31}P\text{-}^{13}C)$ = 2.8 Hz), 134.47 (d, C-6, $^{3}J(^{31}P\text{-}^{13}C)$ = 9.8 Hz), 134.08 (d, C-3, $^{2}J(^{31}P\text{-}^{13}C)$ = 9.6 Hz), 131.33 (d, C-11, $^{3}J(^{31}P\text{-}^{13}C)$ = 5.6 Hz), 130.36 (d, C-7, $^{3}J(^{31}P\text{-}^{13}C)$ = 12.6 Hz), 128.97 (d, C-12, $^{4}J(^{31}P\text{-}^{13}C)$ = 3.1 Hz), 128.64 (d, C-13, $^{5}J(^{31}P\text{-}^{13}C)$ = 3.6 Hz), 126.97 (d, C-10, $^{2}J(^{31}P\text{-}^{13}C)$ = 8.5 Hz), 121.29 (d, C-4, $^{1}J(^{31}P\text{-}^{13}C)$ = 83.8 Hz), 117.07 (d, C-5, $^{1}J(^{31}P\text{-}^{13}C)$ = 85.7 Hz), 31.11 (d, C-9, $^{1}J(^{31}P\text{-}^{13}C)$ = 47.0 Hz),

^{29}Si NMR ($CDCl_3$, 79.46 MHz)

δ = -15.46 (s)

^{31}P NMR ($CDCl_3$, 202.28 MHz)

δ = 23.12 (s)

5.4.4 Synthesis of 21

Tetraphosphonium salt **20** (0.1149 g, 0.06538 mmol) is suspended in toluene (25 mL) in a Schlenk flask. Then ^{n}BuLi (0.11 mL, 0.25 mol, 4.2 eq) is added to the flask, and the contents are allowed to stir for 15 h. Then the product is extracted in toluene, resulting in **21**, an orange solid (0.0854 g, 88.4%).

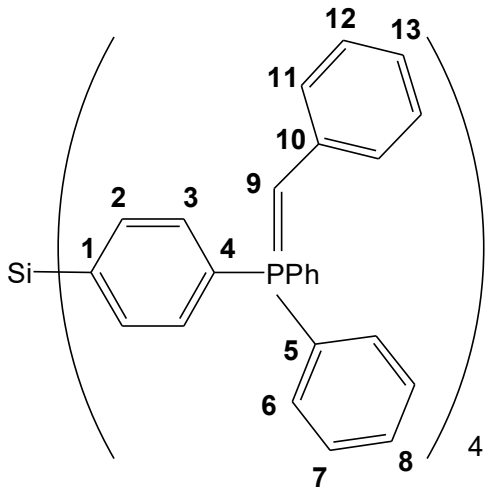

21

$C_{100}H_{80}P_4Si$

Mol. Wt.: 1433.688 g/mol

^{1}H NMR ($CDCl_3$, 499.69 MHz)

δ = 8.00 (8H, H-3, dd, $^{3}J(^{1}H\text{-}^{1}H)$ = 8.0 Hz, $^{3}J(^{31}P\text{-}^{1}H)$ = 4.4 Hz), 7.84 (8H, H-2, dd, $^{3}J(^{1}H\text{-}^{1}H)$ = 7.8 Hz, $^{4}J(^{31}P\text{-}^{1}H)$ = 3.2 Hz), 7.78 (8H, H-8, t, $^{3}J(^{1}H\text{-}^{1}H)$ = 7.7 Hz), 7.67 (32H, H-6/H-7, m) 7.32 (8H, H-11, t, $^{3}J(^{1}H\text{-}^{1}H)$ = 7.3 Hz), 7.11 (12H, H-12/H-13, m), 5.29 (2H, H-9, d, $^{2}J(^{31}P\text{-}^{1}H)$ = 14.4 Hz).

^{13}C NMR ($CDCl_3$, 125.66 MHz)

δ = 138.07 (s, C-1), 137.20 (d, C-2, $^{3}J(^{31}P\text{-}^{13}C)$ = 11.9 Hz), 134.93 (d, C-8, $^{4}J(^{31}P\text{-}^{13}C)$ = 2.8 Hz), 134.03 (d, C-6, $^{3}J(^{31}P\text{-}^{13}C)$ = 9.8 Hz), 133.67 (d, C-3, $^{2}J(^{31}P\text{-}^{13}C)$ = 9.6 Hz), 131.89 (d, C-13, $^{5}J(^{31}P\text{-}^{13}C)$ = 2.7 Hz), 130.56 (d, C-11, $^{3}J(^{31}P\text{-}^{13}C)$ = 9.8 Hz), 129.99 (d, C-7, $^{3}J(^{31}P\text{-}^{13}C)$ = 12.6 Hz), 127.89 (d, C-12, $^{4}J(^{31}P\text{-}^{13}C)$ = 13.5 Hz), 126.44 (d, C-10, $^{2}J(^{31}P\text{-}^{13}C)$ = 8.6 Hz), 120.95 (d, C-4, $^{1}J(^{31}P\text{-}^{13}C)$ = 83.6 Hz), 117.07 (d, C-5, $^{1}J(^{31}P\text{-}^{13}C)$ = 85.7 Hz), 23.44 (d, C-9, $^{1}J(^{31}P\text{-}^{13}C)$ = 15.6 Hz),

^{29}Si NMR ($CDCl_3$, 79.46 MHz)

δ = -15.01 (s)

^{31}P NMR (C_6D_6, 202.28 MHz)

δ = 8.04 (s)

5.4.5 Synthesis of 21i

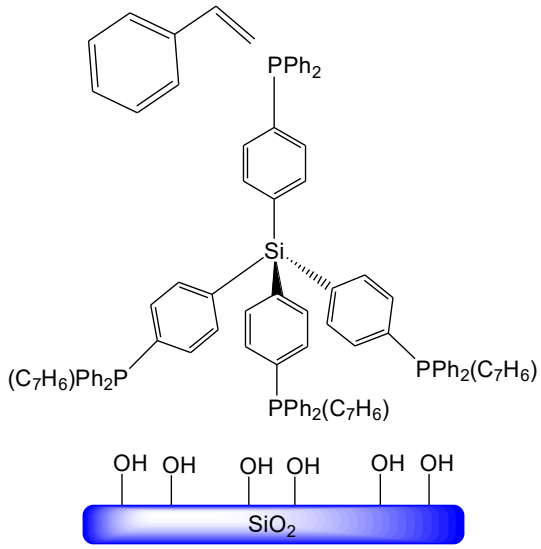

21i

0.0366 g **21** (0.02082 mmol) is suspended in toluene, and 0.04 mL ^{n}BuLi (0.1 mmol, 4.8 eq.) is added. The reaction proceeds for 1 h. Separately, 0.250 g SiO_2 is suspended 10 mL toluene. The ylide **9**, having formed from deprotonation of **8**, is added via cannula to the SiO_2 suspension. The mixture is then stirred at room temperature overnight. The product **14** is decanted and washed with 20 mL toluene. The product is then dried *in vacuo*, leaving 0.260 g **14 (**92.8%), an orange solid. The mass of **9** remaining in the supernatant was 0.0070 g, so the mass of ylide on the surface was 0.0229 g (0.0155 mmol). Therefore, the surface coverage was 4.98 particles/100 nm^2 (91.6 mg/g SiO_2, $6.20 \cdot 10^{-2}$ mmol/g SiO_2).

5.4.6 Synthesis of 22i

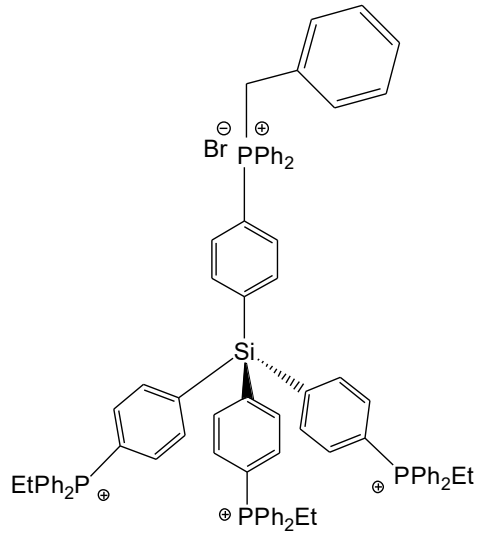

22i

0.162 g of **3i** are placed in a Schlenk flask, along with 20 mL toluene. Then 0.50 mL benzyl bromide (4.2 mmol, exc.) are added, and the mixture is heated to 100°C. After 18 h, the mixture is cooled, the supernatant is decanted, and the product is washed twice with 20 mL toluene. The solid, slightly yellow product **21i** is then dried *in vacuo*, giving a yield of 0.1584 g (97%).

5.4.7 Synthesis of 23i

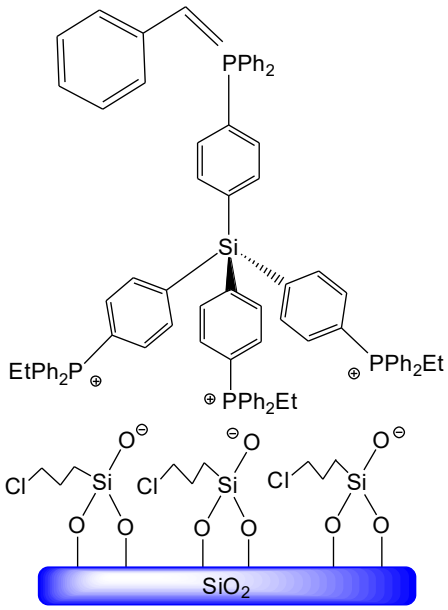

23i

0.240 g of **22i** are suspended in 20 mL toluene. Then 0.30 mL 2.5 M ^{n}BuLi (0.75 mmol) are added, and the reaction proceeds for 2 h. The supernatant is decanted and the product **22i** is washed with 20 mL toluene, leaving an orange powder with a mass of 0.238 g (99%).

5.4.8 General Procedure for Wittig Reaction

Compound **22i** (0.238 g) is immediately added to a flask and suspended in THF (10 mL). Benzaldehyde (0.123 g) is added to the suspension. The orange color of the particles vanishes over the span of about 1 minute. The reaction proceeds overnight, then the solution is decanted and the solvent is removed *in vacuo*. The yield is 0.0089 g *E/Z*-stilbene (73%), of which 87% is determined to be the *E* isomer by ^{1}H NMR.

CHAPTER VI

SUMMARY

In this thesis various tetraphosphines with tetraphenylelement cores with silicon and tin as the center atoms, for example, Si(*p*-$C_6H_4PCy_2)_4$, were synthesized. Synthetic routes have been explored in detail and optimized for each tetraphosphine. These tetraphenylelement compounds have the advantage of incorporating a rigid backbone. This feature makes them ideal scaffold-like linkers that prevent interactions of coordinated metal complexes with the reactive silica surface after being immobilized, and it diminishes the probability of deactivation of the metal complexes by dimerization. Derivatives of these molecules were obtained in a straightforward manner to meet the needs of the application desired. There are two principal routes for synthesizing these scaffolds, depending on whether the tetraphenyl core is generated in the first or second step. Both routes are used to synthesize compound **3** as well as derivatives thereof. All of these compounds have been fully characterized. It is possible to modify the scaffolds by incorporating different substituents at phosphorus and to choose alternative elements from the carbon group for the core. For example, compounds with four dicyclohexylphosphine groups can be generated, and a Sn, or alternatively a Si core can be incorporated. This is demonstrated for compounds **12**, **13**, and **14**. All of the scaffolds with cyclohexylphosphines display an interesting ^{13}C NMR phenomenon where six aliphatic signals are found per cyclohexyl ring while four would be expected at first glance. For synthesizing compounds **14**, **15**, and **16**, it is necessary to use ^{t}BuLi to lithiate compound **2**, which proves to be the only successful synthesis route.

Next, the research focus was placed on interactions of the tetraphosphines and their phosphonium salts with the silica surface. The tetraphosphine scaffolds can be immobilized onto silica using ethoxysilanes. During this process the immobilization is occurring via three generated phosphonium groups, leaving one free phosphine that will eventually be coordinated to a catalyst or transformed into a reagent. Monophosphonium salts are mobile on surfaces in the presence of solvents. To determine the modes of mobility, four salts were checked regarding their solubility, and whether this correlates with the ^{31}P HRMAS linewidths. There was no strong correlation, and therefore the mechanism involving surface detachment in a solvent could be ruled out with respect to the surface mobility of phosphonium salts. Furthermore, while simply impregnated phosphonium salts can be leached off the surface, they are not detached after being immobilized with ethoxysilanes, as in these cases the counteranions are covalently tethered to the support. This was demonstrated by placing batches of **3i** in eight different solvents, where less than 3% leaching occurred, even in very polar solvents.

Using the tetraphosphine scaffold linkers, a new class of immobilized Wilkinson-type Rh catalysts, **3iRh**, **12iRh**, and **13iRh**, could be obtained. The Wilkinson's catalyst can be coordinated to the immobilized scaffold via a simple ligand exchange. These new catalysts can easily be recycled almost indefinitely, they work at very low temperatures, have no active species leaching into the supernatant, and they are resistant to oxidation in air. The only functional difference between the catalysts is that **12iRh** and **13iRh** require 50 °C to initiate catalytic activity, while **3iRh** was already active at room temperature. Unfortunately, the catalyst is reduced during the batchwise catalytic run, resulting in the formation of Rh nanoparticles. Importantly, it could be demonstrated that the core element of the scaffold

linker, Si or Sn, plays no part in catalysis. The last catalyst synthesized was **18iRh**, which is distinct from the other catalysts because it does not feature a rigid linker, and was coordinated to the Rh center in a chelating manner. The catalyst is effective at room temperature, but under these conditions it needs to form nanoparticles before any catalytic reaction can commence. Therefore, it can be concluded that using a chelating linker to bind to the Rh center did not prevent nanoparticle formation.

In the final section of this thesis, surface-supported Wittig reactions for easy removal of the phosphine oxide byproduct were explored. The rigid linker scaffolds are ideal for this purpose because the sensitive ylide group that is needed as an intermediate in this reaction is prevented sterically from decomposition by interacting with the reactive silica surface. The conditions for this reaction were optimized using a molecular Wittig reagent, $Ph_3P{=}CHPh$. The Wittig reaction, when performed in THF at RT, with benzaldehyde as the carbonyl compound, produces two isomers of stilbene, *E* and *Z*, in nearly equal amounts. There were no cooperative effects when applying the tetraylide **21**. In the next step an immobilized ylide was synthesized. This was achieved in two different ways.

Using the first method, the remaining phosphine at the top of the scaffold, which had been immobilized via three phosphonium centers, was quaternized with benzyl bromide, then transformed into the ylide **23i** using ^{n}BuLi. Solid-state NMR confirmed that the synthesis was successful. This ylide was then subjected to the Wittig reaction under the optimized conditions. The result was approximately the same yield as for the reaction with $Ph_3P{=}CHPh$ in solution (73%), but with a substantially higher *E*/*Z* ratio (84%). The formed phosphine oxide byproduct remained on the surface with no scaffold leaching into solution.

The second method involved synthesizing the tetraylide **21** using the tetraphosphine **3**, then adding benzyl bromide to form **20**, before adding ^{n}BuLi to deprotonate the tetraphosphonium salt. The tetraylide was then reacted with the silica surface to create **21i**. This method produced results that were similar to those when using the first method (75% yield, 87% *E* isomer), but the crucial difference was that the scaffold could easily be washed off with THF.

REFERENCES

1. Guenther, J.; Reibenspies, J.; Blümel, J. *Adv. Synth. Catal*. **2011**, *353*, 443-460.

2. Posset, T.; Guenther, J.; Pope, J.; Oeser, T.; Blümel, J. *Chem. Commun*. **2011**, *47*, 2059-2061.

3. Beele, B.; Guenther, J.; Perera, M.; Stach, M.; Oeser, T.; Blümel, J. *New J. Chem*. **2010**, *34*, 2729-2731.

4. Guenther, J.; Blümel, J. *ACS Catal*., *in preparation*.

5. Posset, T.; Pope, J.; Oeser, T.; Blümel, J. *Adv. Synth. Catal*., *in preparation*.

6. Beele, B.; Yang, Y.; Perera, M.; Stach, M.; Oeser, T. *Eur. J. Inorg. Chem*., *in preparation*.

7. Stach, M. Masters Thesis, Texas A&M University, College Station, TX, 2009.

8. Perera, M. Masters Thesis, Texas A&M University, College Station, TX, 2011.

9. Beele, B. Ph.D. Thesis, University of Heidelberg, Heidelberg, Germany, 2009.

10. Guenther, J. Ph.D. Thesis, Texas A&M University, College Station, TX, 2012.

11. (a) Barbaro, P.; Liguori, F.; Editors. *Heterogenized Homogeneous Catalysts for Fine Chemicals Production*. Springer: New York, 2010; (b) *Supported Metal Complexes*., Hartley, F. R., D. Reidel Publishing Co.: Holland, 1985; (c) Clark, J. H. *Supported Reagents in Organic Reactions*. Wiley-VCH: Weinheim, 1994; (d) Gladysz, J. A.; Editor. *Recoverable Catalysts and Reagents*. Special Issue of *Chem. Rev*. **2002**, *102*; (e) DeVos, D. E.; Vankelecom, I. F. J.; Jacobs, P. A.; Editors. *Chiral Catalyst Immobilization and Recycling*. Wiley-VCH: Weinheim, 2000; (f) Rothenberg, G. *Catalysis: Concepts and Green Applications*. Wiley-VCH: Weinheim: 2008.

12. Reinhard, S.; Behringer, K. D.; Blümel, J. *New J. Chem.* **2003**, *27*, 776-778.

13. Merckle, C.; Blümel, J. *Top. Catal.* **2005**, *34*, 5-15.

14. Merckle, C.; Blümel, J. *Adv. Synth. Catal*. **2003**, *345*, 584-588.

15. Silbernagel, R.; Diaz, A.; Steffensmeier, E.; Clearfield, A.; Blümel, J. *J. Mol. Catal*. *A* **2014**, *394*, 217-223.

16. (a) Nicolaou, K. C.; Hanko, R.; Hartwig, W.; Editors. *Handbook of Combinatorial Chemistry*. Wiley-VCH: Weinheim, 2002; Vol. 1, 2; (b) Wilson, S. R.; Czarnik, A. W.

Combinatorial Chemistry. John Wiley & Sons: New York, 1997; (c) Bannworth, W.; Felder, E. *Combinatorial Chemistry*. Wiley-VCH: Weinheim, 2000; (d) Jung, G. *Combinatorial Chemistry*. Wiley-VCH: Weinheim, 1999.

17. (a) Seneci, P. *Solid-Phase Synthesis and Combinatorial Technologies*. John Wiley & Sons: New York, 2000. (b) Zaragoza Dörwald, F. *Organic Synthesis on Solid Phase*, Wiley-VCH: Weinheim, 2000. (c) Smith, K.; Editor. *Solid Supports and Catalysts in Organic Synthesis*. Ellis Horwood and PTR Prentice Hall: New York, 1992; (d) Hodge, P., Sherrington, D.C.; Editor. *Polymer-Supported Reactions in Organic Synthesis*. John Wiley & Sons: New York, 1980; (e) *Solid-Phase Organic Synthesis*; Burgess, K.; Editor.; Wiley-Interscience: New York, 2000. (f) Kates, S. A., Albericio, F. *Solid-Phase Synthesis: a Practical Guide*. Marcel Dekker, Inc.: New York, 2000.

18. (a) Vansant, E. F.; VanDer Voort, P.; Vrancken, K. C. *Characterization and Chemical Modification of the Silica Surface*. Elsevier: Amsterdam, 1995; (b) Scott, R. P. W. *Silica Gel and Bonded Phases*. John Wiley and Sons: New York, 1993.

19. (a) Subramanian, G. A. *Practical Approach to Chiral Separations by Liquid Chromatography*. Wiley-VCH: Weinheim, 1994; (b) Iler, R. K. *The Chemistry of Silica*, John Wiley: New York, 1979.

20. Chen, K.-Y.; Ivashenko, O.; Carroll, G. T.; Robertus, J.; Kistemaker, J. C. M.; London, G.; Browne, W. R.; Rudolf, P.; Feringa, B. L. *J. Am. Chem. Soc*. **2014**, *136*, 3219−3224.

21. "Improved Process for Production of Alkenylphosphonic Acid Derivatives by Addition of Hydrophosphonate Diesters to Alkynes in the Presence of Nickel Catalyst and a Base", Biel, M. C.; Kessinger, R. (BASF); Sommer, J.; Blümel,J., U.S. Patent, WO 2008113777, PCT Int. Appl. **2008**, *Chemical Abstracts* number: 149:402503.

22. Merckle, C.; Blümel, J. *Chem. Mater*. **2001**, *13*, 3617-3623.

23. Blümel, J. *Coord. Chem. Rev*. **2008**, *252*, 2410-2423.

24. (a) Blümel, J. *J. Am. Chem. Soc*. **1995**, *117*, 2112-2113; (b) Behringer, K. D.; Blümel, J. *J. Liquid Chromatogr.* **1996**, *19*, 2753-2765.

25. Blümel, J. *Inorg. Chem*. **1994**, *33*, 5050-5056.

26. Sommer, J.; Yang, Y.; Rambow, D.; Blümel, J. *Inorg. Chem.* **2004**, *43*, 7561-7563.

27. (a) Fetouaki, R.; Seifert, A.; Bogza, M.; Oeser, T.; Blümel, J. *Inorg. Chim. Acta* **2006**, *359*, 4865-4873; (b) Pope, J. C.; Posset,T.; Bhuvanesh, N.; Blümel, J. *Organometallics* **2014**, *33*, 6750-6753.

28. Tsiavaliaris, G.; Haubrich, S.; Merckle, C.; Blümel, J. *Synlett* **2001**, 391-393.

29. Piestert, F.; Fetouaki, R.; Bogza, M.; Oeser, T.; Blümel, J. *Chem. Commun.* **2005**, 1481-1483.

30. Posset, T.; Rominger, F.; Blümel, J. *Chem. Mater*. **2005**, *17*, 586-595.

31. Bogza, M.; Oeser, T.; Blümel, J. *J. Organomet. Chem.* **2005**, *690*, 3383-3389.

32. Behringer, K. D.; Blümel, J. *Chem. Commun*. **1996**, 653-654.

33. Behringer, K. D.; Blümel, J. *Inorg. Chem.* **1996**, *35*, 1814-1819.

34. (a) Reinhard, S.; Soba, P.; Rominger, F.; Blümel, J. *Adv. Synth. Catal*. **2003**, *345*, 589-602; (b) Cluff, K. J.; Bhuvanesh, N.; Blümel, J. *Chem. Eur. J*. **2015**, *21*, 10138-10148.

35. (a) Merckle, C.; Haubrich, S.; Blümel, J. *J. Organomet. Chem.* **2001**, *627*, 44-54.

36. (a) Stanger, K. J.; Wiench, J. W.; Prusik, M.; Espenson, J. H.; Kraus, G. A.; Angelici, R. J. *J. Mol. Catal*. **2006**, *243*, 158-169; (b) Lucas, N. T.; Hook, J. M.; McDonagh, A. M.; Colbran, S. B. *Eur. J. Inorg. Chem*. **2005**, 496-503; (c) Mehendale, N. C.; Bezemer, C.; Van Walree, C. A.; Klein Gebbink, R. J. M.; Van Koten, G. *J. Mol. Catal. A* **2006**, *257*, 167-175; (d) Zeidan, R. K.; Dufaud, V.; Davis, M. E. *J. Catal*. **2006**, *239*, 299-306; (e) Nunes, C. D.; Pillinger, M.; Valente, A. A.; Rocha, J.; Lopes, A. D.; Goncalves, I. S. *Eur. J. Inorg. Chem*. **2003**, 3870-3877; (f) DeClercq, B.; Lefebvre, F.; Verpoort, F. *Appl. Catal. A: General* **2003**, *247*, 345-364; (g) Heckel, A.; Seebach, D. *Chem. Eur. J.* **2002**, *8*, 559-572; (h) Uusitalo, A.-M.; Pakkanen, T. T.; Iiskola, E. I. *J. Mol. Catal. A: Chemical* **2002**, *177*, 179-194.

37. Ozin, G. A.; Arsenault, A. C., *Nanochemistry: A Chemical Approach to Nanomaterials,* RSC Publishing: Cambridge, 2005.

38. (a) Jones, C. W. *Top. Catal.* **2010**, *53*, 942-952; (b) Ping, E. W.; Pierson, J.; Wallace, R.; Miller, J. T.; Fuller, T. F.; Jones, C. W. *Applied Catalysis A* **2011**, *396*, 85-90; (c) Richardson, J. M.; Jones, C. W. *J. Catal*. **2007**, *251*, 80-93; (d) Weck, M.; Jones, C. W. *Inorg. Chem*. **2007**, *46*, 1865-1875; (e) Richardson, J. M.; Jones, C. W. *Adv. Synth. Catal*. **2006**, *348*, 1207-1216; (f) Phan, N. T. S.; Van Der Sluys, M.; Jones, C. W. *Adv. Synth. Catal*. **2006**, *348*, 609-679.

39. (a) Cassol, C. C.; Umpierre, A. P.; Machado, G.; Wolke, S. I.; Dupont, J. *J. Am. Chem. Soc*. **2005**, *127*, 3298-3299; (b) Durán Pachón, L.; Rothenberg, G., *Appl. Organomet. Chem*. **2008**, *22*, 288-299; (c) Gaikwad, A. V.; Holuigue, A.; Thathagar, M. B.; ten Elshof, J. E.; Rothenberg, G. *Chem. Eur. J*. **2007**, *13*, 6908-1913; (d) Thathagar, M. B.; ten Elshof, J. E.; Rothenberg, G. *Angew. Chem., Int. Ed.* **2006**, *45*, 2886-2890; (e) Gaikwad, A. V.; Holuigue, A.; Thathagar, M. B.; Ten Elshof, J. E.; Rothenberg, G. *Chem. Eur. J*. **2007**, *13*, 6908-6913; (f) Dupont, J.; Fonseca, G. S.; Umpierre, A. P.; Fichtner, P. F. P. Teixeira, S. R. *J. Am. Chem. Soc*. **2002**, *124*, 4228-4229.

40. (a) Myers, V. S.; Weir, M. G.; Carino, E. V.; Yancey, D. F.; Pande, S.; Crooks, R. M. *Chem. Sci*. **2011**, *2*, 1632-1646; (b) Carino, E. V.; Crooks, R. M. *Langmuir* **2011**, *27*, 4227-4235; (c) Scott, R. W.; Wilson, O. M.; Crooks, R. M. *J. Phys. Chem. B* **2005**, *109*, 692-704.

41. Yamauchi, Y.; Itagaki, T.; Yokoshima, T.; Kuroda, K. *J. Dalton Trans*. **2012**, *41*, 1210-1215.

42. Niemantsverdriet, J. W. *Spectroscopy in Catalysis*. Wiley-VCH: Weinheim, 1995; (b) Sibilia, J. P.; Ed. *A Guide to Materials Characterization and Chemical Analysis*. Wiley-VCH: Weinheim, 1988; (c) Webb, P. A.; Orr, C.; Editors. *Analytical Methods in Fine Particle Technology*. Micromeritics Instrument Corporation: Norcross, GA, 1997; (d) Larkin, P. *Infrared and Raman Spectroscopy*. Elsevier: Amsterdam, 2011.

43. (a) Fyfe, C. A. *Solid-State NMR for Chemists*. C. F. C. Press: Guelph, Canada, 1983; (b) Bell, A. T.; Pines, A.; Editors. *NMR Techniques in Catalysis*. Marcel Dekker, Inc.: New York, 1994; (c) Engelhardt, G.; Michel, D. *High-Resolution Solid-State NMR of Silicates and Zeolites*. John Wiley & Sons: New York, 1987; (d) Stejskal, E. O.; Memory, J. D. *High Resolution NMR in the Solid State*. Oxford University Press: New York, 1994; (e) Fitzgerald, J. J.; Ed. *Solid-State NMR Spectroscopy of Inorganic Materials*. American Chemical Society: Washington DC, 1999; (f) Duer, M. J. *Introduction to Solid-State NMR Spectroscopy*. Blackwell Publishing: Oxford, 2004.

44. Reinhard, S.; Blümel, J. *Magn. Reson. Chem*. **2003**, *41*, 406-416.

45. Brenna, S.; Posset, T.; Furrer, J.; Blümel, J. *Chem. Eur. J.* **2006**, *12*, 2880-2888.

46. Posset, T.; Blümel, J. *J. Am. Chem. Soc.* **2006**, *128*, 8394-8395.

47. Yang, Y.; Beele, B.; Blümel, J. *J. Am. Chem. Soc.* **2008**, *130*, 3771-3773.

48. (a) Hilliard, C. R.; Bhuvanesh, N.; Gladysz, J. A.; Blümel, J. *Dalton Trans*. **2012**, *41*, 1742-1754; (b) Ahn, S. H.; Cluff, K. J.; Bhuvanesh, N.; Blümel, J. *Angew. Chem. Int. Ed.* **2015**, *54*, 13341-13345; (c) Hilliard, C. R.; Kharel, S.; Cluff, K. J.; Bhuvanesh, N.; Gladysz, J. A.; Blümel, J. *Chem. Eur. J.* **2014**, *20*, 17292-17295.

49. Ng, S.; Sathasivam, R. V.; Lo, K. *J. Phys. Chem. A* **2005**, *109*, 12059-12063.

50. Krannich, L. K.; Kanjolia, R. K.; Watkins, C. L. *Magn. Reson. Chem*. **1987**, *25*, 320.

51. Van Overschelde, M.; Vervecken, E.; Modha, Sachin G.; Cogen, S.; Van der Eycken, E.; Van der Eycken, J. *Tetrahedron* **2009**, *65*, 6410–6415.

52. Schraml, J.; Čapka, M.; Blechta, V. *Magn. Reson. Chem*. **1992**, *30*, 544-547.

53. Thomas, C. M.; Peters, J. C. *Inorg. Chem.* **2004**, *43*, 8-10.

54. Kermagoret, A.; Braunstein, P. *Dalton Trans*. **2008**, *41*, 822-831.

55. (a) Cluff, K. J.; Bhuvanesh, N.; Blümel, J. *Organometallics* **2014**, *33*, 2671−2680. (b) Cluff, K. J.; Schnellbach, M.; Hilliard C. R.; Blümel, J. *J. Organomet. Chem.* **2013**, *744*, 119-124.

56. (a) Timerbulatova, M. G.; Gatus, M. R. D.; Vuong, K. Q.; Bhadbhade, M.; Algarra, A. G.; Macgregor, S. A.; Messerle, B. A. *Organometallics* **2013**, *32*, 5071−5081. (b) Greco, R.; Goessler, W.; Cantillo, D.; Kappe, C. O. *ACS Catal*. **2015**, *5*, 1303−1312.

57. (a) Posner, G. H.; Runquist, A. W.; Chapdelaine, M. J. *J. Org. Chem.* **1977**, *42*, 1202-1208. (b) Ali, M. H.; Stevens, W. C. *Synthesis* **1997**, 764-768. (c) Braibante, M. E. F.; Braibante, H. T. S.; Rosso, G. B.; da Roza, J. K. *Synthesis* **2001**, 1935-1937.

58. Byrne, P.A.; Gilheany; D.G. *Chem. Soc. Rev.,* **2013**, *42*, 6670-6696.

59. Manoni, F; Connon, S. J. *Angew. Chem. Int. Ed*. **2014**, *53*, 2628-2632.

60. Yang, Y. Ph.D. Thesis, University of Heidelberg, Heidelberg, Germany, 2007.

61. (a) *Spectral Database for Organic Compounds (SDBS)*; ^{1}H NMR spectrum; SDBS No.: 1844; RN 103-30-0; http://riodb01.ibase.aist.go.jp/sdbs/ (accessed July 15, 2014). (b) *Spectral Database for Organic Compounds (SDBS)*; ^{1}H NMR; SDBS No.: 7295; RN 645-49-8; http://riodb01.ibase.aist.go.jp/sdbs/ (accessed July 15, 2014).

APPENDIX A

COMPOUND LIST

MOLECULAR COMPOUNDS

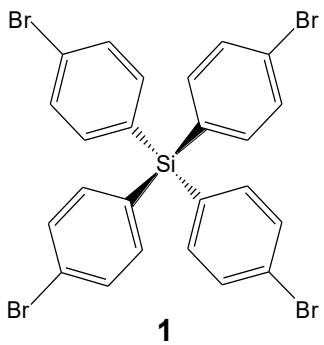
Br
Br
Si
Br
Br

1

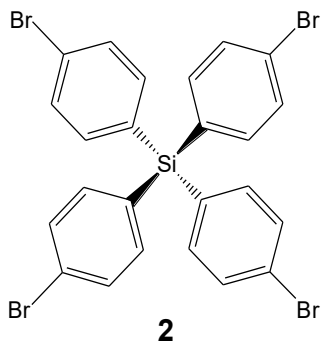
Br
Br
Si
Br
Br

2

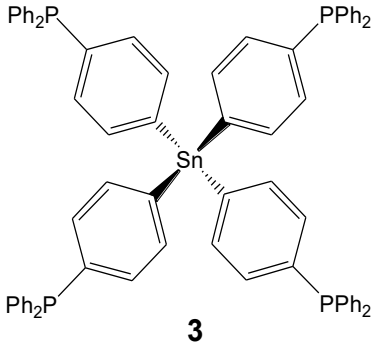
Ph2P
PPh2
Sn
Ph2P
PPh2

3

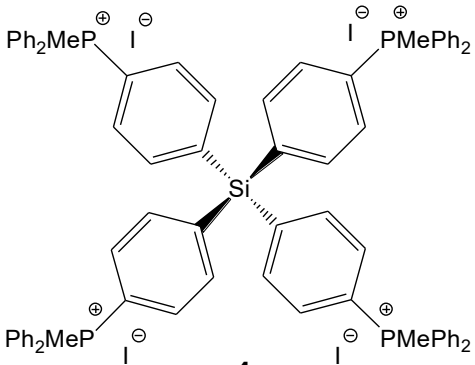
Ph2MeP
I
I
PMePh2
Si
Ph2MeP
I
I
PMePh2

4

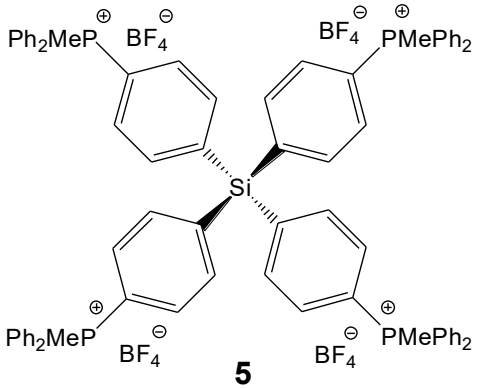
Ph2MeP
BF4
BF4
PMePh2
Si
Ph2MeP
BF4
BF4
PMePh2

5

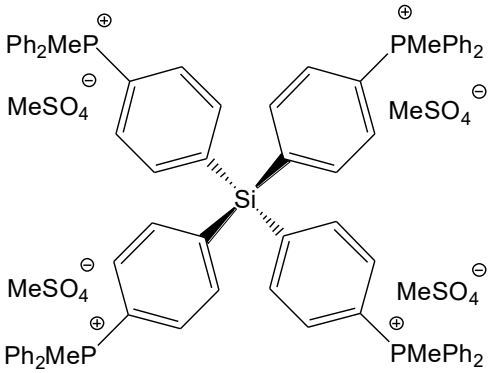
Ph2MeP
PMePh2
MeSO4
MeSO4
Si
MeSO4
MeSO4
Ph2MeP
PMePh2

6

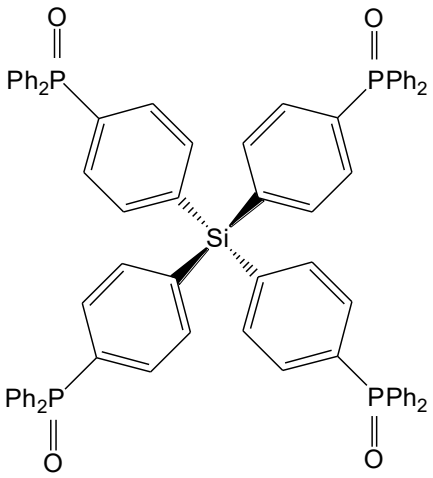
O
Ph2P
O
PPh2
Si
Ph2P
PPh2
O
O

7

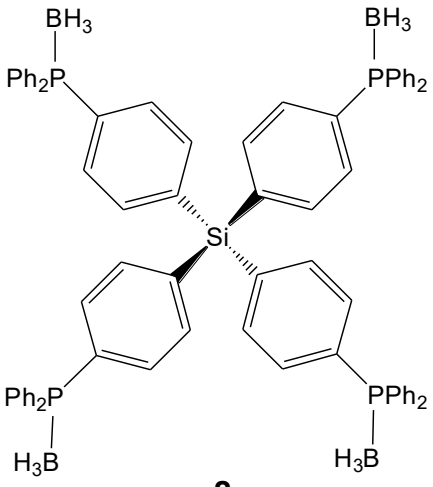
BH3
Ph2P
BH3
PPh2
Si
Ph2P
PPh2
H3B
H3B

8

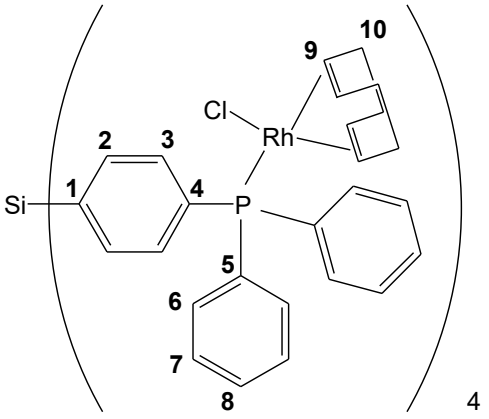
10
9
Cl
Rh
2
3
1
4
Si
P
5
6
7
8
4

9

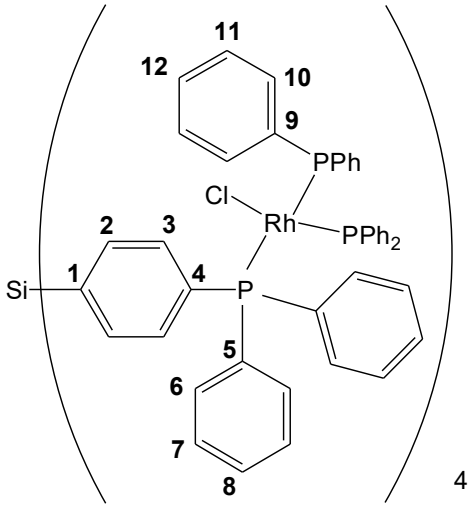
11
12
10
9
PPh
Cl
Rh
PPh2
2
3
1
4
Si
P
5
6
7
8
4

10

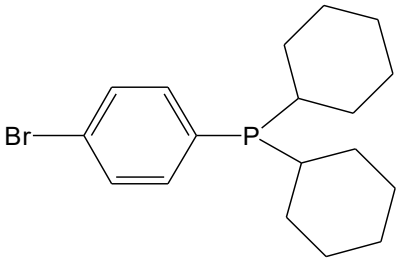

11

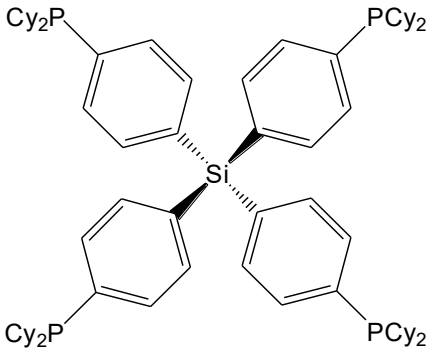

12

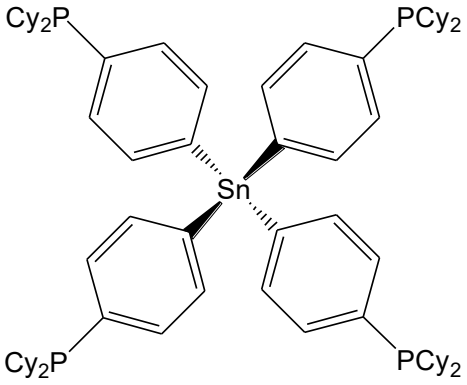

13

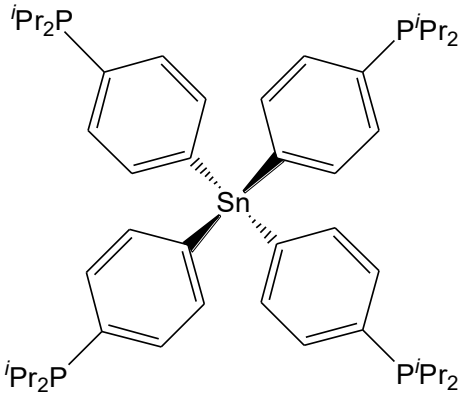

14

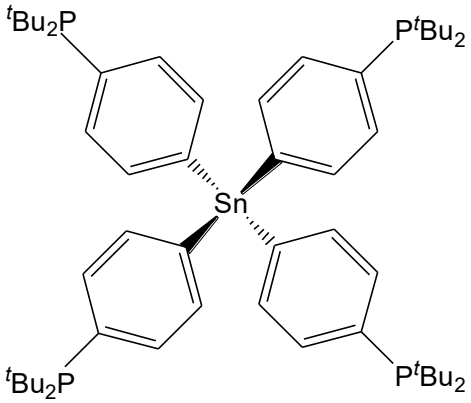

15

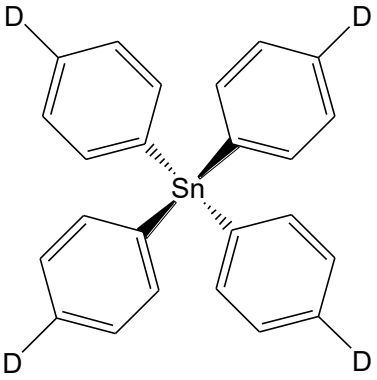

16

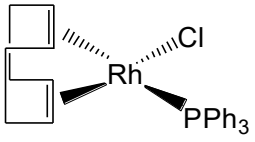
Cl
Rh
PPh3

17

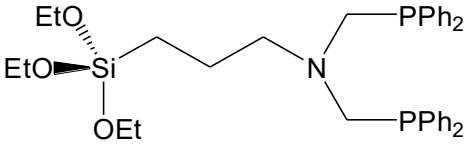
EtO
EtO
Si
OEt
N
PPh2
PPh2

18

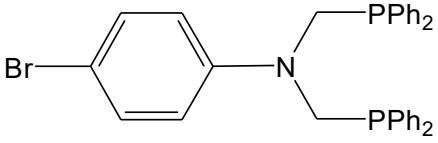
Br
N
PPh2
PPh2

19

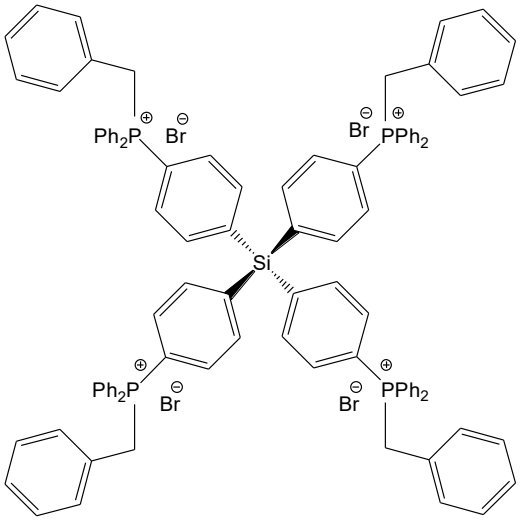
Ph2P
Br
Br
PPh2
Si
Ph2P
Br
Br
PPh2

20

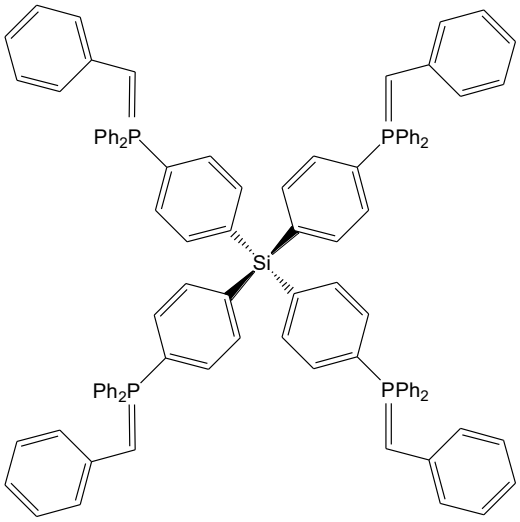
Ph2P
PPh2
Si
Ph2P
PPh2

21

IMMOBILIZED COMPOUNDS

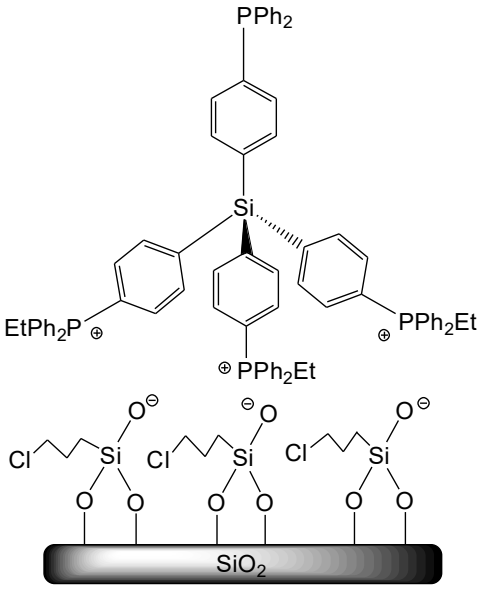

3i

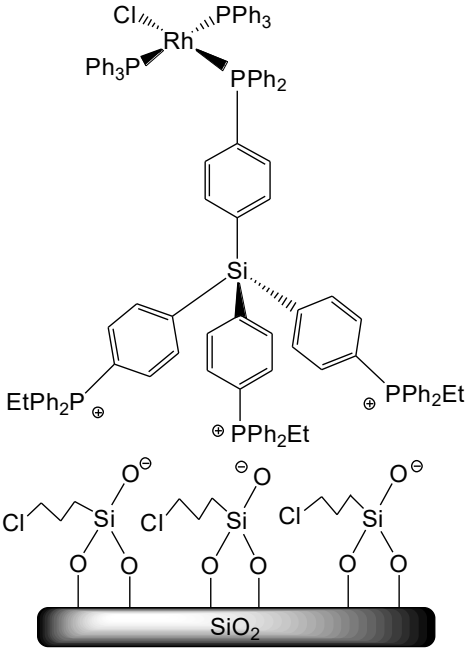

3iRh

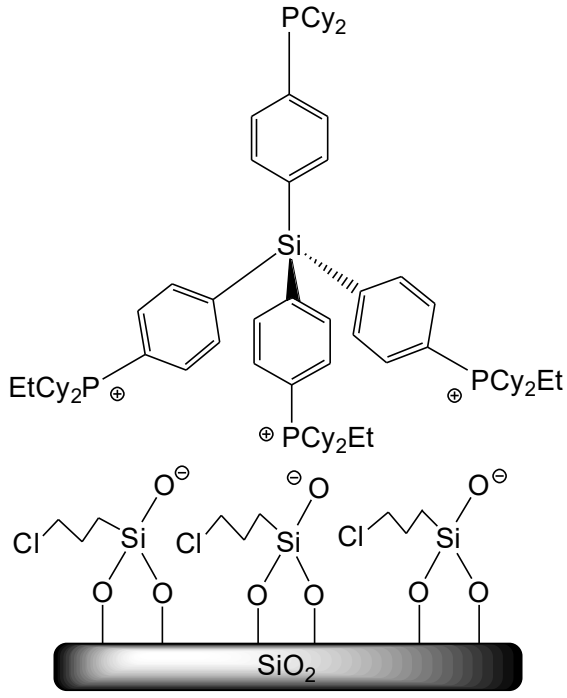

12i

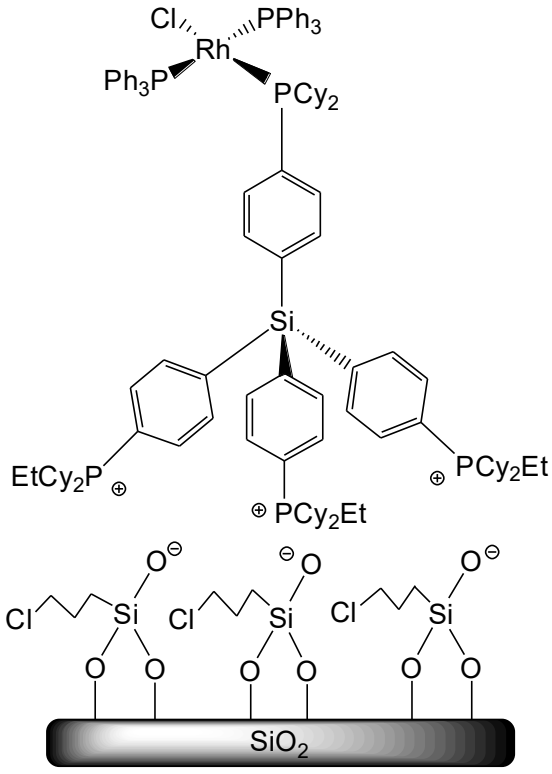

12iRh

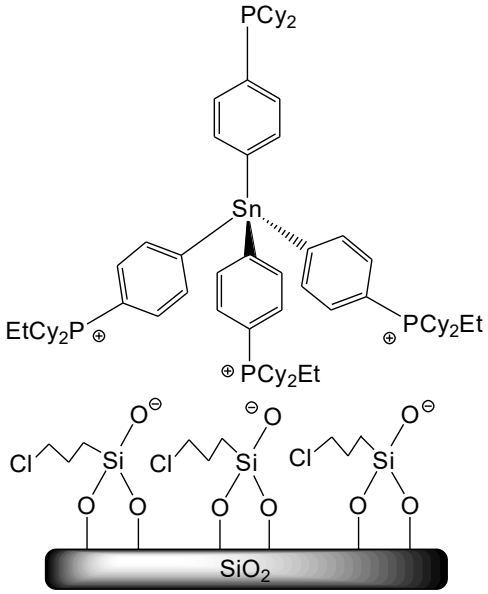

13i

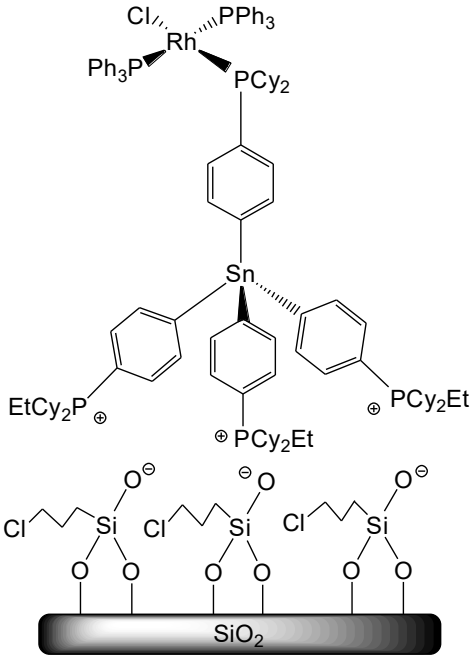

13iRh

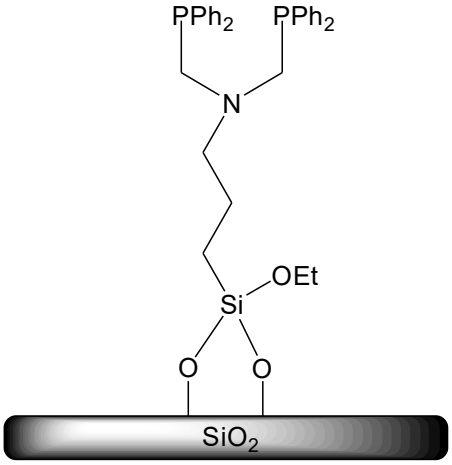

20i

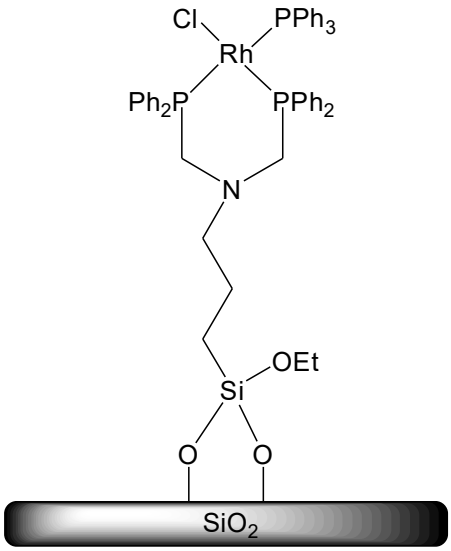

20iRh

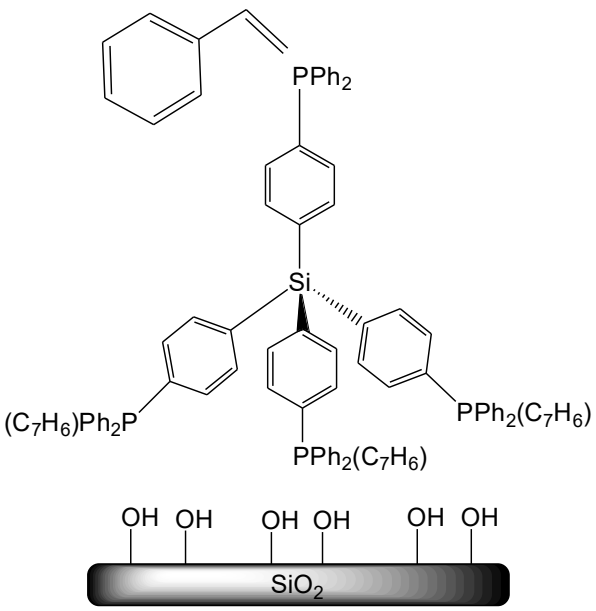

21i

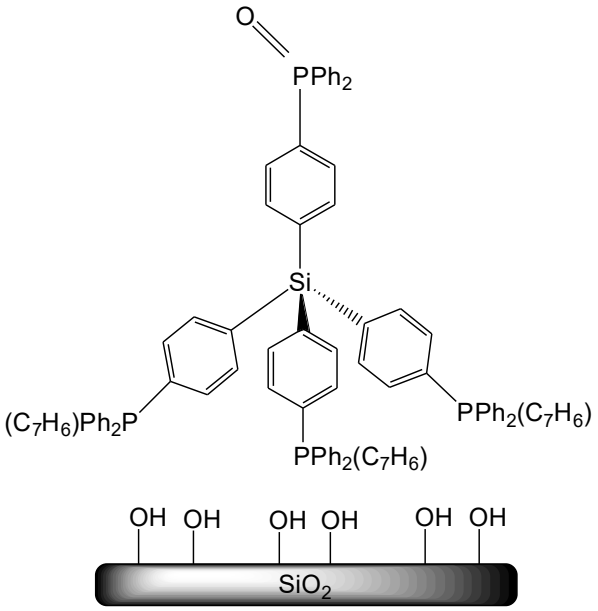

25i

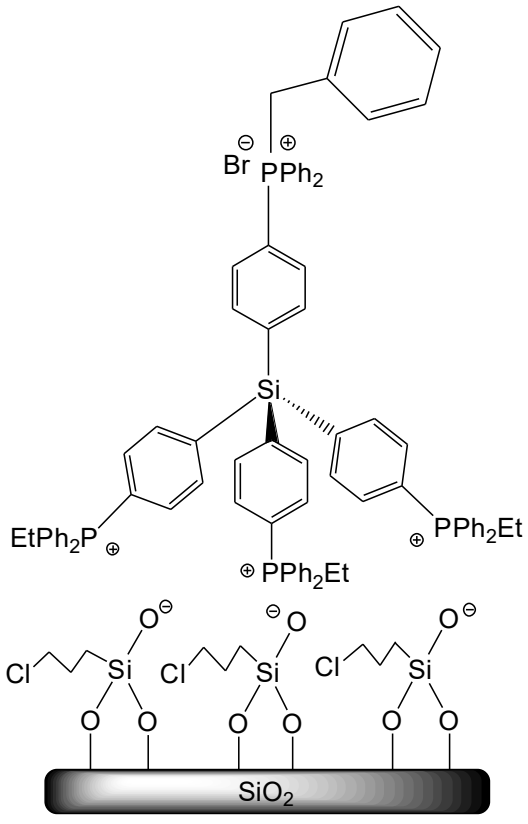

22i

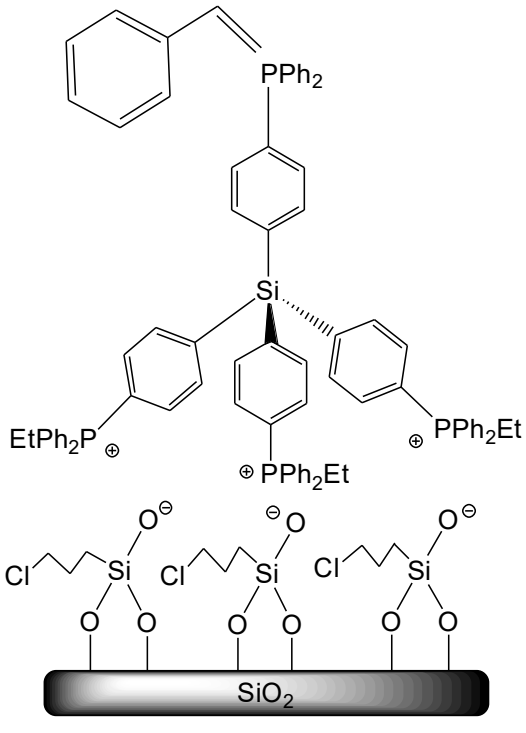

23i

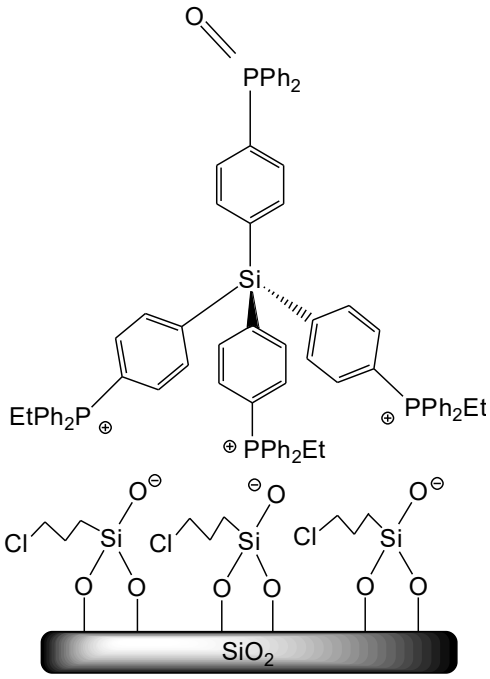
O
PPh2
Si
EtPh2P
PPh2Et
PPh2Et
O
Cl
Si
O
O
O
O
O
O
Cl
Si
O
O
O
O
Cl
Si
O
O
SiO2

24i

APPENDIX B

NMR SPECTRA

^{1}H NMR (DMSO-d_6)

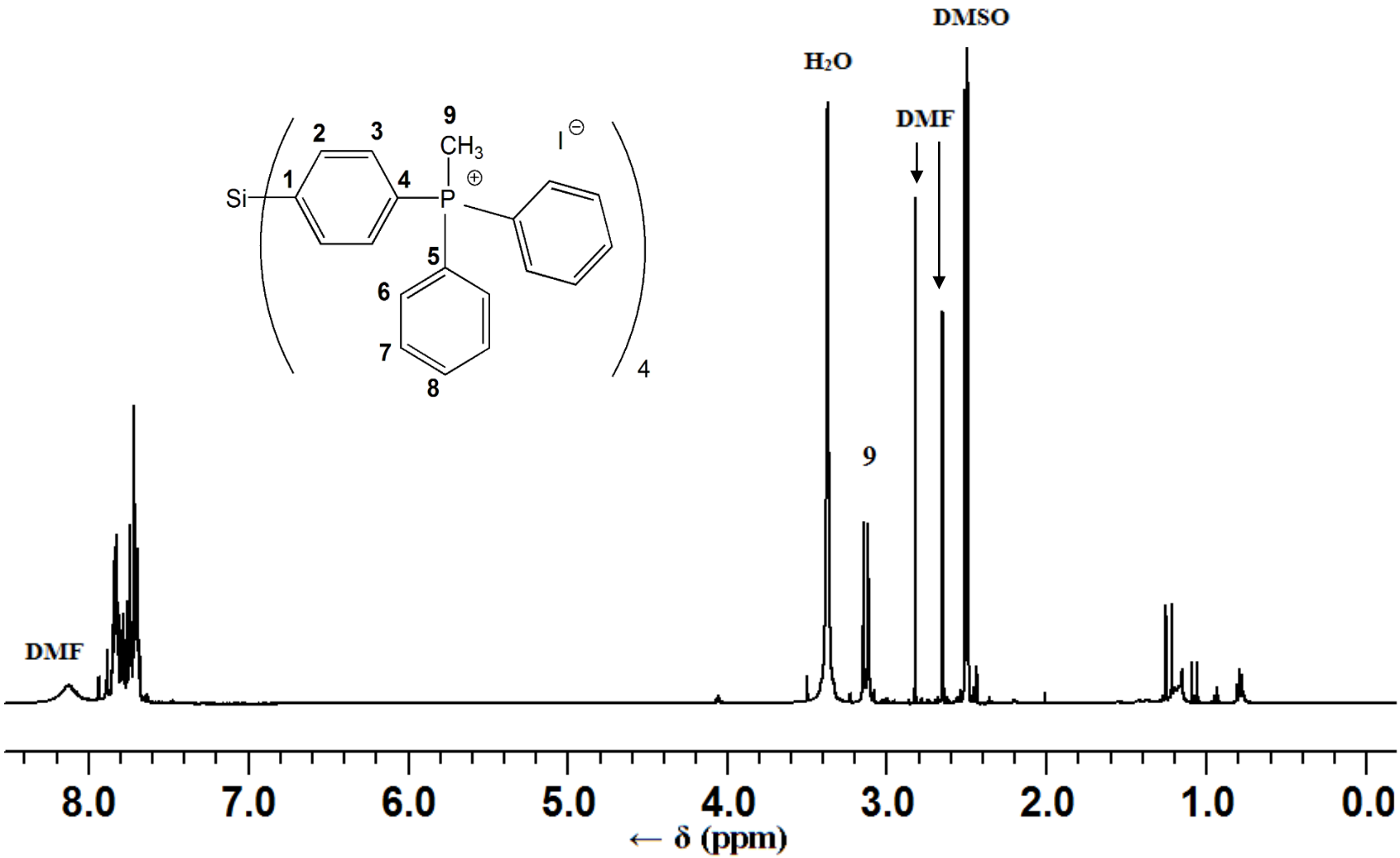

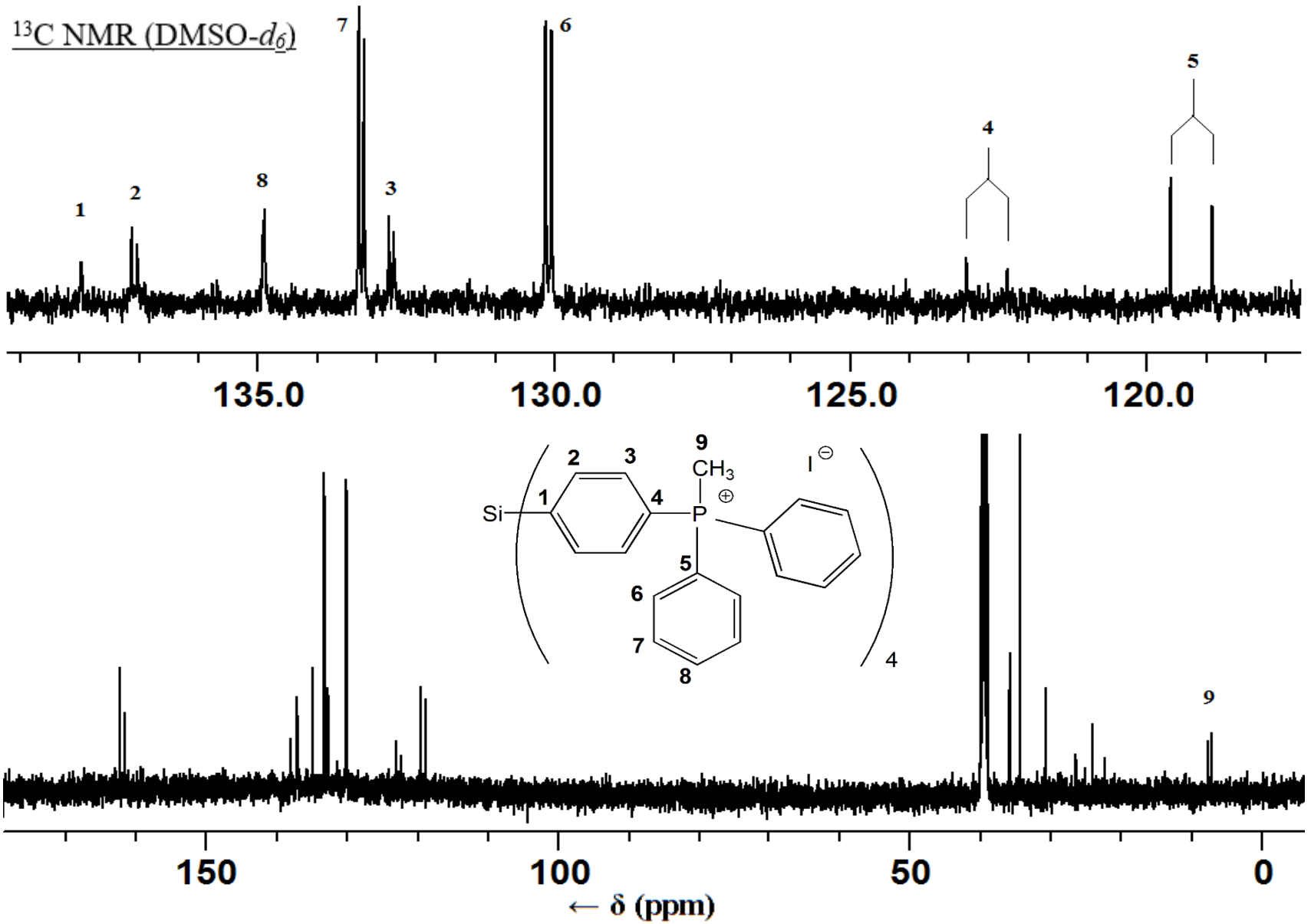
13C NMR (DMSO-d6)
1
2
8
7
3
6
4
5
135.0
130.0
125.0
120.0
Si
CH3
P
I
9
150
100
50
0
← δ (ppm)

^{1}H NMR (DMSO-d_6)

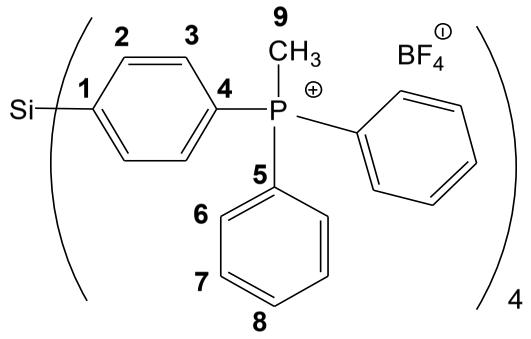

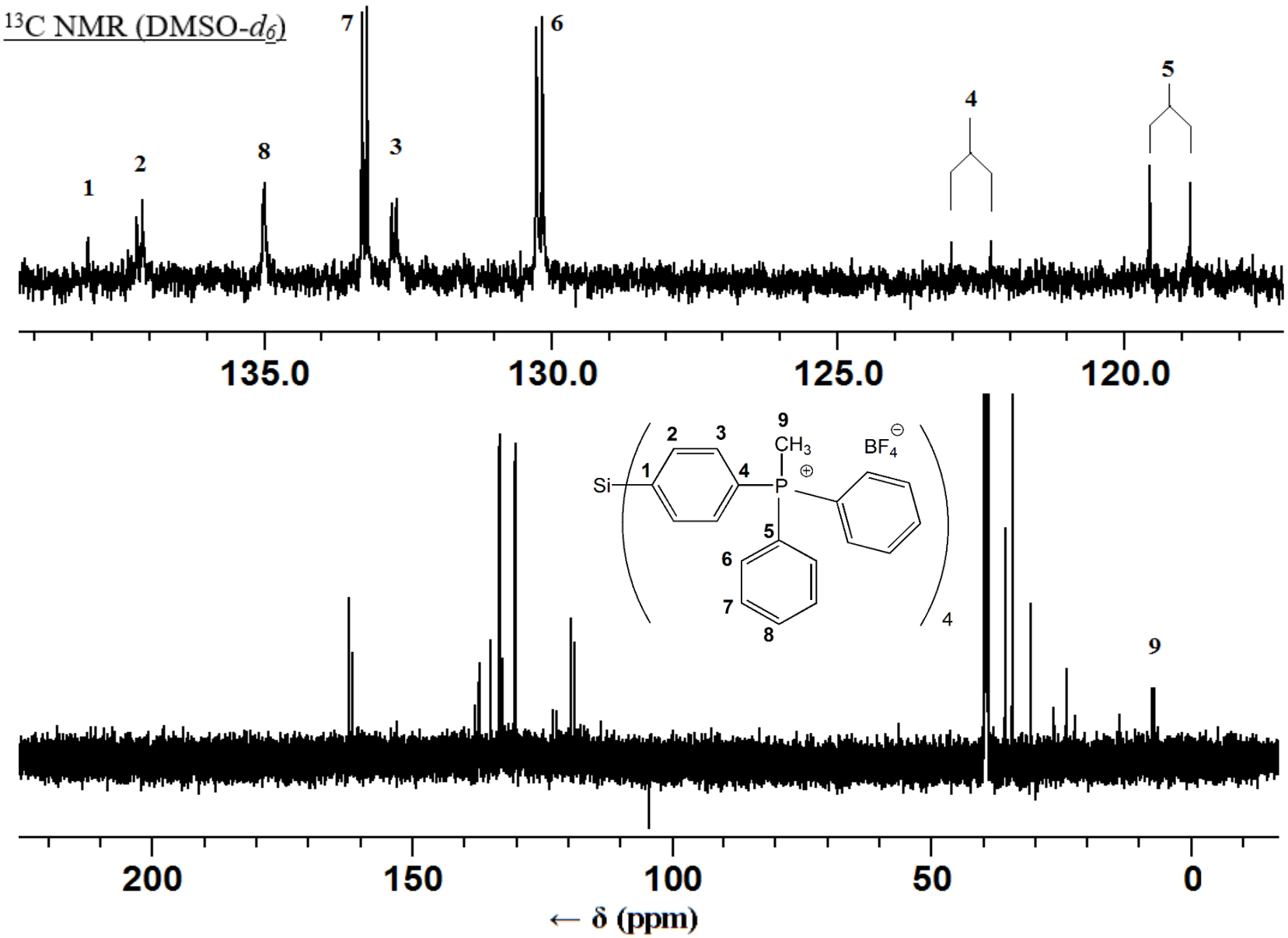
13C NMR (DMSO-d6)
1
2
8
7
3
6
4
5
135.0
130.0
125.0
120.0
Si
P
CH3
BF4
9
200
150
100
50
0
← δ (ppm)

^{29}Si NMR (DMSO-d_6)

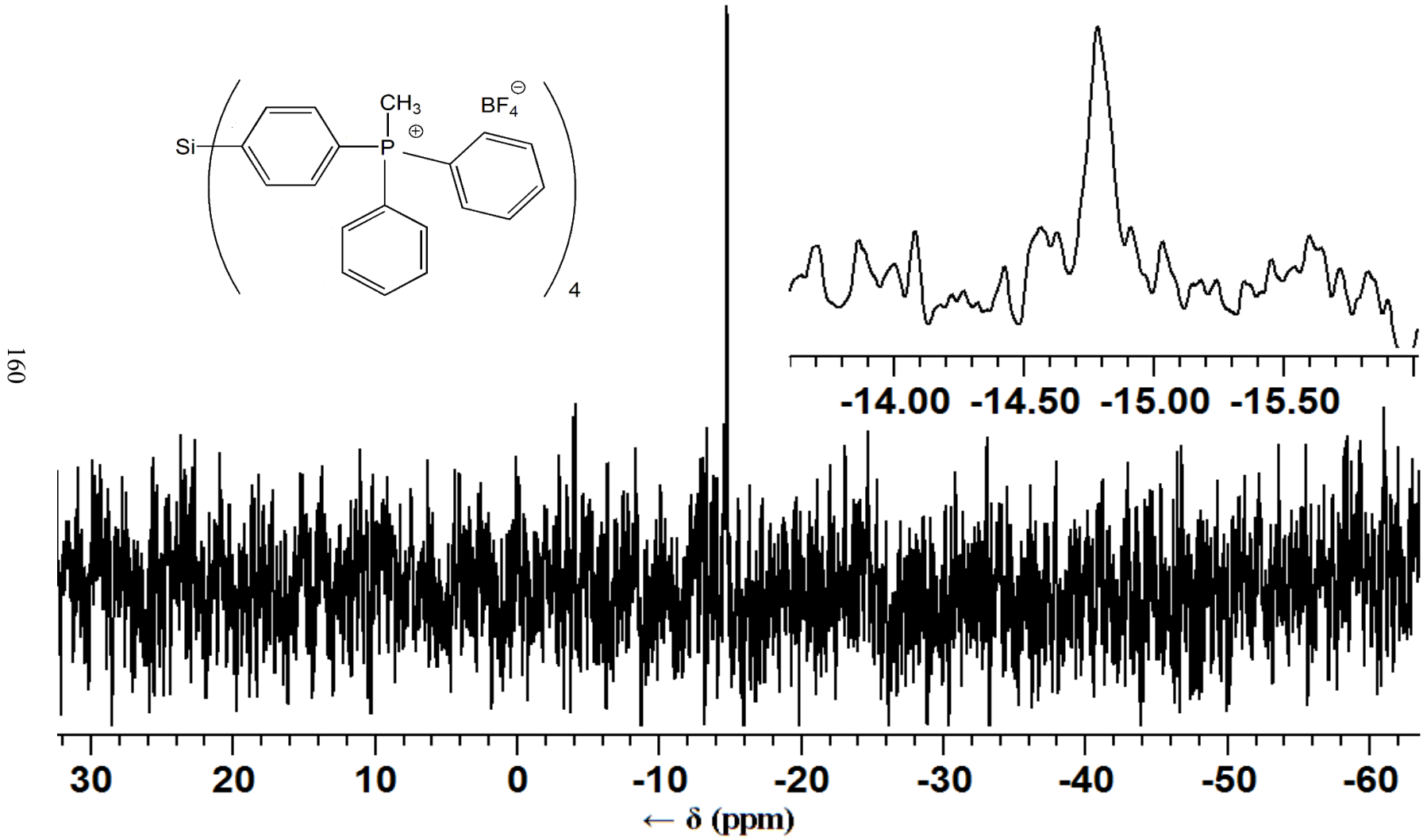

^{31}P NMR (DMSO-d_6)

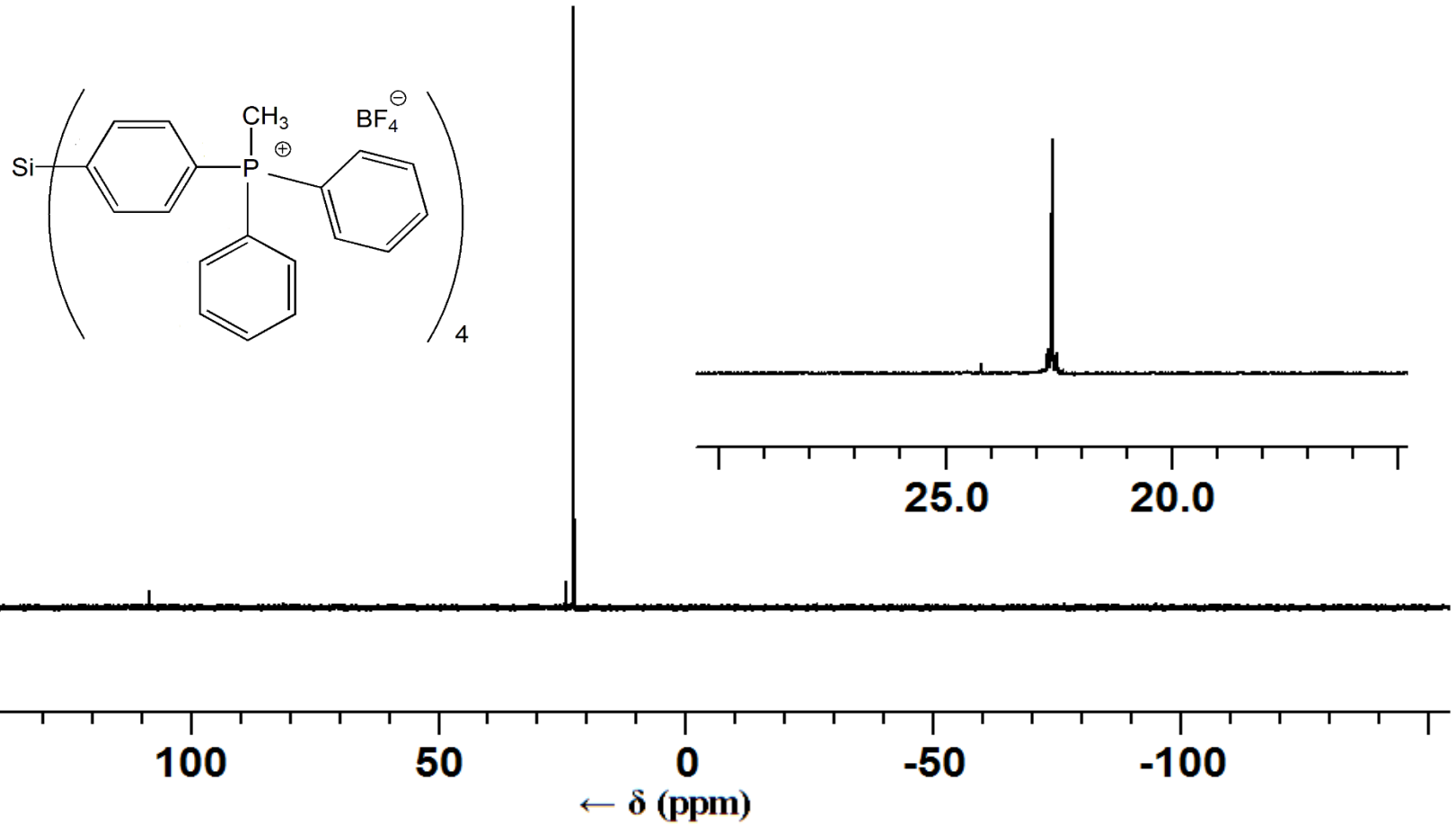

^{1}H NMR ($CDCl_3$)

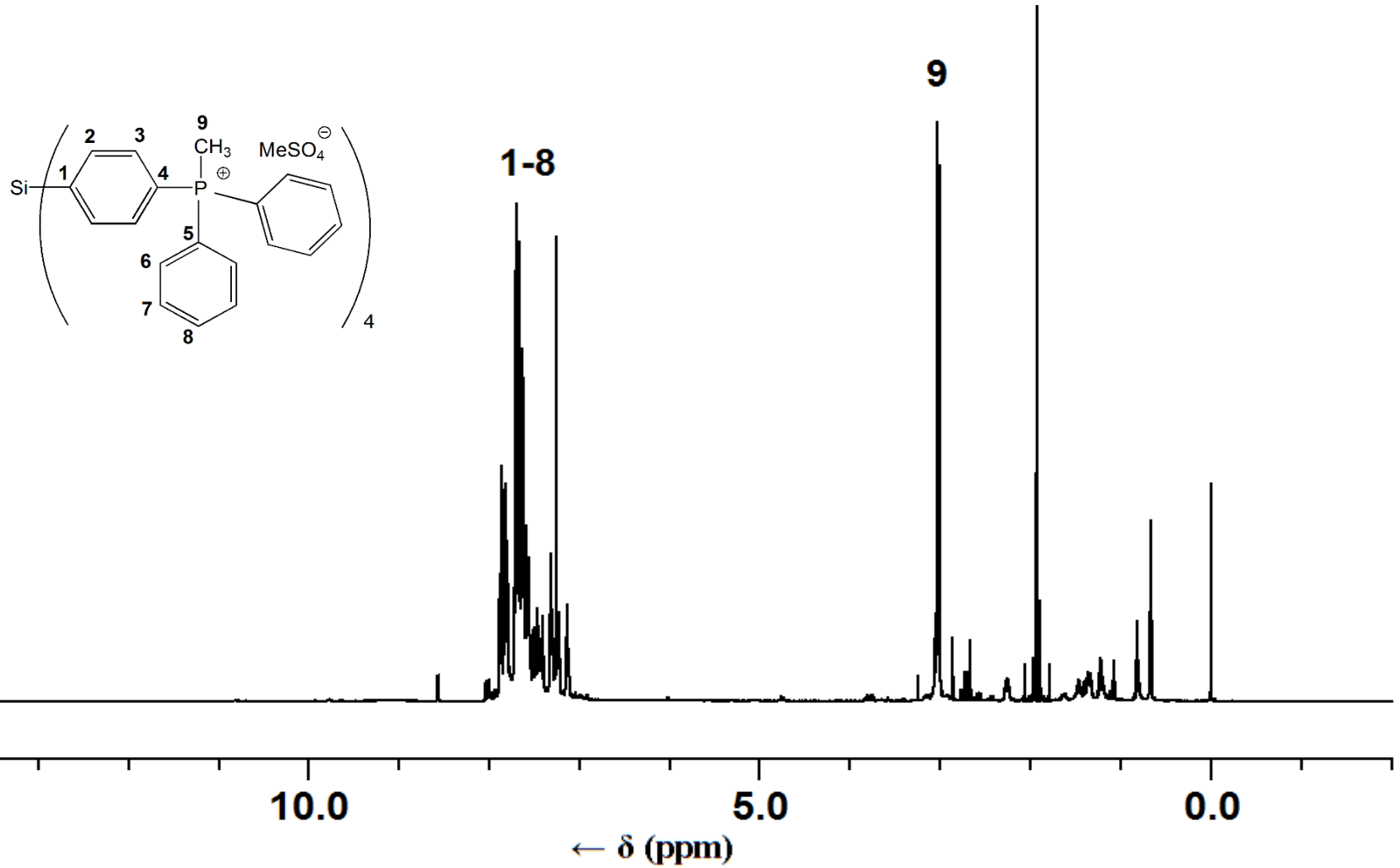

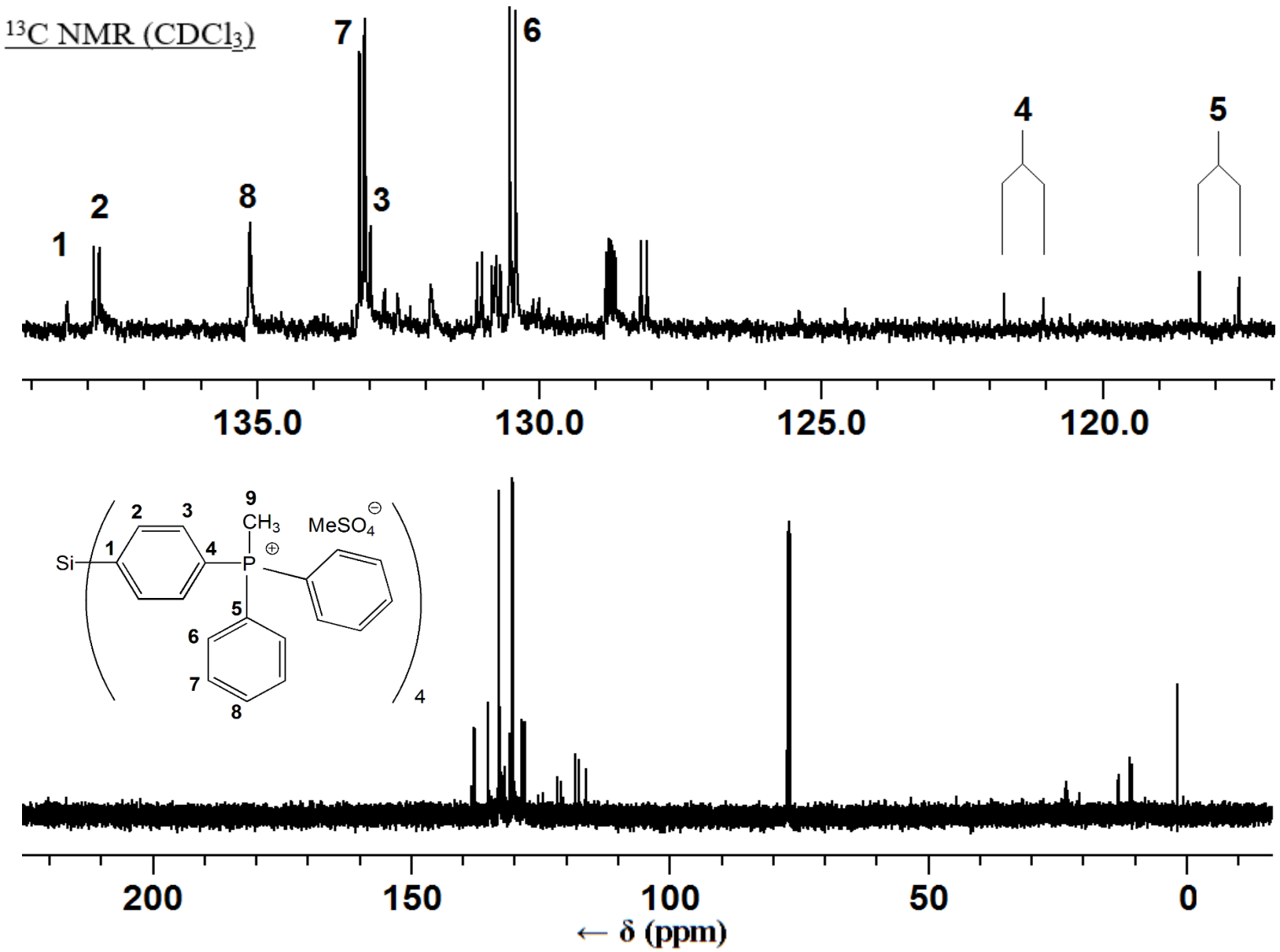
13C NMR (CDCl3)
1
2
8
7
3
6
4
5
135.0
130.0
125.0
120.0
Si
CH3
MeSO4
200
150
100
50
0
← δ (ppm)

^{29}Si NMR ($CDCl_3$)

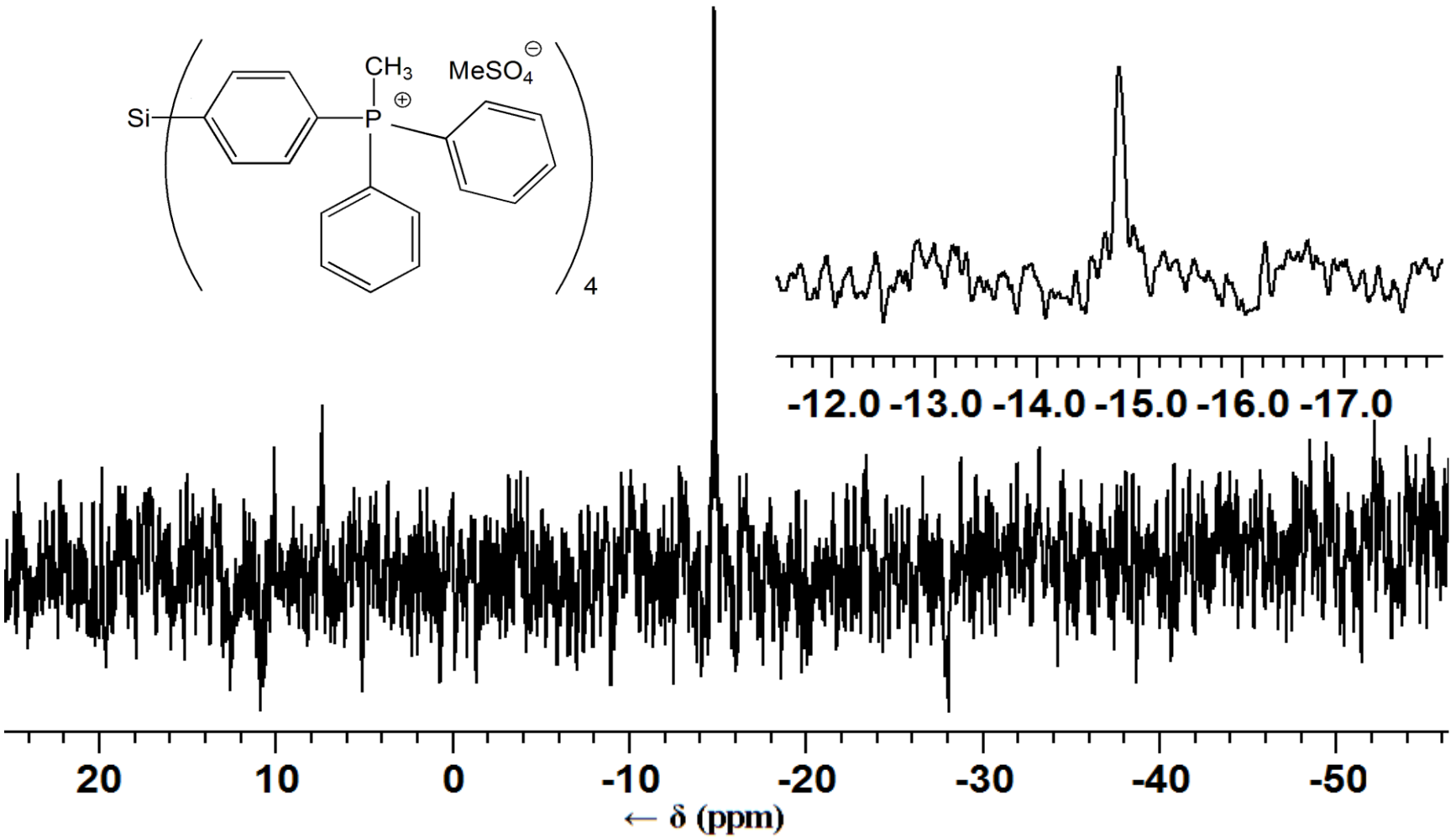

^{31}P NMR ($CDCl_3$)

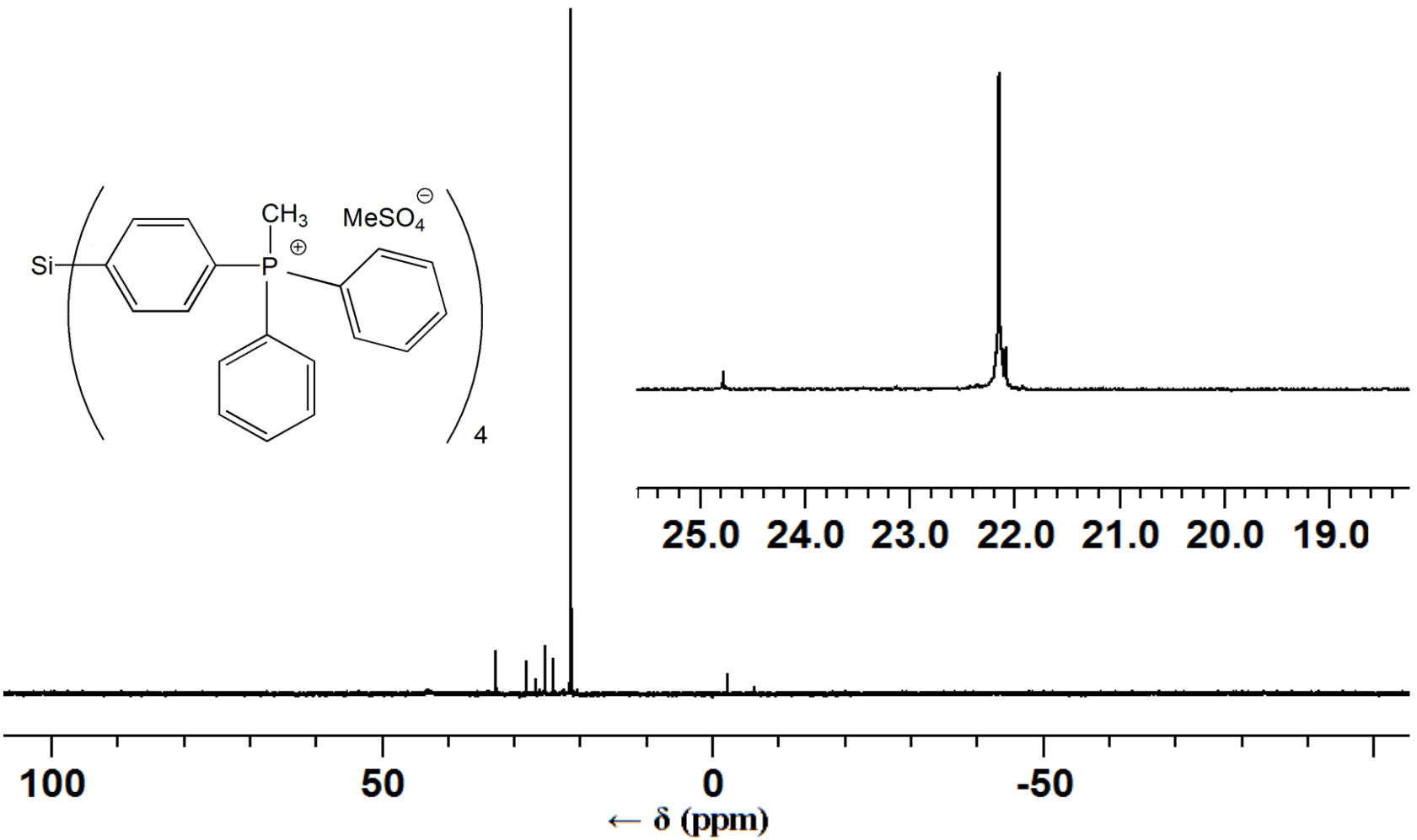

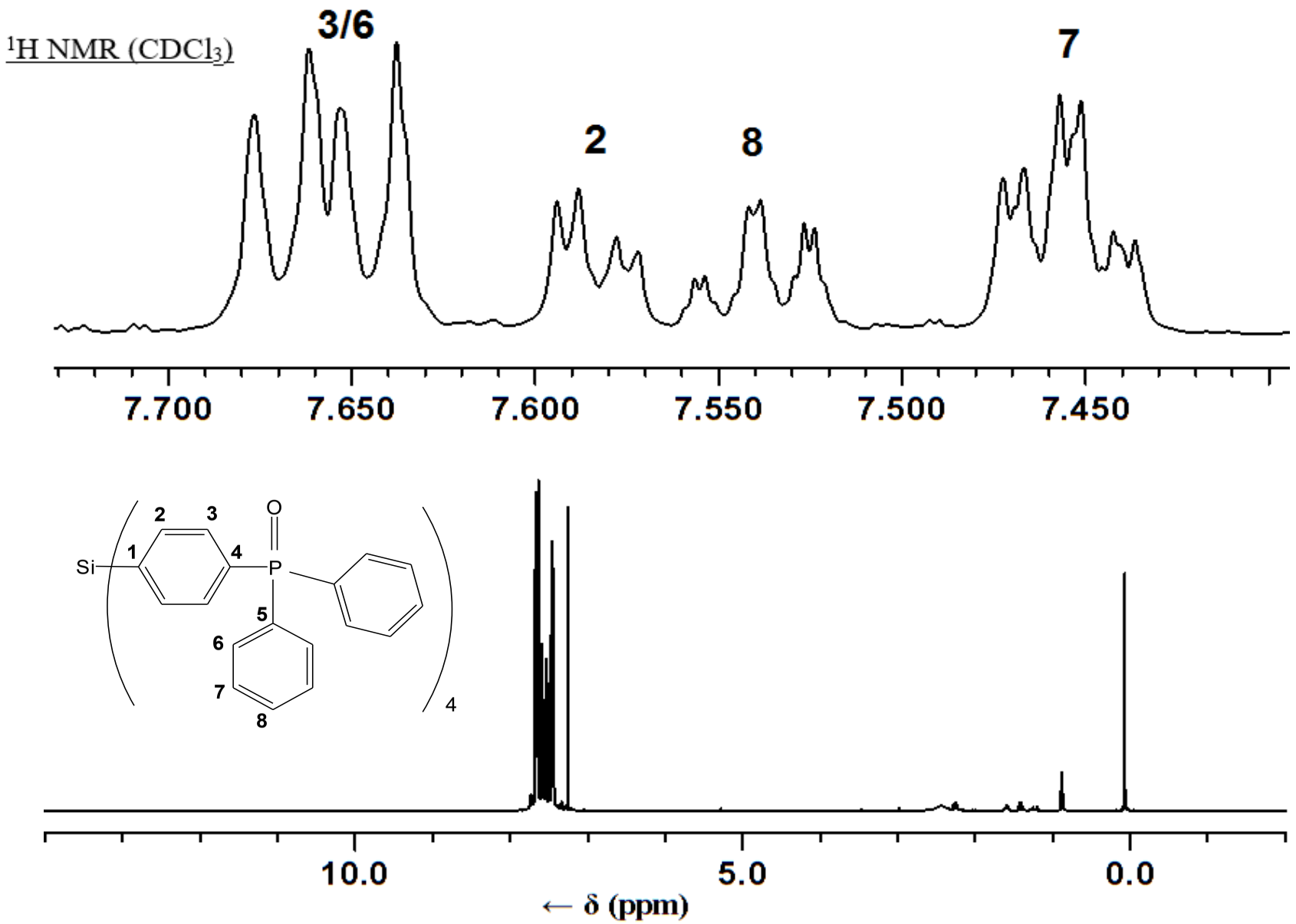
^{1}H NMR ($CDCl_3$)
3/6
2
8
7
7.700
7.650
7.600
7.550
7.500
7.450
Si
O
P
1
2
3
4
5
6
7
8
4
10.0
5.0
0.0
← δ (ppm)

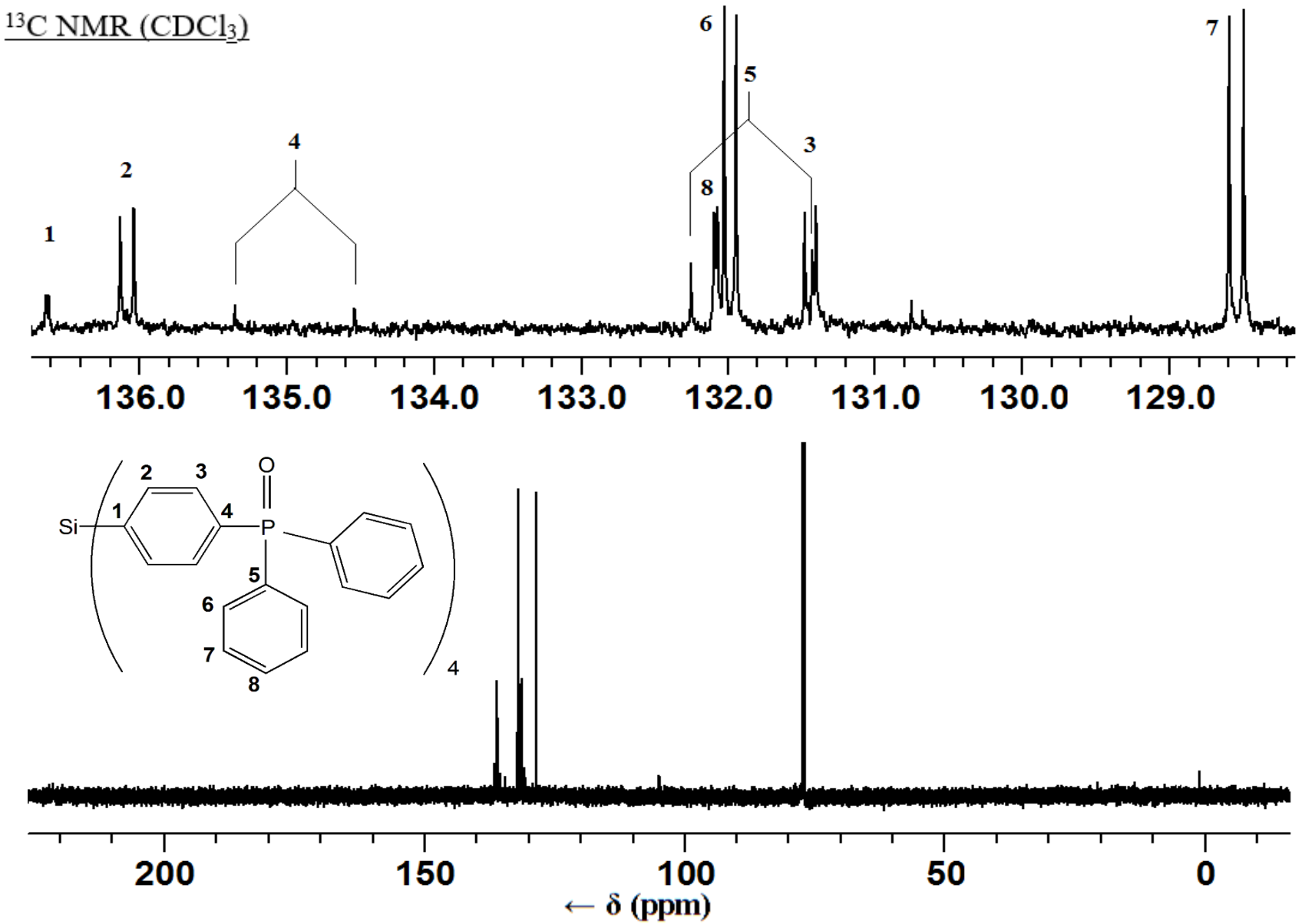
^{13}C NMR ($CDCl_3$)
1
2
4
8
6
5
3
7
136.0
135.0
134.0
133.0
132.0
131.0
130.0
129.0
Si
O
P
4
200
150
100
50
0
← δ (ppm)

^{29}Si NMR ($CDCl_3$)

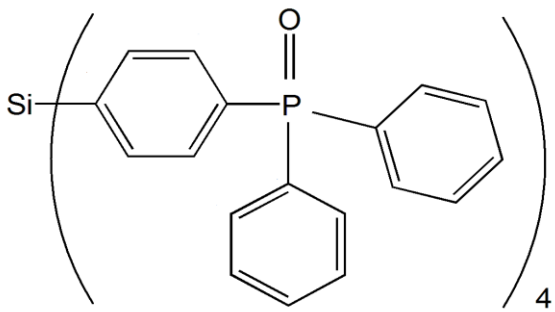

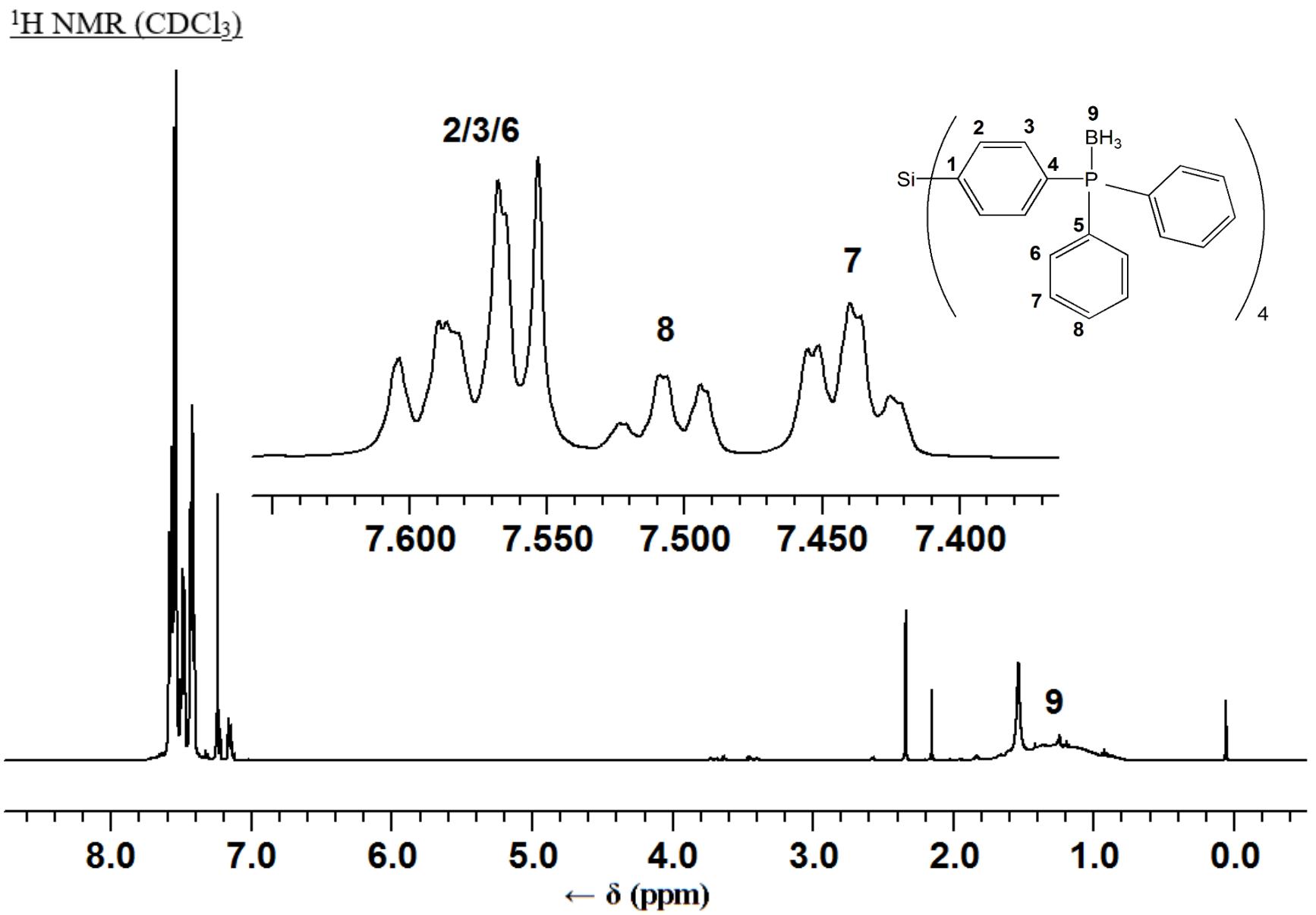
^{1}H NMR ($CDCl_3$)
2/3/6
8
7
9
7.600
7.550
7.500
7.450
7.400
8.0
7.0
6.0
5.0
4.0
3.0
2.0
1.0
0.0
← δ (ppm)
Si
P
BH_3
1
2
3
4
5
6
7
8
9
4

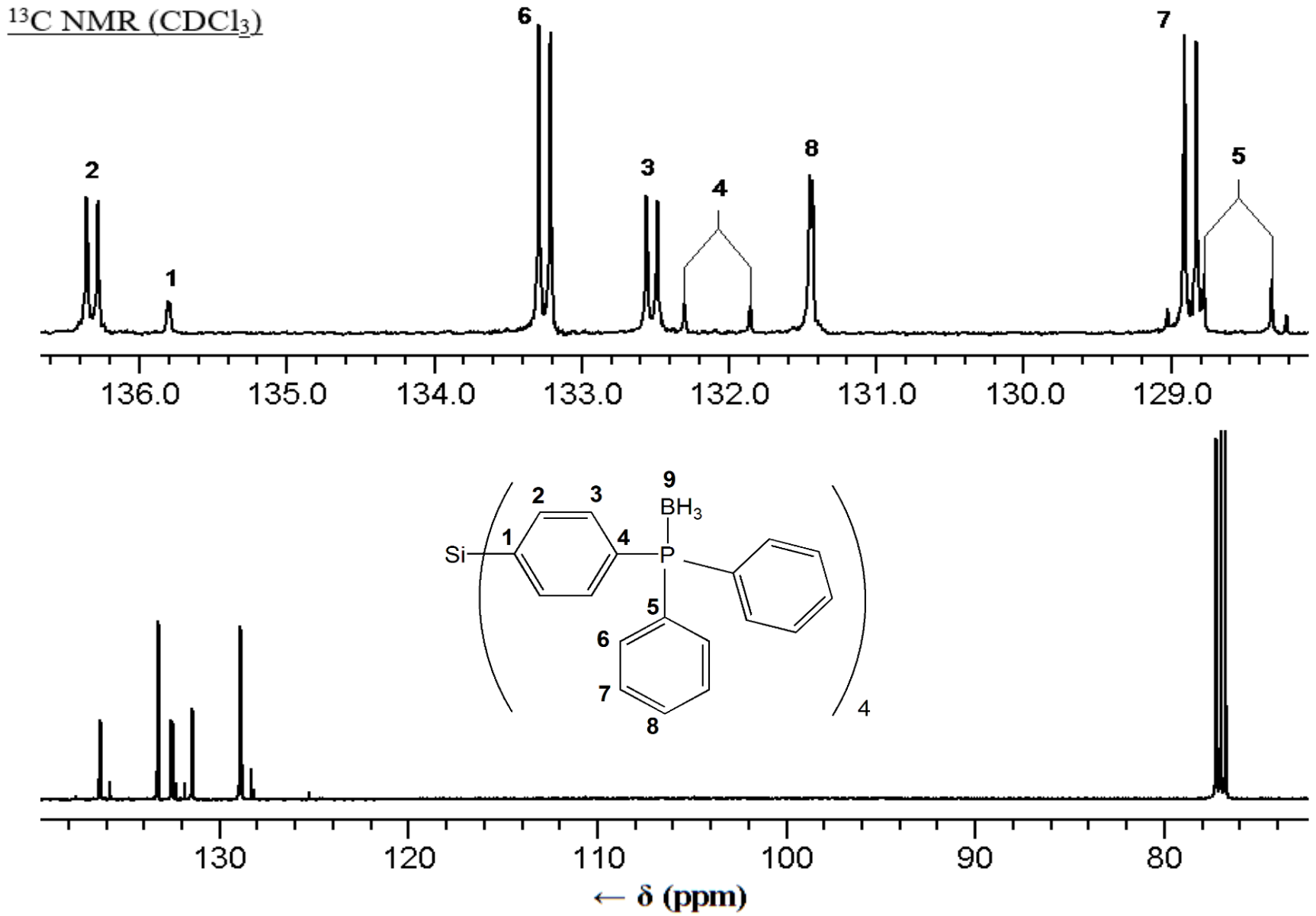
13C NMR (CDCl3)
6
7
2
3
8
4
5
1
136.0
135.0
134.0
133.0
132.0
131.0
130.0
129.0
9
BH3
2
3
1
4
Si
P
5
6
7
8
4
130
120
110
100
90
80
← δ (ppm)

^{29}Si NMR ($CDCl_3$)

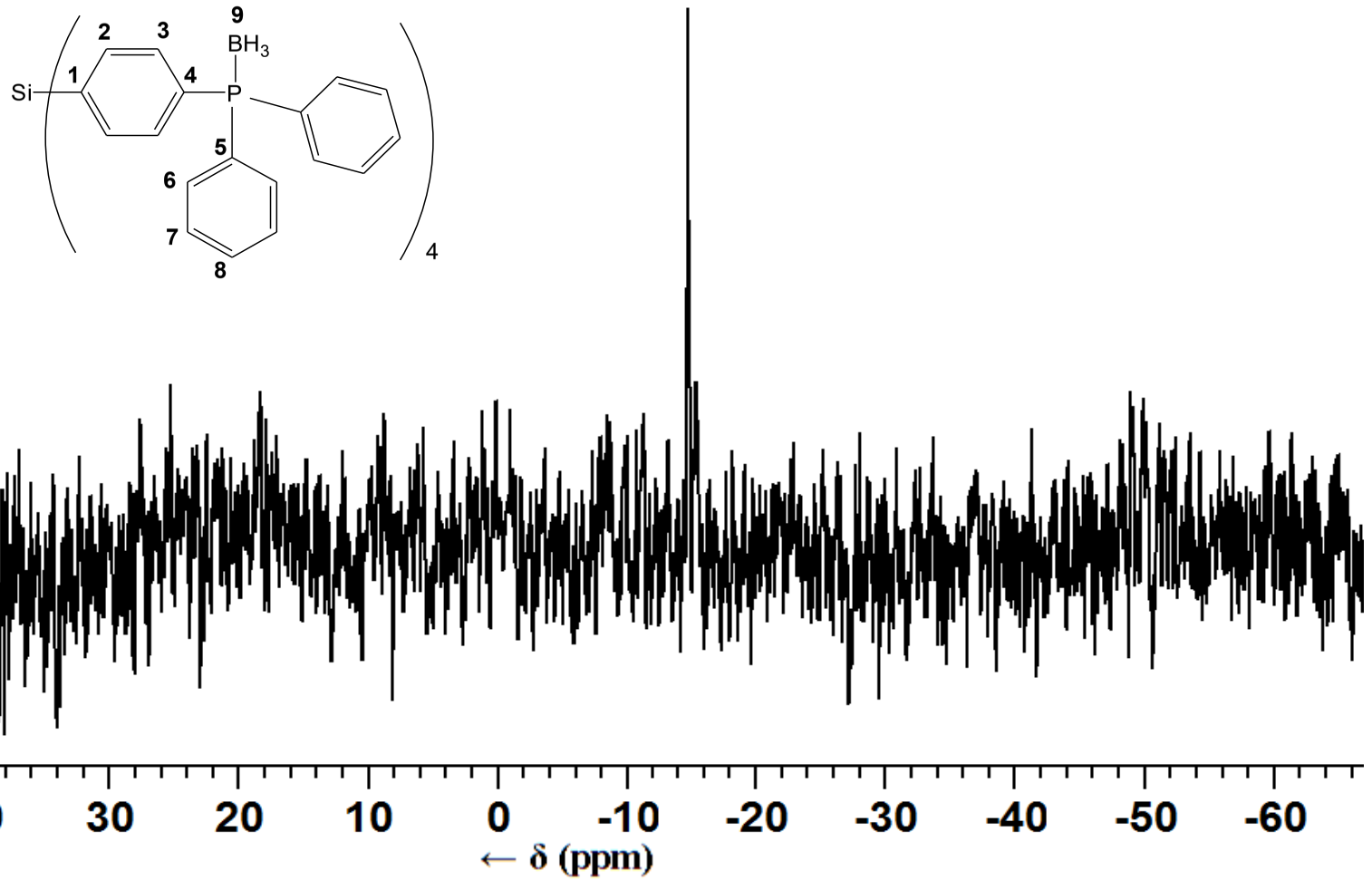

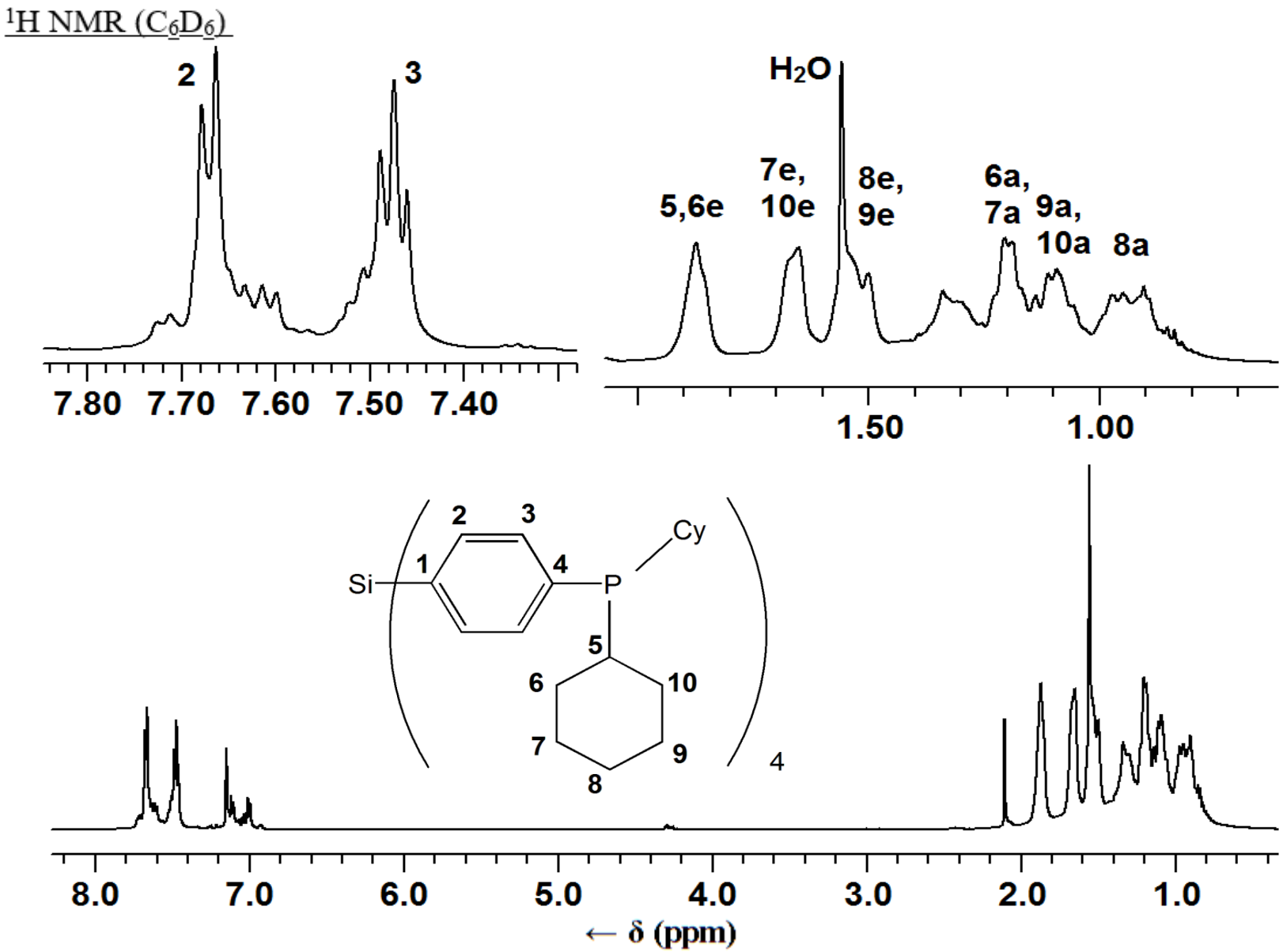
^{1}H NMR (C_6D_6)
2
3
H_2O
5,6e
7e,
10e
8e,
9e
6a,
7a
9a,
10a
8a
7.80 7.70 7.60 7.50 7.40
1.50 1.00
Si
1
2
3
4
P
Cy
5
6
7
8
9
10
4
8.0 7.0 6.0 5.0 4.0 3.0 2.0 1.0
← δ (ppm)

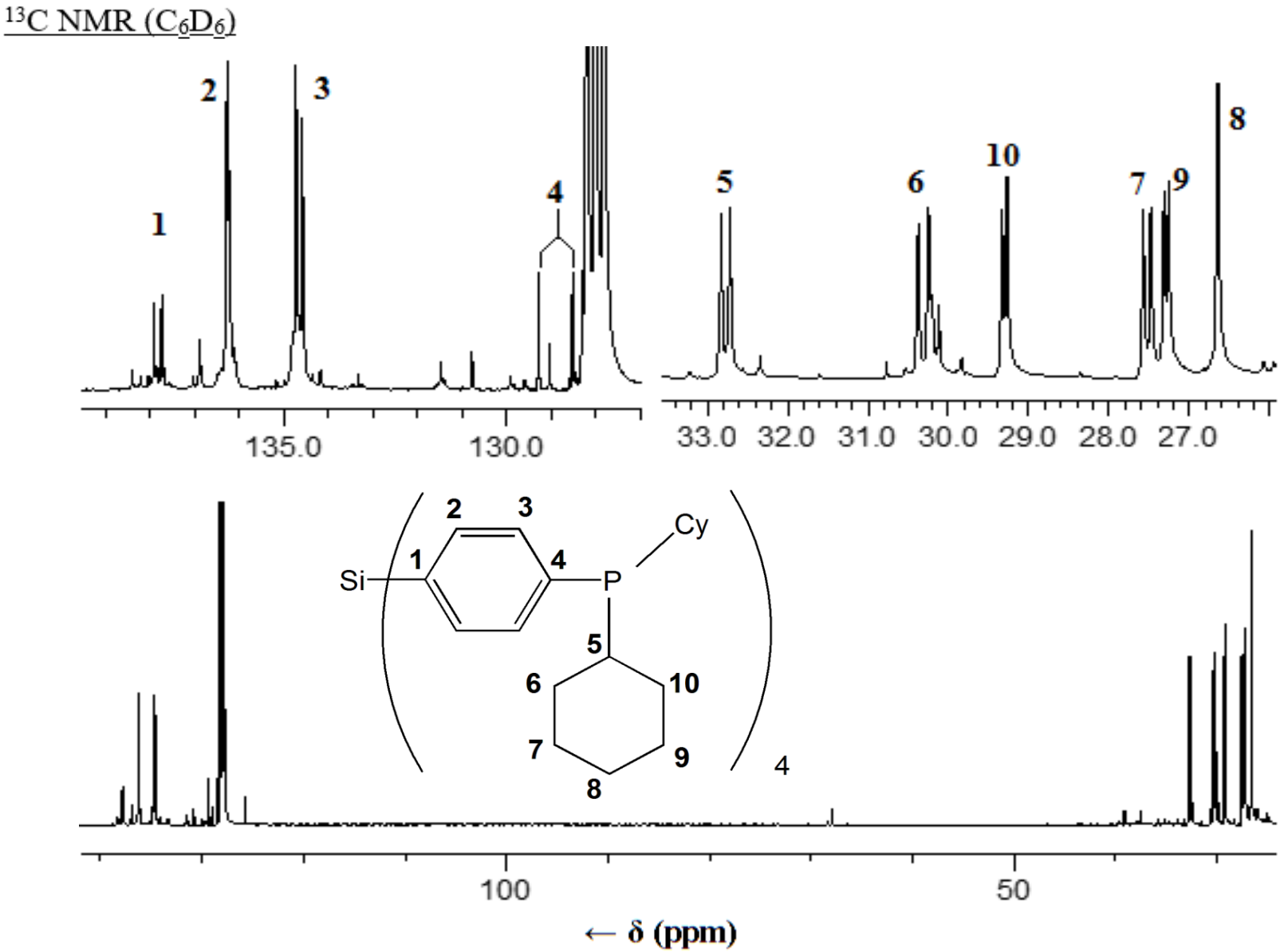
13C NMR (C6D6)
1
2
3
4
5
6
10
7
9
8
135.0
130.0
33.0 32.0 31.0 30.0 29.0 28.0 27.0
Si
P
Cy
4
100
50
← δ (ppm)

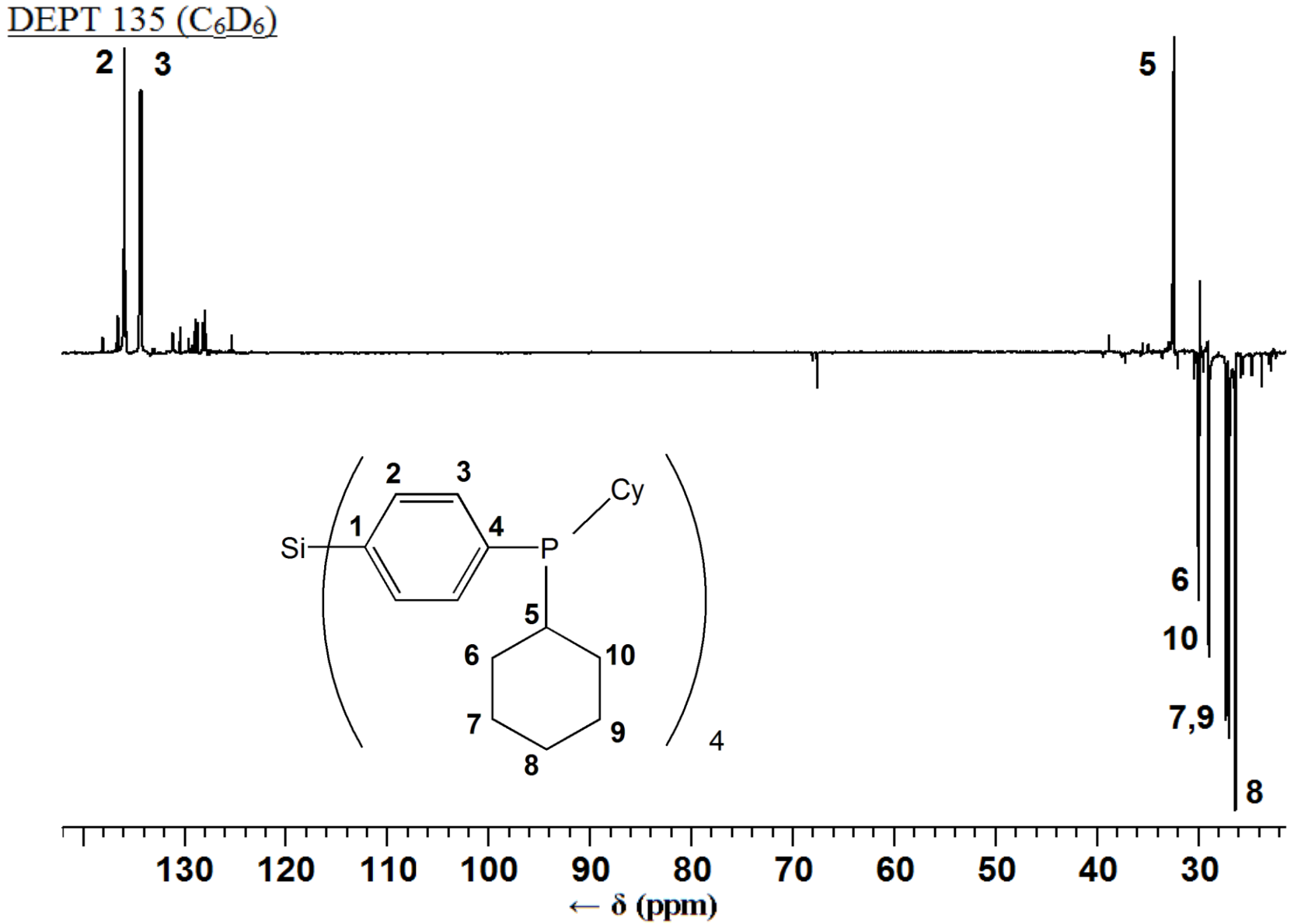
DEPT 135 (C_6D_6)
2
3
5
6
10
7,9
8
Si
P
Cy
1
2
3
4
5
6
7
8
9
10
4
130
120
110
100
90
80
70
60
50
40
30
← δ (ppm)

^{1}H-^{1}H COSY (C_6D_6)

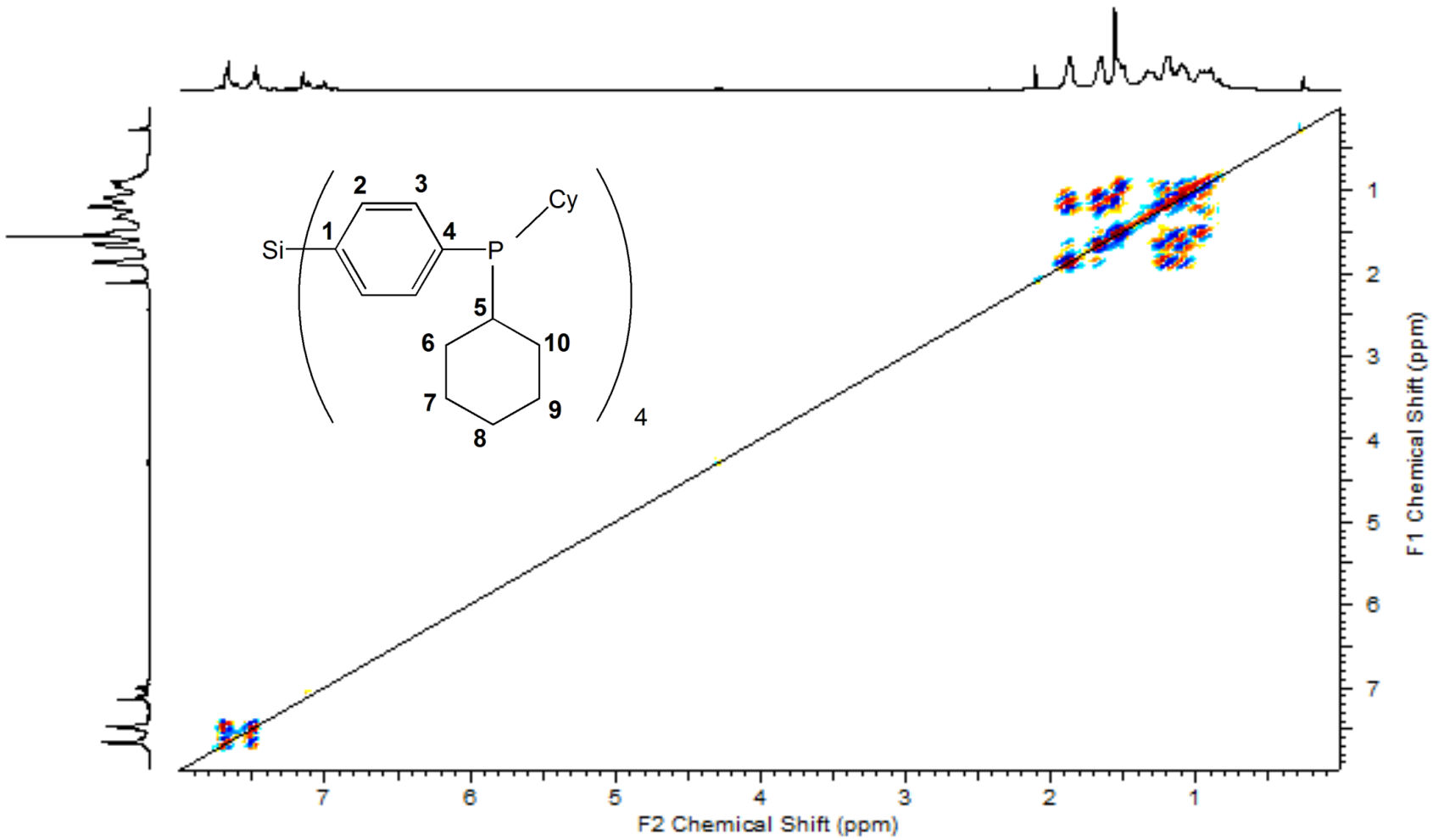

^{13}C-^{1}H HSQC (C_6D_6)

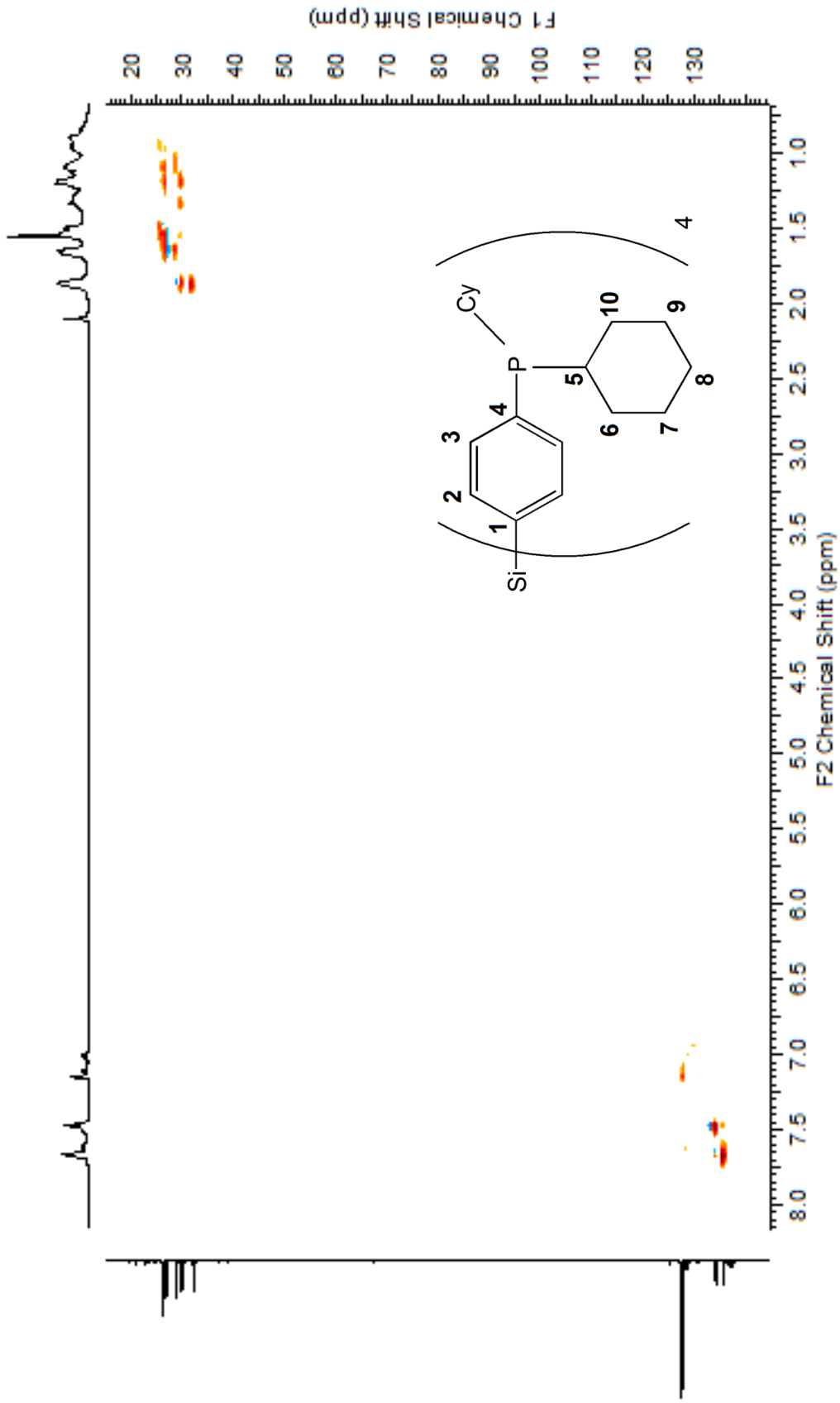

^{29}Si NMR (C_6D_6)

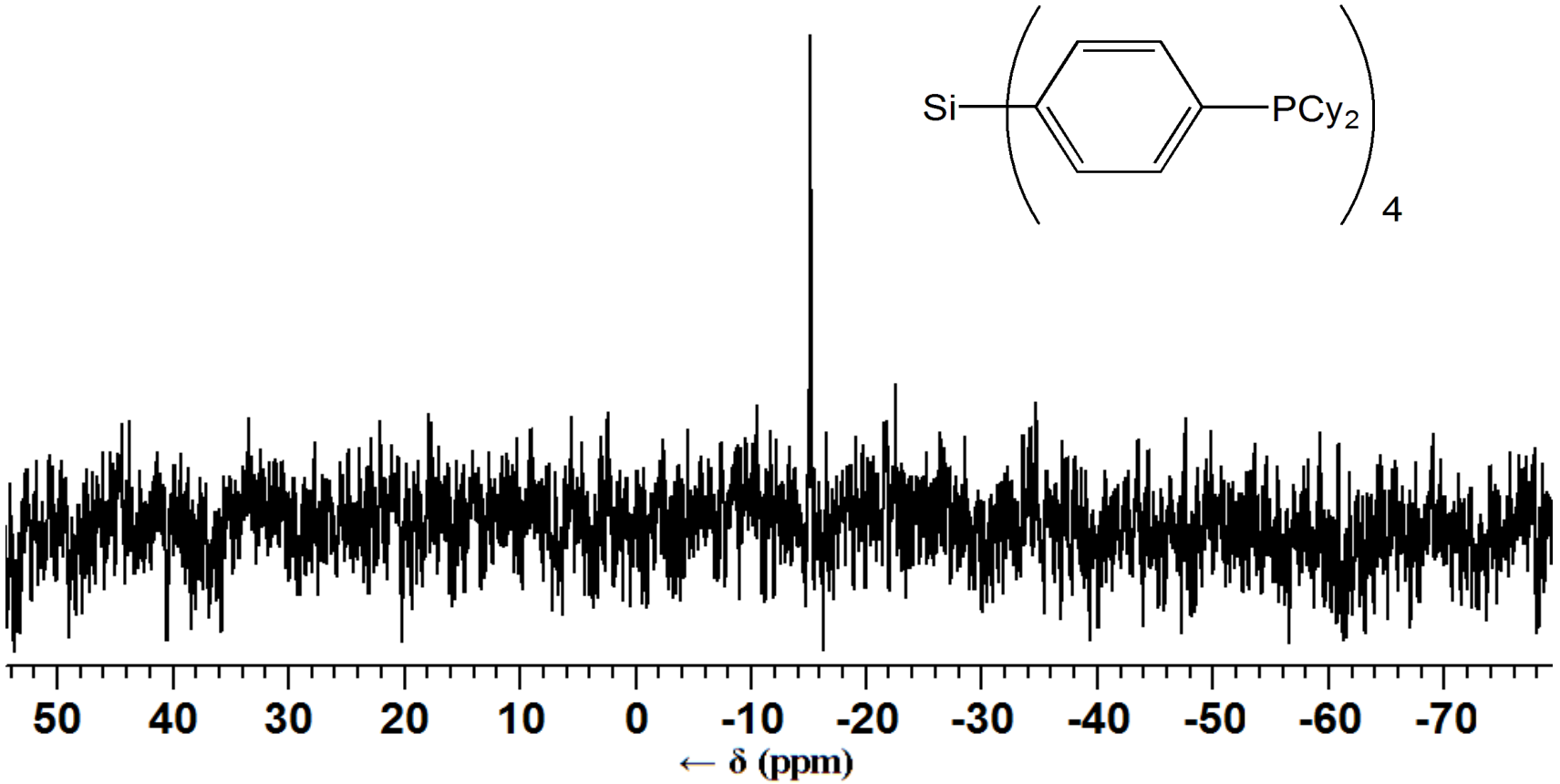

^{29}Si CP/MAS NMR

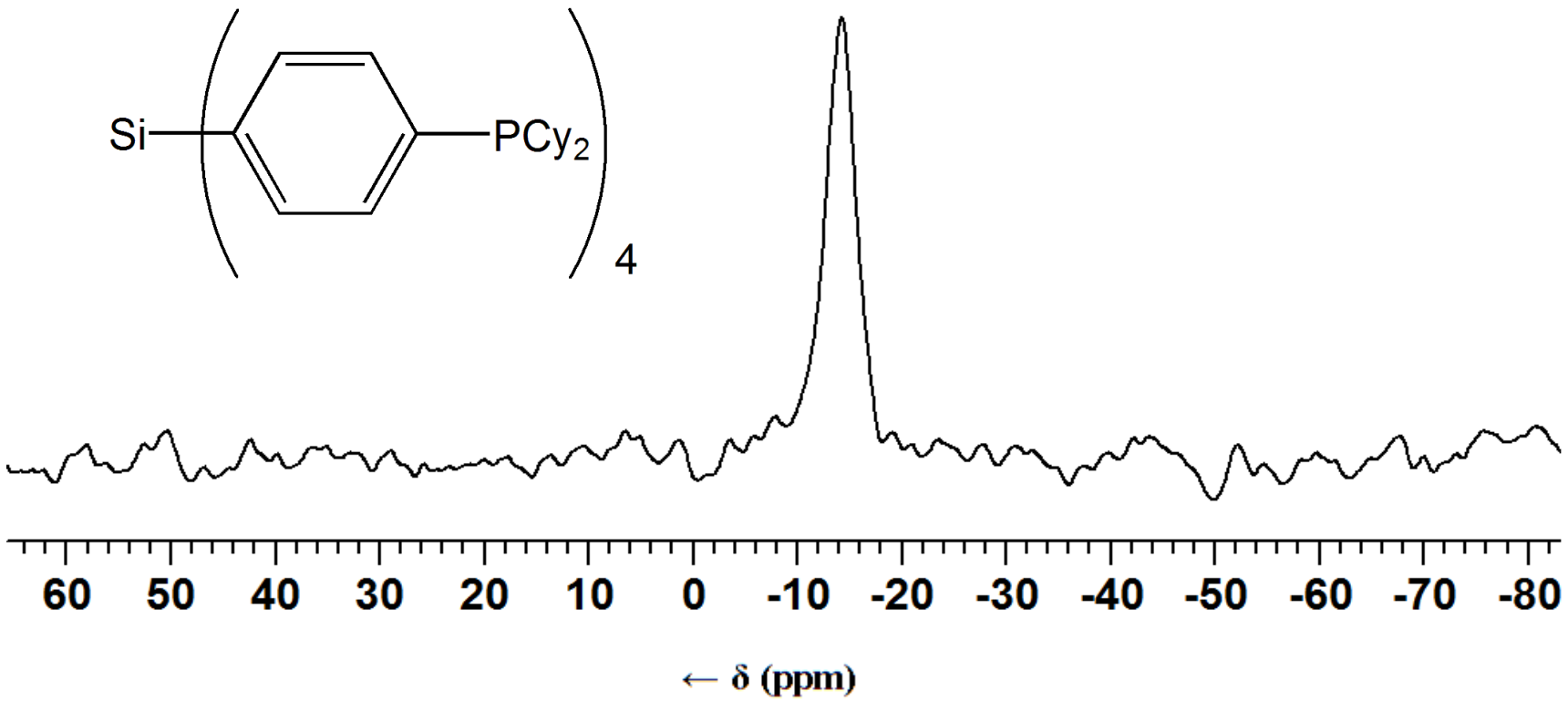

^{31}P CP/MAS NMR

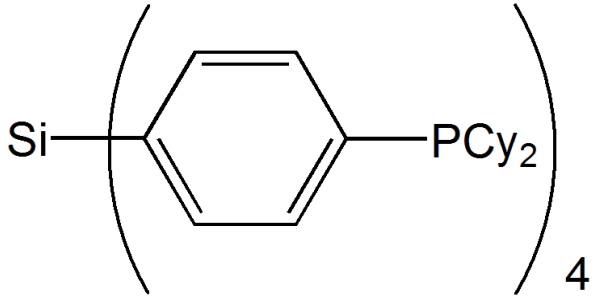

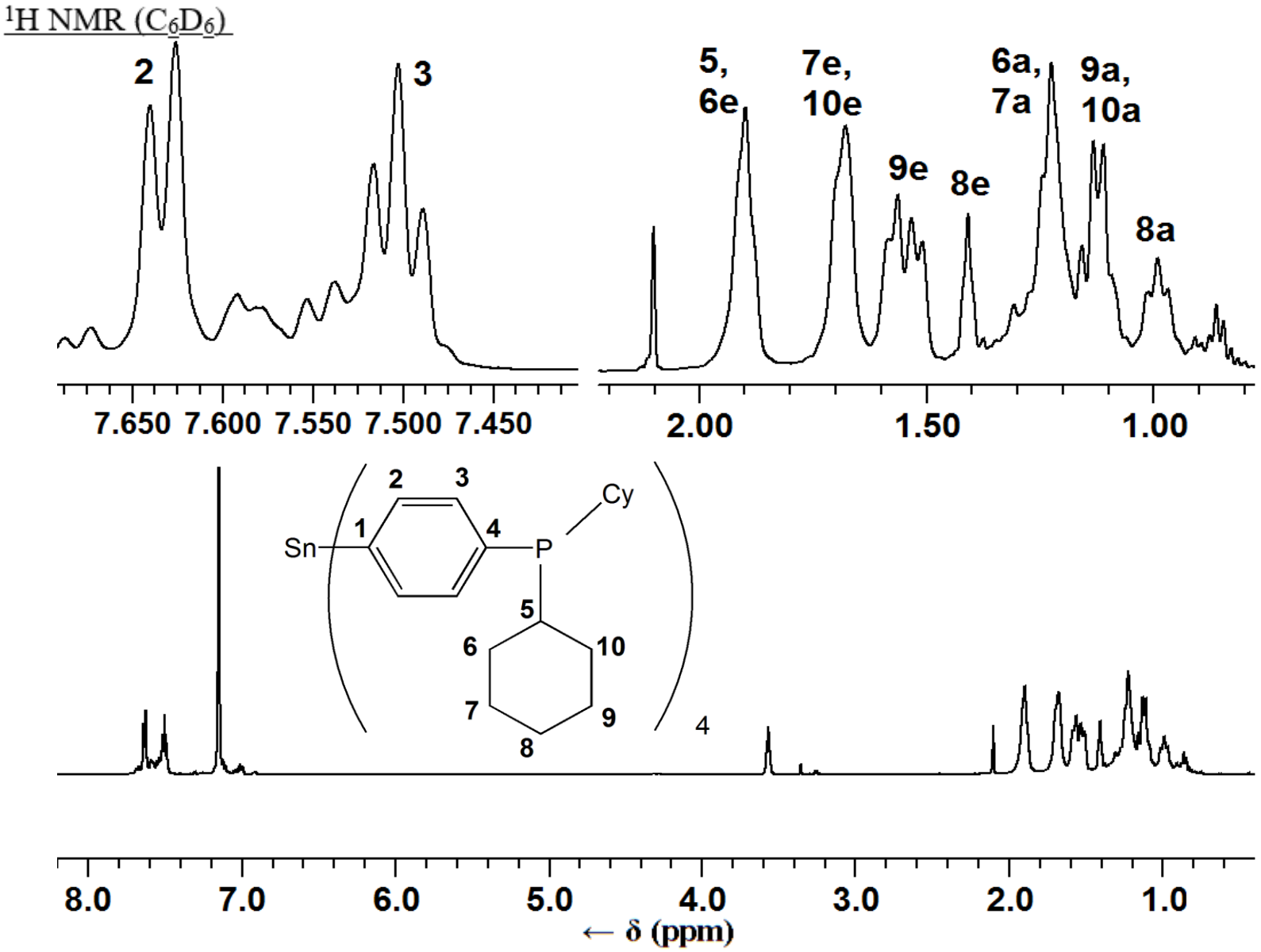
^{1}H NMR (C_6D_6)
2
3
5, 6e
7e, 10e
9e
8e
6a, 7a
9a, 10a
8a
7.650 7.600 7.550 7.500 7.450
2.00
1.50
1.00
Sn
P
Cy
1
2
3
4
5
6
7
8
9
10
4
8.0
7.0
6.0
5.0
4.0
3.0
2.0
1.0
← δ (ppm)

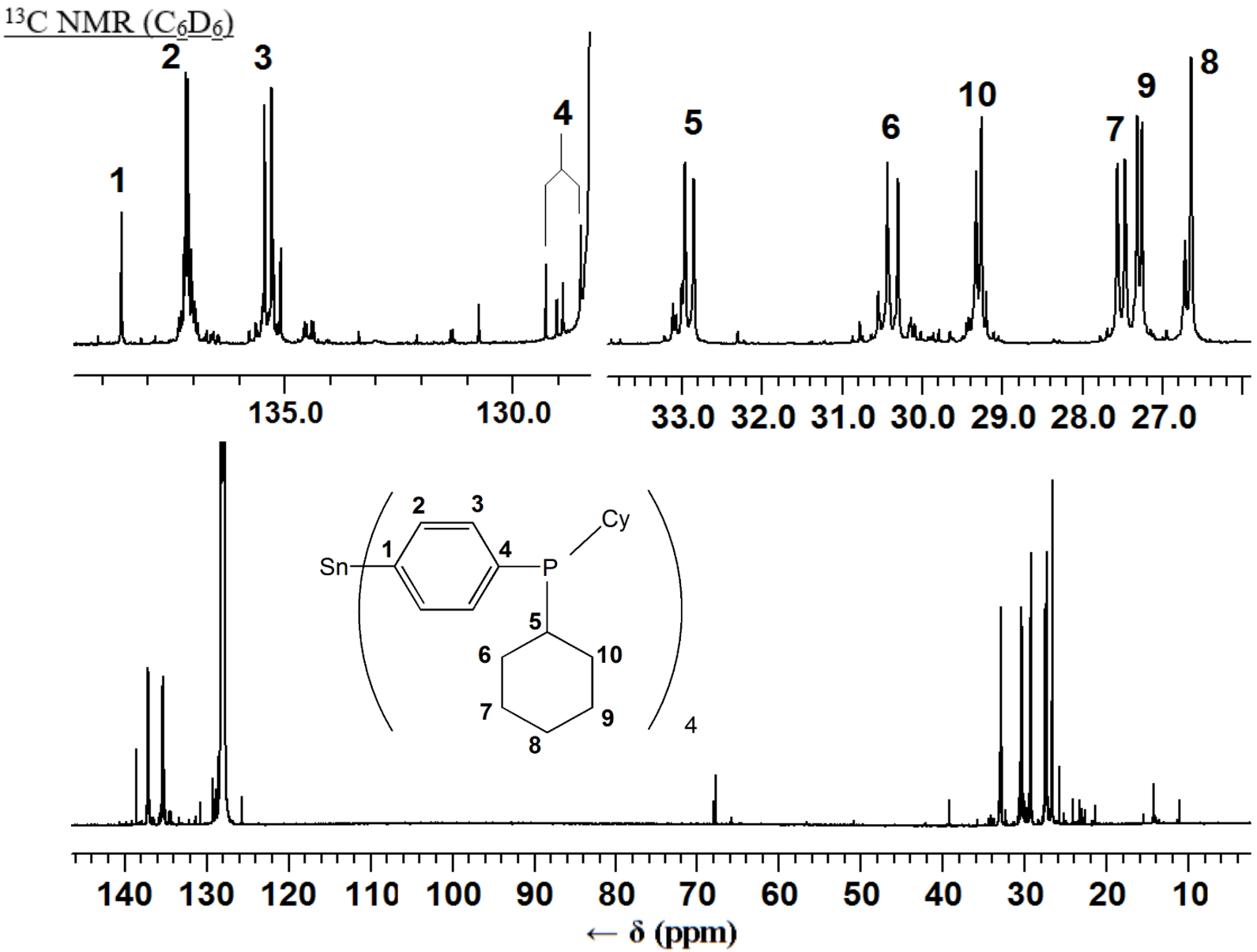
13C NMR (C6D6)
1
2
3
4
5
6
10
7
9
8
135.0
130.0
33.0 32.0 31.0 30.0 29.0 28.0 27.0
Sn
P
Cy
140 130 120 110 100 90 80 70 60 50 40 30 20 10
← δ (ppm)

^{1}H-^{1}H COSY (C_6D_6)

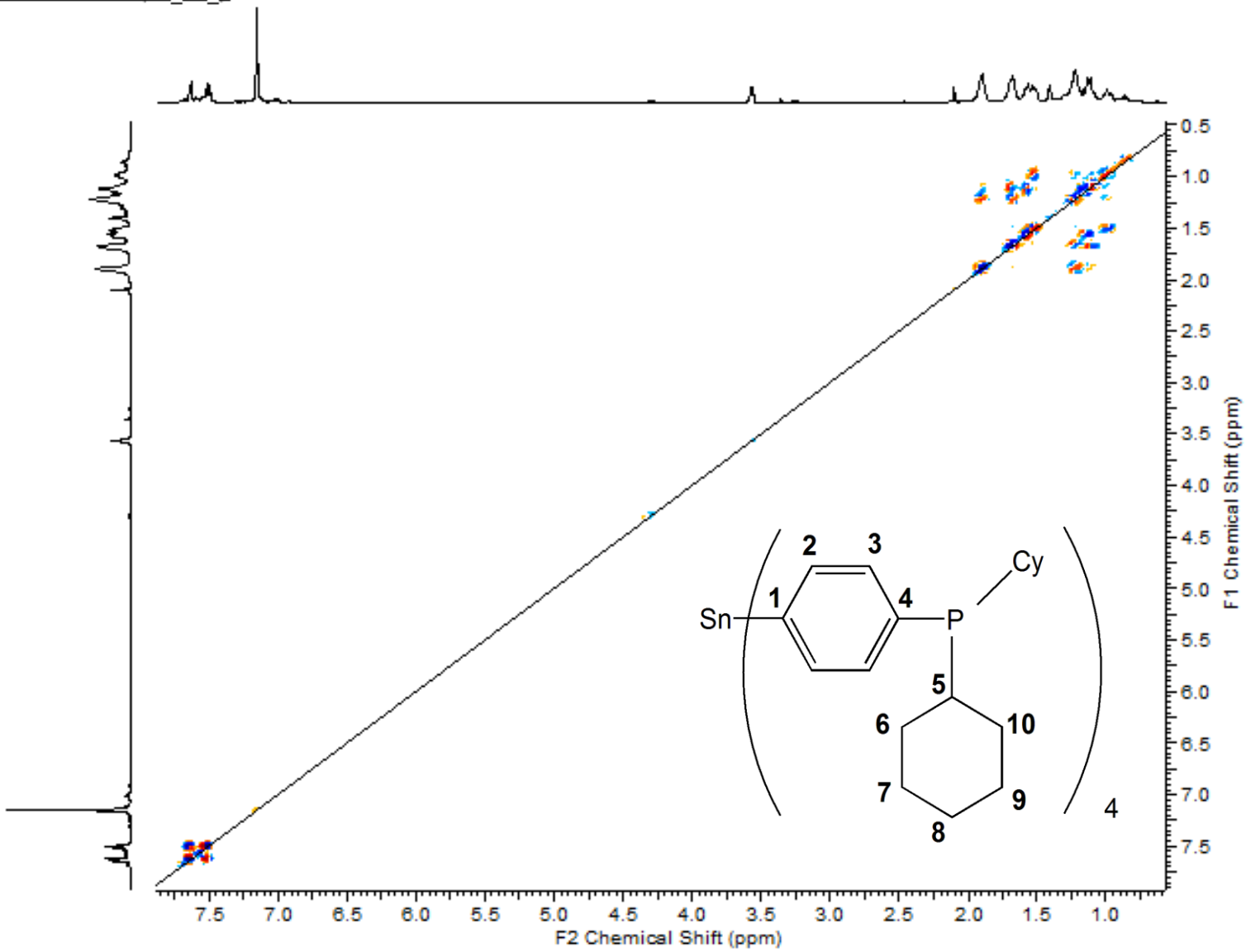

^{1}H-^{1}H COSY (expansion) (C_6D_6)

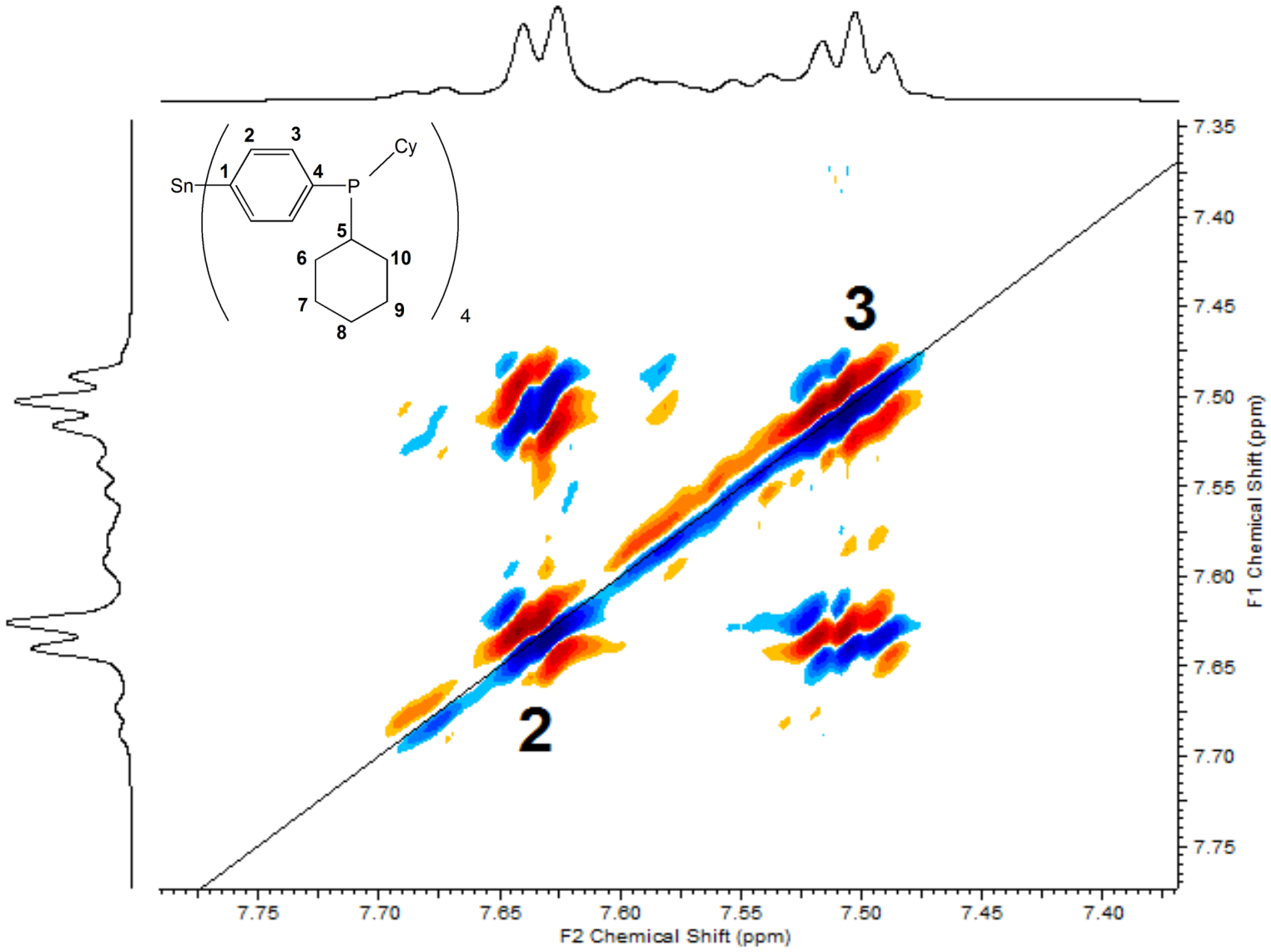

^{1}H-^{1}H COSY (expansion) (C_6D_6)

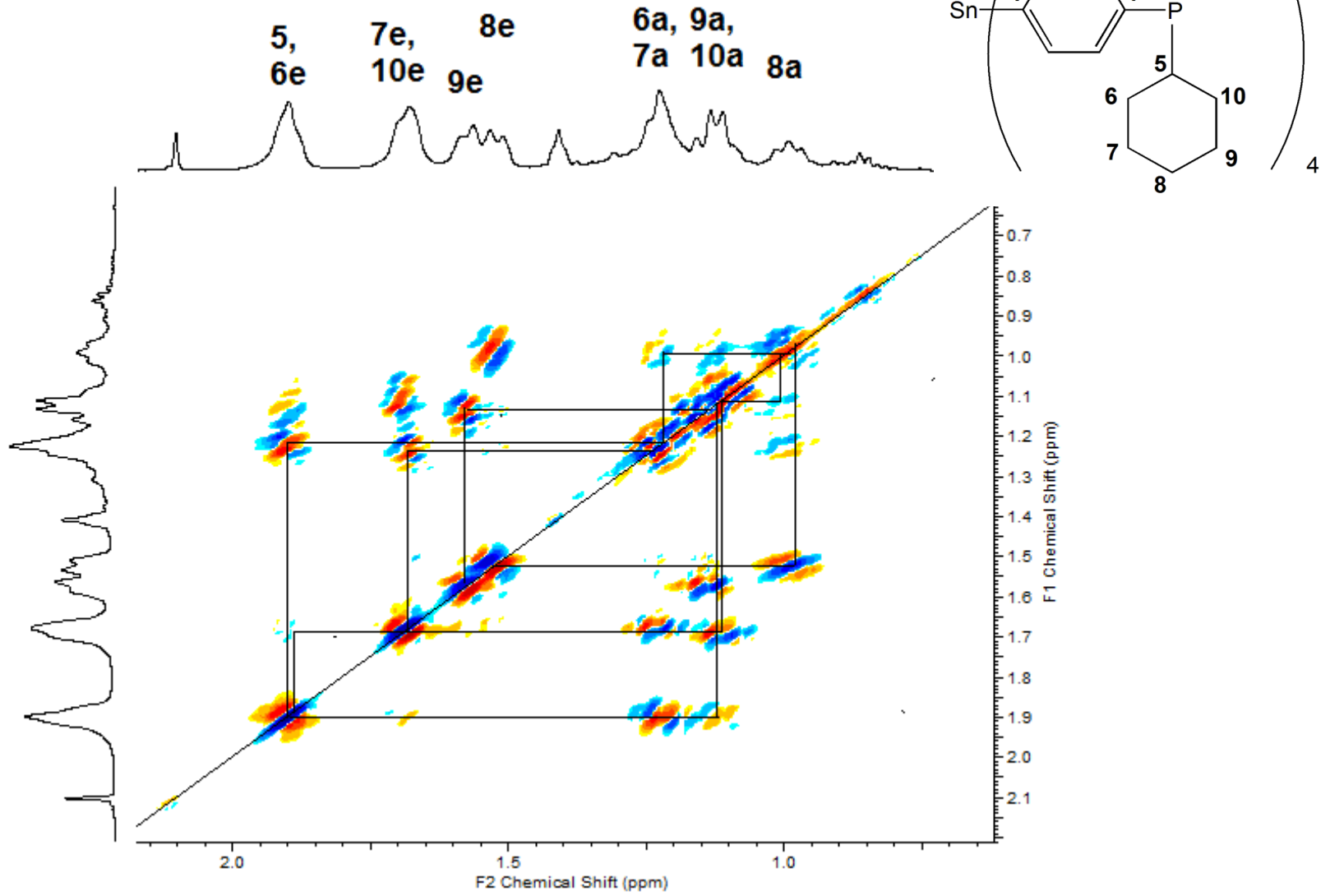

^{13}C-^{1}H HSQC (C_6D_6)

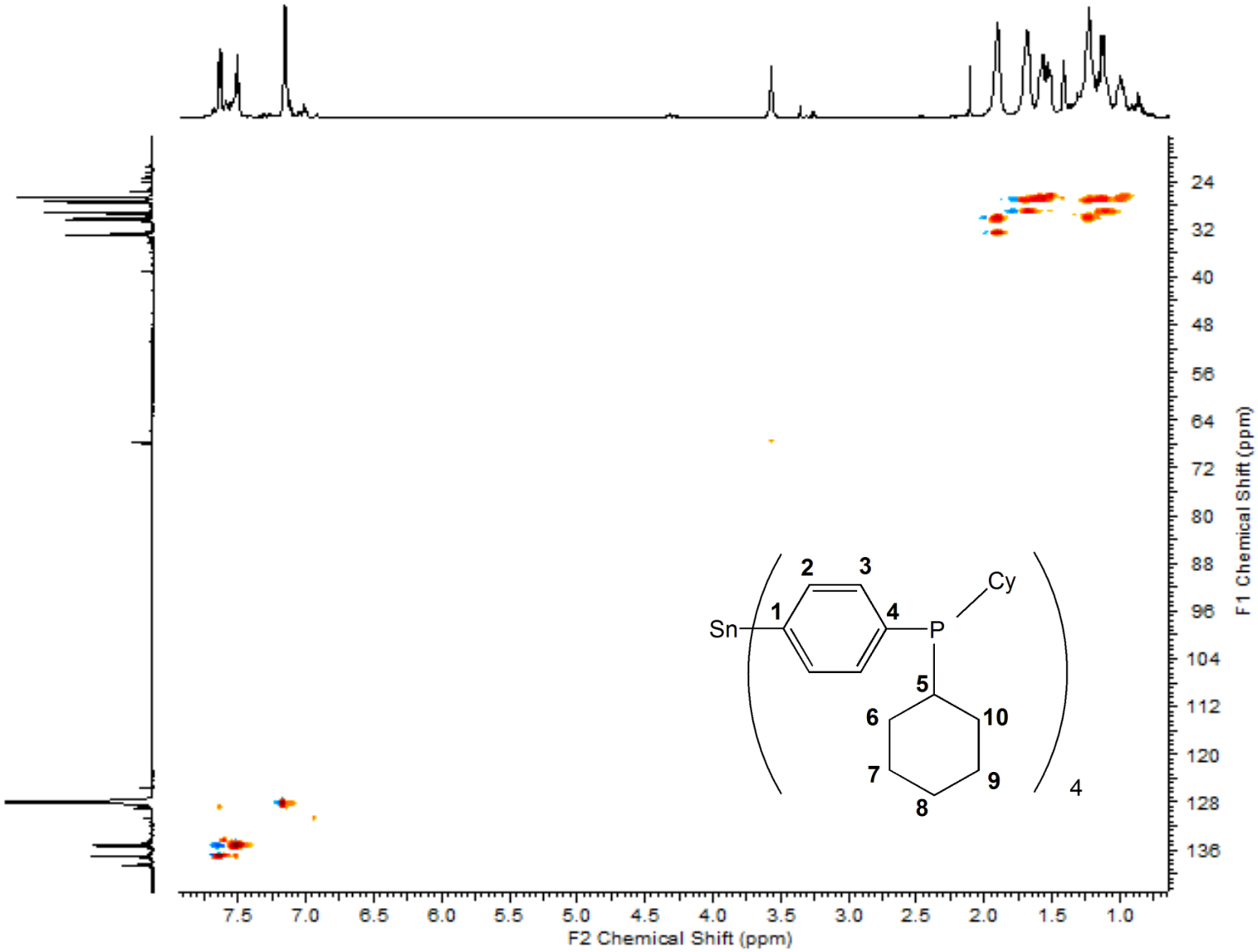

^{13}C-^{1}H HSQC (expansion) (C_6D_6)

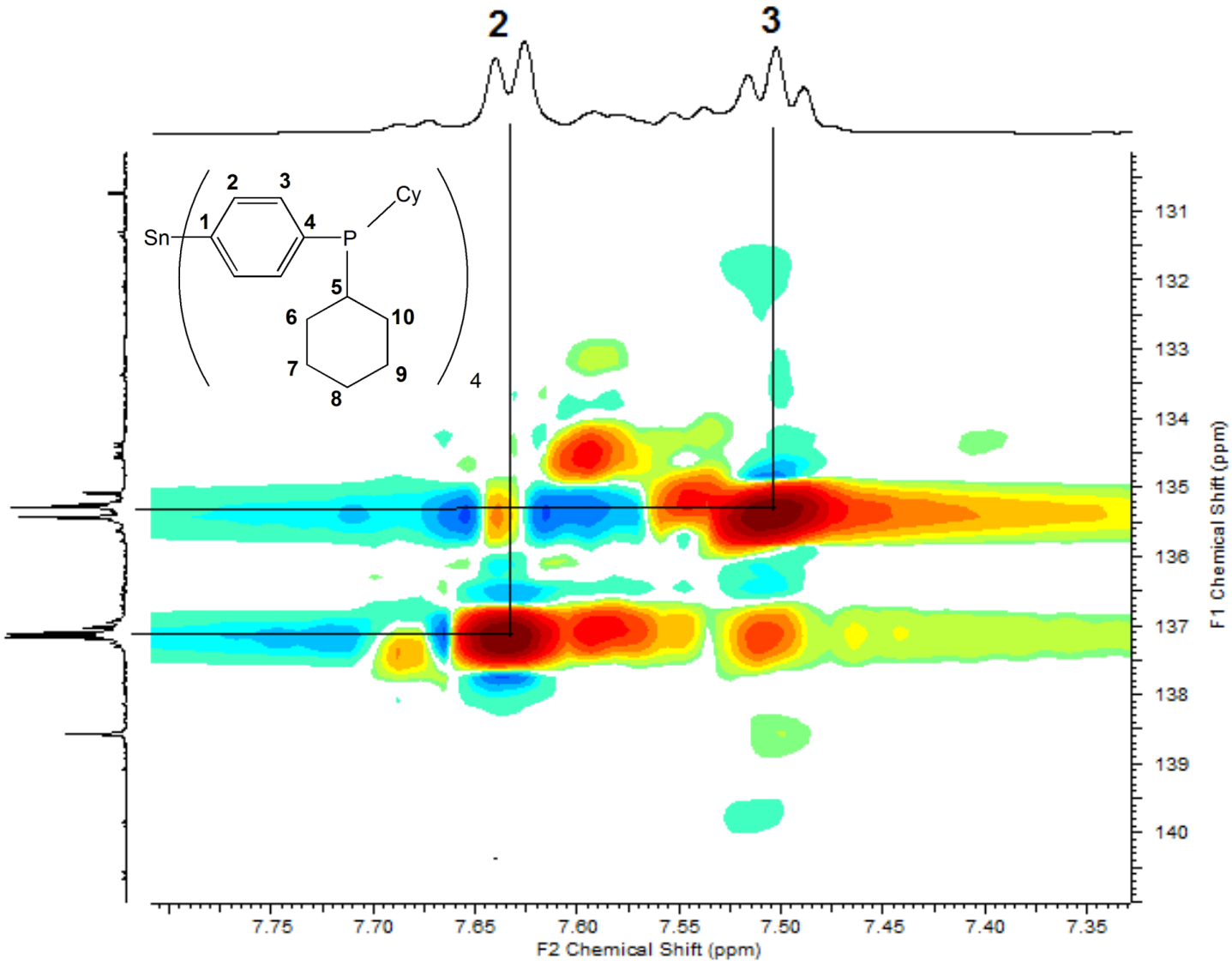

^{31}P NMR (C_6D_6)

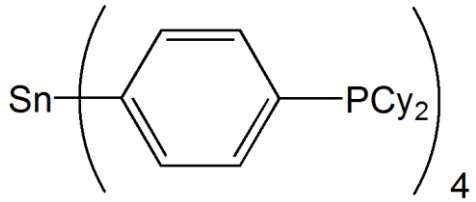

^{119}Sn NMR (C_6D_6)

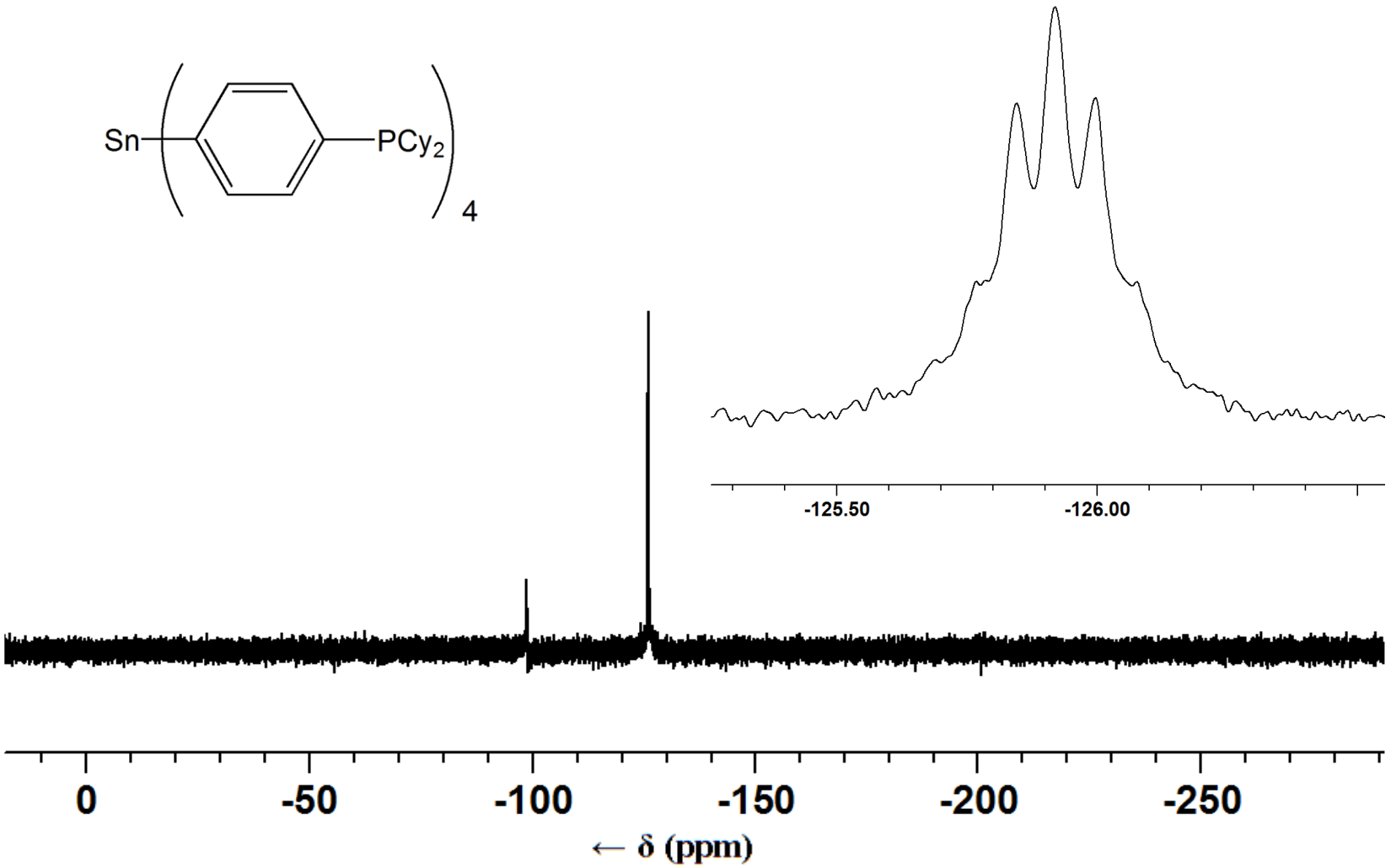

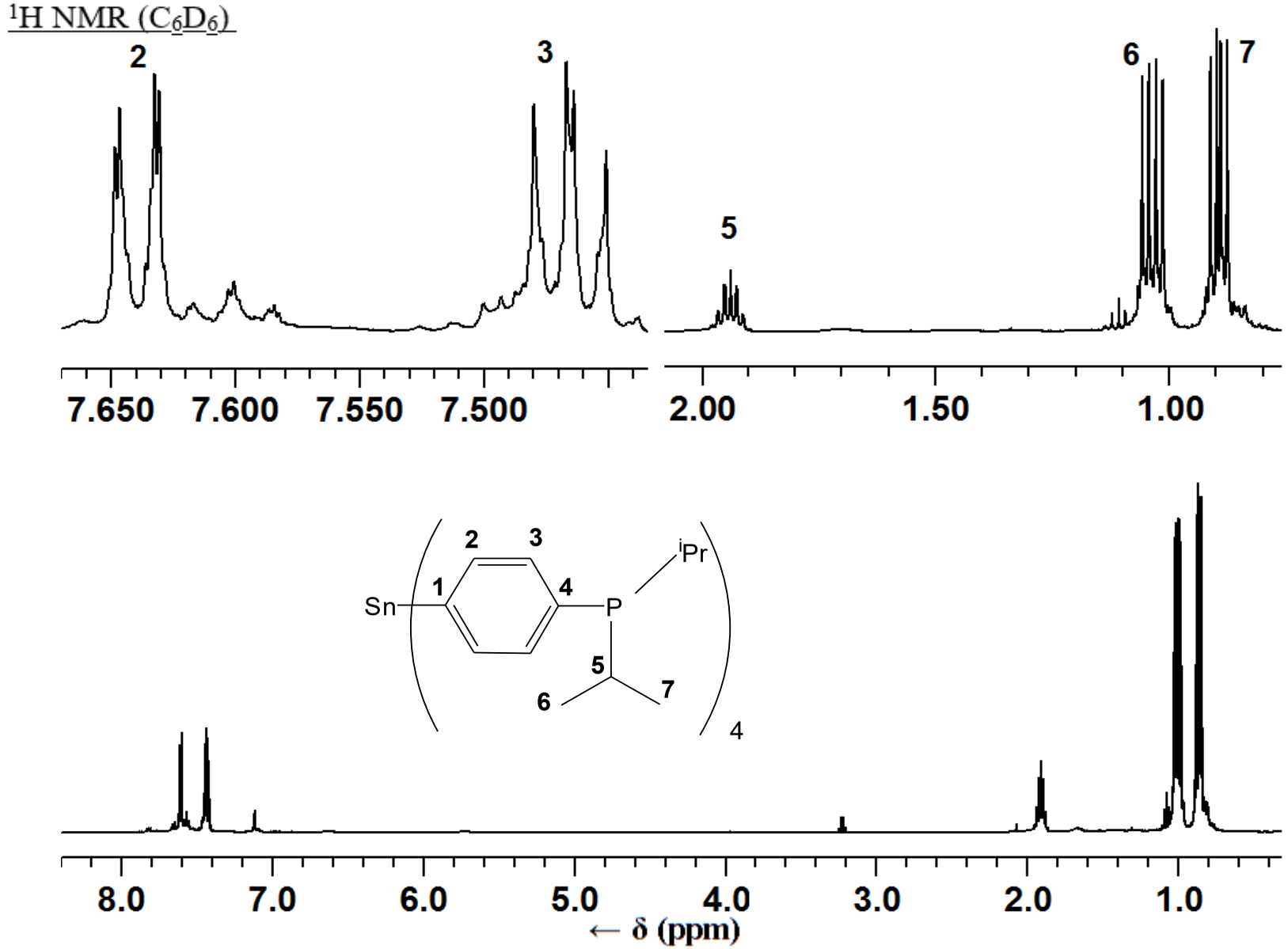
1H NMR (C6D6)
2
3
6
7
5
7.650
7.600
7.550
7.500
2.00
1.50
1.00
Sn
1
2
3
4
P
iPr
5
6
7
4
8.0
7.0
6.0
5.0
4.0
3.0
2.0
1.0
← δ (ppm)

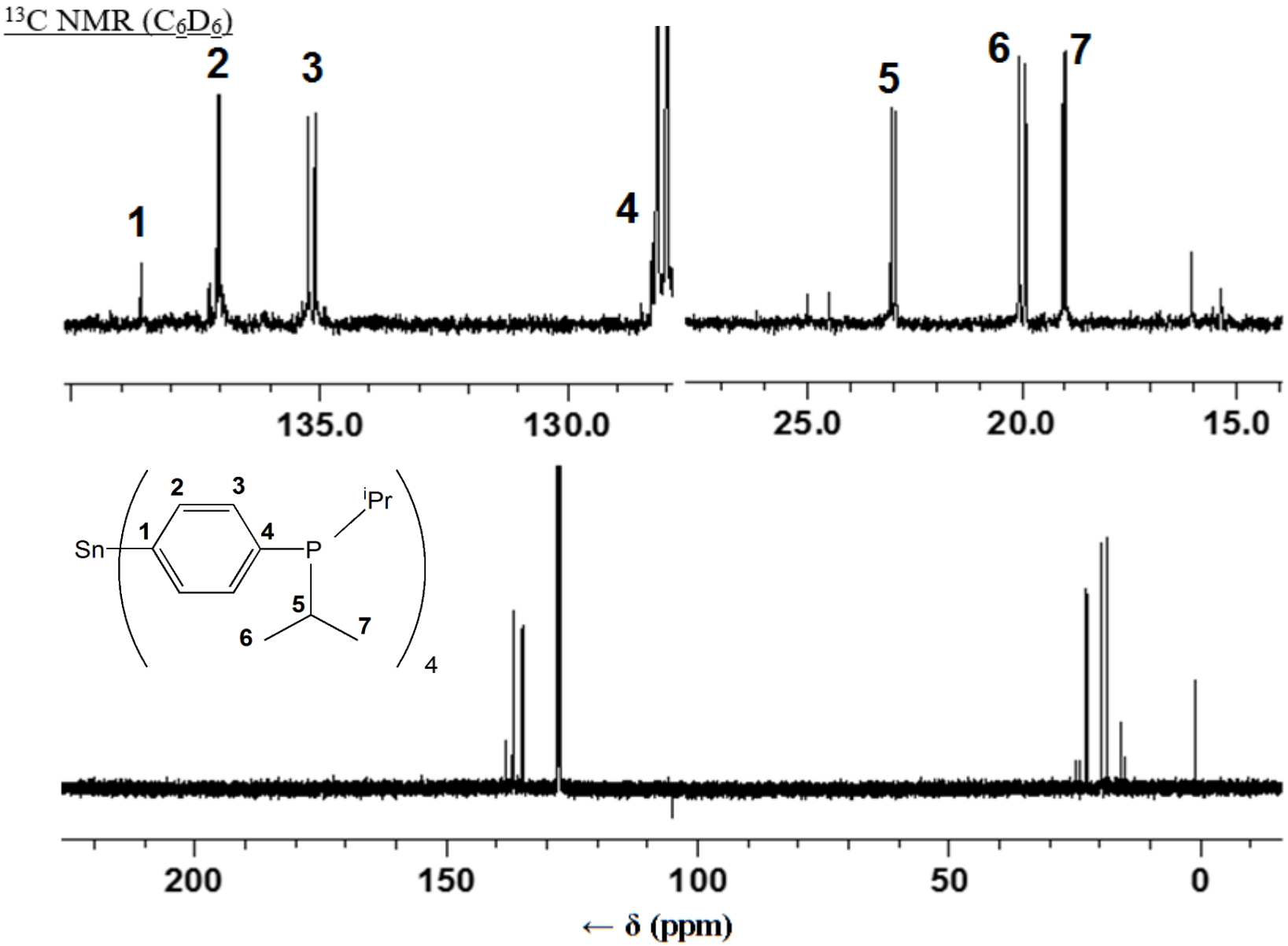
13C NMR (C6D6)
1
2
3
4
5
6
7
135.0
130.0
25.0
20.0
15.0
Sn
P
iPr
4
200
150
100
50
0
← δ (ppm)

^{119}Sn NMR (C_6D_6)

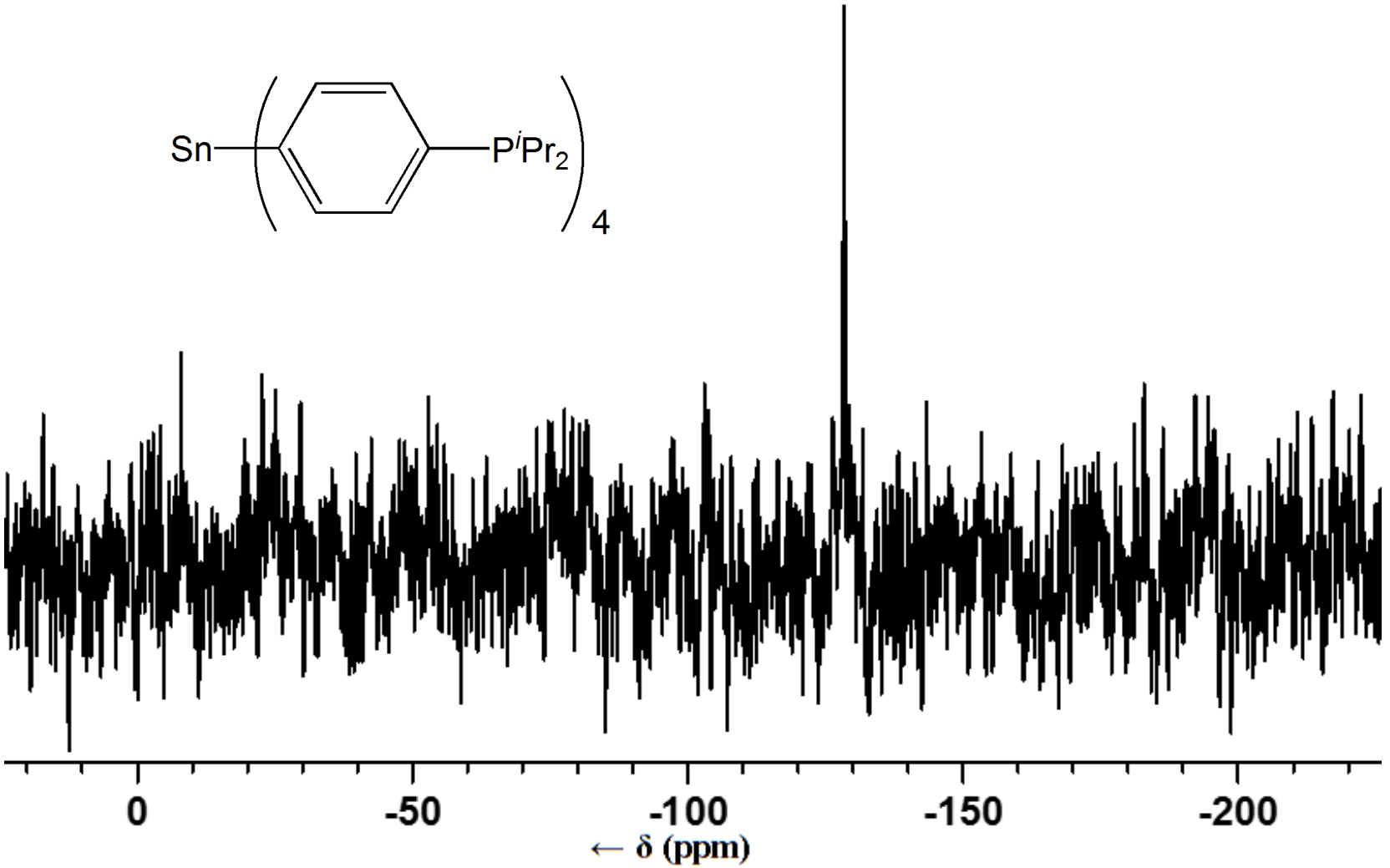

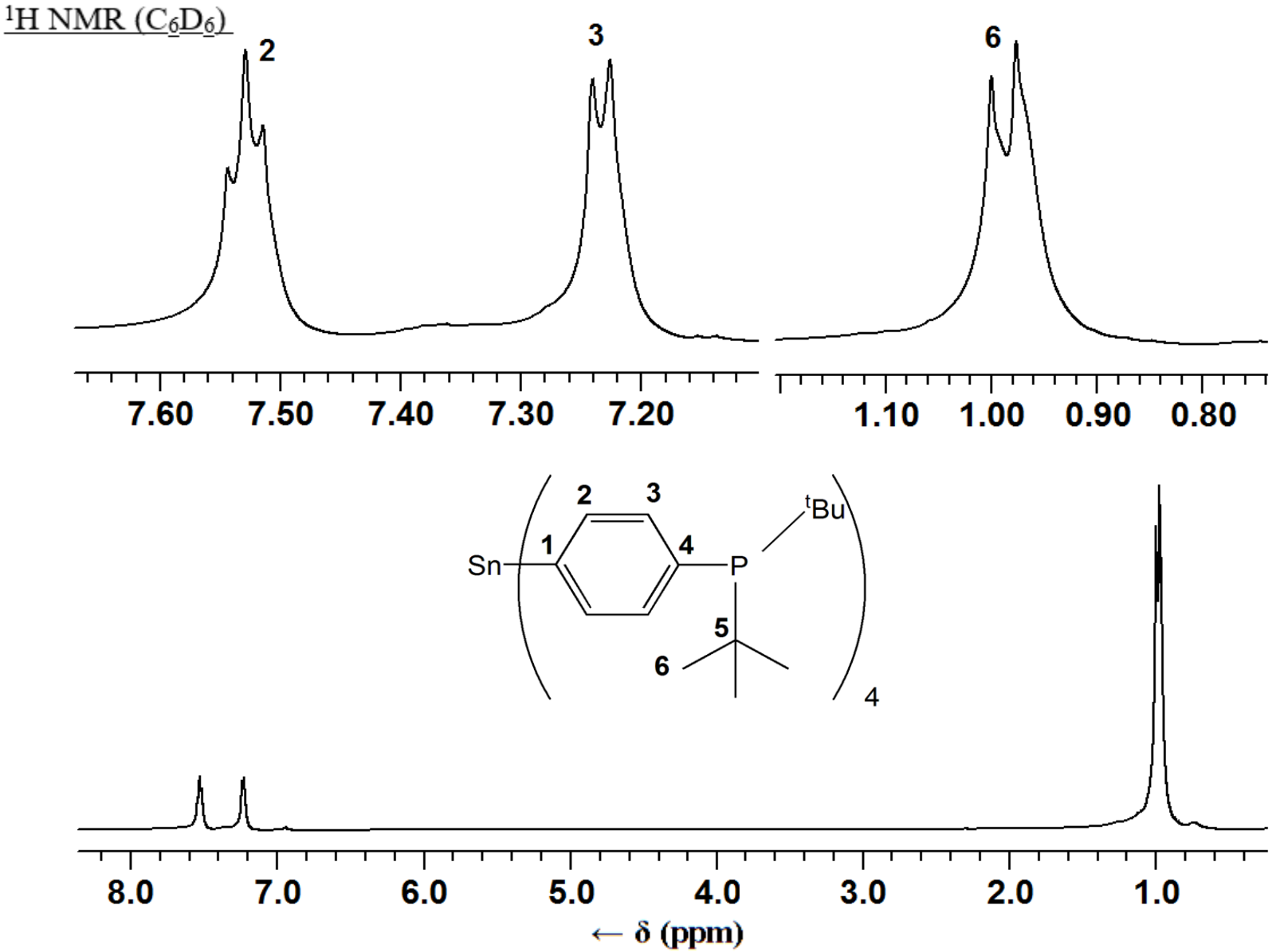
^{1}H NMR (C_6D_6)
2
3
6
7.60
7.50
7.40
7.30
7.20
1.10
1.00
0.90
0.80
Sn
P
^{t}Bu
1
2
3
4
5
6
4
8.0
7.0
6.0
5.0
4.0
3.0
2.0
1.0
← δ (ppm)

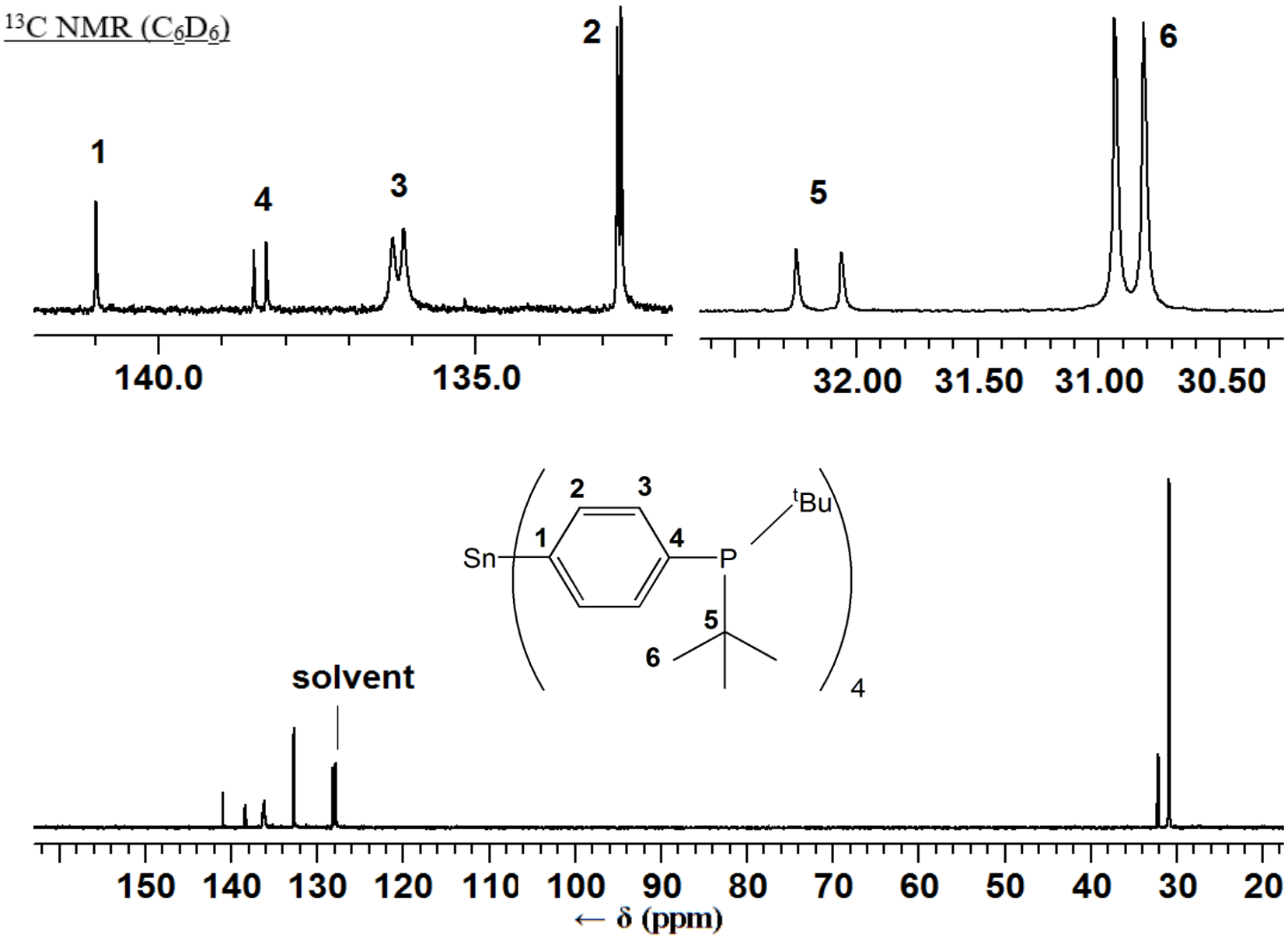
^{13}C NMR (C_6D_6)
1
2
3
4
5
6
140.0
135.0
32.00
31.50
31.00
30.50
Sn
P
^{t}Bu
solvent
150
140
130
120
110
100
90
80
70
60
50
40
30
20
← δ (ppm)

^{119}Sn NMR (C_6D_6)

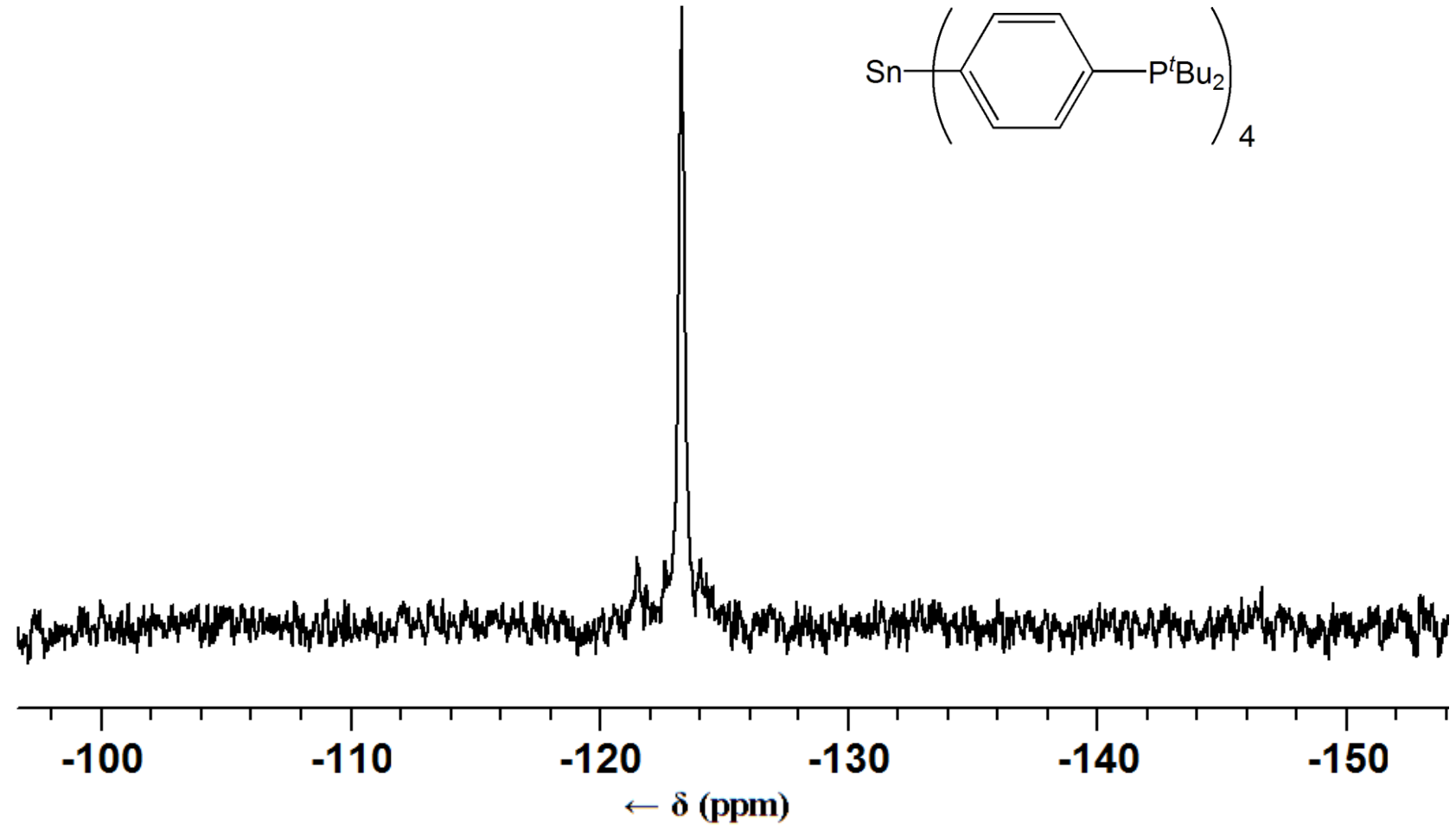

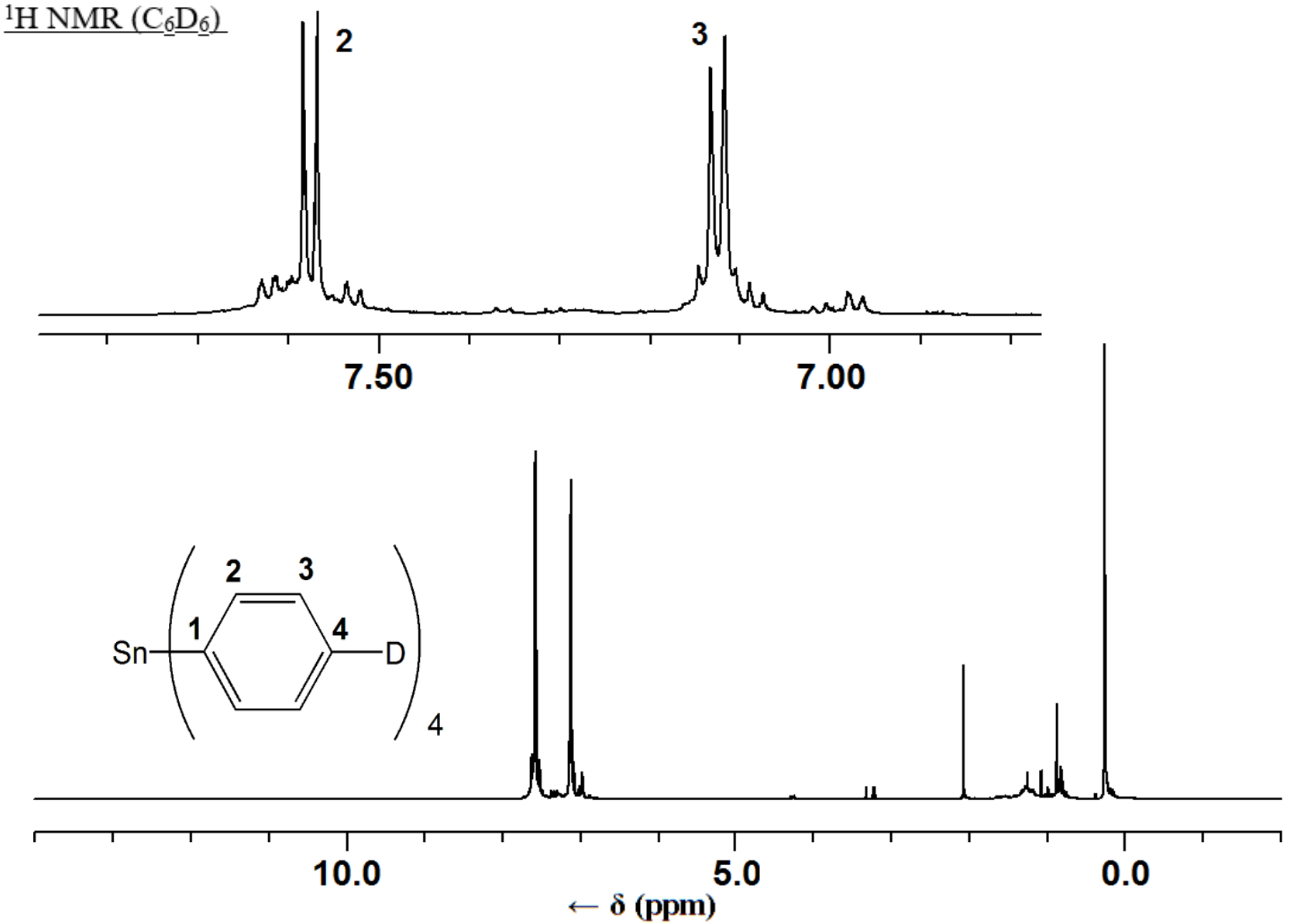
^{1}H NMR (C_6D_6)
2
3
7.50
7.00
Sn
D
1
2
3
4
4
10.0
5.0
0.0
← δ (ppm)

^{2}H NMR (CH_2Cl_2)

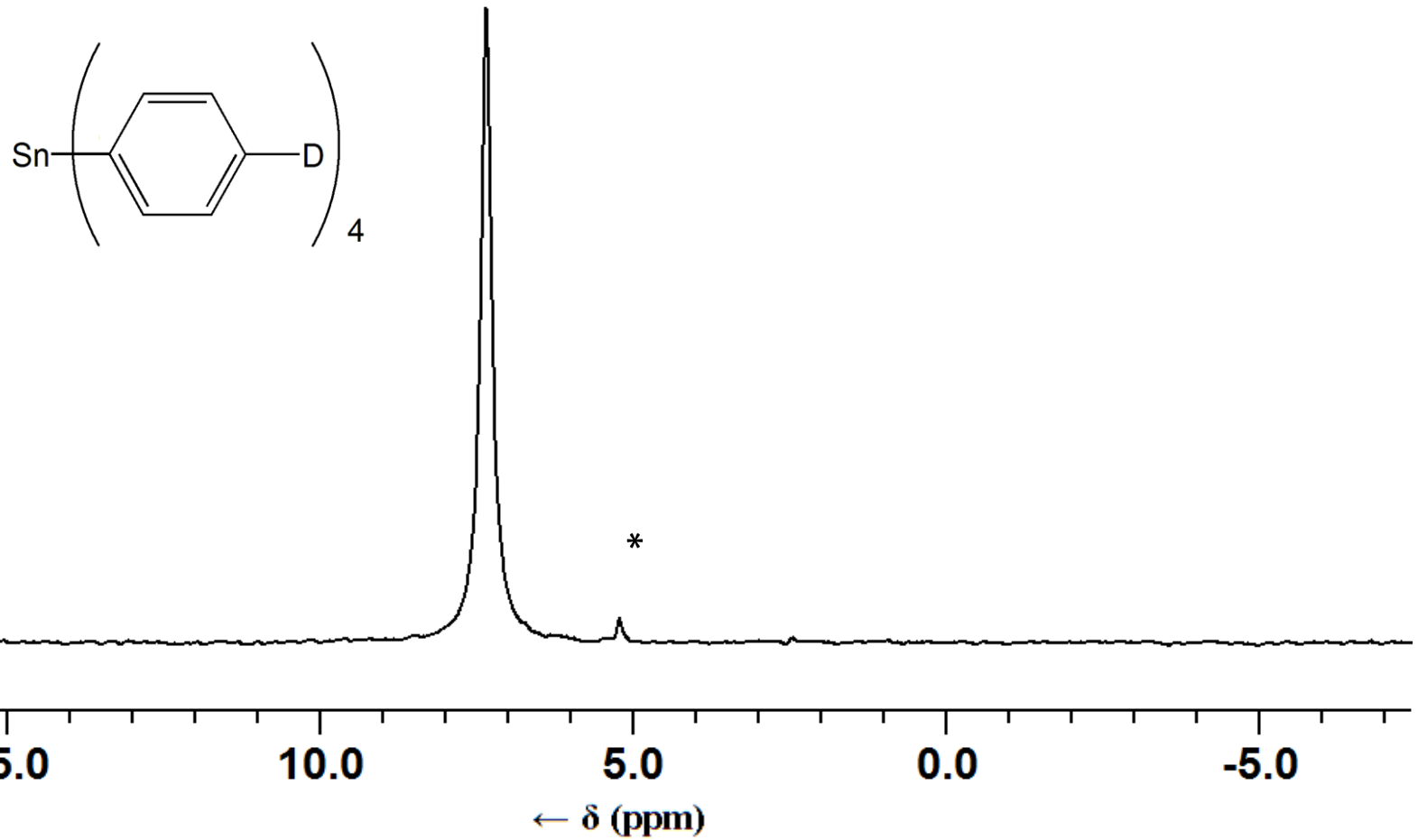

^{119}Sn NMR (C_6D_6)

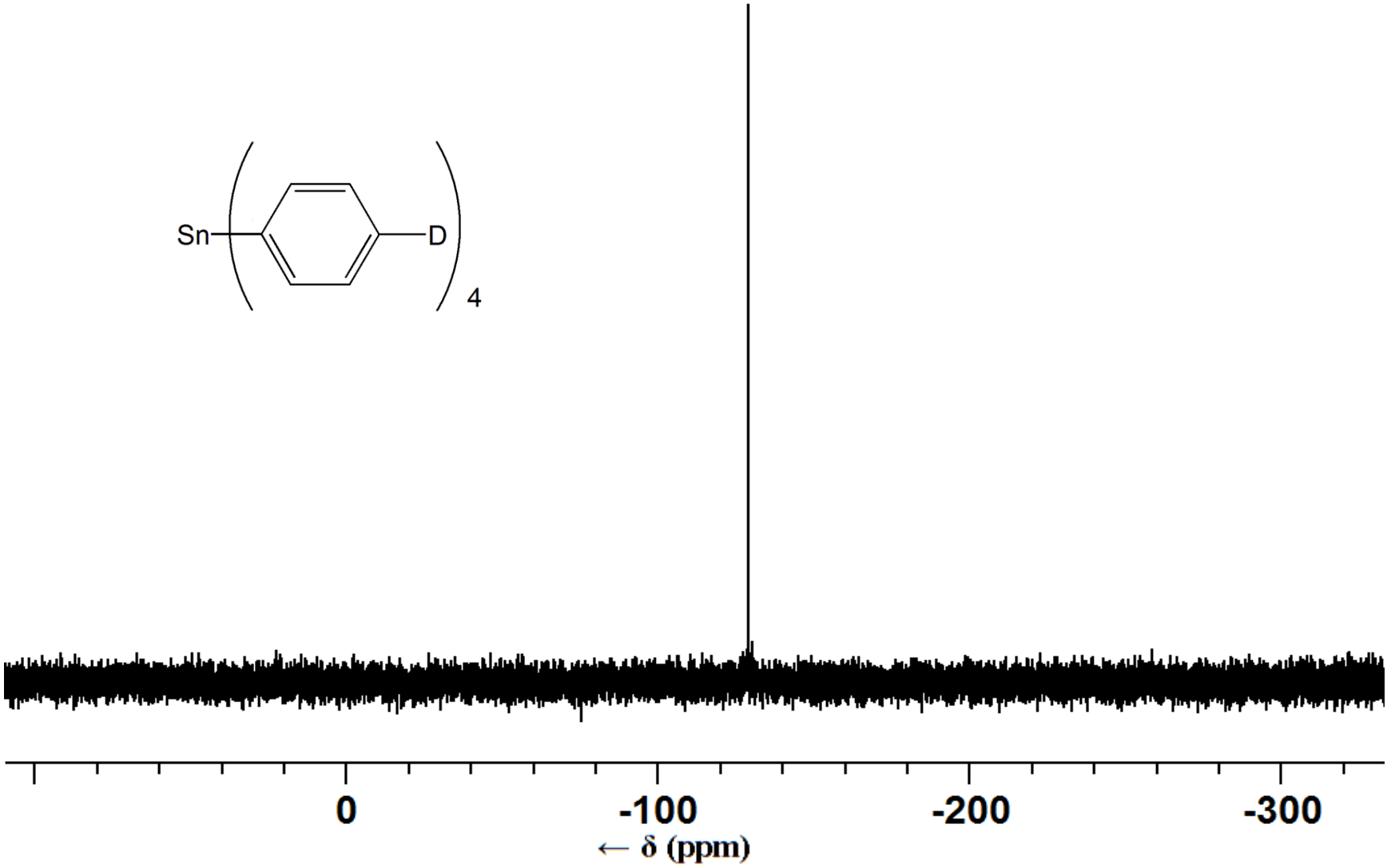

^{2}H MAS NMR

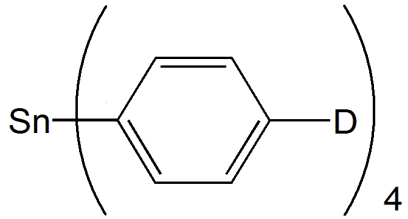

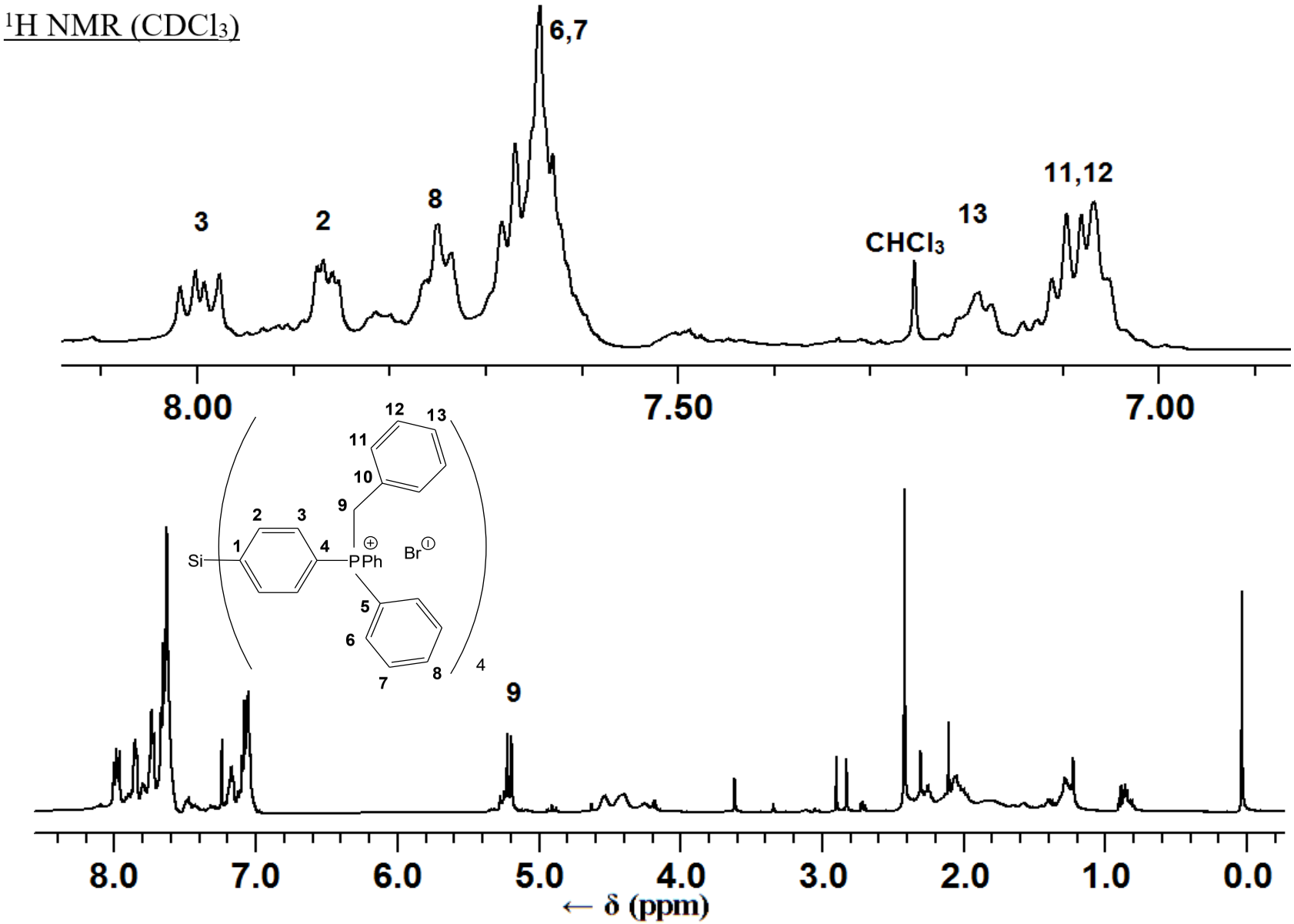
1H NMR (CDCl3)
6,7
3
2
8
CHCl3
13
11,12
8.00
7.50
7.00
12
13
11
10
9
2
3
1
4
Si
PPh
Br
5
6
7
8
4
9
8.0
7.0
6.0
5.0
4.0
3.0
2.0
1.0
0.0
← δ (ppm)

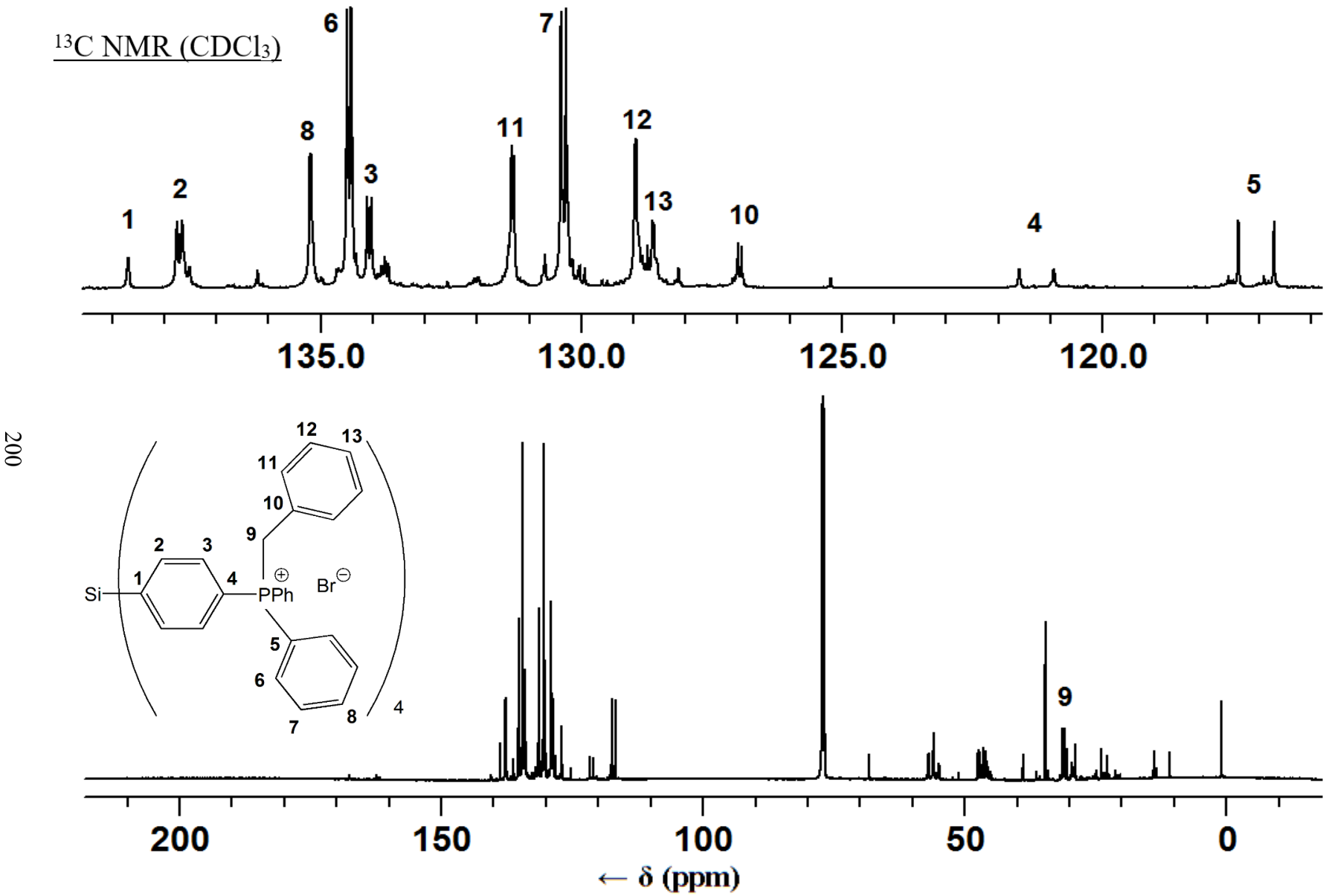
13C NMR (CDCl3)
1
2
8
6
3
11
7
12
13
10
4
5
135.0
130.0
125.0
120.0
Si
PPh
Br
200
150
100
50
0
← δ (ppm)

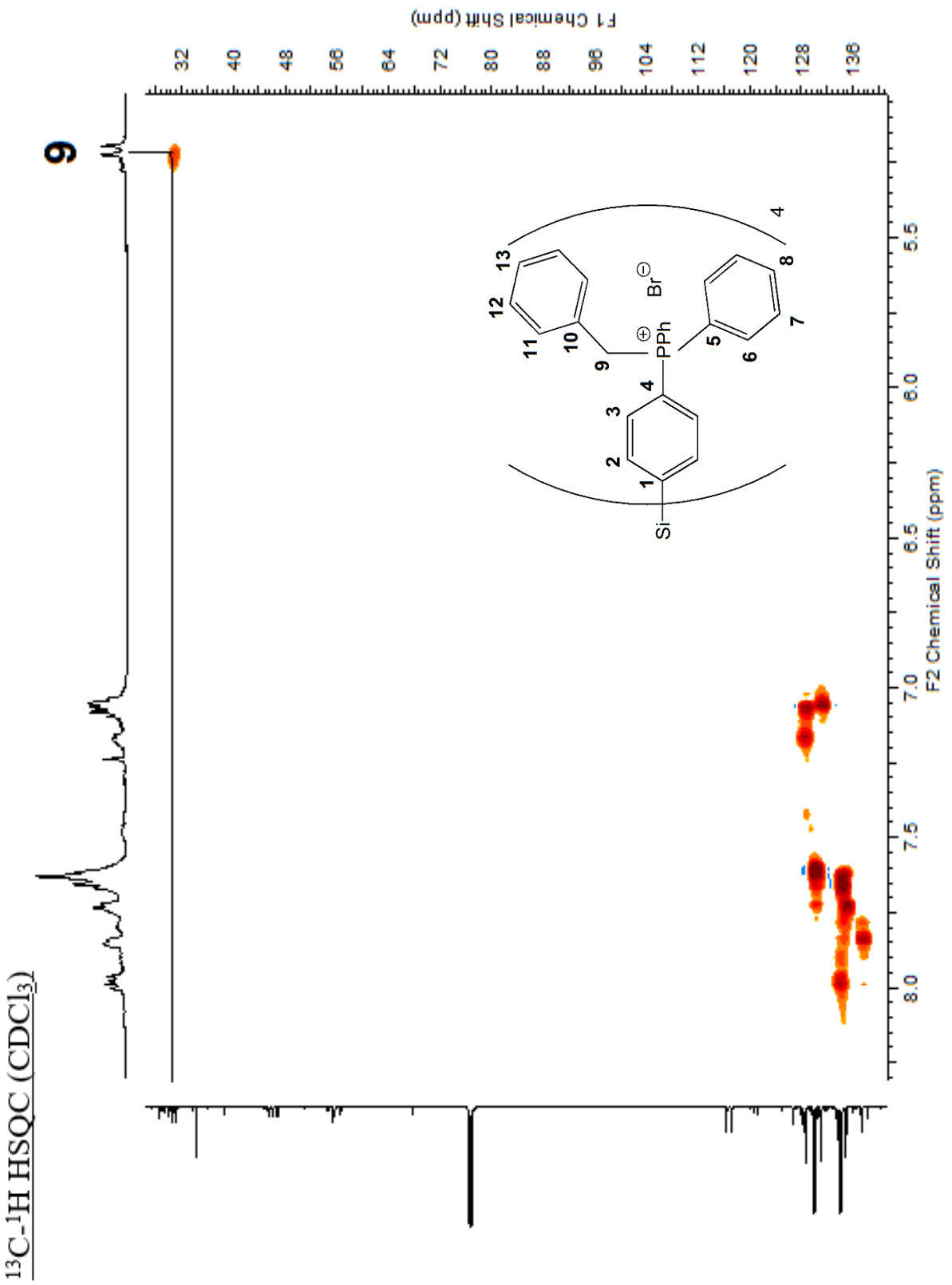
^{13}C-^{1}H HSQC ($CDCl_3$)
9
F1 Chemical Shift (ppm)
F2 Chemical Shift (ppm)
Br
PPh
Si

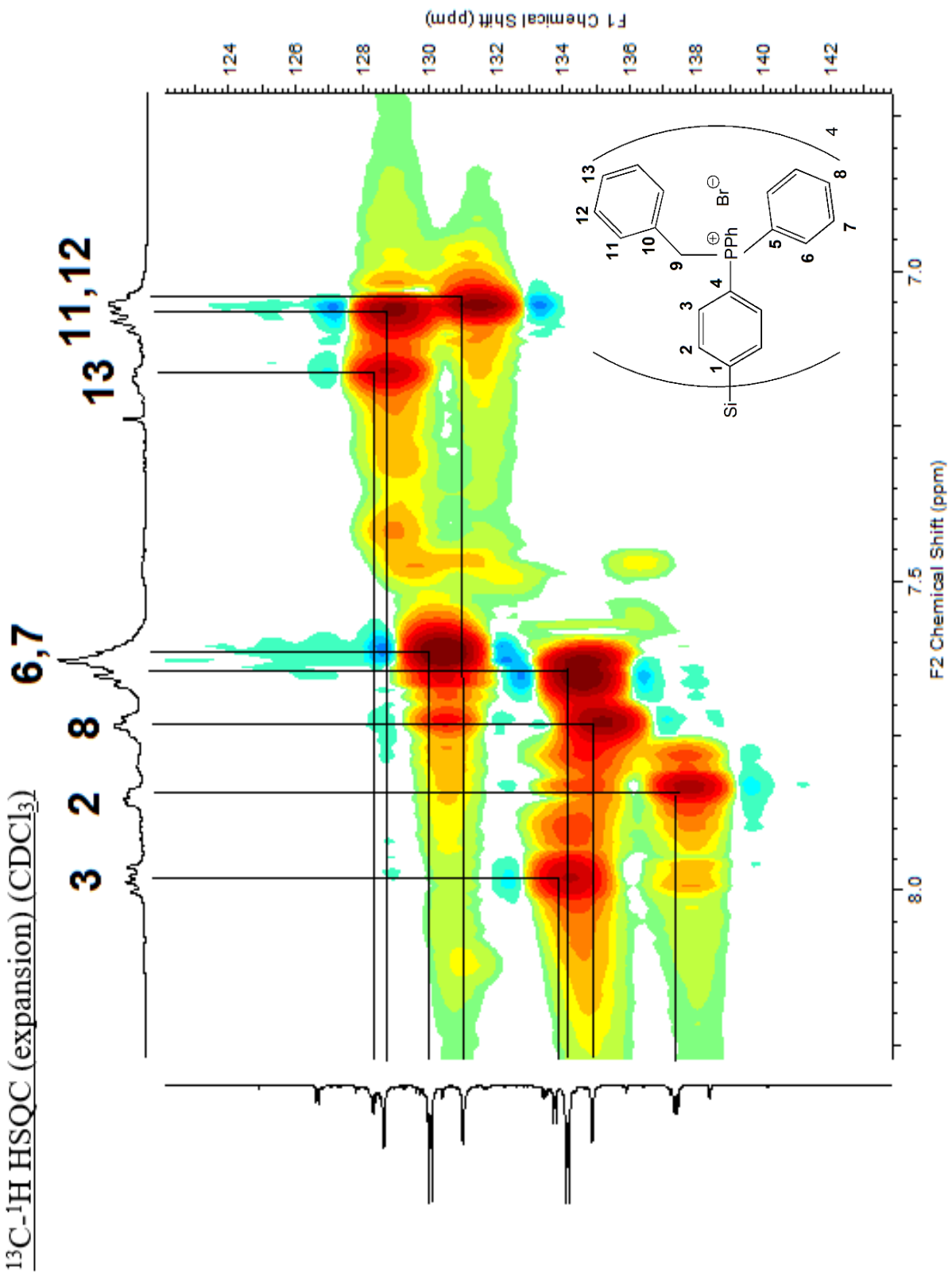
^{13}C-^{1}H HSQC (expansion) ($CDCl_3$)
3
2
8
6,7
13
11,12
F1 Chemical Shift (ppm)
F2 Chemical Shift (ppm)
124
126
128
130
132
134
136
138
140
142
8.0
7.5
7.0
Si
PPh
Br

^{29}Si NMR ($CDCl_3$)

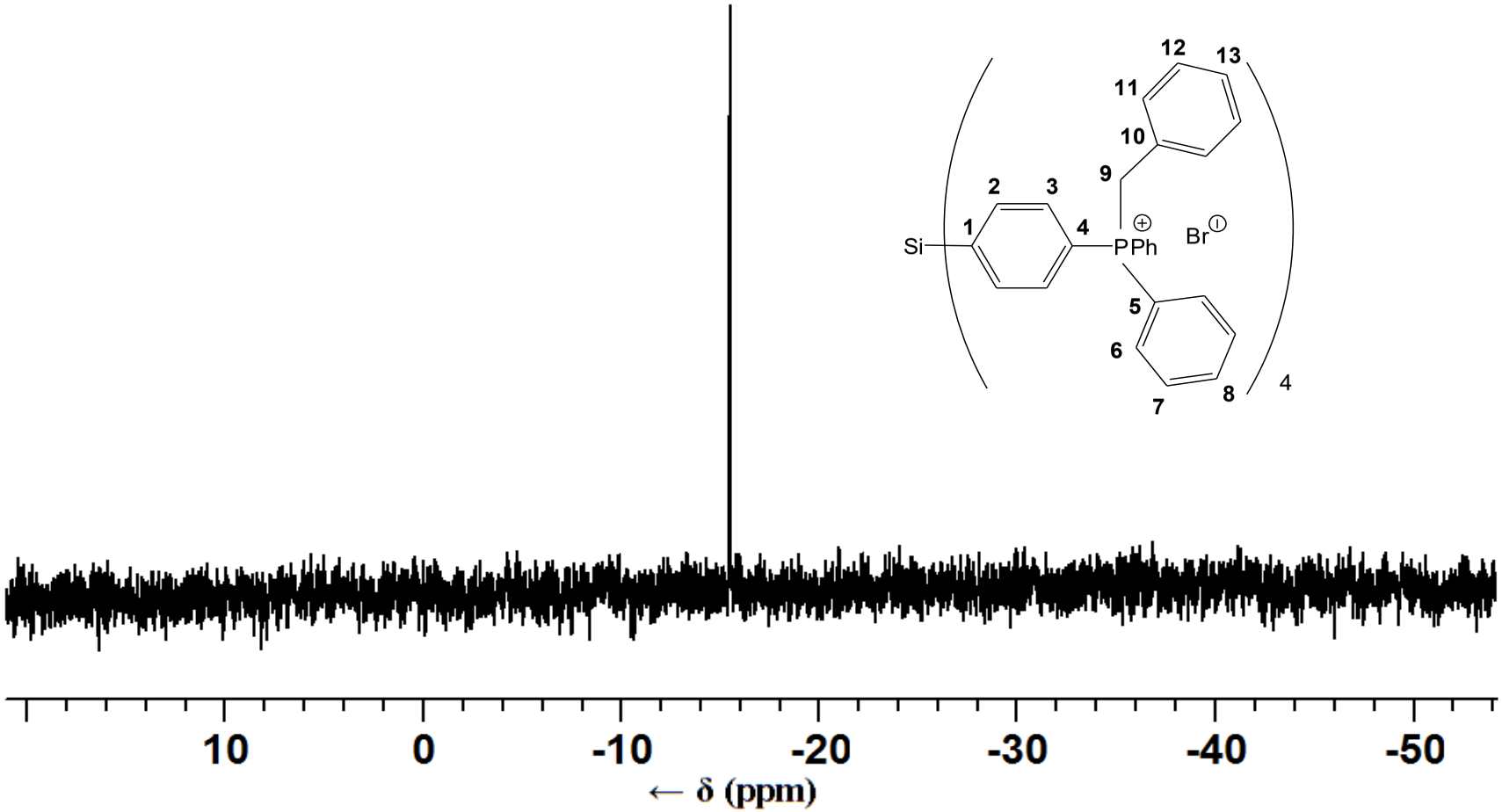

^{31}P NMR ($CDCl_3$)

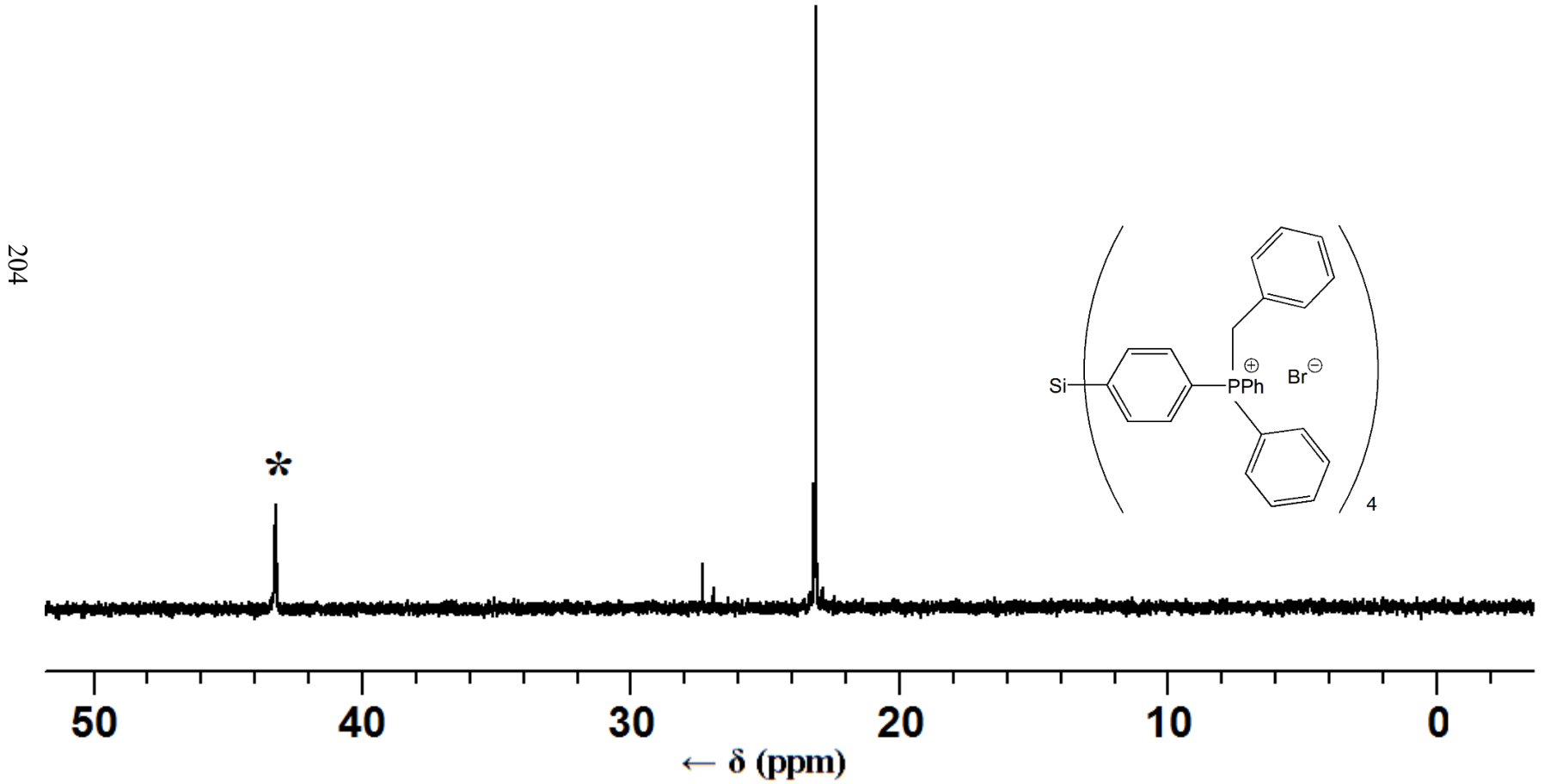

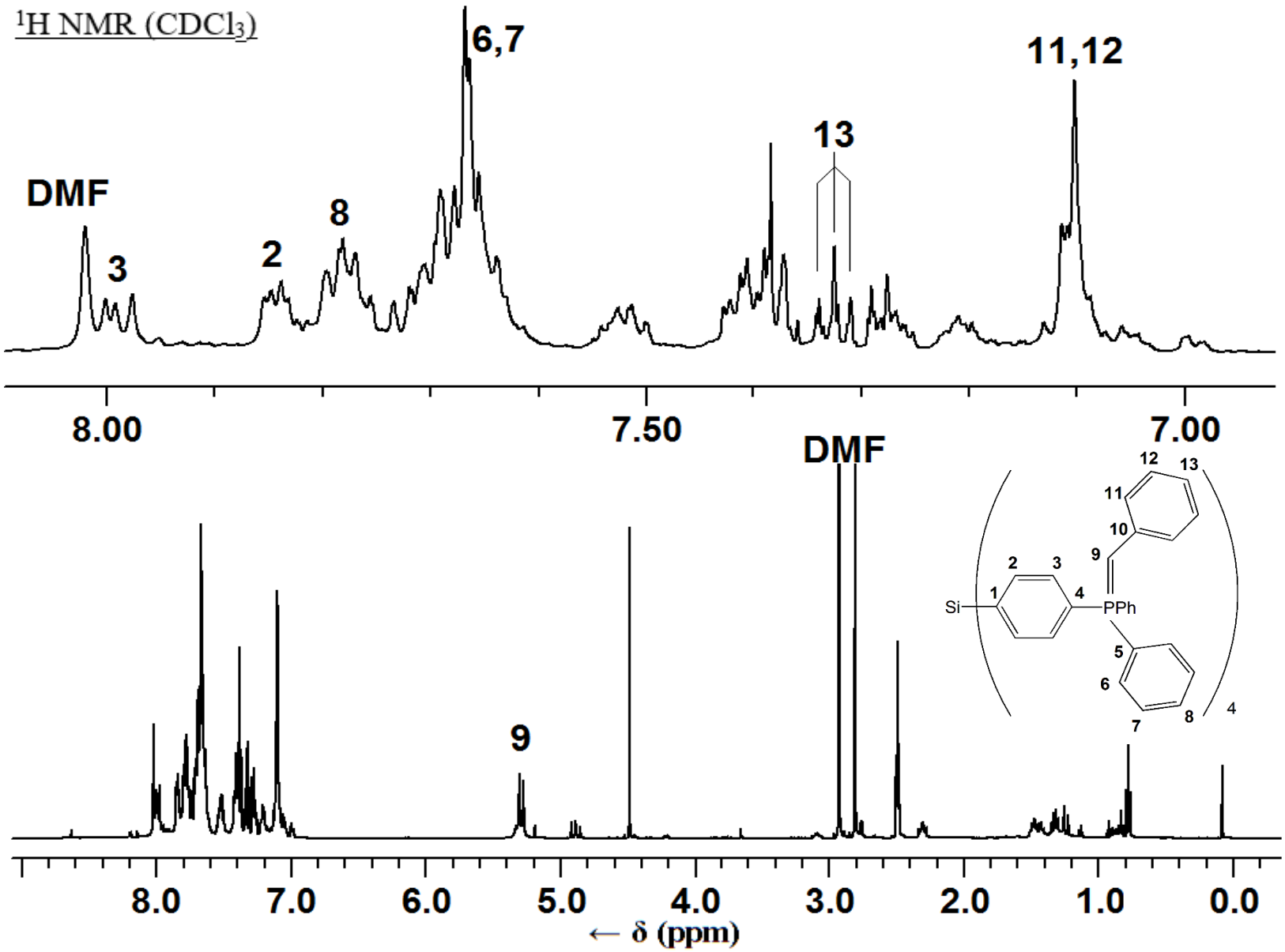
^{1}H NMR ($CDCl_3$)
6,7
11,12
13
DMF
8
3
2
8.00
7.50
7.00
DMF
9
12
13
11
10
9
2
3
1
4
Si
PPh
5
6
8
7
4
8.0
7.0
6.0
5.0
4.0
3.0
2.0
1.0
0.0
← δ (ppm)

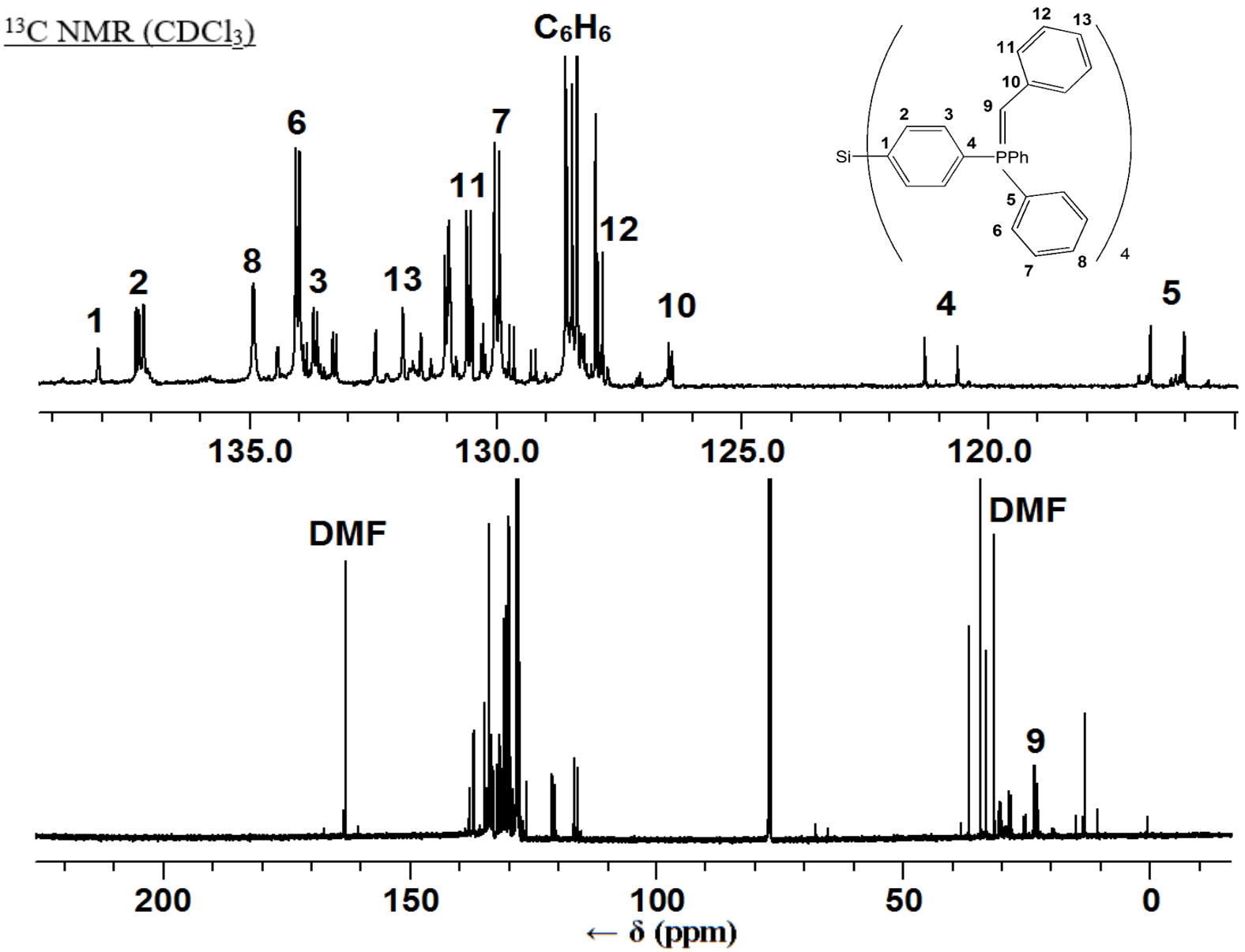
13C NMR (CDCl3)
C6H6
1
2
8
6
3
13
11
7
12
10
4
5
135.0
130.0
125.0
120.0
DMF
DMF
9
200
150
100
50
0
← δ (ppm)
Si
PPh

^{29}Si NMR ($CDCl_3$)

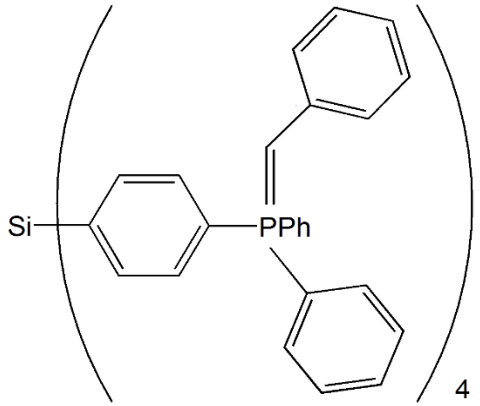

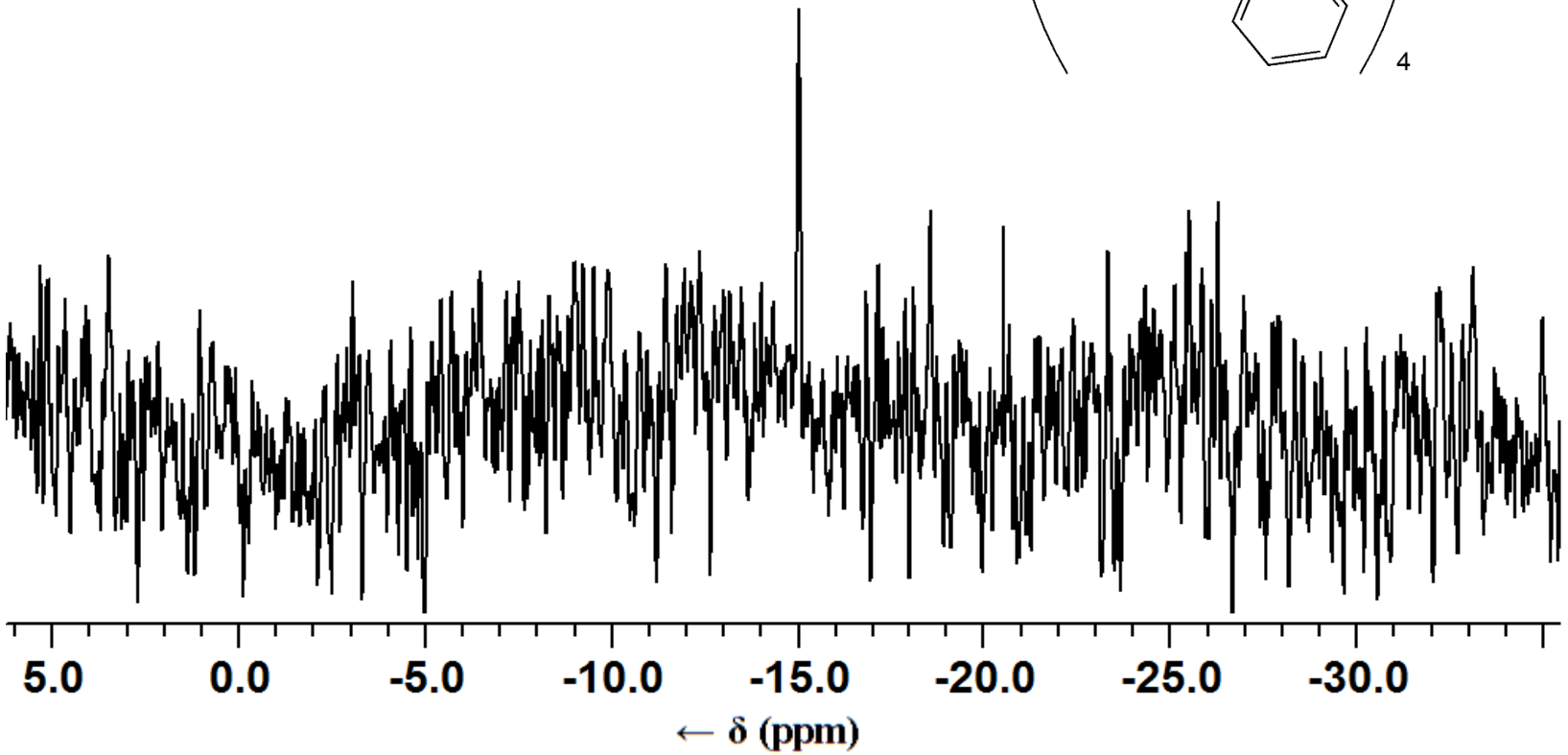

^{31}P NMR (C_6D_6)